

**Synthesis and  
Optical Properties of  
Monodisperse Oligodiacetylenes**

**Promotoren**

Prof. dr. H. Zuilhof

Hoogleraar in de Organische Chemie

Wageningen Universiteit

Prof. dr. E.J.R. Sudhölter

Hoogleraar in de Nano-Organische Chemie

Technische Universiteit Delft

**Promotiecommissie**

Prof. dr. H. van Amerongen (Wageningen Universiteit)

Prof. dr. F.P.J.T. Rutjes (Radboud Universiteit Nijmegen)

Prof. dr. W.J. Buma (Universiteit van Amsterdam)

Dr. J.M. Kroon (Energieonderzoek Centrum Nederland, Petten)

Dit onderzoek is uitgevoerd binnen de onderzoeksschool VLAG

# **Synthesis and Optical Properties of Monodisperse Oligodiacetylenes**

**Gregor Stefan Pilzak**

Proefschrift  
ter verkrijging van de graad van doctor  
op gezag van de rector magnificus  
van Wageningen Universiteit  
Prof.dr. M.J. Kropff,  
in het openbaar te verdedigen  
op vrijdag 19 juni 2009  
des namiddags te 13.30 uur in de Aula.

Pilzak, G.S.

*Synthesis and Optical Properties of Monodisperse Oligodiacetylenes*

PdD-thesis Wageningen University, Wageningen, The Netherlands (2009)

ISBN: 978-90-8585-396-1

# Table of Contents

<b>Chapter 1</b>	<b>9-18</b>
General Introduction	
<b>Chapter 2</b>	<b>19-46</b>
Synthesis and Optical Properties of <i>all-trans</i> -Oligodiacetylenes	
<b>Chapter 3</b>	<b>47-70</b>
Synthesis and Optoelectronic Properties of Nanometer-Sized and Highly Soluble Homocoupled Oligodiacetylenes	
<b>Chapter 4</b>	<b>71-100</b>
Hybrid Conjugated Organic Oligomers Consisting of Oligodiacetylene and Thiophene Units: Synthesis and Study of Their Optical Properties	
<b>Chapter 5</b>	<b>101-112</b>
Divergent Synthesis and Optoelectronic Properties of Oligodiacetylene Building Blocks	
<b>Chapter 6</b>	<b>113-128</b>
Radical Cations of <i>all-trans</i> Oligodiacetylenes: Optical Absorption and Reactivity towards Nucleophiles	
<b>Chapter 7</b>	<b>129-136</b>
Summary and General Discussion	
Samenvatting	137-141
Dankwoord	143
Curriculum Vitae	145
List of publications	147
Overview of completed training activities	149

## Propositions

1. The effective conjugation length of  $\pi$ -conjugated polymers based on enyne units extends up to at least 20 double and triple bonds.

*This thesis*

2. A practically useful solubility of nanometer-sized oligodiacetylenes requires laterally attached alkyl chains.

*This thesis*

3. Ishikawa's synthesis of the anti-influenza neuramidase inhibitor (–)-Oseltamivir is claimed to proceed efficiently by 3 "one-pot" operations, but still requires "multi-step" and "multi-pot" preparations and purifications of complex starting materials.

H. Ishikawa, T. Suzuki, Y. Hayashi, *Angew Chem Int Ed Engl.* **2009**, *48*, 1304-1307.

4. Close, reciprocal and long-term oriented relationships with the supplier demonstrably pay off for buyers.

A. Blonska, F.A. Rozemeijer, M.G.M. Wetzels, *The Influence of Supplier Development on Gaining Preferential Buyer Status, Supplier Adaptation and Supplier Relational Embeddedness*. 24th IMP-conference in Uppsala, Sweden, **2008**, 1-19.

5. Electronic laboratory notebook is efficient and versatile while still providing the functionality of the traditional paper version.
6. The transition to sustainable energy is slowed down mostly by economic and political powers that fight to protect the short-term profits of their current positions.
7. Current methods to fuel the hydrogen economy are not environmentally attractive, and thus do not yet warrant the required large investments in novel infrastructure.

Propositions belonging to the thesis, entitled:  
*"Synthesis and Optical Properties of Monodisperse Oligodiacetylenes"*

Gregor S. Pilzak  
Wageningen, 19 juni 2009

*mojej mamie*





# ***Chapter 1***

## **General Introduction**

## 1.1 Conducting polymers

Synthetic polymers have changed the world tremendously over the last century. Polymers are widely distributed and are the basic constituents of plastics, clothing, and coatings such as used in dyes, paints, pharmaceuticals and special "high-tech" materials. Whereas modern chemistry in general has its roots well before the nineteenth century, polymer science results from much more recent developments in the twentieth century.<sup>[1]</sup> This development is clearly characterized by polymer chemistry-related Nobel Prizes in Chemistry: The first in 1953, for Staudinger's discovery of macromolecules, *i.e.* polymers. This was followed by the Nobel Prize for Ziegler and Natta (1963), who invented novel polymerization catalysts that triggered the development of a wide range of engineering plastics in various industries. Subsequently, Flory received the Nobel Prize in 1974 for his work on polymerization kinetics and polymer dynamics. Electrically conducting polymers are a relatively young generation of polymers, and for the discovery of semi-conductive polymers Heeger, MacDiarmid and Shirakawa were awarded by the Nobel Prize in 2000. In more general terms this related to the discovery and development of the new class of conducting polymers: materials that exhibit (some of) the optical and electrical properties of metals or semi-conductors.

Because saturated polymers (in which all of the four valence electrons of carbon are used in covalent bonds) are insulators, they are viewed as fundamentally uninteresting materials for electronic devices. The electronic configuration, however, is fundamentally different in conjugated polymers, which gives them their special conducting properties. Conjugated polymers have a  $\sigma$ -bond backbone of overlapping  $sp^2$  hybrid orbitals. The remaining out-of-plane  $p_z$  orbitals on the carbon (or nitrogen, sulphur, ...) atoms overlap with neighboring  $p_z$  orbitals to give  $\pi$ -bonds, leading to delocalization of the electrons over the entire (macro)molecule. Figure 1 presents the chemical structure of polyacetylene (PA) ( $\pi$ -conjugated polymer synthesized *via* polymerization of acetylene units) on the left-hand side, and on the right-hand side a sketch of the distribution of the  $\pi$ -electrons.

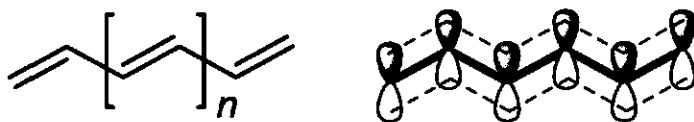


Figure 1. (left) Structure of polyacetylene, with indicated repeat unit. (right) Clouds of  $\pi$  electrons positioned above and below the plane of carbon-carbon backbone. The thick lines connecting the carbon atoms represent the  $\sigma$ -bonds.

The electronic structure in conducting polymers is determined by the number and kind of atoms within the repeat unit (monomer). The resonance interaction between the  $\pi$  bonds in the delocalized  $\pi$  electron states (*i.e.* the conjugation) provides charge mobility along the backbone of the polymer. The coalescence of the energies of these interacting molecular orbitals of the constituent monomer units occurs in a manner reminiscent of the band structure of solid-state semiconductors and inorganic quantum dots. (Figure 2).<sup>[2, 3]</sup> The mechanism of conductivity in these polymers is based on the motion of charge carriers along the conjugated backbone. The charge carriers, holes or electrons, are formed as a result of oxidation or reduction of the polymer, respectively.<sup>[4-7]</sup>

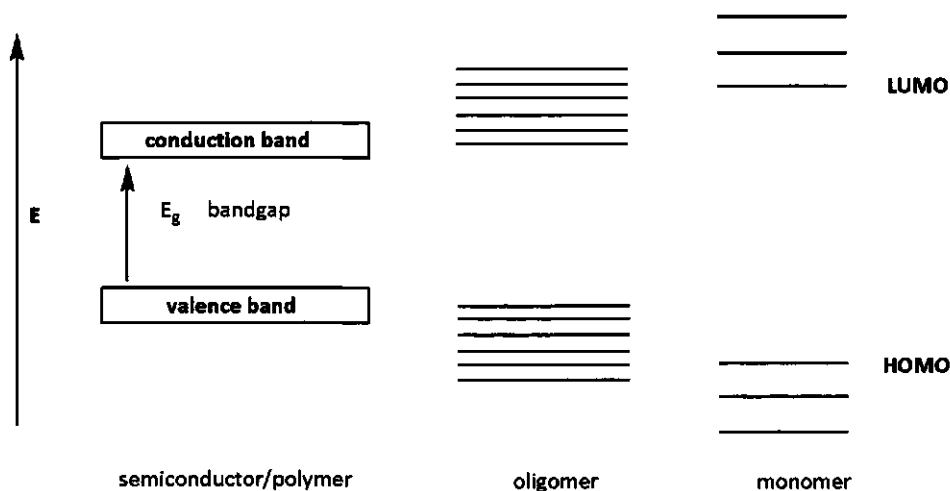


Figure 2. (left) Electronic band structure in a solid-state semiconductor or polymer, and orbital energy levels in a  $\pi$ -conjugated oligomer (center) and monomer (right).

Optical and electrical properties of  $\pi$ -conjugated polymers attract a lot of scientific investigations because of their crucial role in a wide variety of photoinduced processes.<sup>[8-11]</sup> In particular, organic  $\pi$ -electron systems have received attention as potential photo- and electro-active materials,<sup>[12-14]</sup> which warrants the significant body of fundamental work performed on these systems.

## 1.2 Polydiacetylenes (PDAs)

An important class of linearly  $\pi$ -conjugated non-aromatic all-carbon polymers are the polydiacetylenes (PDAs). PDAs can be obtained as near-perfect macroscopic single crystals formed by topochemical solid-state polymerization of suitably pre-arranged and substituted buta-1,3-dienes.<sup>[15, 16]</sup> This special requirement, however, severely limits their accessibility. There are, generally, two types of PDA crystals, corresponding to two different electronic structures, *i.e.* "blue" ( $\lambda_{\text{max}} \approx 630$  nm) and "red" ( $\lambda_{\text{max}} \approx 540$  nm) PDAs. In earlier studies, this blue/red dichotomy was associated with two resonance structures,<sup>[17]</sup> *i.e.* the "enynne" and the "butatriene" structures as depicted in Figure 2. The enynne structure was associated with the blue-absorbing polymer and the butatriene with the red-absorbing material. Recent studies show that the structural differences between these two crystals, such as bond lengths alternations, are small and not unequivocally established.<sup>[18, 19]</sup> Furthermore, comparative crystallographic studies of a red and blue PDA crystals fail to show any significant differences between the chain geometries.<sup>[20]</sup> Therefore, new models for the chains in the red-absorbing polymer have been proposed (Figure 3),<sup>[19, 20]</sup> for example, one in which the repeating units of the backbone are slightly tilted above and below the main plain of the polymer backbone. The chains in the blue-absorbing polymer are known to be planar.<sup>[21]</sup>

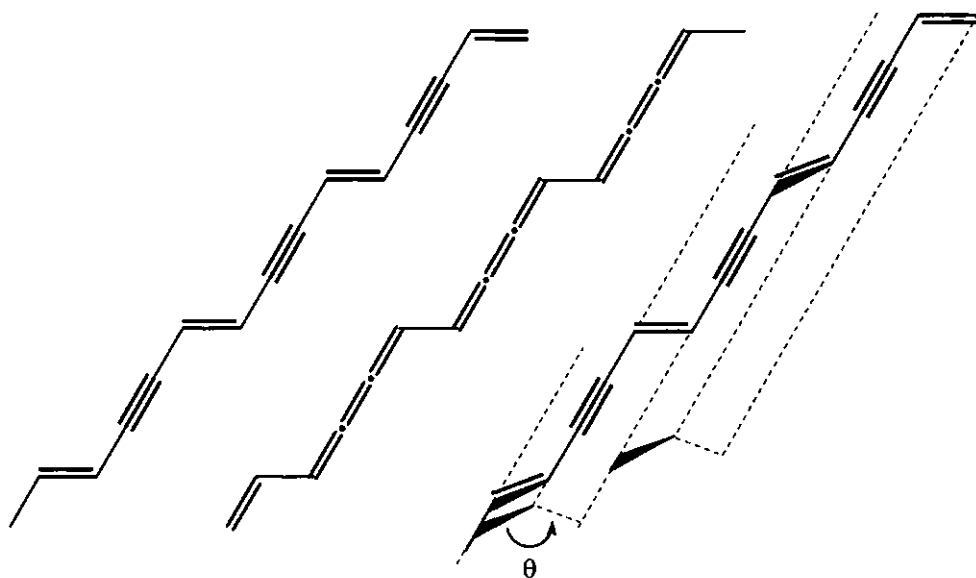


Figure 3. (left) Enynne structure. (middle) Butatriene structure. (right) Chain conformation in the "red" PDAs. (Repeating units are tilted by an angle of  $\theta$  relative to the average plain; dotted line indicates polymer backbone axis).

Another remarkable feature of PDAs is the possibility of a thermally induced color change, either occurring in the solid state or in solution (so-called thermochromism). A deeply colored low-temperature phase can e.g. be changed reversibly into a pale yellow high-temperature phase.<sup>[22-24]</sup> The different colors that are observed for PDA in Langmuir-Blodgett films are frequently described using the concept of an effective conjugation length. This effective conjugation length of polymers is defined as the minimum number of repeating units that is required to obtain the same properties as obtained for the polymer.

PDAs possess interesting properties such as a significant photoconductivity<sup>[19]</sup> and show large third-order nonlinear coefficients.<sup>[25, 26]</sup> PDAs are considerably more stable than PAs which degrade relatively fast by oxidation or aging.<sup>[27]</sup> The backbone of (planar) PDAs is roughly centrosymmetric with  $C_{2h}$  symmetry.<sup>[28]</sup> The vibrational and electronic states will thus have either ungerade (*u*) or gerade (*g*) symmetry, i.e. be either allowed or forbidden in one-photon absorption and emission, with the reverse selection rules in two-photon absorption. Under these symmetry restrictions, the lowest energy absorption band of polydiacetylenes is due to the allowed transition from the  $1A_g$  ground state to the lowest  $1B_u$  state, which has an excitonic character.<sup>[29]</sup>

### 1.3 Monodisperse oligomers as model for polymers

Most synthetic reactions that afford polymeric compounds generate polydisperse materials, i.e. mixtures of polymer chains of varying molecular weights.<sup>[3]</sup> In addition, the formation of structural defects during the polymerization is frequently inevitable, and this provides an additional obstacle towards obtaining relevant physical data. Therefore, obtaining the specific information concerning the optoelectronic properties of a high-molecular weight polymer is in this case more difficult. The synthesis and study of *precisely defined oligomers* gives an opportunity to overcome this problem and to explore the complex world of the corresponding polydisperse macromolecular analogues.<sup>[30, 31]</sup> Such studies allow the establishment of a direct correlation between the physical properties and the molecular structure of a polymer. Several detailed studies on the basic electronic structure of polymers are reported for oligoenes,<sup>[32, 33]</sup> oligothiophenes,<sup>[34-40]</sup> oligoarylenevinylenes,<sup>[41, 42]</sup> oligoaryleneethynyls,<sup>[43]</sup> *iso/cis*-oligodiacetylenes,<sup>[44-46]</sup> and oligotriacetylenes.<sup>[47-53]</sup> Despite the enormous interest, as shown by over 1500 publications in this area since 1990,<sup>[28]</sup> systematic investigations of the synthesis and optoelectronic properties of monodisperse all *trans*-oligodiacetylenes (ODAs) as a model for PDAs remain, however, rather scarce. This is a shortcoming, given several of the unique properties of *trans*-PDAs, such as nonlinear optical (NLO) properties.<sup>[28, 54-59]</sup> Furthermore, most

of the optoelectronic studies on PDAs are performed on PDA crystal structures, *i.e.* quasi one-dimensional organic quantum wires,<sup>[28, 58, 59]</sup> which are formed during the topochemical polymerization process in the crystalline phase.<sup>[21]</sup> A major disadvantage of this process is the presence of neighboring, parallel conjugated backbones that will likely influence the optoelectronic properties of the conjugated chain significantly. Monodisperse, all-*trans*-ODAs can be studied both in isolated form (at micromolar concentrations in solution or as dilute components in films or solids) and with adjacent conjugated chains (in the solid state as pure compounds). Therefore, they can function as models for a more detailed understanding of the effects of the conjugation length on the optoelectronic properties of conjugated polymers. In fact, the systematic study of a series of tailor-made monodisperse model compounds can clarify the distinction between inter and intra-molecular optoelectronic effects in PDA, that has muddled the discussion on optoelectronic effects in PDAs for almost three decades.<sup>[28]</sup>

## 1.4 Purpose and outline of this thesis

This thesis deals with the synthesis and optoelectronic properties of several novel series of ODAs and related oligomers. First, novel synthetic routes are developed that for the first time provide access to gram-scale amounts of these well-defined oligomers. Subsequently, a detailed study was made of the optical absorption and emission properties of these materials as a function of the chain length, using both steady-state and picosecond time-resolved spectroscopy. This allows a detailed clarification of a long-standing issue in the literature regarding PDAs, namely the origin of the visible-light absorption. Moreover, the more general question “when does an oligomer start to ‘look like’ a polymer?” is addressed and discussed by the analysis of several precisely defined series of oligomers.

In Chapter 2 the synthesis and photophysical behavior of a series - from monomer up to octamer - of ODAs that bears unsymmetrical alkyl side chains and different endcapping groups is described. The synthetic approach is based on a sequence of Sonogashira coupling reactions between monomeric building block and the oligomeric chain; detailed optoelectronic studies of this ODA series both in solution as in thin-film are described.<sup>[60]</sup>

In Chapter 3 the synthesis and optoelectronic characterization of homocoupled ODA (HODAs) up to 8.2 nm in length is described. This new series consists of two symmetric oligodiacetylene units, and is synthesized with high yield and on a multi-milligram scale under mild, catalytic Sonogashira conditions.<sup>[61]</sup>

A new and divergent synthesis route of oligodiacetylene (ODA) building blocks *via* Sonogashira reactions under a reductive atmosphere is described in Chapter 4. It is shown that

the optoelectronic properties are to some extent dependent on the end cap moiety. Finally, the formation of their radical cations, and their optical properties and reactivity towards nucleophiles are investigated.<sup>[62]</sup>

This precise tuning of the electronic properties of ODAs *via* well-controlled molecular variations was continued in the research described in Chapter 5. Here a novel series of hybrid conjugated oligomers is described that consist of oligodiacetylene and thiophene units. Several novel series are synthesized *via* iterative and divergent approaches based on highly accessible sequences of Sonogashira reactions. The photophysical behavior of the resulting materials is discussed as a function of chain length, resulting from both, studies in solution and in the solid state.<sup>[63]</sup>

The use of conjugated materials in optoelectronic devices is limited frequently by the high reactivity of the corresponding radical cations. Nanosecond laser transient absorption spectroscopy was therefore employed to determine the optical absorption spectra of ODA radical cations, and their reactivity towards nucleophiles.<sup>[64]</sup> The experimental and theoretical studies of the optical absorption spectra of charged ODAs that have been investigated are described in Chapter 6.<sup>[65]</sup>

In the final chapter of this thesis a summary of the research is presented, as well as a discussion of future prospects. Parts of this thesis are already published or will be published in the near future.

## 1.5 References

- [1] B. G. Rånby, W. R. Salaneck and I. Lundström, *Conjugated Polymers and Related Materials: The Interconnection of Chemical and Electronic Structures*, Oxford University Press, Oxford U.K., 1993, p. 502.
- [2] S. Stafstrom in *Theory of Conjugated Polymers*, (Eds.: T. A. Skotheim and J. R. Reynolds), CRC Press, Boca Raton, 1998, pp. 19-87.
- [3] W. Schnabel, *Polymers and Light: Fundamentals and Technical Applications*, Wiley-VCH, Weinheim, 2007, p. 398.
- [4] T. Ito, H. Shirakawa and S. Ikeda, *J. Polym. Sci. Chem Ed.* **1974**, *12*, 11-20.
- [5] C. K. Chiang, C. R. J. Fincher, Y. W. Park and A. J. Heeger, *Phys. Rev. Lett.* **1977**, *39*, 1098-1101.
- [6] J. Roncali, *Chem. Rev.* **1992**, *92*, 711-738.
- [7] K. Wilbourn and R. W. Murray, *J. Phys. Chem.* **1988**, *92*, 3642-3648.
- [8] M. Surin, R. Lazzaroni, W. J. Feast, A. P. H. J. Schenning, E. W. Meijer and P. Leclerc, *Synth. Met.* **2004**, *147*, 67-72.
- [9] J. G. Rodriguez and J. L. Tejedor, *J. Org. Chem.* **2002**, *67*, 7631-7640.
- [10] A. Aviram and M. A. Ratner, *Chem. Phys. Lett.* **1974**, *29*, 277-283.
- [11] A. Pron and P. Rannou, *Prog. Polym. Sci.* **2002**, *27*, 135-190.
- [12] G. G. Wallace, P. C. Dastoor, D. L. Officer and C. O. Too, *Chem. Innov.* **2000**, *30*, 15-22.
- [13] C. J. Brabec, N. S. Sariciffci and J. C. Hummelen, *Adv. Funct. Mat.* **2001**, *11*, 15-26.

- [14] J. J. M. Halls and R. H. Friend in *Organic Photovoltaic Devices*, (Eds.: M. D. Archer and R. Hill), Imperial College Press, London, **2001**, pp. 377-445.
- [15] J. L. Brédas, R. Silbey, D. S. Boudreaux and R. R. Chance, *J. Am. Chem. Soc.* **1983**, *105*, 6555-6559.
- [16] A. J. Campbell and C. K. L. Davies, *Polymer* **1994**, *35*, 4787-4793.
- [17] M. Schott and G. Wegner in *Nonlinear Optical Properties of Organic Molecules and Crystals*, Vol. 2, (Eds.: J. Zyss and D. S. Chemla), Academic Press, Orlando, **1987**, p. 3.
- [18] H. Tanaka, M. A. Gomez, A. E. Tonelli and M. Thakur, *Macromolecules* **1989**, *22*, 1208-1215.
- [19] M. Schott in *Photophysics of Molecular Materials*, (Ed. G. Lanzani), Wiley-VCH, Weinheim, **2006**, pp. 49-151.
- [20] A. Kobayashi, H. Kobayashi, Y. Tokura, T. Kanetake and T. Koda, *J. Chem. Phys.* **1987**, *87*, 4962-4966.
- [21] V. Enkelmann, *Adv. Polym. Sci.* **1984**, *63*, 91-136.
- [22] H. Tanaka, M. Thakur, M. A. Gomez and A. E. Tonelli, *Macromolecules* **1987**, *20*, 3094-3097.
- [23] A. J. Heeger and K. C. Lim, *J. Chem. Phys.* **1985**, *82*, 522-530.
- [24] A. J. Berlinsky, F. Wudl, K. C. Lim, C. R. Fincher and A. J. Heeger, *J. Polym. Sci. Phys.* **1984**, *22*, 847-852.
- [25] H. S. Nalwa in *Nonlinear Optics of Organic Molecules and Polymers*, (Eds.: H. S. Nalwa and S. Miyata), CRC, New York, **1997**, pp. 611-797.
- [26] H. S. Nalwa, *Adv. Mater.* **1993**, *5*, 341-358.
- [27] K. J. Steenberg-Harrell and S. T. Nguyen in *Polyacetylene and its analogs: Synthesis and physical properties*, Vol. 8, (Ed. H. S. Nalwa), Academic Press, San Diego, **2001**, pp. 132-158.
- [28] H. Zuilhof, H. M. Barentsen, M. Dijk van, E. J. R. Sudhölter, R. J. O. M. Hoofman, L. D. A. Siebbeles, M. P. Haas de and J. M. Warman in *Polydiacetylenes*, (Ed. H. S. Nalwa), Academic Press, San Diego, San Francisco, New York, Boston, London, Sydney, Tokyo, **2001**, pp. 339-437.
- [29] T. Kobayashi, M. Ikuta and Y. Yuasa in *Photophysics of Molecular Materials*, (Ed. G. Lanzani), Wiley-VCH, Weinheim **2006**, pp. 497-524.
- [30] J. M. Tour, *Trends Polym. Sci.* **1994**, *2*, 332-342.
- [31] H. S. Creel, *Trends Polym. Sci.* **1994**, *1*, 336-342.
- [32] M. R. Bryce, M. A. Coffin, P. J. Skabara, A. J. Moore, A. S. Batsanov and J. A. K. Howard, *Chem. Eur. J.* **2000**, *6*, 1955-1962.
- [33] C. Czekelius, J. Hafer, Z. J. Tonzetich, R. R. Schrock, R. L. Christensen and P. Mueller, *J. Am. Chem. Soc.* **2006**, *128*, 16664-16675.
- [34] G. Zotti, G. Schiavon, A. Berlin and G. Pagani, *Chem. Mater.* **1993**, *5*, 430-436.
- [35] G. Zotti, G. Schiavon, A. Berlin and G. Pagani, *Chem. Mater.* **1993**, *5*, 620-624.
- [36] G. Zotti, G. Schiavon, A. Berlin and G. Pagani, *Adv. Mater.* **1993**, *5*, 551-554.
- [37] W. Ten Hoeve, H. Wynberg, E. E. Havinga and E. W. Meijer, *J. Am. Chem. Soc.* **1991**, *113*, 5887-5889.
- [38] S. S. Zade and M. Bendikov, *J. Org. Chem.* **2006**, *71*, 2972-2981.
- [39] D. Fichou, G. Horowitz, B. Xu and F. Garnier, *Synth. Met.* **1990**, *39*, 243-259.
- [40] U. Segelbacher, N. S. Sariciftci, A. Grupp, P. Baeuerle and M. Mehring, *Synth. Met.* **1993**, *57*, 4728-4733.
- [41] J. Roncali, *Chem. Soc. Rev.* **2005**, *34*, 483-495.
- [42] R. Sander, V. Stuempflen, J. H. Wendorff and A. Greiner, *Macromolecules* **1996**, *29*, 7705-7708.
- [43] K. A. Walters, K. D. Ley and K. S. Schanze, *Langmuir* **1999**, *15*, 5676-5680.
- [44] M. B. Nielsen and F. Diederich, *Chem. Rev.* **2005**, *105*, 1837-1867.
- [45] B. Leibrock, O. Vostrowsky and A. Hirsch, *Eur. J. Org. Chem.* **2001**, 4401-4409.
- [46] J.-M. Kim, Y. B. Lee, D. H. Yang, J.-S. Lee, G. S. Lee and D. J. Ahn, *J. Am. Chem. Soc.* **2005**, *127*, 17580-17581.
- [47] R. E. Martin and F. Diederich, *Angew. Chem. Int. Ed.* **1999**, *38*, 1351-1377.
- [48] R. E. Martin, U. Gubler, J. Cornil, M. Balakina, C. Boudon, C. Bosshard, J.-P. Gisselbrecht, F. Diederich, P. Gunter, M. Gross and J.-L. Bredas, *Chem. Eur. J.* **2000**, *6*, 3622-3635.



- 
- [49] J. F. Nierengarten, D. Guillon, B. Heinrich and J. F. Nicoud, *Chem. Commun.* **1997**, 1233-1234.
- [50] Y. Zhao and R. R. Tykwinski, *J. Am. Chem. Soc.* **1999**, *121*, 458-459.
- [51] Y. Zhao, R. McDonald and R. R. Tykwinski, *J. Org. Chem.* **2002**, *67*, 2805-2812.
- [52] S. C. Ciulei and R. R. Tykwinski, *Org. Lett.* **2000**, *2*, 3607-3610.
- [53] Y. Zhao, S. C. Ciulei and R. R. Tykwinski, *Tetrahedron Lett.* **2001**, *42*, 7721-7723.
- [54] C. Sauteret, J. P. Hermann, R. Frey, F. Pradère, J. Ducuing, R. H. Baughman and R. R. Chance, *Phys. Rev. Lett.* **1976**, *36*, 956-959.
- [55] A. F. Garito, C. C. Teng, K. Y. Wong and O. Zammani-Khamiri, *Mol. Cryst. Liq. Cryst.* **1984**, *106*, 219-258.
- [56] K. J. Donovan and E. G. Wilson, *Synth. Met.* **1989**, *28*, 569-574.
- [57] S. Spagnoli, K. J. Donovan, K. Scott, M. Somerton and E. G. Wilson, *Chem. Phys.* **1999**, *250*, 71-79.
- [58] S. Jo, H. Yoshikawa, A. Fujii and M. Takenaga, *Synth. Met.* **2005**, *150*, 223-226.
- [59] M. Schott, *Synth. Met.* **2003**, *139*, 739-742.
- [60] G. S. Pilzak, B. van Lagen, C. C. J. Hendriks, E. J. R. Sudhölter and H. Zuilhof, *Chem. Eur. J.* **2008**, *14*, 7939-7950.
- [61] G. S. Pilzak, J. Baggerman, B. van Lagen, M. A. Posthumus, E. J. R. Sudhölter and H. Zuilhof, *Chem. Eur. J.* **2009**, *15*, 2296-2304.
- [62] G. S. Pilzak, B. van Lagen, E. J. R. Sudhölter and H. Zuilhof, *Tetrahedron Lett.* **2008**, *49*, 4949-4952.
- [63] G. S. Pilzak, K. van Gruijthuijsen, R. H. van Doorn, B. van Lagen, E. J. R. Sudhölter and H. Zuilhof, *Chem. Eur. J.* *accepted* **2009**.
- [64] I. R. Gould, D. Ege, J. E. Moser and S. Farid, *J. Am. Chem. Soc.* **1990**, *112*, 4290-4301.
- [65] G. S. Pilzak, S. Fratiloiu, J. Baggerman, F. Grozema, E. J. R. Sudhölter, L. D. A. Siebbeles and H. Zuilhof, *J. Chem. Phys. B* *submitted* **2009**.
-

# Chapter 2

## Synthesis and Optical Properties of *all-trans*-Oligodiacetylenes

### Abstract

A new series of pure and highly soluble oligodiacetylenes (ODAs) was synthesized in high yield and on a multi-milligram scale by a sequence of Sonogashira reactions with a strongly reduced homocoupling. The  $\lambda_{\text{max}}$  and  $\epsilon_{\text{max}}$  of these ODAs show an increase with both chain elongation and solvent polarity. A plot of  $\lambda_{\text{max}}$  absorption versus  $1/\text{CL}$  (CL = conjugation length) was shown to be linear. The  $\lambda_{\text{max}}$  converges to 435 nm for the longest members of the series at micromolar concentration. This reveals that the longest wavelength absorption observed for PDA chains ( $\lambda_{\text{max}}$  up to 700 nm) is due to aggregation effects. The fluorescence quantum yield increased from monomer to trimer and decreased for longer ODAs. A similar trend is found for the lifetime of fluorescence with a maximum of 600 ps for the trimer. The observed linearity of the rotational correlation time with the oligomer length implies that the ODA chains in solution lack significant geometrical changes. This implies that the ODAs in solution are fully stretched molecular rods of up to 4 nm in length.

*This chapter was published: Gregor S. Pilzak, Barend van Lagen, Cindy C. J. Hendriks, Ernst J. R. Sudhölter, Han Zuilhof, Chemistry - A European Journal, 2008, 14, 7939-7950.*

## 2.1 Introduction

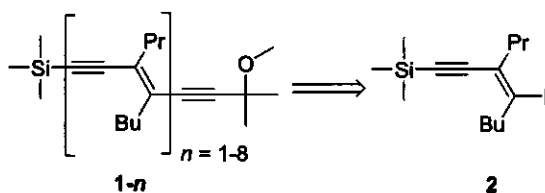
Over the last decade there has been a tremendous growth of interest in the optoelectronic properties of conducting polymers.<sup>[1, 2]</sup> These polymers with linearly  $\pi$ -conjugated scaffolds possess unique properties such as photo-conductivity and third-order nonlinear optical properties.<sup>[3-5]</sup> Most of the conjugated polymers are, however, heterogeneous in conjugation length, which hampers systematic studies of their optoelectronic properties. Moreover, the processing and characterization of these polymers can be difficult due to a low solubility in organic solvents. Therefore, the dependence of the optoelectronic properties on the chain length deserves further clarification for many types of conjugated materials.<sup>[6]</sup> To obtain further insight into the consequences of extended  $\pi$ -conjugation, homologous series of monodisperse analogues can be investigated as a function of the chain length.<sup>[7-9]</sup> Such well-defined oligomers function as model systems to determine the evolution of the electronic, optical, thermal and morphological properties of the corresponding polymeric materials.

Current research on the basic features of conjugated polymers is mostly devoted to the study of oligoenes,<sup>[10, 11]</sup> oligothiophenes,<sup>[12-18]</sup> oligoarylenevinylenes,<sup>[19, 20]</sup> oligoarylene-ethynylene,<sup>[21]</sup> *iso/cis*-oligodiacetylenes,<sup>[5, 22, 23]</sup> and oligotriacetylenes.<sup>[24-30]</sup> However, systematic investigations of the synthesis and optoelectronic properties of monodisperse all *trans*-oligodiacetylenes (or: *trans*-oligoenynes) still remain very scarce. This is remarkable considering that polydiacetylenes (PDAs) figure prominently in current research on electronically conducting polymers (> 1500 publications since 1990<sup>[31]</sup>) and are of interest as nonlinear optical materials.<sup>[31, 32]</sup> Such PDA molecular wires can act as a channel to transfer charges between sites in a molecular electronic device.<sup>[33, 34]</sup> Moreover, PDAs are unique due to their formation by topochemical polymerization from crystalline diacetylenes,<sup>[35]</sup> resulting in quasi one-dimensional organic quantum wires.<sup>[31, 36, 37]</sup> During this process PDA chains are formed in the presence of neighboring, parallel conjugated backbones. Although this may give PDAs some of their unique properties, it also blurs the distinction between intra-chain and inter-chain effects. The synthesis of a systematic series of monodisperse all-*trans*-oligodiacetylenes as model compounds for isolated PDA chains is therefore needed to clarify this distinction, as they can be studied both in isolated form (at micromolar concentrations in solution) and with adjacent conjugated chains (in thin films of pure compound). Therefore all-*trans*-oligodiacetylenes (ODAs) can function as models for a more detailed understanding of the effects of the conjugation length on the optoelectronic properties of PDAs.

The first syntheses of ODAs series ran up to penta- and heptamers,<sup>[38, 39]</sup> but the low solubility of the higher analogues prevented a proper spectroscopic characterization. This was

improved somewhat in the mid-1990s, with the synthesis of a series of ODAs with *tert*-butyl endgroups that allowed a more detailed spectroscopic analysis.<sup>[40]</sup> However, *cis/trans* isomerization of oligodiacetylenes during the synthesis by means of a Peterson-olefination reaction again hampered systematic investigations.<sup>[40, 41]</sup> Short *trans*-ODAs bearing phenyl and trimethylsilyl endgroups have also been synthesized as part of a  $\pi^2$ -complex with cobalt and molybdenum but only UV spectroscopic measurements were performed.<sup>[42]</sup>

Polhuis *et al.* used the Sonogashira coupling of terminal acetylenes with *trans*-1,2-dichloroethene to prepare series of ODAs ranging from monomer up to trimer with different endgroups.<sup>[43]</sup> However, the instability of terminal acetylenes, resulting in polymerization or homocoupling reactions, prevented the formation of longer analogues. Yet, sufficient amounts were isolated up to the trimer, to allow detailed photophysical studies of those materials.<sup>[44, 45]</sup> Recently, Takayama *et al.* reported a synthetic approach to produce a soluble series of ODAs up to a pentamer.<sup>[46, 47]</sup> The key step in this elongation method was the Sonogashira coupling of 1-iodo-4-trimethylsilylbut-1-en-3-yne with terminal acetylenes. The use of two equivalents of the halogenated diacetylene was required to partially suppress the formation of the homocoupling product of the terminal acetylenes. Nevertheless, even under these reaction conditions, 10-20 % of the homocoupling product was always found in the reaction mixture along with the starting material. Although synthetically this opened the door towards further studies, the spectroscopic characterizations of these ODAs were limited to NMR, IR, and UV/Vis steady-state absorption measurements.



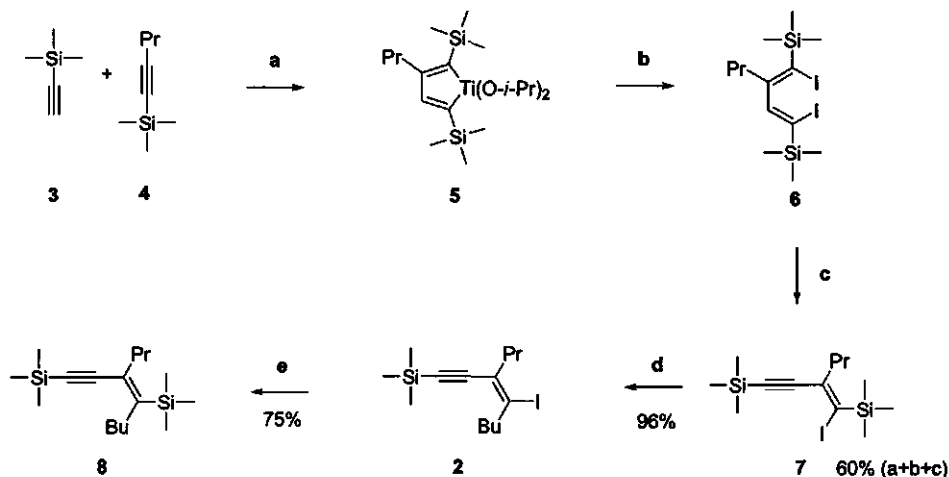
Scheme 1. Retrosynthetic approach for ODAs 1-*n* under present study.

In this study we present an optimized method to synthesize highly soluble ODAs 1-*n*, from monomer 1-1 to octamer 1-8 (Scheme 1) in high yields (70-80%). This allows, for the first time, the synthesis of significant amounts of these oligomers and detailed photophysical studies. Therefore, we can also report on the optical absorption and emission features of these materials using both steady-state and picosecond time-resolved techniques, which allows discussion of a long-standing issue in the literature regarding PDAs, namely, the origin of the visible light absorption of those polymers.<sup>[31]</sup>

## 2.2 Results and Discussion

### 2.2.1 Synthesis of all-*trans*-Oligodiacetylenes

Our approach to synthesize a series of ODAs 1-*n* (Scheme 2) required a simple preparation of enyne 2 equipped with two different alkyl side chains.



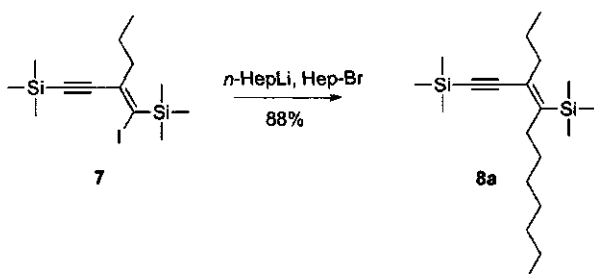
Scheme 2. Synthesis of building block 2.

Two complementary ways to enhance the solubility and to retain the  $\pi$ -overlap between the subunits of the oligodiacetylenes were applied:

- tert*-methoxy and trimethylsilyl groups at both ends of the conjugated chain, and
- short alkyl chains with different sizes on the repeating units.

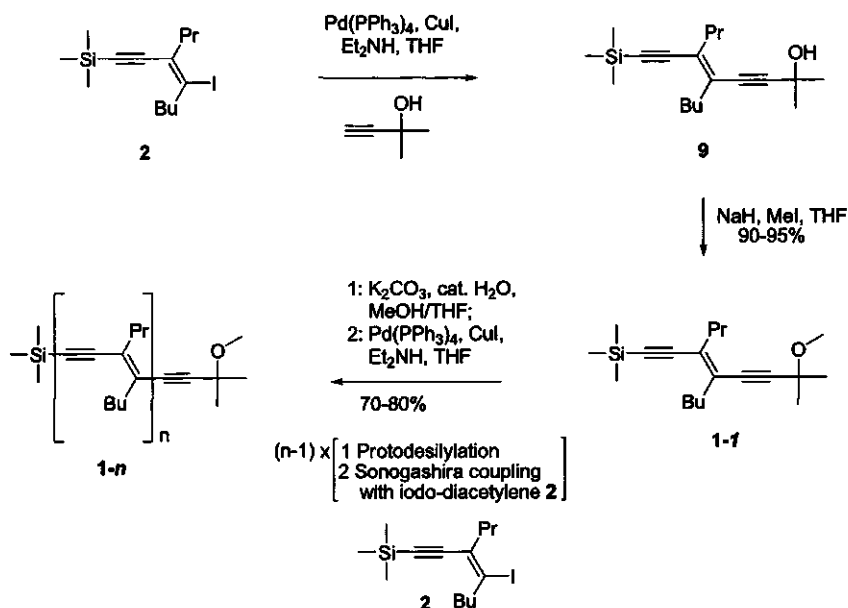
The building block enyne 2 was synthesized by using the multi-step method as shown in Scheme 2. The regioselective coupling<sup>[48, 49]</sup> between terminal acetylene 3 and internal acetylene 4 followed by iodination of titanium complex 5 and subsequent elimination of iodine was performed on a multi-gram scale yielding iodo-diacetylene 7 in a good overall yield (60%).<sup>[46, 47]</sup> Alkylation step (Scheme 2, d) is performed by using  $n\text{-BuLi}/n\text{-BuI}$  providing diacetylene 8 in excellent yield (96%). We found that the use of  $n\text{BuLi}$  reagent instead of a tertiary lithium salt<sup>[46]</sup> improved the yield of the desired product oligodiacetylenes by *in situ* formation of the alkylating reagent,  $n$ -butyl iodide.<sup>[50]</sup> The formation of this compound close to the reaction site speeds up the conversion, and prevents the occurrence of otherwise competing reactions. As a result, the formation of a protonated analogue of 7 is completely

suppressed, however, this is not the case when *t*-BuLi and *n*BuI are used.<sup>[51]</sup> Moreover, other commercially available or easily prepared organolithium salts may be utilized for this alkylation step providing a general route to variation in the side chain length. For example, we used *n*-heptyl lithium and *n*-heptyl bromide to prepare diacetylene **8a** with *trans*-propyl and heptyl side chains in nearly identical yields (Scheme 3), but since further development of this synthesis was out of the scope of this study we have consistently used building block **2**. The iodination step is performed using *N*-iodosuccinimide, which provides enyne **2**. The final purification of this apolar compound requires the use of reversed-phase silica material to remove any traces of the side products.



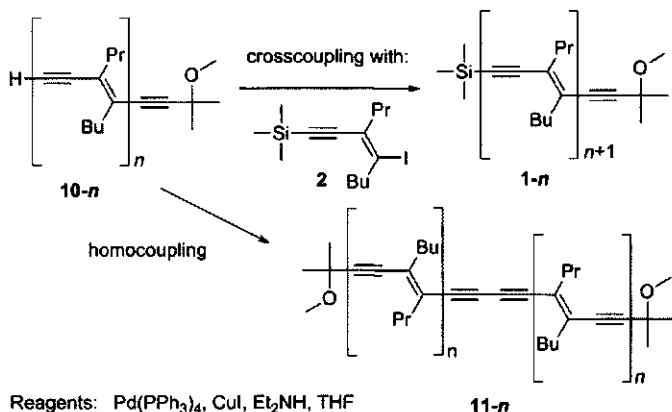
Scheme 3. Alkylation of iodo-diacetylene **7** with *n*-heptyl lithium.

Enyne **2** is catalytically coupled with 2-methylbut-3-yn-2-ol by a Sonogashira coupling,<sup>[52]</sup> which results in the formation of enediyne **9** bearing two different endgroups (Scheme 4). To increase the stability of the radical cations of these conjugated materials (Chapter 6)<sup>[53]</sup> the tertiary hydroxy endgroup is transformed into the redox-insensitive methoxy group. Direct methylation of hydroxy *trans*-oligodiacetylenes with NaH and MeI resulted in the almost quantitative formation of methoxy analogues. These were subsequently subjected to protodesilylation in an alkaline environment (Scheme 4). The difference in reactivity against, for example, nucleophilic attack between these two endcaps makes it possible to remove selectively only the TMS group in order to prepare a terminal acetylene (**10-*n***), which can be subjected to the following chain-elongation step by an iterative coupling with building block **2**. Moreover, the choice of the polar, methoxy-containing endcap is highly useful to increase the polarity of the ODAs and longer analogues and allows easy purification.



Scheme 4. Iterative synthesis of all-*trans* oligodiacetylenes *via* Sonogashira coupling.

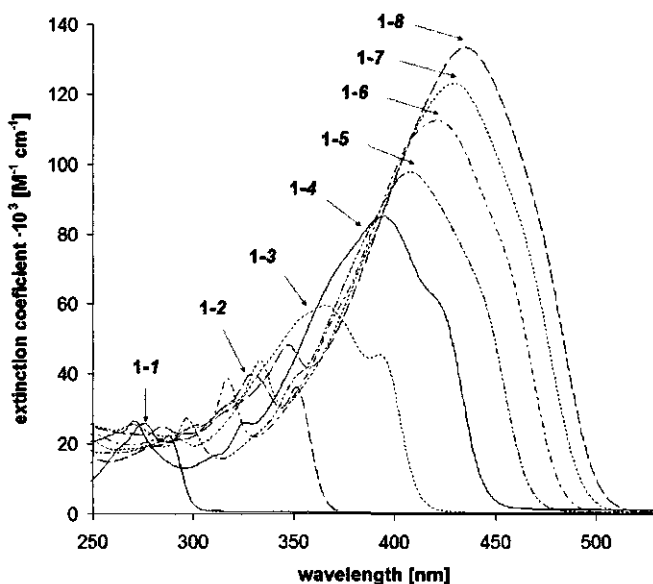
The iterative elongation steps of the ODA chain, such as the formation of dimers, trimers, etc., are subsequently achieved by using the Sonogashira coupling reactions, and have been optimized in our laboratory to achieve very good overall yields and suppression of the formation of the main side product. It is known that the use of copper(I) salts as co-catalyst in the Sonogashira coupling promotes the formation of homocoupled ODA analogues **11-*n*** (Scheme 5).<sup>[43, 46, 47]</sup> This copper-catalyzed oxidative homocoupling reaction has been widely applied in the synthesis of bisacetylenes.<sup>[54]</sup> However, the homocoupling is very undesirable for ODA synthesis because it consumes the terminal acetylene and reduces the yield of cross-coupled product dramatically. We succeeded in suppressing this homocoupling to about 5 mol% by the use of a large excess of **2**, up to 10 equivalents, under a reductive atmosphere of a 1:1 mixture H<sub>2</sub>/Ar. In this reaction, iodo-enyne **2** was recovered quantitatively after each elongation step, which allowed the use of this large excess. A similar procedure for the Sonogashira coupling, which used a diluted atmosphere of hydrogen gas was recently published by Elangovan *et al.*<sup>[55]</sup> Other methods, such as the copper-free Sonogashira coupling published by Urgaonkar *et al.*<sup>[56]</sup> proved to be not suitable for the synthesis of *trans*-oligodiacetylenes bearing TMS endgroups, as the instability of the TMS group against attack from a nucleophilic base such as tetrabutylammonium acetate resulted in polymerization of the ODAs.



**Scheme 5.** Catalytic coupling of ODAs under Sonogashira conditions yielding cross-coupled and homo-coupled ODAs.

## 2.2.2 Steady-state optical absorption in solution

The excellent solubility of the synthesized ODAs, which is largely a consequence of the laterally appended alkyl chains, allowed us to make an extended study of their optical properties. The ground-state absorption of the 1-*n* series was measured in solution and as a drop-casted thin film. The absorption of the ODA series 1-*n* up to the octamer as a monodisperse solution in 1,2-dichloroethane (DCE) is depicted in Figure 1. Similar spectra were obtained in *n*-hexane, which are given in the Supporting Information (Chapter 2.6).



**Figure 1.** Electronic absorption spectra of methoxy-endcapped oligodiacylenes 1-*n* (*n* = 1-8) in DCE.



The  $C_{2h}$  symmetry of the conjugated system of the ODAs under study implies that the absorption spectrum is associated with the  $S_2 (1^1B_u) \leftarrow S_0 (1^1A_g)$  transition.<sup>[44, 45, 57]</sup> The steady-state absorption spectra recorded in both solvents show the expected red-shift of the maximum absorption peak ( $\lambda_{\max}$ ) and an increase of the extinction coefficient ( $\epsilon_{\max}$ ) with an increasing number of repeating enynic units analogous to literature data reported for shorter diacetylene-based series.<sup>[38, 40, 44, 46]</sup> The longest-wavelength absorption maximum shows that this bathochromic shift decreases significantly for the longer oligomers:  $\Delta\lambda_{\max}$  decreases from about 0.75 eV going from **1-1** to **1-2** to about 0.05 eV from **1-7** to **1-8** in both *n*-hexane and DCE. The solvent effect on the shift of the electronic absorption is small for this series of ODAs and is in agreement with previously reported data for shorter all-*trans*-<sup>[31, 44]</sup> and *iso*-PDA oligomers.<sup>[58]</sup> For example, upon changing the solvent from *n*-hexane to DCE the longest-wavelength absorption maximum for ODAs increases from 0.02 eV (1 nm) for monomer **1-1** to 0.05 eV (8 nm) for octamer **1-8** (Table 1). This indicates that, the dipole moment  $\mu$  of the excited state of ODAs is only somewhat larger than that of the ground state.

Table 1. Absorption data of methoxy-endcapped oligodiacetylenes **1-*n*** ( $n=1-8$ ) in *n*-hexane and DCE.

<b>1-<i>n</i></b> (CL) <sup>[a]</sup>	$\lambda_{\max}$ [nm] ([eV])		$\epsilon_{\max}$ [ $\times 10^3$ dm <sup>3</sup> mol <sup>-1</sup> cm <sup>-1</sup> ]	
	<i>n</i> -hexane	DCE	<i>n</i> -hexane	DCE
<b>1-1</b> (3)	274 (4.53)	275 (4.51)	24.0	25.8
<b>1-2</b> (5)	327 (3.79)	330 (3.76)	33.4	39.9
<b>1-3</b> (7)	361 (3.43)	366 (3.39)	45.7	59.6
<b>1-4</b> (9)	388 (3.20)	395 (3.14)	51.9	85.3
<b>1-5</b> (11)	401 (3.09)	410 (3.02)	63.1	100.5
<b>1-6</b> (13)	414 (3.00)	422 (2.94)	72.7	112.6
<b>1-7</b> (15)	422 (2.94)	430 (2.89)	85.5	123.2
<b>1-8</b> (17)	427 (2.90)	435 (2.85)	99.7	133.4

[a] Conjugation length (CL) = number of double/triple bonds.

The extinction coefficient is also slightly affected by the solvent polarity and this solvent effect depends on the number of enynic units as well. For the shorter ODAs the difference between  $\epsilon_{\max}$  in *n*-hexane and DCE is marginal (7.5% in favor of the polar solvent for **1-1**), but this increases evidently for the longer oligomers, up to 64%. Clearly, the  $S_2 \leftarrow S_0$  transition is more probable in polarisable DCE than in *n*-hexane. It is also known that for conjugated polyenes<sup>[59]</sup> the  $S_2$  energy level decreases with solvent refractive index ( $n$ ), and this tendency is displayed for the series of ODA which show lower values in DCE ( $n = 1.445$ ) than in *n*-hexane ( $n = 1.375$ ). The absorption maximum of the oligomers (expressed in energy units) displays a linear relation with the reciprocal number of conjugation length ( $1/CL$ ) with  $CL = 2n + 1$  as

shown in Figure 2. An extrapolated  $\lambda_{\max}$  of 2.55 eV (487 nm) is obtained for a polymer with  $n = \infty$  in *n*-hexane, whereas in DCE a value of 2.48 eV (500 nm) was measured. The absorption maximum of the longest ODA (1-8) in solution is 427 and 435 nm in *n*-hexane and DCE, respectively, and the absorption spectrum of the ODA series does not exceed 500 nm for any of the compounds (see Figure 1). For plots like these, it is known that for extended oligomers they start to deviate from linearity, and curve horizontally.<sup>[60, 61]</sup> In other words: based on the data that can be provided up to the octamer 1-8, it can be expected that the isolated polymer should display its maximum absorption at energies larger than 2.5 eV ( $\approx$  500 nm). From this observation we conclude that the reported longer wavelength absorptions ( $\lambda_{\max}$  up to 700 nm) for PDA chains<sup>[31]</sup> are due to aggregation effects. Such aggregation generally plays a role in conjugated polymers, but is in our case negligible for these oligomers in dilute solution. Also at higher concentrations, up to 5 mM, ODA solutions do not show any additional high-wavelength absorption to suggest aggregation in solution. This was also the case when small amounts of methanol or ethanol were added: up to the point that stepwise increase of the alcohol concentration starts to induce precipitation of the ODAs, no long-wavelength band could be observed in the UV/Vis absorption spectrum. This indicates that steric repulsion from the alkyl chains remains dominant for ODAs in solution.

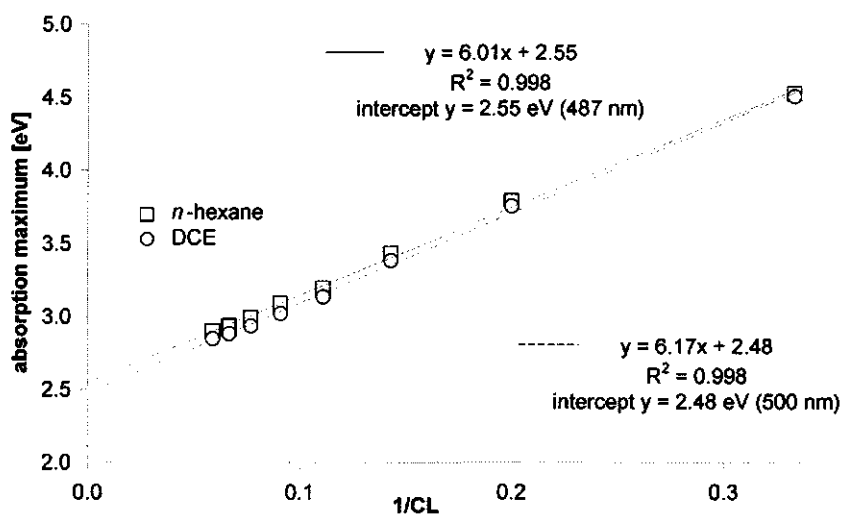


Figure 2.  $\lambda_{\max}$  of the absorption of ODA series 1-*n* (*n* = 1 - 8) in *n*-hexane (□) and DCE (○) solution at micromolar concentrations ( $2 \cdot 10^{-6}$  M) versus 1/CL.

It is important to point out that the linear relation of the absorption maximum with 1/CL indicates that for the longer ODAs elongation of the conjugation length is observed (the curve

does not yet flatten towards the y-axis). As a result, for these oligomers with up to 17 conjugated double and triple bonds, the effective conjugation length (ECL), in which the delocalization is predominantly present in only part of the chain, is at least 17 and most likely  $> 20$ . This is in contrast with the estimated ECL of 12 for PDA by Wenz et al.,<sup>[62]</sup> and more in line with predictions of Giesse en Schulz,<sup>[40]</sup> who suggest that saturation should not occur below  $CL = 20$ . In the present case, conjugation is not significantly reduced by kinks or torsions in the oligomeric chains, which shows the importance of detailed studies of extensive series of well-defined conjugated oligomers. Analogous data presented for polytriacetylenes by Martin et al. show truncation effects for that type of oligomers only with more than 24 conjugated bonds.<sup>[63]</sup> Finally, a recent study of oliogenes with up to 15 conjugated C=C bonds by Czeakalius et al.<sup>[11]</sup> is also in good agreement with the presented linear correlation of the absorption maximum with  $1/CL$ .

### 2.2.3 Steady-state optical absorption in thin films

The optical absorption of the ODA series in the solid state was investigated in drop-casted thin films. The absorption spectrum was taken 30 min after the evaporation of the solvent, and for **1-8** also after 12, 24 and 48 h.

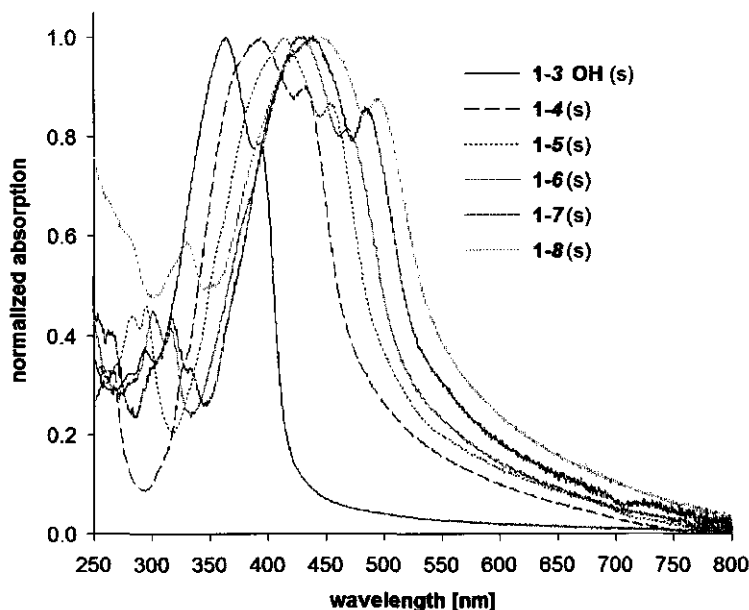


Figure 3. Normalized absorption spectra drop-casted thin films of methoxy end-capped ODAs **1-4** to **1-8** and hydroxy end-capped ODA **1-3 OH** taken after 12 h.

Because the shorter oligomers up to  $n = 3$  are liquids we prepared a trimer **1-3 OH** having a  $-\text{C}(\text{CH}_3)_2\text{CH}_2\text{OH}$  endcap rather than a  $-\text{C}(\text{CH}_3)_2\text{CH}_2\text{OCH}_3$  endcap by a similar approach as shown in Scheme 4. This oligomer is a solid at room temperature, thus readily allowing absorption measurements of its drop-casted thin films. The absorption spectra are shown in Figure 3 for all solid-state ODAs. A comparison between solution and thin-film absorption is depicted in Figure 4 for **1-3** and **1-8**; other oligomers show similar effects and their absorption data are part of the Supporting Information (Chapter 2.6).

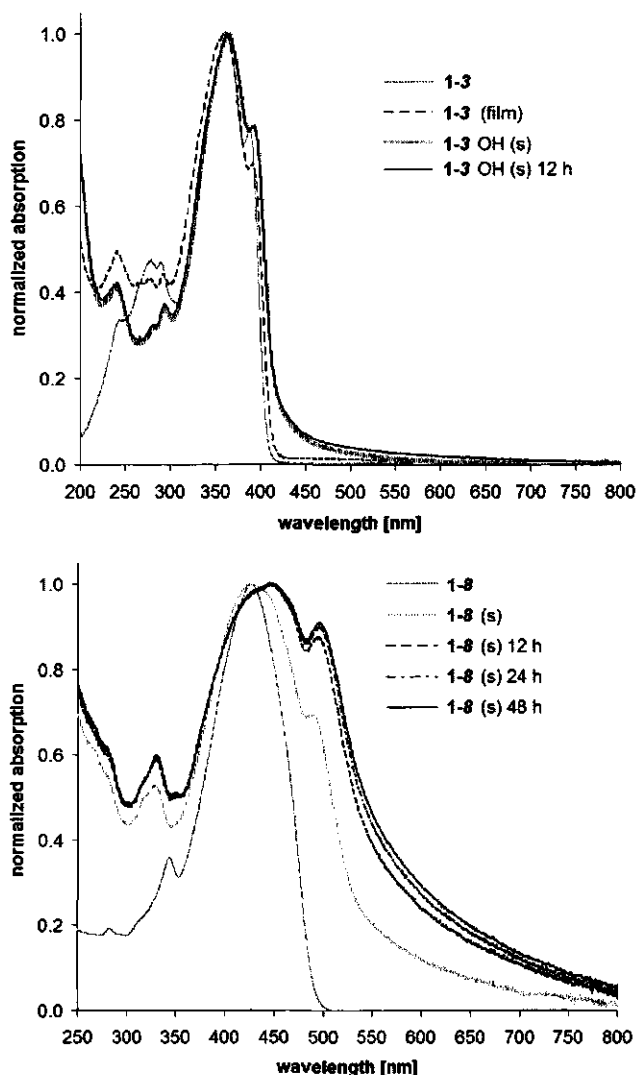


Figure 4. Normalized absorption spectra of ODAs **1-3**, **1-3OH** (top) and **1-8** in *n*-hexane solution versus solid state (s) (bottom).

The solid-state absorption of the oligomers under study consistently shows two features that more or less deviate from the data in solution (see Table 2). First, additional higher-wavelength absorption occurs. Second, a clearly visible red-shifted shoulder occurs that is already present for shorter oligomers in solution, but not for longer oligomers. The long-wavelength absorption feature is already detectable for the solid  $-OH$  endcapped **1-3 OH**, in contrast to the liquid  $-OCH_3$  endcapped **1-3** (Figure 4, top). Because the endcap modification has no significant effects on the  $\pi$ -system and thus on the nature of the electronic transitions, any differences between the absorption spectra of **1-3 OH** and **1-3** are due to differences in the phase (solid or liquid). We attribute this solid-state effect to forced aggregation of the chains, inducing the overlap of the  $\pi$ - $\pi$  orbitals and the red-shift of the  $\lambda_{max}$ . In other words: the absorption  $> 425$  nm is due to solid-state effects. [The increase in the absorption of the left shoulder in the spectrum is attributed to light scattering.] This effect leads to substantial long-wavelength absorption for longer oligomers as well, and for **1-8** for example, the absorption  $> 550$  nm is clearly not due to properties of isolated oligomer chains. It should be noted that this long-wavelength absorption feature (absorption  $> 550$  nm) does not occur in concentrated solutions (up to 5 mM), indicating that the lateral alkyl chains provide sufficient repulsion to prevent aggregation of the ODAs.

Table 2. Solid-state absorption data of methoxy-endcapped oligodiacetylenes **1-*n*** ( $n=4-8$ ) and **1-3 OH** with a *tert*-OH endcap.

<b>1-<i>n</i></b> (CL) <sup>[a]</sup>	$\lambda_{max}$ [nm] ([eV])	$\lambda_{max}$ right shoulder [nm] ([eV])
<b>1-3 OH</b> (7)	363 (3.42)	392 (3.16)
<b>1-4</b> (9)	392 (3.16)	431 (2.88)
<b>1-5</b> (11)	413 (3.00)	452 (2.74)
<b>1-6</b> (13)	425 (2.92)	467 (2.66)
<b>1-7</b> (15)	438 (2.83)	483 (2.57)
<b>1-8</b> (17)	445 (2.79)	495 (2.51)

[a] Conjugation length (CL) = number of double/triple bonds.

For longer oligomers, such as **1-8**, the absorption spectrum displays no features in solution, but in the solid-phase a shoulder appears, which is already present for shorter oligomers, such **1-3**, in both phases (liquid or solid). We interpret this to mean that for short oligomers, the completely flat oligomer geometry ( $C_{2h}$ -like) is dominant, as was confirmed from detailed photophysical studies.<sup>[44, 45]</sup> For longer oligomers, entropic reasons might also allow other geometries to play a role (e.g. with slight rotations around the C-C bonds), and the lowest

energy transition may in solution even be fully suppressed for these reasons. In the solid state, interchain interactions may force planarity, and thus bring back the shoulder.

For long oligomers, such as **1-8**, an additional 20 nm red-shift of  $\lambda_{\text{max}}$  in the spectrum is detected after 12 h, together with significantly increased long-wavelength absorption ( $> 550$  nm for **1-8**). We assign this to increased  $\pi$ - $\pi$  stacking, for which there is apparently sufficient driving force; even though the process is relatively slow (time scale of several hours) due to the restrictions of the solid phase, and/or slow evaporation of trace remnants of the solvent. No marked changes in the spectra occur after 24 or 48 h, which indicates that the stacking process for these materials is largely finished within 12 h. Similar irreversible chromatic changes have also been observed for a variety of PDAs.<sup>[31]</sup> For the first time this systematic study of the optical properties of this series of oligomers thus enables to clearly distinguish intra- and intermolecular effects on the light absorption of elongated enynic systems.

## 2.2.4 Steady-state fluorescence in solution

Emission spectra measured for near-equimolar ( $2 \cdot 10^{-6}$  M) homogeneous solutions of ODA series were recorded in *n*-hexane and DCE. The emission spectra recorded in DCE are shown in Figure 5. This plot shows a red-shift of  $\lambda_{\text{max}}$  with an increasing chain length *n*, whereas a maximum fluorescence quantum yield ( $\Phi_f$ ) is observed for the trimer ( $\Phi_f = 0.325$ ; see Table 3); both shorter and longer oligomers display less fluorescence. The obtained quantum yields for the methoxy-endcapped ODAs up to the trimer are similar to those previously reported for analogous ODAs of similar length.<sup>[44]</sup> Upon further extension of the conjugation the  $\Phi_f$  becomes smaller again. These values are in line with reported PDA polymer data, which show marginal fluorescence quantum yields, mostly lower than 0.001.<sup>[64]</sup> This can be explained by considering the electronic states involved in the light absorption process and subsequent relaxation: after excitation to  $S_2$  ( $1^1B_u$ ) (excitation to  $S_1$  ( $1^1A_g$ ) is symmetry forbidden),<sup>[44, 65]</sup> rapid internal conversion takes place to the  $S_1$  state with a time constant of  $\sim 200$  fs for trimer ODA.<sup>[45]</sup> This value matches rather closely with the lifetime of the photoexcited  $1^1B_u$  exciton in blue-phase PDAs, which was concluded to relax to the  $2^1A_g$  exciton.<sup>[31, 66]</sup> As a result, efficient population of the  $S_1$  state through the  $S_2$  state is expected, irrespective of conjugation length. The marked dependence of  $\Phi_f$  is therefore related to a faster internal conversion from  $S_1$  to  $S_0$  for longer ODAs, because longer conjugated chains provide an increasing density of states, which promotes internal conversion. Similar correlations have been found for series of polyenes.<sup>[67, 68]</sup> While for larger ODAs the symmetry restriction to  $C_{2h}$  might be less strict than for shorter ones due to increased conformational freedom, the increase of the rate for internal

conversion will be likely to be substantially larger. The overall result is thus the remarkable decrease of the fluorescence quantum yield.

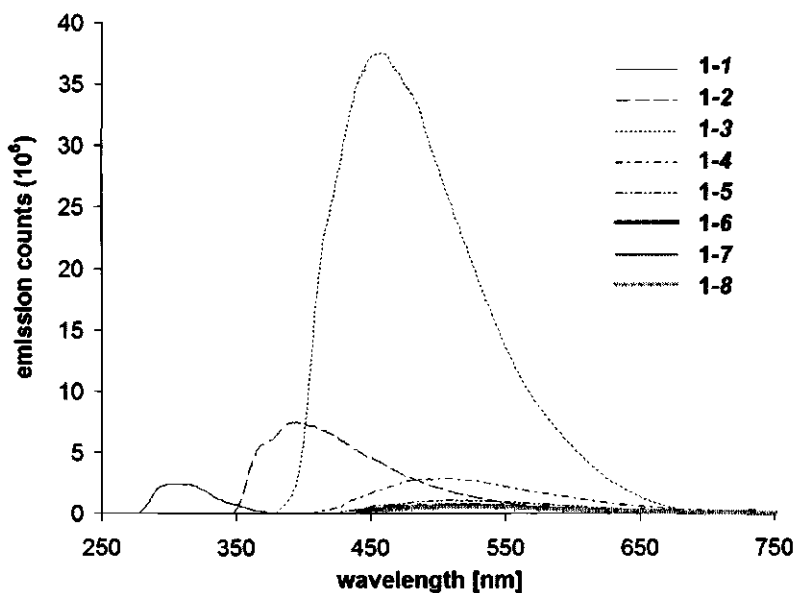


Figure 5. Fluorescence spectra of methoxy-endcapped oligodiacylenes **1-n** ( $n = 1 - 8$ ) in DCE.

Table 3. Emission data of methoxy-endcapped oligodiacylenes **1-n** ( $n = 1 - 8$ ) in DCE and *n*-hexane.

<b>1-n (CL)<sup>[a]</sup></b>	Emission $\lambda_{\text{max}}$ [nm] ([eV])		Quantum Yield $\Phi_f$ <sup>[b,c]</sup>	
	<i>n</i> -hexane	DCE	<i>n</i> -hexane	DCE
<b>1-1 (3)</b>	307 (4.04)	309 (4.01)	0.004	0.009
<b>1-2 (5)</b>	404 (3.07)	395 (3.14)	0.029	0.057
<b>1-3 (7)</b>	471 (2.63)	457 (2.71)	0.159	0.325
<b>1-4 (9)</b>	515 (2.41)	510 (2.43)	0.015	0.029
<b>1-5 (11)</b>	515 (2.41)	515 (2.41)	0.004	0.011
<b>1-6 (13)</b>	<sup>d</sup>	516 (2.40)	<sup>d</sup>	0.011
<b>1-7 (15)</b>	<sup>d</sup>	518 (2.39)	<sup>d</sup>	0.008
<b>1-8 (17)</b>	<sup>d</sup>	520 (2.38)	<sup>d</sup>	0.008

[a] Conjugation length (CL) = number of double/triple bonds; [b] quantum yield determined by comparison with quinine bisulfate in 0.1M H<sub>2</sub>SO<sub>4</sub>:  $\Phi_f = 0.535$  <sup>[69]</sup>; [c] experimental error  $\pm 0.002$ ; [d] not available due to marginal emission.

The fluorescence quantum yield recorded for the tetramer **1-4** up to the octamer **1-8** decreases more rapidly in *n*-hexane than in the more polar solvent DCE, with the emission recorded in DCE on average more than two times higher than in *n*-hexane. The 0-0 transition is only clearly visible for the emission of dimer **1-2**. The shoulder at the high energy side of the fluorescence band is less visible for trimer **1-3** and cannot be resolved for monomer and longer ODAs with more than three monomeric units. With the present data it is therefore not possible to study the evolution of the Stokes shift with increasing conjugation length. This would have been interesting given the significant Stokes shifts of the smaller ODAs.<sup>[44]</sup>

## 2.2.5 Fluorescence lifetimes and anisotropy

Picosecond time-resolved single photon counting at four different excitation wavelengths (283 nm, 304 nm, 372 nm and 444 nm) was used to determine the fluorescence lifetimes of the oligomers series **1-*n***. The observed lifetimes in the ODA series measured in *n*-hexane and DCE are listed in Table 4.

Table 4. Fluorescence lifetimes  $\tau_i$  (in ps), their relative weights  $A_i$ , and average lifetimes  $\tau_{\text{AVG}}$  (in ps).

1- <i>n</i> (CL) <sup>[a]</sup>	<i>n</i> -hexane					DCE				
	$\tau_1$	(% $A_1$ )	$\tau_2$	(% $A_2$ )	$\tau_{\text{AVG}}$ <sup>[b]</sup>	$\tau_1$	(% $A_1$ )	$\tau_2$	(% $A_2$ )	$\tau_{\text{AVG}}$ <sup>[b]</sup>
<b>1-1 (3)</b>	24 <sup>[c]</sup>	(100)				24 <sup>c</sup>	(98)	647	(2)	37
<b>1-2 (5)</b>	29 <sup>[c]</sup>	(98)	843	(2)	45	47 <sup>c</sup>	(99)	850	(1)	55
<b>1-3 (7)</b>	278	(14)	647	(87)	596	237	(14)	663	(86)	603
<b>1-4 (9)</b>	76	(93)	697	(7)	120	67	(83)	523	(17)	145
<b>1-5 (11)</b>	15	(93)	563	(7)	53	31	(85)	678	(15)	128
<b>1-6 (13)</b>	[d]		[d]		[d]	21	(96)	288	(4)	32
<b>1-7 (15)</b>	[d]		[d]		[d]	24	(98)	284	(2)	29
<b>1-8 (17)</b>	[d]		[d]		[d]	20	(98)	250	(2)	25

[a] Conjugation length (CL) = number of double/triple bonds; [b] calculated using eq.1; [c] values not accurate, as instrument response time is 560 and 460 ps, respectively; [d] not available due to marginal emission.

The decay curves can be fitted with a sum of two exponentials. The data in Table 4 indicate that the excited-state lifetimes of oligomers are positively affected by the solvent polarity: in DCE the lifetimes are generally longer than in *n*-hexane. Moreover, the longest lifetime, in both solvents, is recorded for trimer **1-3**. The average fluorescence lifetime  $\tau_{\text{AVG}}$  was calculated according to:



$$\tau_{\text{AVG}} = \frac{A_1}{A_1 + A_2} \tau_1 + \frac{A_2}{A_1 + A_2} \tau_2 \quad (1)$$

where  $A_1$  and  $A_2$  are the contributions of the decays obtained from the curve fitting. The average lifetimes are < 60 ps for monomer and dimer, with a maximum around 600 ps for the trimer. For oligomers longer than 3 enynic units the lifetime  $\tau_{\text{AVG}}$  in DCE decreases from 145 ps recorded for **1-4** to 25 ps for **1-8**. In *n*-hexane a similar trend is found, analogous to the trends shown for the fluorescence quantum yields of the ODAs in Table 4.

Fluorescence depolarization ( $r$ ) of the ODAs under present study was studied by picosecond time-resolved fluorescence anisotropy measurements.<sup>[70]</sup> This technique can provide information regarding the transition dipole moment and molecular geometry, and has proven to be useful in recent investigations of the conformational behavior of (water)-soluble polymers in solution.<sup>[71, 72]</sup> Since all-*trans* ODAs are roughly rod-shaped in their most extended conformation, and possess a relatively large axial ratio, the rotation of the molecules around the longitudinal axis progresses evidently much than the rotation around the two short, perpendicular axes, which are not expected to differ significantly from each other. In line with this, the observed anisotropy decay kinetics  $r(t)$  of ODAs are mono-exponential, characterized by an initial anisotropy value  $r_0$  and one rotation correlation time ( $\tau_R$ ):<sup>[69]</sup>

$$r(t) = r_0 \cdot \exp(-t / \tau_R) \quad (2)$$

in which  $r_0$  is determined by the angle  $\gamma$  between the absorption and emission transition moment:

$$r_0 = (3\cos^2 \gamma - 1) / 5 \quad (3)$$

The recorded initial anisotropy value  $r_0$  for all ODAs under study was  $\sim 0.3$ , similar to that of trimeric ODAs investigated previously.<sup>[31, 44, 45]</sup> This indicates a small angle ( $\sim 15^\circ$ ) between absorption and emission transition moments.

The rotation correlation times of anisotropy  $\tau_R$  for ODAs recorded in *n*-hexane and DCE are listed in Table 5 for those oligomers with sufficient fluorescence to determine this (to **1-5** in *n*-hexane and to **1-8** in DCE). The anisotropy lifetimes increase with the oligomer length, which means that the rotation time around the perpendicular axis increases for longer oligomers. The overall trend is illustrated in Figure 6, and shows a linear dependence for  $\tau_R$  and the length of the fully stretched oligomer. Such linearity has recently also been observed for conformationally rigid species of similar sizes.<sup>[73]</sup> Under simplifying conditions<sup>[72]</sup>  $\tau_R = \eta V / RT$ , and the molecular volume  $V \approx \ell r^2$ , in which  $\eta$  = viscosity,  $\ell$  = length of the molecule, and  $r$  = molecular diameter. In other words:  $\tau_R$  is should be proportional to the length of the molecule. Since the observed linear correlation is with the length of the molecule in its fully extended

shape, this provides clear evidence that there are no significant geometrical changes of ODA structures within this series. In other words: ODA oligomers in solution are indeed largely fully stretched nanometer-sized molecular rods.

Table 5. The rotation correlation time  $\tau_R$  of 1-*n* (*n* = 1 - 8).

1- <i>n</i> (CL) <sup>[a]</sup>	$\tau_R$ [ps]	
	<i>n</i> -hexane	DCE
1-1 (3)	65 <sup>[b]</sup>	95 <sup>[b]</sup>
1-2 (5)	106 <sup>[b]</sup>	180 <sup>[b]</sup>
1-3 (7)	155	321
1-4 (9)	204	395
1-5 (11)	263	468
1-6 (13)	[c]	540
1-7 (15)	[c]	577
1-8 (17)	[c]	631

[a] Conjugation length (CL) = number of double/triple bonds; [b] values relatively inaccurate due to low emission; [c] not available due to marginal emission.

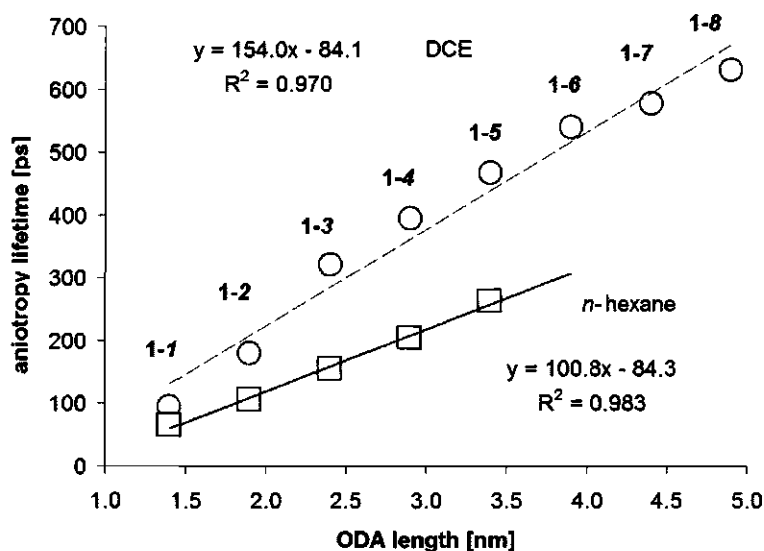


Figure 6. Anisotropy lifetimes vs. the length of a fully stretched ODA molecule for 1-1 to 1-8 in DCE (○), and for 1-1 to 1-5 in *n*-hexane (□).

## 2.3 Conclusion

A Sonogashira reaction-based synthesis of a series of highly soluble oligodiacetylenes (ODAs) was developed, with both high yields in the chain elongation step (70-80%) and high purity (> 99%). The series ranges from monomer to octamer, which contain up to 17 double and triple bonds ( $\approx 3.9$  nm) and having different endcaps and alkyl side chains. The oxidative homocoupling of terminal acetylenes, which is an undesirable side reaction, has been strongly reduced by the use of an  $H_2/Ar$  atmosphere, which improves the yield of the main product significantly.

Two effects were observed for the  $S_2 \leftarrow S_0$  transition of ODAs:

- (a) The linearity of the plot of  $\lambda_{max}$  versus  $1/CL$  (conjugation length (CL) = number of double/triple bonds) displays the undiminished elongation of the conjugation length for oligomers up to 3.9 nm;
- (b) Solid-state absorption measurements display an additional band in the visible region. This extra band is attributed to intermolecular  $\pi$ - $\pi$  stacking, which is marginal for oligomers at micromolar concentrations ( $\lambda_{max} \leq 435$  nm for all ODAs), but apparently dominant in PDAs for which  $\lambda_{max}$  up to 700 nm have been observed.

The rotation correlation time of the anisotropy increases linearly with the oligomer length, which shows that the oligomers lack significant geometrical changes and kinks in their conjugation. This provides evidence that the ODA oligomers in solution are indeed fully stretched molecular rods.

## 2.4 Experimental Section

### 2.4.1 Solvents and reagents

For all dry reactions performed under a steady stream of argon (or reductive atmosphere of argon/hydrogen mixture 1:1), the equipment was dried in an oven at 150 °C for several hours and allowed to cool down in an atmosphere of dry nitrogen or argon. Pure, dry, and degassed ether and tetrahydrofuran (THF) were obtained by distillation of the commercial material over sodium particles.  $CH_2Cl_2$  was distilled and dried over calcium hydride or sodium hydride. Dry DMF was purchased from Sigma-Aldrich and stored under argon. All other specified chemicals were commercially purchased (Aldrich, Fluka or Riedel-de Haën) and used without further purification.

### 2.4.2 General work up & purification procedure

Reaction monitoring and reagents visualization was performed on silica gel or reversed phase silica gel plates with UV-light (254 and 366 nm) combined with GC/MS. Usually the reaction mixture was diluted with water and extracted (3x) with an organic solvent (petroleum ether 40-60, hexane, or ethyl acetate).

The combined organic extracts were washed with brine and dried over anhydrous sodium sulfate prior to filtration and evaporation of the solvent under reduced pressure. Flash chromatography was performed on commercially available silica gel (0.035-0.070 nm pore diameter) and mixtures of freshly distilled petroleum ether 40/60 and ethyl acetate or reversed phase silica gel (0.04-0.06 nm pore diameter Screening Devices) with freshly distilled mixtures of acetonitrile and ethyl acetate. Final purification was performed on Shimadzu preparative HPLC by using a C18 column (Alltech Alltima 250 mm × 22mm; 5μ) with HPLC-grade water, acetonitrile and ethyl acetate mixture.

### 2.4.3 Nuclear Magnetic Resonance spectroscopy and Mass Spectroscopy

$^1\text{H}$  NMR and  $^{13}\text{C}$  NMR spectra were determined on a Bruker CXP 300 NMR-spectrometer in  $\text{CDCl}_3$  solutions unless indicated otherwise. Chemical shifts are reported in ppm downfield relative to tetramethylsilane ( $\delta=0$  ppm for  $^1\text{H}$ ) or based on the solvent peak ( $\text{CDCl}_3$ ) ( $\delta=77.00$  ppm for  $^{13}\text{C}$  NMR) as an internal standard. HRMS was performed on Finnigan Mat95 mass spectrometer.

### 2.4.4 Steady-state absorption and fluorescence

Absorption spectra of the oligodiacetylenes in *n*-hexane (spectrophotometric grade, Riedel-de Haën) and DCE (spectrophotometric grade, Sigma-Aldrich) were recorded using a Cary 100 UV-Vis spectrophotometer (scan range: 200-800 nm, scan rate: 300 nm min<sup>-1</sup>, data interval 0.5 nm) and steady-state fluorescence using a FLS920P Spectrometer (slit exc.: 2 nm, slit em.: 2 nm, step: 1.0, dwell: 0.2 s). Absorption spectra of oligodiacetylenes in film via drop casting were recorded on a Cary 50 UV-Vis spectrophotometer (scan range 200-800 nm, scan rate 300 nm/min, data interval 0.5 nm).

### 2.4.5 Determination of fluorescence quantum yield in solution

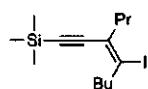
In order to evaluate the fluorescence quantum yield ( $\Phi_F$ ) of the ODA's solution in *n*-hexane and DCE, the areas of the corrected emission spectra were compared to a spectrum of a reference solution of quinine bisulfate in 0.1 M  $\text{H}_2\text{SO}_4$  measured at 366 nm having  $\Phi_F=0.535$ .<sup>[69]</sup> The fluorescence quantum yields of the ODA's were determined using the relationship:

$$\Phi_F = \Phi_F \frac{I_{OD_R} n^2}{I_R OD n^2} \quad (4)$$

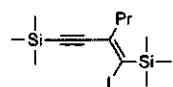
where  $I$  and  $I_R$  are the integrated emission intensities of the ODA and quinine bisulfate solutions, respectively, OD refers to the optical densities of the respective solutions and  $n$  is the refractive index.

### 2.4.5 Lifetime of fluorescence and fluorescence anisotropy in solution

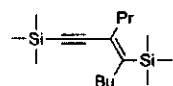
The fluorescence lifetime and anisotropy were recorded using a FLS920P Spectrometer (Edinburgh Instruments) for time-correlated photon counting (TCSP) (time set up: 5 or 10 ns, 4096 channels; measurements stopped after 10.000 counts were obtained, and for 1-8 in a separate experiment also after 24 hours of data collection to check the influence of photochemistry occurring after prolonged irradiation). Pulsed diode lasers (372 nm, FWHM: 54 ps; 444 nm, FWHM: 63 ps) and pulsed LEDs (283 nm, FWHM <500 ps; 304 nm, FWHM: < 350 ps) from PicoQuant were used as light sources. The anisotropy measurements were performed using vertical and horizontal polarizations. All spectroscopic measurements were carried out under magic angle conditions to avoid the possible influence of rotational motions of the probe molecules.

**2.4.6 ((E)-4-iodo-3-propyloct-3-en-1-ynyl)trimethylsilane (2)**

A brown, 500 ml, two-necked, round-bottomed flask containing a solution of 250 ml (distilled and degassed)  $\text{CH}_2\text{Cl}_2$ , (E)-5-(trimethylsilyl)-4-(2-(trimethylsilyl)ethynyl)non-4-ene **8** (42.5 mmol, 12.50 g) and *N*-iodosuccinimide (88.9 mmol, 20.0 g) was vigorously stirred for 3 hours at room temperature under an argon atmosphere. After addition of a saturated aqueous solution of  $\text{Na}_2\text{S}_2\text{O}_3$ , the reaction mixture was worked up according to the general procedure and purified on reversed phase silica ( $\text{CH}_3\text{CN}$ ) to give a crude oil which was purified by reversed phase chromatography ( $\text{CH}_3\text{CN}/\text{H}_2\text{O}$ , 90/10) to afford pure **2** (31.9 mmol, 11.09 g, 75%) as a colorless oil:  $^1\text{H}$  NMR:  $\delta$  0.20 (s, 9H), 0.95 (t,  $J = 7.5$  Hz, 3H), 0.96 (t,  $J = 7.7$  Hz, 3H), 1.35 (t,  $J = 7.4$  Hz, 2H), 1.49–1.63 (m, 4H), 2.30 (t,  $J = 7.7$  Hz, 3H), 2.88 (t,  $J = 7.4$  Hz, 3H);  $^{13}\text{C}$  NMR:  $\delta$  0.0, 13.7, 14.1, 21.2, 21.5, 31.4, 43.3, 43.6, 99.4, 101.7, 119.2, 128.1; HRMS: observed 348.0771; calculated 348.0770.

**2.4.7 (Z)-3-(iodo(trimethylsilyl)methylene)-1-(trimethylsilyl)hex-1-yne (7)**

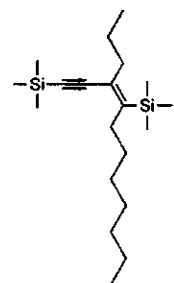
A brown, two liter, two-necked, round-bottomed flask filled with 12000 ml (dry and degassed) ether and equipped with four pressure-equalized dropping funnels containing 1-trimethylsilyl-1-pentyne **4** (106.9 mmol, 15.00 g, 19.6 ml),  $\text{Ti}(\text{O}-i\text{-Pr})_4$  (139.0 mmol, 39.51 g, 41.0 ml), 2.0 M solution of *i*-PrMgCl in ether (267.3 mmol, 133.6 ml), and ethynyl trimethylsilane **3** (74.8 mmol, 7.35 g, 10.6 ml) was flushed with constant flow of argon, stirred, and slowly cooled down to  $-78^\circ\text{C}$ . At  $-78^\circ\text{C}$   $\text{Ti}(\text{O}-i\text{-Pr})_4$  were dropwise added along with the 2.0 M solution of *i*-PrMgCl. The solution was warmed up to  $-50^\circ\text{C}$  over 60 min and its color changed from pale yellow to brown. After the solution was stirred at  $-55^\circ\text{C}$  for 2 h, ethynyltrimethylsilane was drop wise added and the stirring at  $-50^\circ\text{C}$  was continued further for 2 h. Iodine (245.9 mmol, 62.4 g) was added as powder at  $-60^\circ\text{C}$  and then the mixture was slowly warmed up to room temperature and stirred for 2 h. The resulting mixture was filtered through a pad of Celite and washed with sodium thiosulfate solution and worked up according to the general procedure to give a crude oil of (1Z,3Z)-1-iodo-3-(iodo(trimethylsilyl)methylene)-1-(trimethylsilyl)hex-1-ene **6**, which was subjected to the elimination reaction. The crude oil was stirred at  $0^\circ\text{C}$  in pyrrolidine (100 ml) during 1 h in a brown three-necked flask under an argon atmosphere. After dilution of the mixture with 100 ml of petroleum ether 40/60, ammonium chloride was added at  $0^\circ\text{C}$ . The reaction mixture was worked up according to the general procedure, pre-purified on silica gel column (5%  $\text{Et}_3\text{N}$  solution in petroleum ether 40/60) and finally purified on reversed phase silica ( $\text{CH}_3\text{CN}/\text{H}_2\text{O}$ , 80/20) to give pure **7** (45.21 mmol, 16.45 g, 60%) as a colorless oil:  $^1\text{H}$  NMR:  $\delta$  0.24 (s, 9H), 0.31 (s, 9H), 0.93 (t,  $J = 7.4$  Hz, 3H), 1.54–1.69 (m, 2H), 2.29–2.34 (m, 2H);  $^{13}\text{C}$  NMR:  $\delta$  0.0, 2.1, 13.7, 22.7, 39.2, 99.9, 109.6, 117.3, 142.1; HRMS: observed 364.0539; calculated 364.0540.

**2.4.8 (E)-5-(trimethylsilyl)-4-(2-(trimethylsilyl)ethynyl)non-4-ene (8)**

A brown, one liter, three-necked, round-bottomed flask filled with 500 ml (dry and degassed) THF, under continuous flow of argon, containing (Z)-3-(iodo(trimethylsilyl)methylene)-1-(trimethylsilyl) hex-1-yne **7** (45.2 mmol, 16.45 g) was equipped with two pressure-equalized dropping funnels with 1.6 M *n*-BuLi solution in hexane (90.6 mmol, 145 ml) and 1-iodobutane (48.3 mmol, 8.89 g, 5.5 ml). The solution was stirred vigorously at  $-78^\circ\text{C}$  and *n*-BuLi was added drop wise during 60 min. After an additional 30 min 1-iodobutane was added to complete the reaction. The mixture was warmed up to room temperature, quenched with a saturated solution of  $\text{NH}_4\text{Cl}$  at  $0^\circ\text{C}$  and worked up according to the general procedure. The residue was purified on reversed phase silica (ACN) to give pure **8** (43.2 mmol, 12.71 g, 96%) as a colorless oil:  $^1\text{H}$  NMR:  $\delta$  0.24 (s, 9H), 0.31 (s, 9H), 0.92 (t,  $J = 7.4$  Hz, 3H), 0.93 (t,  $J = 7.4$  Hz, 3H), 1.35 (t,  $J =$

7.3 Hz, 2H), 1.49 - 1.63 (m, 4H), 2.34 (t,  $J = 7.5$  Hz, 3H), 2.41 (t,  $J = 7.4$  Hz, 3H);  $^{13}\text{C}$  NMR:  $\delta$  0.0, 0.3, 13.6, 14.0, 21.3, 21.5, 31.1, 43.5, 43.6, 99.4, 101.7, 119.2, 129.6; HRMS: observed 294.2199; calculated 294.2200.

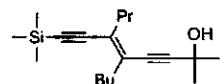
#### 2.4.9 (E)-5-(trimethylsilyl)-4-(2-(trimethylsilyl)ethynyl)dodec-4-ene (8a)



1-bromoheptane (5.58 mmol, 1.00 g, 1.14 ml) was dropwise added to a stirred suspension of lithium (100 mmol, 6.94 g) in dry and degassed ether (50 ml) at room temperature under an argon atmosphere until the reaction became cloudy. Then the reaction mixture was cooled to  $-20^\circ\text{C}$  and the remaining 1-bromoheptane (94.4 mmol, 16.91 g, 14.8 ml) was added dropwise. The reaction mixture was allowed to warm to room temperature and stirred for 1 h. The solution was stored under argon and used without further purification. A brown 50 ml, three-necked, round-bottomed flask filled with **7** (1.24 mmol, 450 mg) in THF (25 ml; dry and degassed) was equipped with two pressure-equalized dropping funnels filled with  $\sim 2.0$  M *n*-HepLi solution in ether (2.5 mmol, 5 ml) and 1-bromoheptane (1.25 mmol, 223.9 mg, 0.20

ml). The apparatus was kept under a continuous flow of argon. The solution was stirred vigorously at  $-78^\circ\text{C}$  and *n*-HepLi is added dropwise over 30 min. After an additional 30 min, 1-bromoheptane was added to complete the reaction. The mixture was warmed up to room temperature, quenched with a saturated solution of  $\text{NH}_4\text{Cl}$  at  $0^\circ\text{C}$  and worked up according to general procedure. The residue was purified on reversed phase silica ( $\text{CH}_3\text{CN}$ ) to give **8a** (1.10 mmol, 381 mg, 88 %) as a colorless oil:  $^1\text{H}$  NMR:  $\delta$  0.24 (s, 9H), 0.31 (s, 9H), 0.91 (t,  $J = 7.4$  Hz, 3H), 0.92 (t,  $J = 7.4$  Hz, 3H), 1.35 (t,  $J = 7.3$  Hz, 2H), 1.48 - 1.64 (m, 10H), 2.34 (t,  $J = 7.5$  Hz, 3H), 2.41 (t,  $J = 7.4$  Hz, 3H);  $^{13}\text{C}$  NMR:  $\delta$  0.0, 0.4, 13.4, 14.1, 21.3, 21.50, 31.1, 33.4, 34.2, 34.5, 43.4, 43.5, 99.3, 101.6, 119.0, 129.4; HRMS: observed 336.2666; calculated 336.2669.

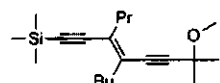
#### 2.4.10 (E)-5-butyl-2-methyl-6-(2-(trimethylsilyl)ethynyl)non-5-en-3-yn-2-ol (9)



A mixture of ((E)-4-iodo-3-propyloct-3-en-1-ynyl)trimethylsilane (**2**) (28.7 mmol, 10.0 g), 2-methylbut-3-yn-2-ol (57.7 mmol, 4.83 g, 5.6 ml),  $\text{Pd}(\text{PPh}_3)_4$  (1.4 mmol, 1.62 g),  $\text{CuI}$  (0.7 mmol, 133 mg), and dry, degassed diethyl amine (70 ml) and

THF (180 ml) was placed anaerobically in a dried 500 ml two-necked round-bottomed flask, equipped with a magnetic stirrer, an argon in- and outlet, and a pressure-equalized dropping funnel. The mixture was stirred for 4 h at  $30^\circ\text{C}$ , concentrated and filtered over short silica gel column (5%  $\text{Et}_3\text{N}$  solution in petroleum ether 40/60). The residue was purified on reversed phase silica ( $\text{CH}_3\text{CN}/\text{EtOAc}$  8.5:1.5) to give pure **9** (23.0 mmol, 6.98 g, 80 %) as a pale yellow oil:  $^1\text{H}$  NMR:  $\delta$  0.20 (s, 9H), 0.92 (t,  $J = 7.4$  Hz, 3H), 0.93 (t,  $J = 7.4$  Hz, 3H), 1.35 (t,  $J = 7.3$  Hz, 2H), 1.49 (s, 6H), 1.49 - 1.63 (m, 4H), 2.35 (t,  $J = 7.5$  Hz, 3H), 2.42 (t,  $J = 7.4$  Hz, 3H);  $^{13}\text{C}$  NMR:  $\delta$  0.0, 13.6, 13.9, 21.6, 22.0, 31.5, 32.4, 34.6, 36.8, 68.7, 81.6, 101.3, 102.8, 104.4, 129.0, 130.7; HRMS: observed 304.2235; calculated 304.2222.

#### 2.4.11 ((E)-4-butyl-7-methoxy-7-methyl-3-propylocta-3-en-1,5-diynyl)trimethylsilane (1-1)



A solution of **9** (21.4 mmol 6.50 g) in dry, degassed THF (125 ml) was placed anaerobically in a dried 250 ml two-necked round-bottomed flask, equipped with a magnetic stirrer and an argon in- and outlet. Sodium hydride (25.0 mmol, 1.0 g, 60 % dispersion in mineral oil) was added in small portions. After hydrogen evolution had ceased,  $\text{MeI}$  (30 mmol, 4.26 g, 1.87 ml) was added slowly and the mixture was warmed gently. After  $\sim 30$  min  $\text{NaI}$  precipitated from the solution. The reaction was then quenched with  $\text{H}_2\text{O}$  (30 mL), and petroleum ether 40/60 (75 ml) was added followed by working up according to the general procedure. After purification on reversed phase silica ( $\text{CH}_3\text{CN}/\text{EtOAc}$  8.0:2.0) pure **1-1** (19.6 mmol, 6.24 g, 92 %) was obtained as a pale

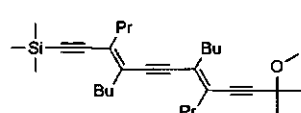
yellow oil:  $^1\text{H}$  NMR:  $\delta$  0.20 (s, 9H), 0.92 (t,  $J = 7.4$  Hz, 3H), 0.93 (t,  $J = 7.4$  Hz, 3H), 1.35 (t,  $J = 7.3$  Hz, 2H), 1.49 (s, 6H), 1.49 - 1.63 (m, 4H), 2.35 (t,  $J = 7.5$  Hz, 3H), 2.42 (t,  $J = 7.4$  Hz, 3H), 3.37 (s, 3H);  $^{13}\text{C}$  NMR:  $\delta$  0.0, 13.6, 13.9, 21.6, 22.0, 28.4, 30.4, 34.6, 36.8, 51.7, 71.2, 83.6, 100.3, 103.1, 104.4, 129.1, 130.5; HRMS: observed 318.2381; calculated 318.2379.

#### 2.4.12 General method for protodesilylation of oligodiacetylenes series (1-*n*) followed by catalytic Sonogashira coupling with iodo-diacetylene (2) (Scheme 5)

(i) A solution of (1-*n*) (1 equiv.) in THF/MeOH (1:1, 5ml/mmol) was stirred in round-bottomed flask.  $\text{H}_2\text{O}$  (3 drops/mmol) and  $\text{K}_2\text{CO}_3$  (2 equiv.) was added to the solution and stirred for 3 h. After working up following the general procedure, the terminal acetylene (10-*n*) was submitted to the catalytic chain elongation step (ii).

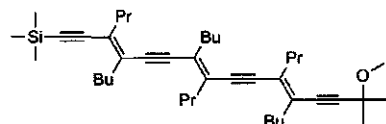
(ii) A mixture of 2 (10 equiv.),  $\text{Pd}(\text{PPh}_3)_4$  (5 mol%), CuI (2 mol %), and dry, degassed diethyl amine (2 ml/mmol) and THF (5 ml/mmol) was placed anaerobically in a dried, brown two-necked round-bottomed flask, equipped with a magnetic stirrer, an argon/hydrogen in- and outlet, and a pressure-equalized dropping funnel containing terminal acetylene (10-*n*) (1 equiv.). The terminal acetylene was added slowly (over 6 h) to the stirred mixture under a constant flow of argon/hydrogen (1:1). The mixture was further stirred overnight at 25 °C, concentrated and filtrated over a short silica gel column (5%  $\text{Et}_3\text{N}$  solution in petroleum ether 40/60). The residue was pre-purified on reversed phase silica ( $\text{CH}_3\text{CN}/\text{EtOAc}$ ) and finally purified on preparative HPLC to give pure (99.5%) diacetylene (1-*n*) and a quantitative recovery of iodo-diacetylene 2.

#### 2.4.13 ((3E,7E)-4,8-dibutyl-11-methoxy-11-methyl-3,7-dipropyldodeca-3,7-dien-1,5,9-triynyl) trimethyl- silane (1-2)



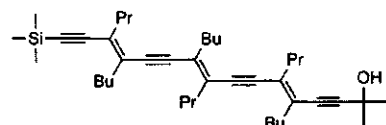
pale yellow oil (4.76 mmol, 2.22 g, 82%) from (1-1) (5.81 mmol, 1.85 g);  $^1\text{H}$  NMR:  $\delta$  0.20 (s, 9H), 0.89-0.95 (m, 12H), 1.28-1.41 (m, 4H), 1.46 (s, 6H), 1.46-1.62 (m, 8H), 2.32-2.49 (m, 6H), 3.38 (s, 3 H);  $^{13}\text{C}$  NMR:  $\delta$  0.0, 13.6, 13.6, 13.9, 14.0, 21.7, 22.1, 22.2, 28.4, 30.5, 30.7, 34.7, 34.9, 36.9, 37.1, 51.7, 71.2, 84.0, 97.9, 98.5, 100.2, 103.7, 104.8, 128.8, 128.9, 129.4, 131.2; HRMS: observed 466.3634; calculated 466.3631.

#### 2.4.14 (3E,7E,11E)-4,8,12-tributyl-15-methoxy-15-methyl-3,7,11-tripropylhexadeca-3,7,11-trien-1,5,9,13-tetraynyl) trimethylsilane (1-3)



yellow oil (1.76 mmol, 1.08 g, 78%) from (1-2) (2.25 mmol, 1.05 g);  $^1\text{H}$  NMR:  $\delta$  0.21 (s, 9H), 0.90-0.96 (m, 18H), 1.30-1.42 (m, 6H), 1.51 (s, 6H), 1.51-1.66 (m, 12H), 2.36-2.50 (m, 12H), 3.39 (s, 3H);  $^{13}\text{C}$  NMR:  $\delta$  0.0, 13.6, 13.6, 13.6, 13.9, 14.0, 14.0, 21.8, 21.9, 22.1, 22.2, 22.3, 28.4, 30.5, 30.7, 30.8, 34.7, 34.9, 35.0, 37.0, 37.1, 37.3, 51.7, 71.2, 84.0, 98.4, 98.6, 98.6, 99.0, 100.30, 103.8, 104.8, 128.8, 128.9, 129.1, 129.5, 129.7, 131.3; HRMS: observed 614.4888; calculated 614.4883.

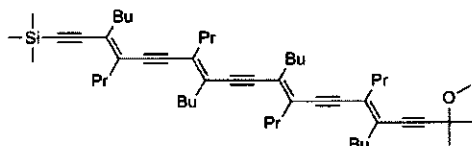
#### 2.4.15 (5E,9E,13E)-5,9,13-tributyl-2-methyl-14-(2-(trimethylsilyl) ethynyl)-6,10-dipropylheptade-5,9,13-trien-3,7,11-triyn-2-ol (1-3 OH)



pale yellow solid.  $^1\text{H}$  NMR:  $\delta$  0.20 (s, 9H), 0.90-0.96 (m, 18H), 1.30-1.42 (m, 6H), 1.51 (s, 6H), 1.51-1.66 (m, 12H), 2.36-2.50 (m, 12H);  $^{13}\text{C}$  NMR:  $\delta$  0.0, 13.6, 13.6, 13.6, 13.9, 14.0, 14.0,

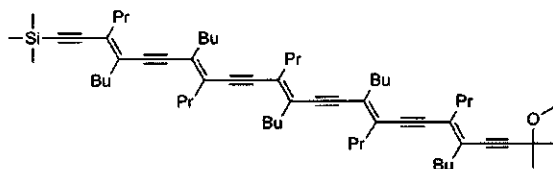
21.8, 21.9, 22.1, 22.2, 22.3, 28.4, 30.5, 30.7, 30.8, 34.7, 34.9, 35.0, 37.0, 37.1, 37.3, 71.2, 84.0, 98.4, 98.6, 98.6, 99.1, 100.3, 103.8, 104.8, 128.8, 128.9, 129.1, 129.5, 129.7, 131.3; HRMS: observed 600.4719; calculated 600.4726.

**2.4.16 ((3E,7E,11E,15E)-4,8,12,16-tetrabutyl-19-methoxy-19-methyl-3,7,11,15-tetrapropylcosa-3,7,11,15-tetraen-1,5,9,13,17-pentaynyl)trimethylsilane (1-4)**



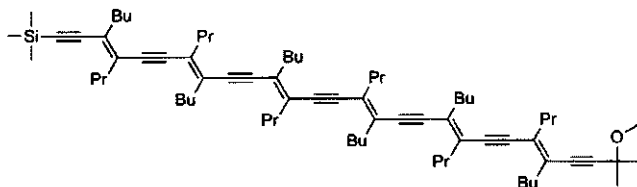
yellow solid (1.72 mmol, 1.31 gram, 75%) from (1-3) (2.29 mmol, 1.41 g);  $^1\text{H}$  NMR:  $\delta$  0.21 (s, 9H), 0.91-0.97 (m, 24H), 1.30-1.42 (m, 8H), 1.51 (s, 6H), 1.51-1.67 (m, 16H), 2.36-2.52 (m, 16H), 3.39 (s, 3H);  $^{13}\text{C}$  NMR:  $\delta$  0.0, 13.6, 13.6, 13.7, 13.9, 14.0, 21.8, 21.9, 22.1, 22.2, 22.3, 28.4, 30.5, 30.7, 30.8, 34.7, 34.9, 35.1, 35.1, 37.0, 37.1, 37.3, 51.7, 71.2, 84.0, 98.5, 98.7, 98.8, 99.2, 100.3, 103.8, 104.8, 128.8, 128.9, 129.2, 129.5, 129.6, 129.7, 131.3; HRMS: observed 762.6131; calculated 762.6135.

**2.4.17 ((3E,7E,11E,15E,19E)-4,8,12,16,20-pentabutyl-23-methoxy-23-methyl-3,7,11,15,19-pentapropyltetracos-3,7,11,15,19-pentaen-1,5,9,13,17,21-hexaynyl)trimethylsilane (1-5)**



yellow solid (0.90 mmol, 0.82 g, 70%) from (1-4) (1.29 mmol, 0.98 g);  $^1\text{H}$  NMR:  $\delta$  0.21 (s, 9H), 0.90-0.97 (m, 30H), 1.30-1.43 (m, 10H), 1.51 (s, 6H), 1.51-1.68 (m, 20H), 2.37-2.52 (m, 20H), 3.39 (s, 3H);  $^{13}\text{C}$  NMR:  $\delta$  0.0, 13.6, 13.6, 13.7, 13.9, 14.0, 21.8, 21.9, 22.1, 22.2, 22.3, 28.4, 30.6, 30.7, 30.9, 34.8, 34.9, 35.1, 37.0, 37.1, 37.3, 51.7, 71.2, 84.0, 98.5, 98.7, 98.8, 99.2, 99.3, 99.3, 100.3, 103.8, 104.9, 128.8, 128.9, 129.2, 129.2, 129.5, 129.6, 129.7, 129.7, 131.3; HRMS: observed 910.7406; calculated 910.7387.

**2.4.18 ((3E,7E,11E,15E,19E,23E)-4,8,12,16,20,24-hexabutyl-27-methoxy-27-methyl-3,7,11,15,19,23-hexapropyloctacos-3,7,11,15,19,23-hexaen-1,5,9,13,17,21,25-heptaynyl)trimethylsilane (1-6)**

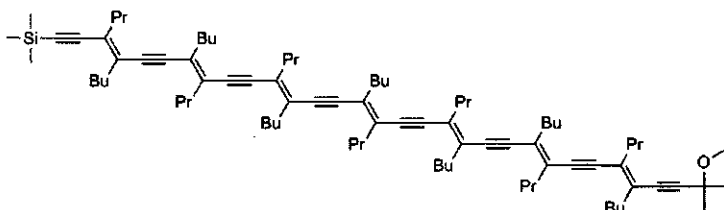


yellow solid (0.42 mmol, 450 mg, 72%) from (1-5) (0.58 mmol, 528 mg);  $^1\text{H}$  NMR:  $\delta$  0.21 (s, 9H), 0.91-0.98 (m, 36H), 1.30-1.43 (m, 12H), 1.51 (s, 6H), 1.51-1.68 (m, 24H), 2.37-2.53 (m, 24H), 3.39 (s, 3H);  $^{13}\text{C}$  NMR:  $\delta$  0.0, 13.6, 13.6, 13.9, 14.0, 21.8, 21.9, 21.9, 22.1, 22.2, 22.3, 28.4, 30.6, 30.7, 30.9, 30.9, 34.8, 34.9, 35.1,



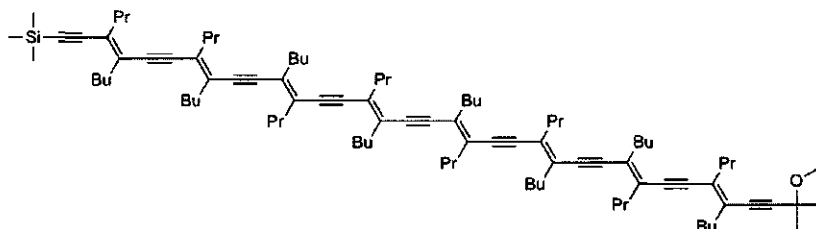
37.0, 37.1, 37.3, 51.7, 71.2, 84.0, 98.5, 98.7, 98.8, 99.2, 99.3, 99.3, 99.4, 99.4, 100.4, 103.8, 104.7, 128.8, 128.9, 129.2, 129.3, 129.5, 129.6, 129.7, 129.7, 131.3; HRMS: observed 1058.8632; calculated 1058.8639.

**2.4.19 ((3E,7E,11E,15E,19E,23E,27E)-4,8,12,16,20,24,28-heptabutyl-31-methoxy-31-methyl-3,7,11,15,19,23,27-heptapropyldotriaconta-3,7,11,15,19,23,27-heptaen-1,5,9,13,17,21,25,29-octaynyl)trimethylsilane (1-7)**



yellow/orange solid (1.16 mmol, 140 mg, 68%) from (1-6) (1.70 mmol, 180 mg);  $^1\text{H}$  NMR:  $\delta$  0.21 (s, 9H), 0.91-0.98 (m, 42H), 1.30-1.44 (m, 14H), 1.51 (s, 6H), 1.51-1.68 (m, 28H), 2.37-2.53 (m, 28H), 3.39 (s, 3H);  $^{13}\text{C}$  NMR:  $\delta$  0.0, 13.6, 13.6, 13.9, 14.0, 21.8, 21.9, 22.1, 22.2, 22.3, 28.4, 30.6, 30.7, 30.9, 30.9, 34.8, 34.9, 35.1, 37.0, 37.1, 37.3, 51.7, 71.2, 84.0, 98.5, 98.7, 98.8, 99.2, 99.3, 99.3, 99.4, 99.4, 99.5, 100.4, 103.9, 104.9, 128.8, 128.9, 129.2, 129.3, 129.5, 129.6, 129.7, 129.7, 131.3; HRMS: observed 1206.9886; calculated 1206.9891.

**2.4.20 ((3E,7E,11E,15E,19E,23E,27E,31E)-4,8,12,16,20,24,28,32-octabutyl-35-methoxy-35-methyl-3,7,11,15,19,23,27,31-octapropylhexatriaconta-3,7,11,15,19,23,27,31-octaen-1,5,9,13,17,21,25,29,33-nonaynyl)trimethylsilane (1-8)**



orange solid (0.06 mmol, 80 mg, 69%) from (1-7) (0.09 mmol, 109 mg);  $^1\text{H}$  NMR:  $\delta$  0.21 (s, 9H), 0.91-0.98 (m, 48H), 1.30-1.44 (m, 16H), 1.51 (s, 6H), 1.51-1.69 (m, 32H), 2.37-2.53 (m, 32H), 3.39 (s, 3H);  $^{13}\text{C}$  NMR:  $\delta$  0.0, 13.6, 13.6, 13.9, 14.0, 21.8, 21.9, 21.9, 22.1, 22.2, 22.3, 28.4, 30.6, 30.7, 30.9, 30.9, 34.8, 34.9, 35.1, 37.0, 37.1, 37.3, 51.7, 71.2, 84.0, 98.5, 98.7, 98.8, 99.2, 99.3, 99.3, 99.4, 99.4, 100.4, 103.9, 104.9, 128.8, 128.9, 129.2, 129.3, 129.5, 129.6, 129.7, 129.7, 131.3; HRMS: observed 1355.1156; calculated 1355.1143.

## 2.5 Acknowledgements

The authors thank the Dutch Technology Foundation STW for generous funding of this research (Project No. WPC 5740), and Dr. Jan Kroon (ECN), Dr. Herman Schoo (TNO), Dr. Joost Smits (Shell) and Prof. Wybren Jan Buma (Univ. of Amsterdam) for helpful discussions.

## 2.6 Supporting Information

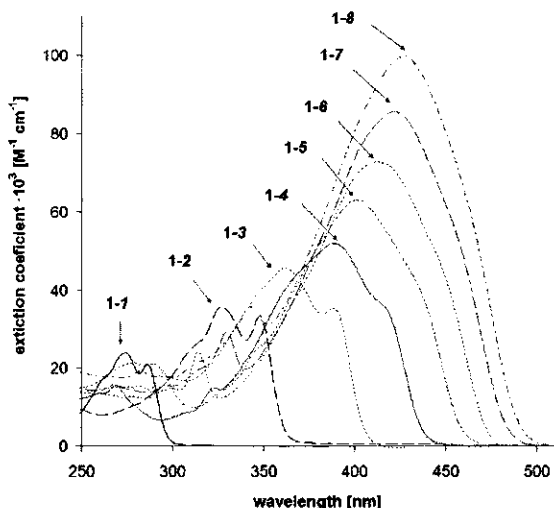


Figure 7. Electronic absorption spectra of methoxy-endcapped oligodiacylenes 1-*n* (*n* = 1-8) in *n*-heptane.

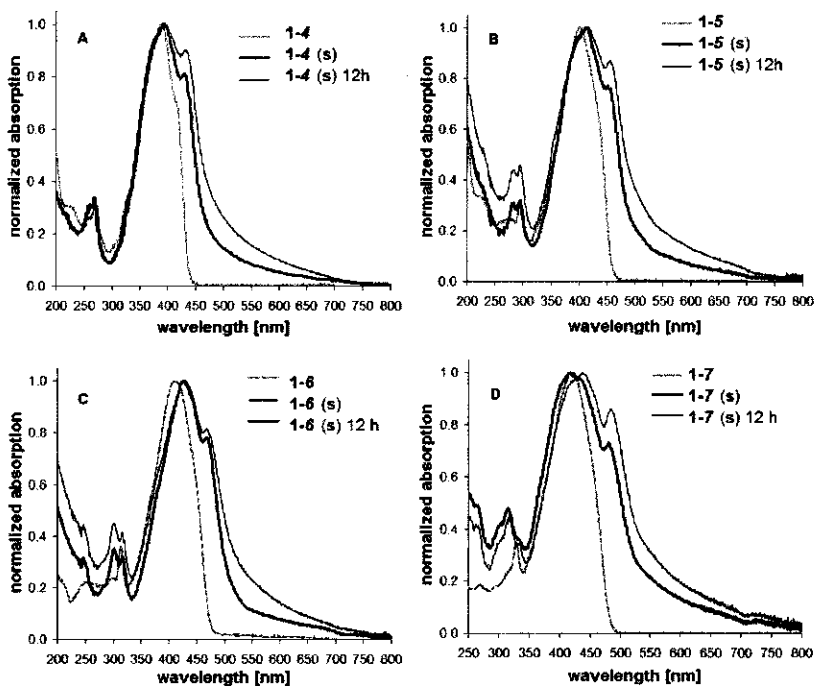


Figure 8. Normalized absorption spectra of ODAs 1-4 to 1-7 in *n*-hexane solution versus solid state (s), either directly after drop-casting or after waiting for another 12 hrs to allow molecular rearrangements.

## 2.7 References

- [1] C. K. Chiang, C. R. J. Fincher, Y. W. Park, A. J. Heeger, H. Shirakawa, E. J. Louis, S. C. Gau and A. G. MacDiarmid, *Phys. Rev. Lett.* **1977**, *39*, 1098-1101.
- [2] H. Shirakawa, E. J. Louis, A. G. MacDiarmid, C. K. Chiang and A. J. Heeger, *J. Chem. Soc., Chem. Commun.* **1977**, 578-580.
- [3] R. H. Friend, R. W. Gymer, A. B. Holmes, J. H. Burroughes, R. N. Marks, C. Taliani, D. D. C. Bradley, D. A. Dos Santos, J. L. Bredas, M. Logdlund and W. R. Salaneck, *Nature* **1999**, *397*, 121-128.
- [4] F. Diederich, *Chem. Commun.* **2001**, 219-227.
- [5] M. B. Nielsen and F. Diederich, *Chem. Rev.* **2005**, *105*, 1837-1867.
- [6] K. Kuriyama, H. Kikuchi and T. Kajiyama, *Langmuir* **1996**, *12*, 6468-6472.
- [7] J. M. Tour, *Chem. Rev.* **1996**, *96*, 537-553.
- [8] Q. Liu, W. Liu, B. Yao, H. Tian, Z. Xie, Y. Geng and F. Wang, *Macromolecules* **2007**, *40*, 1851-1857.
- [9] P. Frere, J.-M. Raimundo, P. Blanchard, J. Delaunay, P. Richomme, J.-L. Sauvajol, J. Orduna, J. Garin and J. Roncali, *J. Org. Chem.* **2003**, *68*, 7254-7265.
- [10] M. R. Bryce, M. A. Coffin, P. J. Skabara, A. J. Moore, A. S. Batsanov and J. A. K. Howard, *Chem. Eur. J.* **2000**, *6*, 1955-1962.
- [11] C. Czekelius, J. Hafer, Z. J. Tonzetich, R. R. Schrock, R. L. Christensen and P. Mueller, *J. Am. Chem. Soc.* **2006**, *128*, 16664-16675.
- [12] G. Zotti, G. Schiavon, A. Berlin and G. Pagani, *Chem. Mater.* **1993**, *5*, 430-436.
- [13] G. Zotti, G. Schiavon, A. Berlin and G. Pagani, *Chem. Mater.* **1993**, *5*, 620-624.
- [14] G. Zotti, G. Schiavon, A. Berlin and G. Pagani, *Adv. Mater.* **1993**, *5*, 551-554.
- [15] W. Ten Hoeve, H. Wynberg, E. E. Havinga and E. W. Meijer, *J. Am. Chem. Soc.* **1991**, *113*, 5887-5889.
- [16] S. S. Zade and M. Bendikov, *J. Org. Chem.* **2006**, *71*, 2972-2981.
- [17] D. Fichou, G. Horowitz, B. Xu and F. Garnier, *Synth. Met.* **1990**, *39*, 243-259.
- [18] U. Segelbacher, N. S. Sariciftci, A. Grupp, P. Baeuerle and M. Mehring, *Synth. Met.* **1993**, *57*, 4728-4733.
- [19] J. Roncali, *Chem. Soc. Rev.* **2005**, *34*, 483-495.
- [20] R. Sander, V. Stuempflen, J. H. Wendorff and A. Greiner, *Macromolecules* **1996**, *29*, 7705-7708.
- [21] K. A. Walters, K. D. Ley and K. S. Schanze, *Langmuir* **1999**, *15*, 5676-5680.
- [22] B. Leibrock, O. Vostrowsky and A. Hirsch, *Eur. J. Org. Chem.* **2001**, 4401-4409.
- [23] J.-M. Kim, Y. B. Lee, D. H. Yang, J.-S. Lee, G. S. Lee and D. J. Ahn, *J. Am. Chem. Soc.* **2005**, *127*, 17580-17581.
- [24] R. E. Martin and F. Diederich, *Angew. Chem. Int. Ed.* **1999**, *38*, 1351-1377.
- [25] R. E. Martin, U. Gubler, J. Cornil, M. Balakina, C. Boudon, C. Bosshard, J.-P. Gisselbrecht, F. Diederich, P. Gunter, M. Gross and J.-L. Bredas, *Chem. Eur. J.* **2000**, *6*, 3622-3635.
- [26] J. F. Nierengarten, D. Guillon, B. Heinrich and J. F. Nicoud, *Chem. Commun.* **1997**, 1233-1234.
- [27] Y. Zhao and R. R. Tykwinski, *J. Am. Chem. Soc.* **1999**, *121*, 458-459.
- [28] Y. Zhao, R. McDonald and R. R. Tykwinski, *J. Org. Chem.* **2002**, *67*, 2805-2812.
- [29] S. C. Ciulei and R. R. Tykwinski, *Org. Lett.* **2000**, *2*, 3607-3610.
- [30] Y. Zhao, S. C. Ciulei and R. R. Tykwinski, *Tetrahedron Lett.* **2001**, *42*, 7721-7723.
- [31] H. Zuilhof, H. M. Barentsen, M. Dijk van, E. J. R. Sudhölter, R. J. O. M. Hoofman, L. D. A. Siebbeles, M. P. Haas de and J. M. Warman in *Polydiacetylenes*, (Ed. H. S. Nalwa), Academic Press, San Diego, San Francisco, New York, Boston, London, Sydney, Tokyo, **2001**, pp. 339-437.
- [32] A. F. Garito, C. C. Teng, K. Y. Wong and O. Zammami'Khamiri, *Mol. Cryst. Liq. Cryst.* **1984**, *106*, 219-258.
- [33] K. J. Donovan and E. G. Wilson, *Synth. Met.* **1989**, *28*, 569-574.

- [34] S. Spagnoli, K. J. Donovan, K. Scott, M. Somerton and E. G. Wilson, *Chem. Phys.* **1999**, *250*, 71-79.
- [35] V. Enkelmann, *Adv. Polym. Sci.* **1984**, *63*, 91-136.
- [36] S. Jo, H. Yoshikawa, A. Fujii and M. Takenaga, *Synth. Met.* **2005**, *150*, 223-226.
- [37] M. Schott, *Synth. Met.* **2003**, *139*, 739-742.
- [38] F. Wudl and S. P. Bitler, *J. Am. Chem. Soc.* **1986**, *108*, 4685-4687.
- [39] S. P. Bitler and F. Wudl, *Polym. Mat. Sci. Engin.* **1986**, *54*, 292-296.
- [40] R. Giesa and R. C. Schulz, *Polym. Int.* **1994**, *33*, 43-60.
- [41] D. J. Ager, *Synthesis* **1984**, 384-398.
- [42] W. E. Lindsell, P. N. Preston and P. J. Tomb, *J. Organomet. Chem.* **1992**, *439*, 201-212.
- [43] M. Polhuis, C. C. J. Hendrikx, H. Zuilhof and E. J. R. Sudholter, *Tetrahedron Lett.* **2003**, *44*, 899-901.
- [44] C. C. J. Hendrikx, M. Polhuis, A. Pul-Hootsen, R. B. M. Koehorst, A. Hoek van, H. Zuilhof and E. J. R. Sudholter, *Phys. Chem. Chem. Phys.* **2005**, *7*, 548-553.
- [45] G. M. Balkowski, M. Groeneveld, H. Zhang, C. C. J. Hendrikx, M. Polhuis, H. Zuilhof and W. J. Buma, *J. Phys. Chem. A* **2006**, *110*, 11435-11439.
- [46] Y. Takayama, C. Delas, K. Muraoka and F. Sato, *Org. Lett.* **2003**, *5*, 365-368.
- [47] Y. Takayama, C. Delas, K. Muraoka, M. Uemura and F. Sato, *J. Am. Chem. Soc.* **2003**, *125*, 14163-14167.
- [48] F. Sato and S. Okamoto, *Adv. Synth. Catal.* **2001**, *343*, 759-784.
- [49] K. Fukuhara, Y. Takayama and F. Sato, *J. Am. Chem. Soc.* **2003**, *125*, 6884-6885.
- [50] B. J. Wakefield, *The Chemistry Of Organolithium Compounds*, Pergamon Press Ltd., **1974**, p.
- [51] Alkylation of diacetylene **7** followed by GS/MS using *t*-BuLi and *n*-BuLi resulted in formation of **8** along with protonated analogue in ratio 80/20. The use of *n*-BuLi with *n*-propyllithium resulted in formation of **8** along with its analogue bearing two propyl side chains in ratio 60/40 determined on GC/MS.
- [52] V. A. Solomin and W. Heitz, *Macromol. Chem. Phys.* **1994**, *195*, 303-314.
- [53] G. S. Pilzak, S. Fratiloju, J. Baggerman, F. Grozema, E. J. R. Sudholter, L. D. A. Siebbeles and H. Zuilhof, *J. Chem. Phys. B submitted* **2009**.
- [54] P. Siemsen, R. C. Livingston and F. Diederich, *Angew. Chem. Int. Ed.* **2000**, *39*, 2632-2657.
- [55] A. Elangovan, Y.-H. Wang and T.-I. Ho, *Org. Lett.* **2003**, *5*, 1841-1844.
- [56] S. Urganekar and J. G. Verkade, *J. Org. Chem.* **2004**, *69*, 5752-5755.
- [57] B. E. Kohler and D. E. Schilke, *J. Chem. Phys.* **1987**, *86*, 5214-5215.
- [58] Y. Zhao, K. Campbell and R. R. Tykwinski, *J. Org. Chem.* **2002**, *67*, 336-344.
- [59] S. M. Bachilo, E. V. Bachilo and T. Gillbro, *Chem. Phys.* **1998**, *229*, 75-91.
- [60] J. Gierschner, J. Cornil and H. Egelhaaf, *J. Adv. Mat.* **2007**, 173-191.
- [61] S. S. Zade and M. Bendikov, *Org. Lett.* **2006**, 5243-5246.
- [62] G. Wenz, M. A. Müller, M. Schmidt and G. Wegner, *Macromolecules* **1984**, *17*, 837-850.
- [63] R. E. Martin, U. Gubler, J. Cornil, M. Balakina, C. Boudon, C. Bosshard, J.-P. Gisselbrecht, F. Diederich, P. Günter, M. Gross and J.-L. Brédas, *Chem. Eur. J.* **2000**, *6*, 3622-3635.
- [64] R. Lecuiller, J. Berrehar, C. Lapersonne-Meyer and M. Schott, *Phys. Rev. Lett.* **1998**, *80*, 4068-4071.
- [65] B. E. Kohler and D. E. Schilke, *J. Chem. Phys.* **1987**, *86*, 5214-5215.
- [66] M. Yoshizawa, A. Kubo and S. Saikan, *Phys. Rev. B* **1999**, *60*, 15632-15635.
- [67] T. Itoh, B. E. Kohler and C. W. Spangler, *Spectrochim. Acta* **1994**, *50A*, 2261-2263.
- [68] S. M. Bachilo, C. W. Spangler and T. Gillbro, *Chem. Phys. Lett.* **1998**, *283*, 235-242.
- [69] J. R. Lakowicz, *Principles of Fluorescence Spectroscopy*, Kluwer Academic / Plenum Publishers, **2006**, p. 420-421.
- [70] P. Kapusta, R. Erdmann, U. Ortmann and M. Wahl, *J. Fluoresc.* **2003**, *13*, 179-183.
- [71] I. Soutar and L. Swanson, *Polym. Int.* **2006**, *55*, 729-739.
- [72] X. Dou, Q. Y. Shang and B. S. Hudson, *Chem. Phys. Lett.* **1992**, *189*, 48-53.
- [73] N. Aratani, Z. S. Yoon, D. Kim and A. Osuka, *J. Chin. Chem. Soc.* **2006**, *53*, 41-46.

# Chapter 3

## Synthesis and Optoelectronic Properties of Nanometer-Sized and Highly Soluble Homocoupled Oligodiacetylenes

### Abstract

A new series of pure, nanometer-sized and highly soluble homocoupled oligodiacetylenes (HODA) consisting of two symmetrical oligodiacetylene units was synthesized with high yield and on a multi-milligram scale under mild, catalytic Sonogashira conditions. The  $\lambda_{\text{max}}$  and the  $\epsilon_{\text{max}}$  of absorption for these HODAs show an increase with the chain elongation. The  $\lambda_{\text{max}}$  converges to 450 nm for the longest members of the series at micromolar concentration and to 462 nm for thin drop-casted films. An additional red-shifted absorption is observed in the solid state and in solution at low temperatures, which is caused by aggregation. The  $\lambda_{\text{max}}$  of the fluorescence emission increases with the chain length and reaches 492 nm for the longest oligomer. The fluorescence quantum yield has its maximum for the shortest oligomer and decreases rapidly for the longer ones. A similar trend is found for the fluorescence lifetime with a maximum of 100 ps for the homocoupled monomer. The rotational correlation time shows a linear increase with the oligomer length. This reveals a significant persistence length and indicates that the HODA molecules are fully stretched molecular rods (up to 8.2 nm).

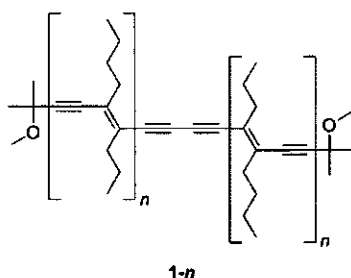
*This chapter was published: Gregor S. Pilzak, Jacob Baggerman, Barend van Lagen, Maarten A. Posthumus, Ernst J. R. Sudhölter, Han Zuilhof, Chemistry - A European Journal, 2009, 15, 2296-2304.*

### 3.1 Introduction

The development of nanometer-sized conjugated molecules, which play a crucial role in a wide variety of photoinduced processes, has attracted a lot of scientific interest in the last decade.<sup>[1-4]</sup>

Various potential applications in optoelectronic devices such as photo-voltaic cells,<sup>[5]</sup> light-emitting diodes,<sup>[6]</sup> and field-effect transistors<sup>[7]</sup> are emerging from this.<sup>[8]</sup> The design of accurately defined  $\pi$ -conjugated oligomers is important, since this provides information about the evolution of the electronic, optical, thermal and morphological properties of the corresponding polymeric materials. However, the synthesis of long  $\pi$ -conjugated oligomers is often difficult, owing to a low solubility of the molecules, possible limitations of the synthetic route (specifically for longer oligomers), or purification problems.<sup>[9]</sup> Novel methods for the preparation of conjugated oligomers are thus frequently required to obtain series of soluble monodisperse oligomers.<sup>[10]</sup>

Oligomers based on repeating enyne units, such as oligodiacetylenes, act as models of polydiacetylene (PDA) for understanding the influence of the precise conjugation length on the electronic properties.<sup>[11-16]</sup> Recently, we have published an iterative approach to construct a new series of oligodiacetylenes ranging from monomer up to octamer bearing 17 conjugated double and triple bonds. In this study we extend our method<sup>[15]</sup> to produce nanometer-sized materials reaching up to 30 conjugated double and triple bonds with an estimated length of  $\sim 8$  nanometer.



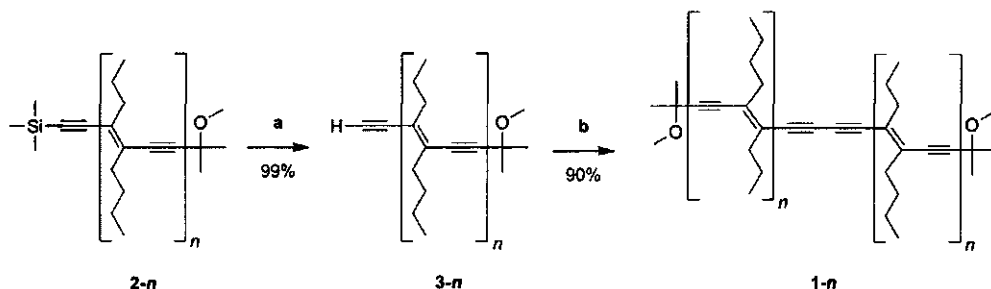
Scheme 1. Series of novel HODAs **1-n** under present study ( $n = 1 - 7$ ).

We describe the synthesis of a new series of highly soluble homocoupled oligodiacetylenes (HODAs) consisting of two symmetrical oligodiacetylene units. The series ranges from monomer **1-1** ( $C_{34}H_{50}O_2$  and  $M_r = 490.38$ ) to heptamer **1-7** ( $C_{166}H_{242}O_2$  and  $M_r = 2267.67$ , Scheme 1), synthesized in high purity ( $\geq 99\%$ ) and with high yields (80-90%), which allows the isolation of significant amounts of these oligomers. We report on the optical properties of these materials using both steady-state and picosecond time-resolved techniques.

## 3.2 Results and Discussion

### 3.2.1 Synthesis of HODAs

A series of soluble oligodiacetylenes bearing two different endcaps and asymmetrical alkyl side chains **2-*n***, ranging from monomer up to heptamer was synthesized according to our previously reported approach.<sup>[15]</sup> The protodesilylation of oligodiacetylene **2-*n*** using a mild alkaline method proceeded quantitatively and resulted in the formation of terminal acetylenes **3-*n***, as shown in Scheme 2.



Reagents: (a) K<sub>2</sub>CO<sub>3</sub>, cat. H<sub>2</sub>O, MeOH/THF; (b) Pd(PPh<sub>3</sub>)<sub>4</sub>, CuI, Et<sub>2</sub>NH, THF.

Scheme 2. Homocoupling of ODAs to yield homocoupled elongated analogs.

The homocoupling of the terminal oligodiacetylene **3-*n*** was performed by means of a mild catalytic reaction under ambient air conditions. Essential for this palladium-catalyzed homocoupling is the presence of both a copper(I) salt and an amine, which results in the formation of Cu(I) acetylides from terminal acetylenes *in situ*. This can be effectively used to induce the desired homocoupling.<sup>[11]</sup> As reported by Elangovan et al.<sup>[17]</sup> the use of tetrakis(triphenylphosphine)palladium(0) under an oxygen atmosphere generates a Pd<sup>II</sup> catalyst *in situ*, which is the active catalyst for the homocoupling of terminal acetylenes. To increase the rate of the reaction and to minimize formation of side products, the concentration of the tetrakis(triphenylphosphine)palladium catalyst and Cu(I) cocatalyst was kept slightly higher (> 5 mol%) than in the case when the crosscoupled Sonogashira product was the target.<sup>[15]</sup> Under such optimized conditions the homocoupling of long oligomers proceeded almost quantitatively (> 90 % isolated yields) and all coupling reactions were completed within 3 hours.

### 3.2.2 Steady-state optical absorption in solution

The high solubility of the synthesized HODAs is the direct result of the laterally attached asymmetrical alkyl side-chains, and allows us to study their optical properties both with *and* without aggregation. The ground-state optical absorption of the **1-*n*** series was measured both in solution and as a drop-casted thin film. The absorption of the HODA series **1-*n*** up to *n* = 7 as a monodisperse solution in *n*-hexane is depicted in Figure 1. Similar spectra were obtained in 1,2-dichloroethane (DCE) and are given in the Supporting Information (Subchapter 3.6; Figure 10).

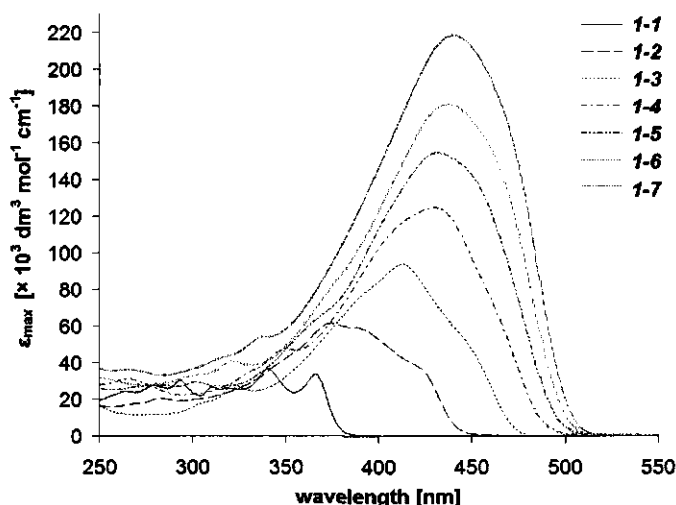


Figure 1. Electronic absorption spectra of methoxy-endcapped oligodiacetylenes **1-*n*** (*n* = 1 - 7) in *n*-hexane.

The steady-state absorption spectra recorded in both solvents show the expected red-shift of the absorption maximum ( $\lambda_{\text{max}}$ ) and an increase of the extinction coefficient ( $\epsilon_{\text{max}}$ ) with an increasing conjugation length. This bathochromic shift is similar to literature data reported for shorter enyne-based oligomer series reported by others<sup>[13, 15, 18, 19]</sup> and us,<sup>[12]</sup> and becomes smaller with chain elongation:  $\Delta\lambda_{\text{max}}$  decreases from  $\sim 0.34$  eV going from **1-1** to **1-2** (in both *n*-hexane and DCE) to  $\sim 0.02$  eV in *n*-hexane and  $\sim 0.04$  eV in DCE going from **1-6** to **1-7** (Table 1).

The  $\lambda_{\text{max}}$  and the  $\epsilon_{\text{max}}$  for the homocoupled oligomers matches rather closely the corresponding values of  $\lambda_{\text{max}}$  for **2-*n*** of similar conjugation length. The optical properties of HODAs are dominated by the  $C_{2h}$  symmetry that is present in fully stretched, planar oligomers. To the degree that this is correct, based on both the analogy with oligodiacetylenes and the



fluorescence quantum yields and time-resolved fluorescence anisotropy data reported below, their absorption spectrum is associated with a  $S_2 (1^1B_u) \leftarrow S_0 (1^1A_g)$  transition.<sup>[12, 15, 16, 20, 21]</sup>

**Table 1.** Absorption data of HODAs **1-*n*** (*n* = 1 - 7) in *n*-hexane and DCE.

<b>1-<i>n</i> (CL)<sup>[a]</sup></b>	<b><math>\lambda_{\max}</math> [nm] ([eV])</b>		<b><math>\epsilon_{\max}</math> [<math>\times 10^3</math> dm<sup>3</sup> mol<sup>-1</sup> cm<sup>-1</sup>]</b>	
	<i>n</i> -hexane	DCE	<i>n</i> -hexane	DCE
<b>1-1 (6)</b>	339 (3.66)	344 (3.60)	36.2	30.1
<b>1-2 (10)</b>	374 (3.32)	380 (3.26)	61.1	54.3
<b>1-3 (14)</b>	412 (3.01)	419 (2.96)	93.8	83.2
<b>1-4 (18)</b>	429 (2.89)	436 (2.84)	124.7	104.2
<b>1-5 (22)</b>	432 (2.87)	441 (2.81)	154.8	133.2
<b>1-6 (26)</b>	437 (2.84)	447 (2.77)	180.7	160.3
<b>1-7 (30)</b>	440 (2.82)	450 (2.76)	218.2	186.6

[a] Conjugation length (CL) = number of double/triple bonds.

The dominant solvent effect is the polarization shift, which is attributed to the difference in solvent refractive index.<sup>[22]</sup> A bathochromic effect is observed upon changing the solvent from *n*-hexane (refractive index,  $n_r = 1.375$ ; empirical solvent polarity parameter,  $E_T(30) = 31.0$ ) to DCE ( $n_r = 1.445$ ;  $E_T(30) = 41.3$ ).<sup>[23, 24]</sup> This relatively small shift ( $\sim 0.06$  eV for all oligomers) is in line with previously reported data for long oligodiacetylene series.<sup>[15]</sup> This shows that the excited-state dipole moment  $\mu_e$  of HODAs **1-*n*** is only marginally larger than the ground-state dipole moment  $\mu_g$ .

The extinction coefficient depends on the solvent polarity and conjugation length (CL), defined as the sum of the number of double and triple bonds with  $CL = 4n + 2$ , as depicted in Figure 2. The  $\epsilon_{\max}$  increases linearly with CL in both solvents, which shows that the  $S_2 - S_0$  energy gap is evenly decreasing during the extension of the conjugated  $\pi$ - $\pi$  systems, and results in a more probable absorption. This observation of linearity indicates that the charge delocalization in the extended chromophoric system is not significantly hampered by kinks or torsions<sup>[25, 26]</sup>, as those would have scaled with the number of possible conformations, which increases exponentially with the chain length and would thus have yielded a less than linear increase.<sup>[27]</sup> For the HODAs the difference between the  $\epsilon_{\max}$  in *n*-hexane and DCE is approximately 20 % in favor of the nonpolar solvent. This observation is similar to the molar extinction decrease for nonpolar and dipole-less  $\beta$ -carotene<sup>[28]</sup> with an increase of solvent

polarity. However, this is in contrast with the previously reported solvent dependence of  $\epsilon_{\max}$  for **2-n** series, which showed an increase of the extinction maximum upon an increase of solvent polarity.<sup>[15]</sup> Apparently, this phenomenon results from the structural differences between both oligomeric series. The **2-n** series have only one  $-\text{C}(\text{CH}_3)_2\text{CH}_2\text{OCH}_3$  endcap, which induces a dipole moment compared to the HODAs where two  $-\text{C}(\text{CH}_3)_2\text{CH}_2\text{OCH}_3$  end groups are placed exactly at the opposite site of the oligodiacetylene chain. This results in structural symmetry of the **1-n** series and thus a low (negligible) dipole moment.

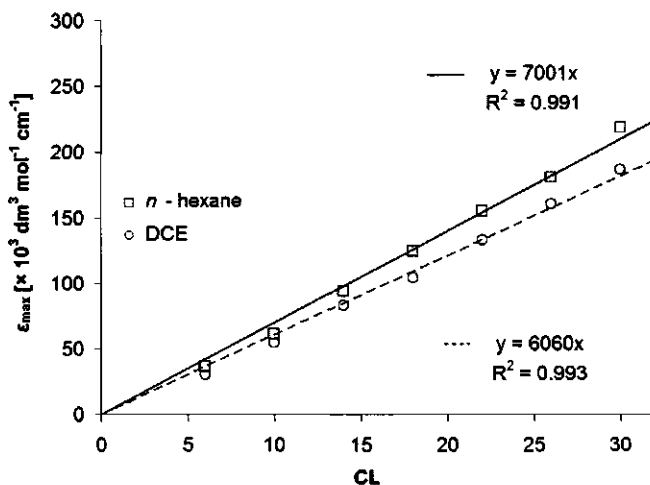


Figure 2. Extinction coefficient maxima of HODA series **1-n** ( $n = 1 - 7$ ) in *n*-hexane ( $\square$ ) and DCE ( $\circ$ ) solution at micromolar concentrations ( $2 \cdot 10^{-6}$  M) versus CL.

The absorption maximum of the oligomers (expressed in eV) displays a linear relation with the reciprocal conjugation length ( $1/\text{CL}$ ) as shown in Figure 3 together with literature data points for the **2-n** series<sup>[15]</sup> ( $\text{CL} = 3 - 17$ ) and oligotriacetylenes (OTA)<sup>[29]</sup> with  $\text{CL} = 3 - 48$ . An extrapolated  $\lambda_{\max}$  of 2.56 eV (484 nm) for a PDA polymer with  $n = \infty$  in *n*-hexane is obtained, while in DCE a value of 2.51 eV (494 nm) is calculated. These extrapolated values match almost exactly the  $\lambda_{\max}$  values reported by us previously for the **2-n** series up to octamer, that is, 2.55 eV (487 nm) in *n*-hexane and 2.48 (500 nm) in DCE.<sup>[15]</sup>

The absorption maximum of the longest HODA (**1-7**) in solution is 440 and 450 nm in *n*-hexane and DCE, respectively. Compared with the **2-n** series (no absorption  $\geq 500$  nm) the absorption spectrum for **1-7** reaches higher, that is, up to 535 nm (see Figure 3). This value is still significantly lower than the reported values for longer-wavelength absorptions ( $\lambda_{\max}$  up to 700 nm) of PDA chains, the most closely related class of conjugated polymers.<sup>[30]</sup> For plots like these, it is known that for extended oligomers they start to deviate from linearity, and curve

horizontally near the y-axis.<sup>[31, 32]</sup> This was previously observed for the highly analogous oligotriacetylenes (OTAs),<sup>[29]</sup> for which truncation effects on the conjugation length are already noticeable for the oligomers with more than 24 conjugated bonds. However, for the HODAs with the elongation of the conjugation length linearity of the plot is retained. This phenomenon is illustrated in Figure 3 where no flattening of the curve towards the y-axis is observed. This observation, together with the linearity of the  $\epsilon_{\max}$  and  $\lambda_{\max}$  of absorption with CL and  $1/CL$ , respectively, clearly shows the continuously increased conjugation in the 1- $n$  series up to 30 double and triple bonds.

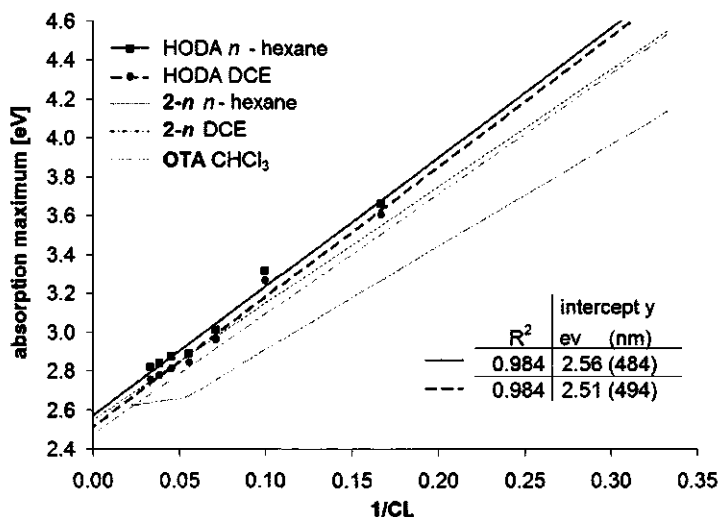


Figure 3.  $\lambda_{\max}$  of the absorption versus  $1/CL$  and its linear fits of HODA series 1- $n$  ( $n = 1 - 7$ ) and 2- $n$ <sup>[15]</sup> ( $CL = 3 - 17$ ) in  $n$ -hexane and DCE solution at micromolar concentrations ( $2 \cdot 10^{-5}$  M) compared to oligotriacetylenes (OTA)<sup>[29]</sup> with  $CL = 3 - 48$  in  $CHCl_3$  solution at room temperature.

### 3.2.3 Steady-state optical absorption in thin films

The optical absorption of oligomer 1-3 to 1-7 in thin solid films is depicted in Figure 4a. The color change between the millimolar solution and the solid state of the conjugated oligomer 1-7 is clearly visible by the naked eye (Figure 4b). To investigate whether this bathochromic shift should be attributed to aggregation or concentration effects, the optical absorption of the 1- $n$  series in the solid state was investigated in drop-casted thin films. The absorption spectrum is recorded 12 hours after the start of the solvent evaporation from the quartz plate containing solid material prepared by means of drop-casting. The solid state absorption spectra of the HODA series 1- $n$  show a bathochromic shift of the absorption maxima with  $\sim 0.07$  eV relatively to the absorption maxima of 1- $n$  solutions in DCE (Table 1).

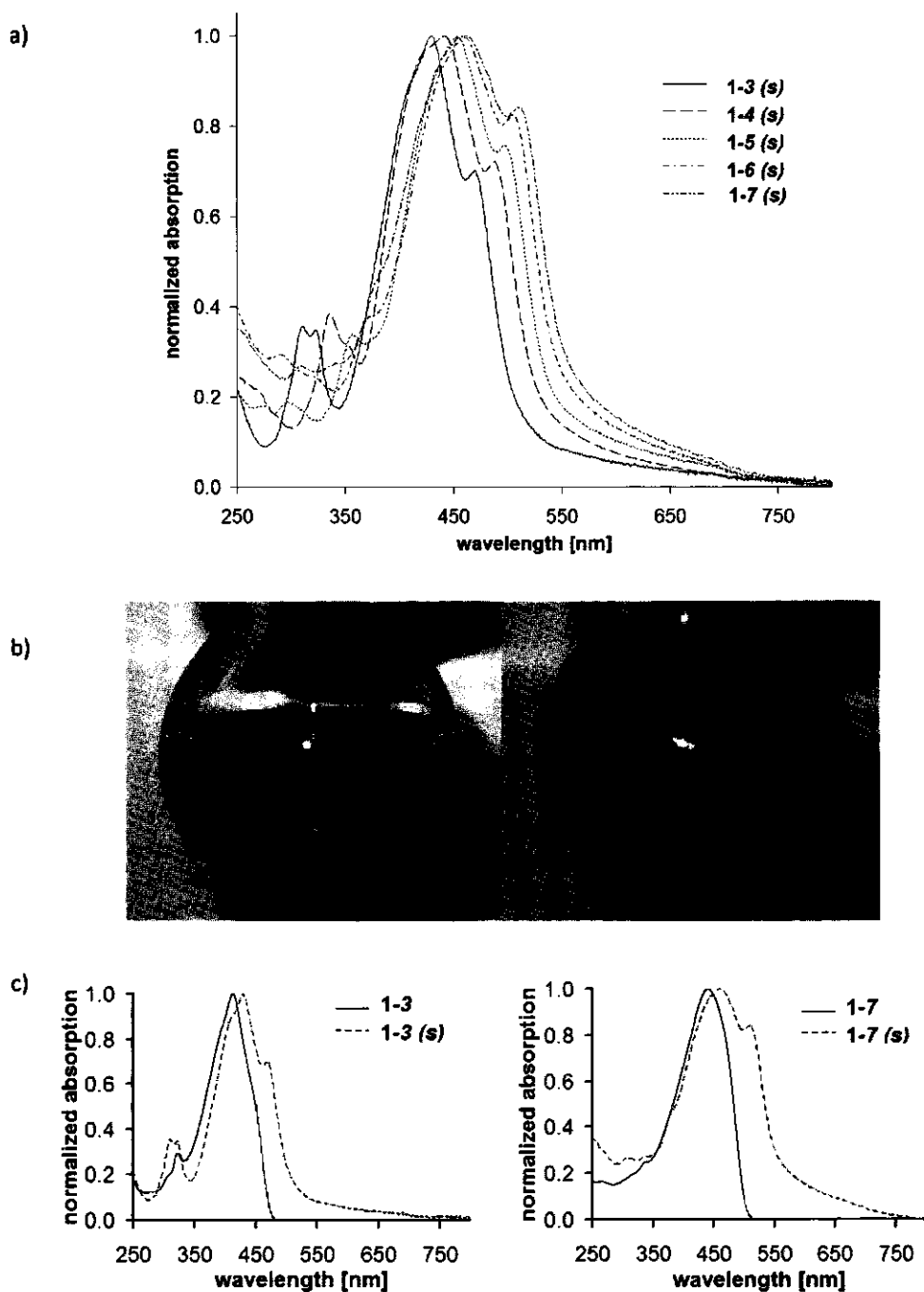


Figure 4. Steady-state optical absorption of HODAs: a) normalized absorption spectra of drop-casted **1-*n*** series ( $n = 3 - 7$ ); b) Color change upon solvent evaporation of **1-7** solution in *n*-hexane (left) versus the **1-7** in thin solid film (right). Normalized absorption spectra of HODA **1-3** (c) and **1-7** (d) in solution versus thin solid film (s).

These data match rather closely the values that were observed for the bathochromic shift of solid 2-*n* oligodiacetylenes ( $\sim 0.10$  eV) of similar CL.<sup>[15]</sup> Furthermore, the spectra are characterized by an additional electronic transition appearing at lower energy,  $\sim 0.23$  eV below the main absorption maxima, followed by a significant absorption increase in the range of 550 - 800 nm. This characteristic pattern for all solid oligomers under study was also reported previously by us for the 2-*n* absorption in thin films.<sup>[15]</sup> Figure 4c and Figure 4d display a comparison between solution and thin-film absorption for the shortest 1-3 and longest 1-7 solid oligomers. The solid-state absorption data of the solid HODAs are summarized in Table 2.

Table 2. Solid state absorption data of HODAs 1-*n* (*n* = 3 - 7)

1- <i>n</i> (CL) <sup>[a]</sup>	$\lambda_{\text{max}}$ [nm] ([eV])	$\lambda_{\text{max right shoulder}}$ [nm] ([eV])
1-3 (14)	430 (2.88)	468 (2.65)
1-4 (18)	441 (2.81)	486 (2.55)
1-5 (22)	453 (2.74)	495 (2.51)
1-6 (26)	459 (2.70)	503 (2.47)
1-7 (30)	462 (2.68)	509 (2.44)

[a] Conjugation length (CL) = number of double/triple bonds.

The correlation between the reciprocal value of the CL and the absorption maximum (expressed in eV) is depicted in Figure 5 for the maxima of both the solid state films and the solutions in DCE. We see a similar linear dependence in both media with a closely matching extrapolated  $\lambda_{\text{max}}$  of 2.50 eV (496 nm) in thin film and 2.51 eV (494 nm) in DCE solution. As the absorption maxima in solid films consistently occur at lower energies than observed in solution, whereas in solution the HODAs were shown to be largely planar (*vide supra*), this suggests that the differences in  $\lambda_{\text{max}}$  between solid and solution phase are largely medium effects. In contrast, the appearance of an additional absorption at the long wavelength in the solid-state measurements is attributed to intermolecular interactions, that is,  $\pi$ - $\pi$  stacking. These interactions are dominant in the solid state but do not manifest itself in monodisperse solutions (up to 3 mM) at room temperature, where the steric hindrance from lateral alkyl chains is dominant. This aggregation leads to substantial long-wavelength absorption for longer oligomers, and for example, 1-7 the absorption  $> 550$  nm is clearly not due to properties of isolated oligomer chains. These findings are supported by our previous

measurements of longer members of 2-*n* series.<sup>[15]</sup> It is important to emphasize that this systematic study of the optical properties of this series of oligomers makes it possible to distinguish intra- and intermolecular effects on the optical absorption of extended conjugated systems.

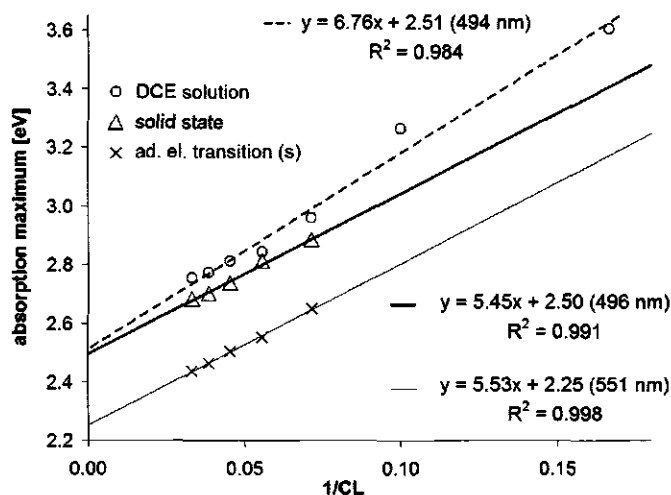


Figure 5.  $\lambda_{\max}$  of the absorption of HODA series 1-*n* (*n* = 3 - 7) in DCE (o) solution at micromolar concentrations ( $2 \cdot 10^{-6}$  M) compared to  $\lambda_{\max}$  of the absorption of drop-casted films ( $\Delta$ ) and  $\lambda_{\max}$  additional electronic transition (x) as function of  $1/CL$ .

### 3.2.4 Temperature-dependent absorption in solution

More insight in the origin of the spectral differences between solution and solid state was obtained by measuring the absorption spectra of HODA 1-7 in methylcyclohexane at lower temperatures (Figure 6). The absorption band at 440 nm shifts upon cooling initially towards the red and a shoulder appears at 470 nm. This is probably owed to restriction of the conformational motion at lower temperatures, resulting in higher population of the lower vibrational levels of the ground state and an slight increase of conjugation. Similar effects were observed by Giesa et. al. for short oligodiacetylenes in methyltetrahydrofuran.<sup>[19]</sup> Upon further cooling an additional absorption band appears around 513 nm, which matches with the additional peak observed in the solid state. Similar thermochromic behavior has been observed for polydiacetylenes in solution<sup>[33]</sup> and other conjugated oligomers<sup>[34]</sup> and polymers,<sup>[35, 36]</sup> and this has been attributed to either intramolecular conformational changes or intermolecular aggregation effects. Yet, for polymers these are frequently difficult to distinguish. To discriminate between these two effects the concentration dependence of the

absorption change was studied. The absorption change at 513 nm upon cooling and subsequent heating of solutions of **1-7** in methylcyclohexane with concentrations of  $\sim 4 \times 10^{-6}$  M and  $\sim 5 \times 10^{-7}$  M is shown in Figure 7.

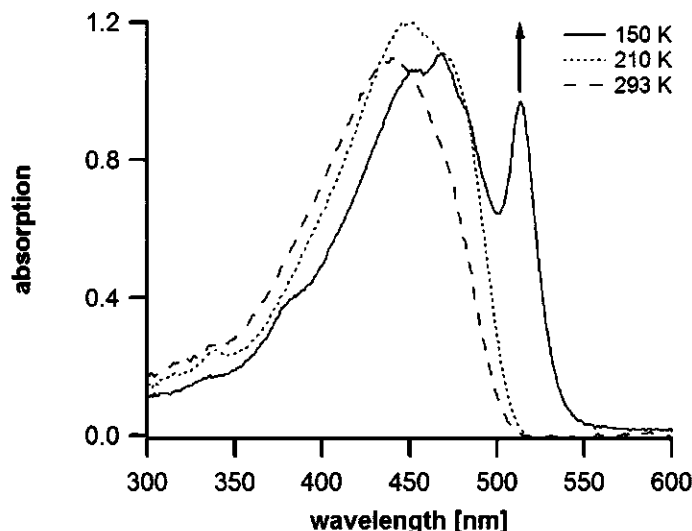


Figure 6. Absorption spectra of HODA **1-7** in methylcyclohexane at 293 K (dashed), 210 K (dotted) and 150 K (solid); data at more intermediate temperatures available in the Supporting Information (Figure 11)

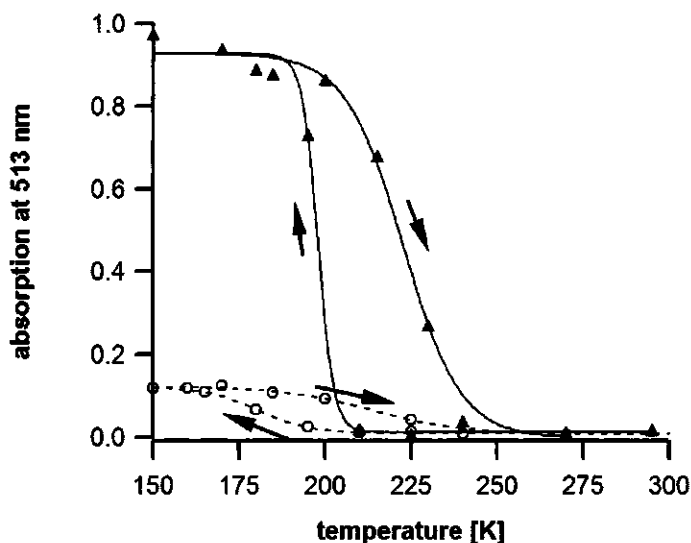


Figure 7. Absorption of HODA **1-7** in methylcyclohexane at 513 nm upon cooling and heating between 293 K and 150 K measured for two solutions with concentrations of  $\sim 4 \times 10^{-6}$  M ( $\blacktriangle$ ) and  $\sim 5 \times 10^{-7}$  M ( $\circ$ ) with sigmoidal curves fitted to the data.

The temperature at which the absorption change takes place is dependent on the concentration of the oligomer. The data was fitted to a sigmoidal curve from which the transition temperature was obtained. The transition temperature is the temperature at which the value of the absorption change is half of the maximum absorption change. In a solution of **1-7** with a concentration of  $\sim 4 \times 10^{-6}$  M the transition temperature upon cooling is 198 K, whereas for a solution of  $\sim 5 \times 10^{-7}$  M the transition takes place at 180 K. The concentration dependence of the chromatic transition shows that the additional absorption band at 513 nm arises as a result of intermolecular  $\pi$ - $\pi$  stacking interactions and is not owed to conformational changes. The system shows significant hysteresis upon heating of the sample. The transition temperatures shift to 224 K and 214 K for the solutions with concentrations of respectively  $4 \times 10^{-6}$  M and  $5 \times 10^{-7}$  M. This suggests that the aggregation process is relatively slow. Similar hysteresis was found for polydiacetylenes in 1,2-dichloroethane by Wenz et al.<sup>[37]</sup> These experiments strongly suggest that the thermochromism of polydiacetylenes in solution is not solely caused by a conformational coil-to-rod transition but that intermolecular interactions play an important role in the absorption change.

### 3.2.5 Steady-state fluorescence in solution

Emission spectra measured for millimolar solutions of the HODA series were recorded in *n*-hexane (Figure 8). The maximum fluorescence quantum yield ( $\Phi_f$ ) is observed for the homocoupled monomer **1-1** ( $\Phi_f = 0.041$ ; see Table 3), and decreases with increasing chain length. The emission maximum (expressed in eV) decreases with an increasing chain length *n* and shows a linear relation with the reciprocal value of the conjugation length (Figure 8 inset), analogous to data previously reported for **2-*n***.<sup>[15]</sup> This supports a continuously increasing conjugation of these oligomers, without major distortions or conformational changes in line with data for the absorption maximum versus 1/CL (Figures 3 and 5). The extrapolated value for the  $\lambda_{\max}$  of the emission for the polymer ( $n = \infty$ ) is 2.43 eV (510 nm; Figure 10 bottom). In addition, for this series of HODAs up to CL = 30 we do not see any saturation in the evolution of  $\lambda_{\max}$  of the emission as function of the chain length. In other words: Up to this length no evidence is observed for truncation of the C-C conjugation as would be suggested by the concept of effective conjugation length.

The values of the  $\lambda_{\max}$  emission are of higher energy compared to the literature data for **2-*n***, that is, **1-7** with CL = 30 has the  $\lambda_{\max}$  emission of 492 nm compared to 520 nm for the shorter **2-8** with 17 conjugated double and triple bonds. Apparently, the chromophore of HODAs is different from that of the **2-*n*** series and deserves future spectroscopic and theoretical studies. The 0-0 transition is not detectable for this series, which was also the



situation for the low emitting **2-*n*** of similar CL. Therefore, it is not possible to study the evolution of the Stokes shift for this series. The fluorescence quantum yield is only marginal ( $\leq 0.012$ ) for the HODAs having CL  $\geq 6$ , which is even lower than the values reported for **2-*n***. The  $\Phi_f$  decreases down to 0.001 for the longest member of this series. This tendency is in line with the observation that PDA polymers show marginal fluorescence quantum yields, mostly lower than 0.001.<sup>[30, 38]</sup>

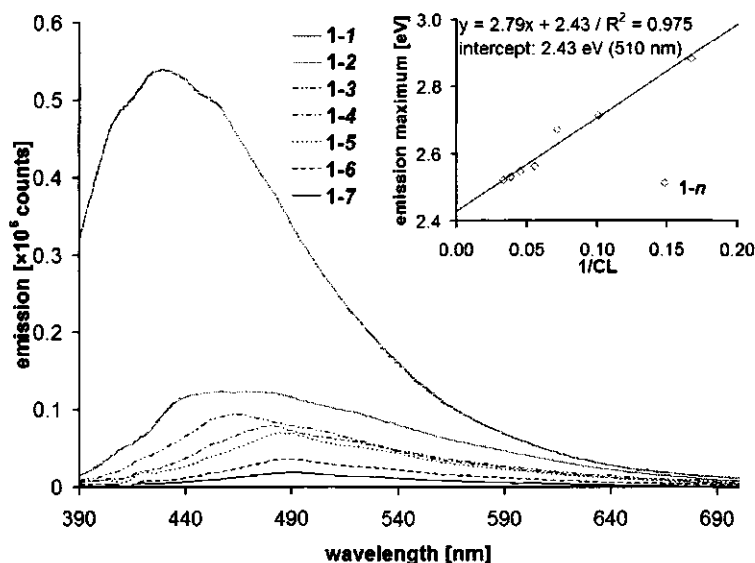


Figure 8. Fluorescence spectra of HODAs **1-*n*** ( $n = 1 - 7$ ) in *n*-hexane; inset: Emission maxima of HODA solutions in *n*-hexane versus  $1/\text{CL}$ .

Table 3. Emission data of HODAs **1-*n*** ( $n = 1 - 7$ ) in *n*-hexane.

<b>1-<i>n</i></b> (CL) <sup>[a]</sup>	Emission $\lambda_{\text{max}}$ [nm] ([eV])	Quantum Yield $\Phi_f$ <sup>[b,c]</sup>
<b>1-1</b> (6)	430 (2.88)	0.041
<b>1-2</b> (10)	457 (2.71)	0.012
<b>1-3</b> (14)	464 (2.67)	0.008
<b>1-4</b> (18)	484 (2.56)	0.006
<b>1-5</b> (22)	487 (2.55)	0.005
<b>1-6</b> (26)	490 (2.53)	0.003
<b>1-7</b> (30)	492 (2.52)	0.001
<b>1-1</b> (6)	430 (2.88)	0.041

[a] Conjugation length (CL) = number of double/triple bonds; [b] quantum yield determined by comparison with quinine bisulfate in 0.1M  $\text{H}_2\text{SO}_4$ ;  $\Phi_f = 0.535$  <sup>[39]</sup>; [c] experimental error  $\pm 0.002$ .

### 3.2.5 Fluorescence lifetimes and anisotropy

Picosecond time-resolved single photon counting with  $\lambda_{\text{ex}} = 372$  nm was used to determine the fluorescence lifetimes ( $\tau_f$ ) of the oligomers series **1-n**. The observed lifetimes in the HODA series measured in *n*-hexane are shown in Table 4. The decay curves of **1-1** to **1-3** required fitting with two exponentials; the marginal decays determined for **1-4** up to **1-7** (lifetimes,  $\tau \leq 10$  ps) required only one exponent. The average lifetime  $\tau_{\text{AVG}}$  was calculated according to Equation 1:

$$\tau_{\text{AVG}} = \frac{A_1}{A_1 + A_2} \tau_1 + \frac{A_2}{A_1 + A_2} \tau_2 \quad (1)$$

where  $A_1$  and  $A_2$  are the contributions of the decays obtained from the curve fitting. The data in Table 4 indicate that the excited-state lifetimes of oligomers are in line with the trend shown for the fluorescence quantum yield:  $\tau_f$  decreases rapidly with increasing chain length. Moreover, the longest lifetimes are recorded for the shortest oligomers **1-1** and **2-2**, which have the conjugation length of CL = 6 and 10, respectively. This tendency is in line with the previously presented data for **2-n**,<sup>[15]</sup> which showed the  $\tau_{\text{AVG}}$  maximum for the trimer with CL = 7.

Table 4. Fluorescence lifetimes  $\tau_f$  (in ps), their relative weights  $A$ , and average lifetimes  $\tau_{\text{AVG}}$  (in ps).

<b>1-n</b> (CL) <sup>[a]</sup>	$\tau_1$ ( $A_1$ ) <sup>[b]</sup>	$\tau_2$ ( $A_2$ ) <sup>[b]</sup>	$\tau_{\text{AVG}}$ <sup>[b, c]</sup>
<b>1-1</b> (6)	40 (71)	252 (29)	101
<b>1-2</b> (10)	54 (49)	126 (51)	91
<b>1-3</b> (14)	19 (94)	576 (6)	55

[a] conjugation length as number of double and triple bonds. [b]  $\tau_f$  [ps] (relative amplitudes) [c] calculated using Eq. 1

Fluorescence depolarization ( $r$ ) of the HODAs under present study was determined by picosecond time-resolved fluorescence anisotropy measurements.<sup>[40]</sup> The resulting anisotropy lifetime is determined by the shape, size, and flexibility of the rotating molecule. This technique has proven to be useful in our recent investigations of the conformational behavior of rod-shaped **2-n**. Based on the experiments that reveal extended conjugation (*vide supra*) it is assumed that the HODAs also possess a relatively large axial ratio, and that their rotation around the longitudinal axis progresses much faster compared to the rotation around the short, perpendicular axes. Therefore, the observed anisotropy decay kinetics  $r(t)$  of HODAs are indeed mono-exponential and characterized by an initial anisotropy value  $r_0$  and one rotation correlation time ( $\tau_R$ ) according to Equation 2:<sup>[39]</sup>

$$r(t) = r_0 \cdot \exp(-t / \tau_R) \quad (2)$$

in which  $r_0$  is determined by the angle  $\gamma$  between the absorption and emission transition moment (Equation 3):

$$r_0 = (3\cos^2 \gamma - 1) / 5 \quad (3)$$

The recorded initial anisotropy values  $r_0$  for HODAs series was 0.3, which indicates a small angle ( $\sim 15^\circ$ ) between absorption and emission transition moments. This tendency is analogous to the trends shown for long oligodiacetylene oligomers **2-n**<sup>[15]</sup> and the trimeric oligodiacetylenes investigated previously.<sup>[12, 21, 30]</sup> The rotation correlation times  $\tau_R$  for HODAs recorded in *n*-hexane are listed in Table 5. Because longer oligomers display a marginal emission the experimental error for these measurements was relatively high.

Table 5. The rotation correlation time  $\tau_R$  of 1-*n* (*n* = 1 - 8).

1- <i>n</i> (CL) <sup>[a]</sup>	$\tau_R$ [ps]
1-1 (6)	$1.25 \times 10^2 (\pm 0.20 \times 10^2)$
1-2 (10)	$1.94 \times 10^2 (\pm 0.20 \times 10^2)$
1-3 (14)	$2.6 \times 10^2 (\pm 0.3 \times 10^2)$
1-4 (18)	$3.0 \times 10^2 (\pm 0.3 \times 10^2)$
1-5 (22)	$3.2 \times 10^2 (\pm 0.4 \times 10^2)$
1-6 (26)	$3.7 \times 10^2 (\pm 0.5 \times 10^2)$
1-7 (30)	$4.3 \times 10^2 (\pm 0.5 \times 10^2)$

[a] Conjugation length (CL) = number of double/triple bonds.

The anisotropy lifetimes showed an increase with the oligomer length indicating an increased rotation time around perpendicular axis for longer oligomers. This is illustrated in Figure 9 in which a linear dependence for  $\tau_R$  and the length of the oligomer is depicted. Such linearity has recently also been reported by us<sup>[15]</sup> and others<sup>[41]</sup> for largely fully stretched species of similar sizes where under simplifying conditions,<sup>[39]</sup>  $\tau_R = \eta V / RT$ , and the molecular volume  $V \approx \ell r^2$  ( $\eta$  = viscosity,  $\ell$  = length of the molecule, and  $r$  = molecular diameter). In other words: The  $\tau_R$  values are proportional to the molecular length  $\ell$ .

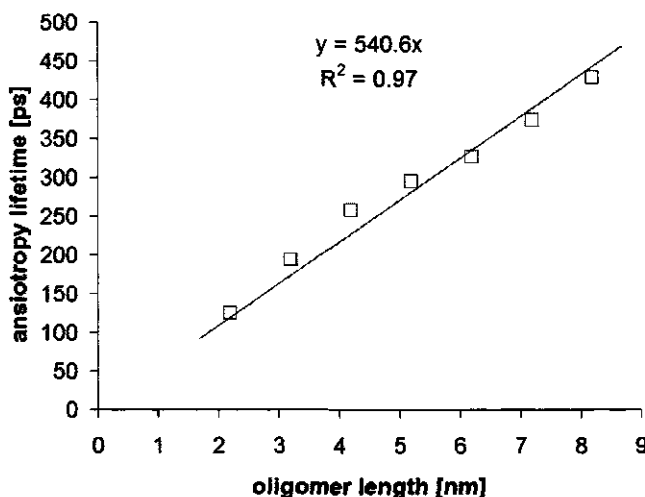


Figure 9. Anisotropy lifetimes vs. the estimated length of HODA series 1-*n* with *n* = 1 – 7 up to 8.2 nm.

The observed correlation of  $\tau_R$  with the molecule in its fully extended shape provides clear evidence, that there are no significant geometrical changes of HODA structures within this series, because otherwise  $\tau_R$  would have increased less than linearly with conjugation length CL or the length of the fully extended system. Therefore, we conclude that the long HODAs up to 30 double and triple bonds do behave like conformationally rigid, molecular rods.<sup>[42]</sup>

### 3.3 Conclusion

A novel, nanometer-sized and highly soluble HODA series was synthesized on a multi-milligram scale through a mild, catalytic coupling under ambient conditions with high yields and purity. The series ranges up to 30 conjugated double and triple bonds with an estimated length of 8.2 nm and therefore is one of the longest synthesized, fully conjugated series of aromatic-free molecular wires.

The absorption and emission of HODAs show a bathochromic shift upon chain elongation. Furthermore, the thin film absorption measurements show an additional high-wavelength absorption for all solid HODAs, which we attribute to the intermolecular stacking of  $\pi$ - $\pi$  systems. In solution at room temperature, the steric hindrance from lateral alkyl chains of the HODA backbone prevents this aggregation up to millimolar concentration. However, cooling of solutions of HODA 1-7 gives rise to formation of aggregates with absorption spectra similar to those of the solid HODA.

The dependency of the maxima of both the absorption and the emission on the reciprocal conjugation length is found to be linear and is similar with the correlation reported for the 2-*n* series. Moreover, this linearity is also observed for the  $\epsilon_{\text{max}}$  of the absorption in *n*-hexane and DCE. These observations are in line with the linear correlation found for the rotational correlation times as a function of the oligomer length. These patterns evidently show the continuously increased conjugation in the 1-*n* series up to 30 double and triple bonds.

## 3.4 Experimental Section

### 3.4.1 Solvents and reagents

For all dry reactions performed under a steady stream of argon (or reductive atmosphere of argon/hydrogen mixture 1:1), the equipment was dried in an oven at 150 °C for several hours and allowed to cool down in an atmosphere of dry nitrogen or argon. Pure, dry, and degassed ether and tetrahydrofuran (THF) were obtained by distillation of the commercial material over sodium particles. CH<sub>2</sub>Cl<sub>2</sub> was distilled and dried over calcium hydride or sodium hydride. Dry DMF was purchased from Sigma-Aldrich and stored under argon. All other specified chemicals were commercially purchased (Aldrich, Fluka or Riedel-de Haën) and used without further purification.

### 3.4.2 General work up & purification procedure

Reaction monitoring and reagents visualization was performed on silica gel or reversed phase silica gel plates with UV-light (254 and 366 nm) combined with GC/MS. Usually the reaction mixture was diluted with water and extracted 3x with an organic solvent (petroleum ether 40-60, hexane, or ethyl acetate). The combined organic extracts were washed with brine and dried over anhydrous sodium sulfate prior to filtration and evaporation of the solvent under reduced pressure. Flash chromatography was performed on commercially available silica gel (0.035 - 0.070 nm pore diameter) and mixtures of freshly distilled petroleum ether 40/60 and ethyl acetate or reversed phase silica gel (0.04 - 0.06 nm pore diameter, Screening Devices) with freshly distilled mixtures of acetonitrile and ethyl acetate. Final purification was performed on Shimadzu preparative HPLC using a C18 column (Alltech Alltima 250 mm × 22mm; 5μ) with HPLC-grade water, acetonitrile and ethyl acetate mixture.

### 3.4.3 Nuclear Magnetic Resonance spectroscopy and Mass Spectroscopy

<sup>1</sup>H NMR and <sup>13</sup>C NMR spectra were determined on a Bruker CXP 300 NMR-spectrometer in CDCl<sub>3</sub> solutions unless indicated otherwise. Chemical shifts are reported in ppm downfield relative to tetramethylsilane ( $\delta$  = 0 ppm for <sup>1</sup>H) or based on the solvent peak (CDCl<sub>3</sub>) ( $\delta$  = 77.00 ppm for <sup>13</sup>C NMR) as an internal standard. HRMS was performed on Finnigan Mat95 mass spectrometer. MALDI-TOF MS analysis was performed on UltraFlex TOF (Bruker Daltonics Bremen).

### 3.4.4 Steady-state absorption and fluorescence

Absorption spectra of the oligodiacetylenes in *n*-hexane (spectrophotometric grade, Riedel-de Haën) and DCE (spectrophotometric grade, Sigma-Aldrich) were recorded using a Cary 100 UV-Vis spectrophotometer (scan range: 200 - 800 nm, scan rate: 300 nm min<sup>-1</sup>, date interval 0.5 nm) and steady-

state fluorescence using a FLS920P Spectrometer (slit exc.: 2 nm, slit em.: 2 nm, step: 1.0, dwell: 0.2 s). Absorption spectra of oligodiacetylenes in film via drop casting were recorded on a Cary 50 UV-Vis spectrophotometer (scan range 200 - 850 nm, scan rate 300 nm/min, data interval 0.5 nm). Absorption spectra at low temperatures in methylcyclohexane (spectrophotometric grade, Sigma-Aldrich) were obtained with an LP920 spectrophotometer (Edinburgh Instruments Limited) fitted with a 450 W Xe arc lamp as probe-light source, a red-sensitive photomultiplier (R928, Hamamatsu) as detector and a cryostat (Optistat DN; Oxford Instruments, UK) with temperature controller (ITC 503S; Oxford Instruments, UK) as sample holder.

### 3.4.5 Determination of fluorescence quantum yield in solution

In order to evaluate the fluorescence quantum yield ( $\Phi_f$ ) of the ODA's solution in *n*-hexane and DCE, the areas of the corrected emission spectra were compared to a spectrum of a reference solution of quinine bisulfate in 0.1 M H<sub>2</sub>SO<sub>4</sub> measured at 366 nm having  $\Phi_f = 0.535$ .<sup>[39]</sup> The fluorescence quantum yields of the ODA's were determined using the relationship:

$$\Phi_f = \Phi_f \frac{I_{OD_R} n^2}{I_R OD n_R^2} \quad (4)$$

where  $I$  and  $I_R$  are the integrated emission intensities of the ODA and quinine bisulfate solutions, respectively, OD refers to the optical densities of the respective solutions and  $n$  is the refractive index.

### 3.4.5 Lifetime of fluorescence and fluorescence anisotropy in solution

The fluorescence lifetime and anisotropy were recorded using a FLS920P Spectrometer (Edinburgh Instruments) for time correlated photon counting (TCSP) (time set up: 5 or 10 ns, 4096 channels, 10000 counts for 1-1 to 1-4, 1000 counts for 1-5 to 1-7). Pulsed diode lasers (372 nm, FWHM: 54 ps; 444 nm, FWHM: 63 ps) and pulsed LED's (283 nm, FWHM <500 ps; 304 nm, FWHM: < 350 ps) from PicoQuant were used as light sources. The anisotropy measurements were performed using vertical and horizontal polarizations. All spectroscopic measurements were carried out under magic angle condition unless stated otherwise to avoid the possible influence of rotational motions of the probe molecules.

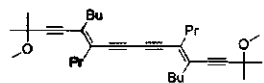
### 3.4.6 General method for synthesis of (1-*n*) series via (a) protodesilylation of oligodiacetylenes (2-*n*) followed by (b) catalytic homocoupling of oligodiacetylenes (3-*n*) under Sonogashira conditions as illustrated in Figure 2

The synthesis of the crosscoupled oligodiacetylene (2-*n*) was performed according to the procedure described elsewhere.<sup>[15]</sup>

(a) A solution of (2-*n*) (1 eq) in THF/MeOH (1:1, 5ml/mmol) was stirred in round-bottomed flask. H<sub>2</sub>O (3 drops/mmol) and K<sub>2</sub>CO<sub>3</sub> (2 eq) is added to the solution and stirred for 3 h. After working up following the general procedure, the terminal acetylene (3-*n*) was submitted to the catalytic homocoupling step (b).

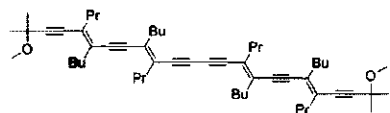
(b) A mixture of terminal acetylene (3-*n*), Pd(PPh<sub>3</sub>)<sub>4</sub> (7 mol%), CuI (8 mol %), distilled diethyl amine (2 ml/mmol) and THF (5 ml/mmol) was placed in a round-bottomed flask, equipped with a magnetic stirrer. The mixture was stirred for 3 h at 25 °C under ambient atmosphere, concentrated and filtrated over a short silica gel column (5% Et<sub>3</sub>N solution in petroleum ether 40/60). The residue was pre-purified on reversed phase silica (ACN/EtOAc) and finally purified on preparative HPLC to give pure (99.5%) HODA (1-*n*).

### 3.4.7 (5E,11E)-5,12-dibutyl-2,15-dimethoxy-2,15-dimethyl-6,11-dipropylhexadeca-5,11-dien-3,7,9,13-tetrayne (1-1)



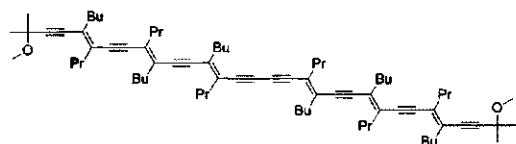
pale yellow liquid (1.00 mmol, 0.490 g, 96%) from (2-1) (2.08 mol, 0.662 g);  $^1\text{H}$  NMR:  $\delta$  = 0.91-0.96 (m, 12H), 1.30-1.43 (m, 4H), 1.50 (12H), 1.50-1.65 (8H), 2.37-2.47 (8H), 3.38 (6H)  $^{13}\text{C}$  NMR:  $\delta$  = 13.57, 13.92, 21.74, 22.00, 28.34, 30.58, 34.96, 36.75, 51.74, 71.18, 82.17, 83.50, 83.60, 102.23, 128.09, 133.33; HRMS: observed (490.3815); calculated (490.3811).

### 3.4.8 (5E,9E,15E,19E)-5,9,16,20-tetrabutyl-2,23-dimethoxy-2,23-dimethyl-6,10,15,19-tetrapropyltetracos-5,9,15,19-tetraen-3,7,11,13,17,21-hexayne (1-2)



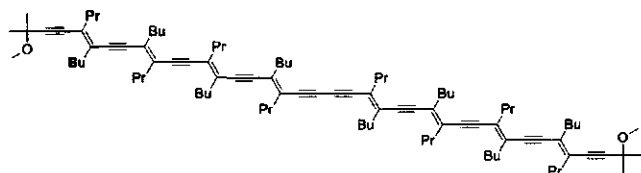
pale yellow liquid (0.29 mmol, 0.231 g, 85%) from (2-2) (0.69 mol, 0.322 g);  $^1\text{H}$  NMR:  $\delta$  = 0.88-0.96 (m, 24H), 1.29-1.41 (m, 8H), 1.51 (s, 12H), 1.49-1.66 (m, 16H), 2.41-2.52 (m, 16H), 3.39 (s, 6H);  $^{13}\text{C}$  NMR:  $\delta$  = 13.59, 13.93, 13.99, 21.75, 21.89, 22.06, 22.22, 28.41, 29.70, 30.67, 30.75, 34.96, 35.13, 36.94, 37.08, 51.72, 71.20, 82.93, 83.90, 84.58, 97.88, 100.46, 100.69, 127.77, 129.23, 129.59, 133.97; HRMS: observed (786.6318); calculated (786.6315).

### 3.4.9 (5E,9E,13E,19E,23E,27E)-5,9,13,20,24,28-hexabutyl-2,31-dimethoxy-2,31-dimethyl-6,10,14,19,23,27-hexapropyltriaconta-5,9,13,19,23,27-hexaen-3,7,11,15,17,21,25,29-octayne (1-3)



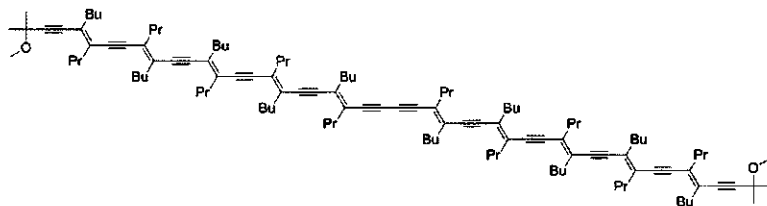
yellow liquid (0.46 mmol, 0.499 g, 84%) from (2-3) (1.10 mol, 0.677 g);  $^1\text{H}$  NMR:  $\delta$  = 0.88-0.97 (m, 36H), 1.28-1.42 (m, 12H), 1.51 (s, 12H), 1.51-1.68 (m, 24H), 2.42-2.53 (m, 24H), 3.39 (s, 6H);  $^{13}\text{C}$  NMR:  $\delta$  = 13.59, 13.61, 13.93, 13.99, 21.74, 21.91, 22.07, 22.23, 22.28, 28.42, 29.69, 30.68, 30.77, 30.83, 34.94, 35.13, 36.97, 37.10, 37.27, 51.71, 71.21, 83.08, 83.98, 84.74, 98.34, 98.63, 99.00, 100.46, 101.05, 127.79, 128.94, 129.13, 129.40, 129.74, 130.31, 134.01; HRMS: observed (1082.8840); calculated (1082.8819).

### 3.4.10 (5E,9E,13E,17E,23E,27E,31E,35E)-5,9,13,17,24,28,32,36-octabutyl-2,39-dimethoxy-2,39-dimethyl-6,10,14,18,23,27,31,35-octapropyltetraconta-5,9,13,17,23,27,31,35-octaen-3,7,11,15,19,21,25,29,33,37-decayne (1-4)



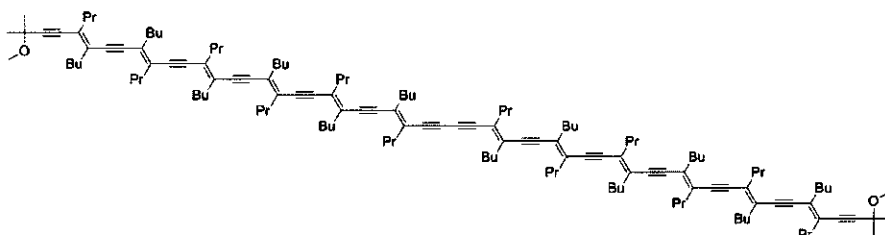
yellow solid (0.29 mmol, 0.400 g, 80%) from (2-4) (0.72 mol, 0.550 g);  $^1\text{H}$  NMR:  $\delta$  = 0.87-0.97 (m, 48H), 1.27-1.41 (m, 16H), 1.51 (s, 12H), 1.51-1.70 (m, 32H), 2.41-2.53 (m, 32H), 3.39 (s, 6H);  $^{13}\text{C}$  NMR:  $\delta$  = 13.59, 13.62, 13.94, 13.99, 21.75, 21.92, 22.08, 22.23, 22.29, 28.42, 29.70, 30.69, 30.78, 30.85, 34.93, 35.10, 35.14, 36.98, 37.11, 37.30, 51.71, 71.21, 83.10, 84.01, 84.78, 98.44, 98.78, 98.80, 99.09, 99.60, 100.39, 101.15, 127.80, 128.98, 129.12, 129.45, 129.86, 129.93, 130.37, 134.02; HRMS: observed (1379.1306); calculated (1379.1323); MALDI-TOF-MS: observed (1379.01).

**3.4.11 (5E,9E,13E,17E,21E,27E,31E,35E,39E,43E)-5,9,13,17,21,28,32,36,40,44-decabutyl-2,47-dimethoxy-2,47-dimethyl-6,10,14,18,22,27,31,35,39,43-decapropyloctatetraconta-5,9,13,17,21,27,31,35,39,43-decaen-3,7,11,15,19,23,25,29,33,37,41,45-dodecayne (1-5)**



yellow/orange solid (0.097 mmol, 0.163 g, 81%) from (2-5) (0.24 mol, 0.219 g);  $^1\text{H}$  NMR:  $\delta$  = 0.83-0.98 (m, 60H), 1.27-1.42 (m, 20H), 1.51 (s, 12H), 1.51-1.70 (m, 40H), 2.43-2.52 (m, 40H), 3.39 (s, 6H);  $^{13}\text{C}$  NMR:  $\delta$  = 13.59, 13.62, 13.93, 13.99, 21.75, 21.92, 22.08, 22.23, 22.30, 28.43, 29.35, 29.69, 30.69, 30.79, 30.86, 34.93, 35.11, 35.14, 36.98, 37.11, 37.30, 51.71, 71.21, 83.11, 84.02, 84.79, 98.48, 98.74, 98.80, 99.20, 99.24, 99.39, 99.69, 100.37, 101.17, 127.81, 128.94, 128.99, 129.16, 129.17, 129.46, 129.50, 129.71, 129.81, 129.92, 130.38, 134.02; HRMS: observed (1675.3814); calculated (1675.3827); MALDI-TOF-MS: observed (1675.25).

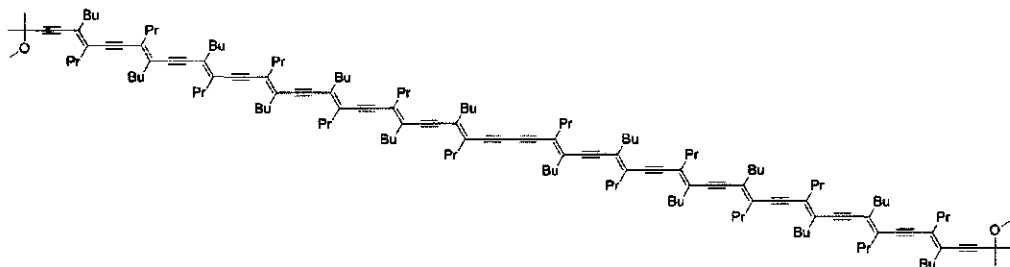
**3.4.12 (5E,9E,13E,17E,21E,25E,31E,35E,39E,43E,47E,51E)-5,9,13,17,21,25,32,36,40,44,48,52-dodecabutyl-2,55-dimethoxy-2,55-dimethyl-6,10,14,18,22,26,31,35,39,43,47,51-dodecapropylhexapentaconta-5,9,13,17,21,25,31,35,39,43,47,51-dodecaen-3,7,11,15,19,23,27,29,33,37,41,45,49,53-tetradecayne (1-6)**



orange solid (0.049 mmol, 0.097 g, 82%) from (2-6) (0.12 mol, 0.127 g);  $^1\text{H}$  NMR:  $\delta$  = 0.85-0.98 (m, 72H), 1.27-1.42 (m, 24H), 1.51 (s, 12H), 1.51-1.69 (m, 48H), 2.45-2.55 (m, 48H), 3.39 (s, 6H);  $^{13}\text{C}$  NMR:  $\delta$  = 13.59, 13.63, 13.94, 14.00, 21.74, 21.92, 22.07, 22.23, 22.30, 28.41, 29.69, 30.68, 30.77, 30.85, 34.92, 35.09, 35.12, 36.96, 37.10, 37.31, 51.71, 71.20, 83.08, 84.01, 84.82, 98.47, 98.52, 98.70, 98.79, 99.26, 99.34, 99.48, 99.71, 100.32, 101.17, 127.81, 128.91, 129.22, 129.47, 129.66, 129.76, 129.93, 130.38, 134.01; MALDI-TOF-MS: observed (1971.41); calculated (1971.63).



**3.4.13 (5E,9E,13E,17E,21E,25E,29E,35E,39E,43E,47E,51E,55E,59E)-5,9,13,17,21,25,29,36,40,44,48,52,56,60-tetradecabutyl-2,63-dimethoxy-2,63-dimethyl-6,10,14,18,22,26,30,35,39,43,47,51,55,59-tetradecapropyltetrahexaconta-3,7,11,15,19,23,27,31,33,37,41,45,49,53,57,61-hexadecayne (1-7)**



orange/red solid (0.040 mmol, 0.091 g, 79%) from (2-7) (0.10 mol, 0.119 g);  $^1\text{H}$  NMR:  $\delta$  = 0.87-0.98 (m, 84H), 1.27-1.41 (m, 28H), 1.51 (s, 12H), 1.51-1.68 (m, 56H), 2.45-2.55 (m, 56H), 3.39 (s, 6H);  $^{13}\text{C}$  NMR:  $\delta$  = 13.59, 13.63, 13.93, 14.00, 21.75, 21.93, 22.08, 22.23, 22.31, 28.42, 29.69, 30.69, 30.79, 30.87, 34.93, 35.10, 35.14, 36.98, 37.11, 37.31, 37.33, 51.71, 71.22, 83.12, 84.03, 84.80, 98.49, 98.71, 98.82, 98.85, 99.26, 99.27, 99.31, 99.38, 99.42, 99.51, 99.71, 99.74, 100.39, 101.17, 127.81, 128.92, 129.00, 129.18, 129.21, 129.24, 129.47, 129.71, 129.77, 129.93, 130.38, 134.02; MALDI-TOF-MS: observed (2267.67); calculated (2267.88).

## 3.5 Acknowledgements

The authors thank the Dutch Technology Foundation STW for generous funding of this research (Project No. WPC 5740), and Dr. Jan Kroon (ECN), Dr. Herman Schoo (TNO), Dr. Joost Smits (Shell) and Prof. Wybren Jan Buma (Univ. of Amsterdam) for helpful discussions.

## 3.6 Supporting Information

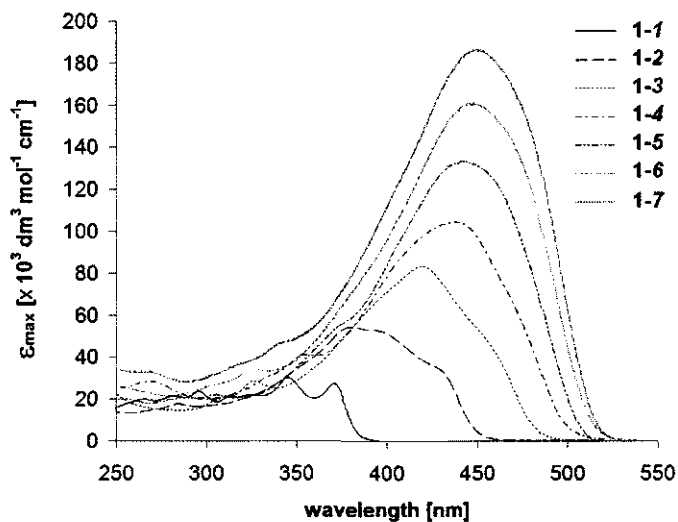


Figure 10. Electronic absorption spectra of homocoupled oligodiacylenes **1-n** ( $n = 1-7$ ) in DCE

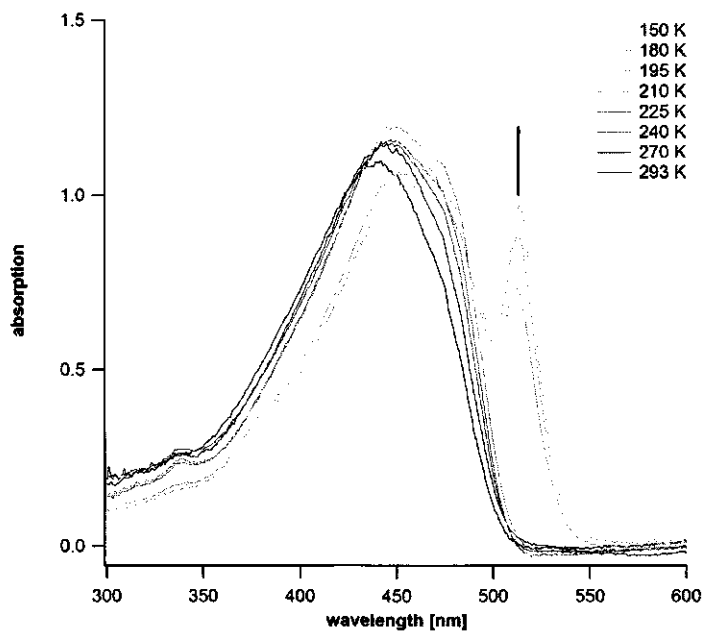


Figure 11. Absorption spectra of HODA **1-7** in methylcyclohexane

## 3.7 References

- [1] M. Surin, R. Lazzaroni, W. J. Feast, A. P. H. J. Schenning, E. W. Meijer and P. Leclerc, *Synth. Met.* **2004**, *147*, 67-72.
- [2] J. G. Rodriguez and J. L. Tejedor, *J. Org. Chem.* **2002**, *67*, 7631-7640.
- [3] A. Aviram and M. A. Ratner, *Chem. Phys. Lett.* **1974**, *29*, 277-283.
- [4] A. Pron and P. Rannou, *Prog. Polym. Sci.* **2002**, *27*, 135-190.
- [5] N. Tessler, D. J. Pinner and P. K. H. Ho, *Opt. Mater.* **2001**, *17*, 155-160.
- [6] J. H. Burroughes, C. A. Jones and R. H. Friend, *Nature* **1988**, *335*, 137-141.
- [7] Y. Zhu, A. Babel and S. A. Jenekhe, *Macromolecules* **2005**, *38*, 7983-7991.
- [8] S. A. Jenekhe, *Chem. Mater.* **2004**, *16*, 4381-4382.
- [9] J. M. Tour, *Chem. Rev.* **1996**, *96*, 537-553.
- [10] R. E. Martin and F. Diederich, *Angew. Chem. Int. Ed.* **1999**, *38*, 1350-1377.
- [11] M. Polhuis, C. C. J. Hendrikx, H. Zuilhof and E. J. R. Sudhölter, *Tetrahedron Lett.* **2003**, *44*, 899-901.
- [12] C. C. J. Hendrikx, M. Polhuis, A. Pul-Hootsen, R. B. M. Koehorst, A. Hoek van, H. Zuilhof and E. J. R. Sudhölter, *Phys. Chem. Chem. Phys.* **2005**, *7*, 548-553.
- [13] Y. Takayama, C. Delas, K. Muraoka and F. Sato, *Org. Lett.* **2003**, *5*, 365-368.
- [14] Y. Takayama, C. Delas, K. Muraoka, M. Uemura and F. Sato, *J. Am. Chem. Soc.* **2003**, *125*, 14163-14167.
- [15] G. S. Pilzak, B. van Lagen, C. C. J. Hendrikx, E. J. R. Sudhölter and H. Zuilhof, *Chem. Eur. J.* **2008**, *14*, 7939-7950.
- [16] G. S. Pilzak, B. van Lagen, E. J. R. Sudhölter and H. Zuilhof, *Tetrahedron Lett.* **2008**, *49*, 4949-4952.
- [17] A. Elangovan, Y.-H. Wang and T.-I. Ho, *Org. Lett.* **2003**, *5*, 1841-1844.
- [18] F. Wudl and S. P. Bitler, *J. Am. Chem. Soc.* **1986**, *108*, 4685-4687.
- [19] R. Giesa and R. C. Schulz, *Polym. Int.* **1994**, *33*, 43-60.
- [20] B. E. Kohler and D. E. Schilke, *J. Chem. Phys.* **1987**, *86*, 5214-5215.
- [21] G. M. Balkowski, M. Groeneveld, H. Zhang, C. C. J. Hendrikx, M. Polhuis, H. Zuilhof and W. J. Buma, *J. Phys. Chem. A* **2006**, *110*, 11435-11439.
- [22] N. S. Bayliss and E. G. McRae, *J. Phys. Chem.* **1954**, *58*, 1002-1006.
- [23] C. Reichardt, *Solvents and Solvent Effects in Organic Chemistry*, Wiley-VCH, **2003**, p. 630.
- [24] D. V. Matyushov, R. Schmid and B. M. Ladanyi, *J. Phys. Chem. B* **1997**, *101*, 1035-1050.
- [25] H. Kuhn, *J. Chem. Phys.* **1949**, *17*, 1198-1212.
- [26] H. Kuhn, *J. Chem. Phys.* **1958**, *29*, 958-959.
- [27] N. Li, K. Jia, S. Wang and A. Xia, *J. Phys. Chem. A* **2007**, *111*, 9393-9398.
- [28] N. E. Craft and J. H. Scares Jr, *J. Agric. Food Chem.* **1992**, *40*, 431-434.
- [29] R. E. Martin, U. Gubler, J. Cornil, M. Balakina, C. Boudon, C. Bosshard, J.-P. Gisselbrecht, F. Diederich, P. Günter, M. Gross and J.-L. Brédas, *Chem. Eur. J.* **2000**, *6*, 3622-3635.
- [30] H. Zuilhof, H. M. Barentsen, M. Dijk van, E. J. R. Sudhölter, R. J. O. M. Hoofman, L. D. A. Siebbeles, M. P. Haas de and J. M. Warman in *Polydiacetylenes*, (Ed. H. S. Nalwa), Academic Press, San Diego, San Francisco, New York, Boston, London, Sydney, Tokyo, **2001**, pp. 339-437.
- [31] J. Gierschner, J. Cornil and H. Egelhaaf, *J. Adv. Mat.* **2007**, *173*-191.
- [32] S. S. Zade and M. Bendikov, *Org. Lett.* **2006**, *8*, 5243-5246.
- [33] B. Chu and R. L. Xu, *Acc. Chem. Res.* **1991**, *24*, 384-389.
- [34] J. J. Apperloo, R. A. J. Janssen, P. R. L. Malenfant and J. M. J. Frechet, *Macromolecules* **2000**, *33*, 7038-7043.
- [35] F. J. M. Hoebe, P. Jonkheijm, E. W. Meijer and A. Schenning, *Chem. Rev.* **2005**, *105*, 1491-1546.
- [36] N. Lebouch, S. Garreau, G. Louarn, M. Belletete, G. Durocher and M. Leclerc, *Macromolecules* **2005**, *38*, 9631-9637.

- [37] G. Wenz, M. A. Müller, M. Schmidt and G. Wegner, *Macromolecules* **1984**, *17*, 837-850.
- [38] R. Lécuyer, J. Berrehar, C. Lapersonne-Meyer and M. Schott, *Phys. Rev. Lett.* **1998**, *80*, 4068-4071.
- [39] J. R. Lakowicz, *Principles of Fluorescence Spectroscopy*, Kluwer Academic / Plenum Publishers, **2006**, p. 420-421.
- [40] P. Kapusta, R. Erdmann, U. Ortmann and M. Wahl, *J. Fluoresc.* **2003**, *13*, 179-183.
- [41] N. Aratani, Z. S. Yoon, D. Kim and A. Osuka, *J. Chin. Chem. Soc.* **2006**, *53*, 41-46.
- [42] Theoretical studies that further clarify this effect are currently ongoing in our laboratories.

# Chapter 4

## Hybrid Conjugated Organic Oligomers Consisting of Oligodiacetylene and Thiophene Units: Synthesis and Study of Their Optical Properties

### Abstract

Novel and highly soluble hybrid conjugated organic oligomers consisting of oligodiacetylene and thiophene units have been synthesized in high purity via iterative and divergent approaches based on a sequence of Sonogashira reactions. The series of thiophene-containing oligodiacetylenes (ThODAs) and homocoupled ThODAs (HThODAs) show – in both solution and solid state – a strong optical absorption, which is progressively red-shifted with increasing chain length. The linear correlation of the absorption maximum ( $\lambda_{\text{max}}^{\text{A}}$ ) with the inverse of conjugation length (CL = number of double and triple bonds) shows that the effective conjugation length of this system is extended up to at least CL = 20. Furthermore, absorption measurements of drop-casted thin films display not only a bathochromic shift of  $\lambda_{\text{max}}^{\text{A}}$  but also a higher wavelength absorption, which is attributed to increased  $\pi$ - $\pi$  interactions. The wavelength of maximum fluorescence emission ( $\lambda_{\text{max}}^{\text{E}}$ ) also increases with CL, and emission is maximal for oligomers with CL = 7 – 12 (fluorescence quantum yield  $\Phi_{\text{f}} \sim 0.2$ ). Both longer and shorter oligomers display marginal emission. The calculated Stokes shifts of these planar materials are relatively large (0.4 eV) for all oligomers, and likely due to excitation to the  $S_2$  state, suggesting that the presence of enyne moieties dominates the ordering of the lowest excited states. The fluorescence lifetimes ( $\tau_{\text{f}}$ ) are short ( $\tau_{\text{f max}} \ll 1$  ns) and follow closely the tendency obtained for  $\Phi_{\text{f}}$ . The anisotropy lifetimes show a near-linear increase with CL, in line with highly rigid oligomers.

*This chapter was accepted for publishing: Gregor S. Pilzak, Kitty van Gruithuysen, Reindert H. van Doorn, Barend van Lagen, Ernst J. R. Sudhölter, and Han Zuilhof, Chemistry - A European Journal, 2009.*

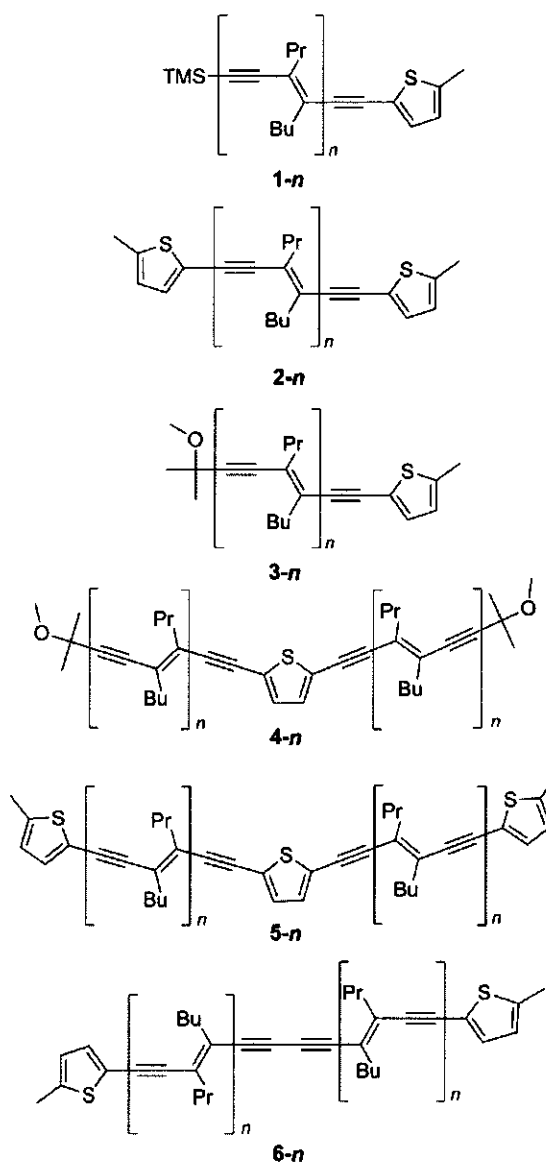
## 4.1 Introduction

Structurally well-defined  $\pi$ -conjugated oligomers such as oligothiophenes, oligoarylvinylenes and oligodiacetylenes have attracted considerable attention as promising nanoscale candidates for organic electronic devices.<sup>[1-4]</sup> In order to study the evolution of the optoelectronic properties of these materials as function of the chain length new series of monodisperse oligomers are designed as model compounds.<sup>[5]</sup> Recently, novel methods for the synthesis of oligodiacetylene-based materials have been developed by us, which has allowed a detailed photophysical study thereof that clarified the optical properties of polydiacetylenes.<sup>[6-8]</sup>

The development of new oligodiacetylene-based materials is often hampered by their low solubility, and a laborious and troublesome synthesis of significantly elongated oligomers.<sup>[9, 10]</sup> While extensive studies based on oligoenes,<sup>[11, 12]</sup> oligoarylenevinylenes,<sup>[4, 13]</sup> oligotriacetylenes<sup>[14-20]</sup> and oligothiophenes,<sup>[21-27]</sup> are known, analogous studies centering around the diacetylene functionality as present in polydiacetylenes are rather scarce. This is a shortcoming, given several of the unique properties of polydiacetylenes, such as nonlinear optical (NLO) properties as well as chromic properties arising due to its  $\pi$ -conjugated system.<sup>[3, 28-33]</sup> Furthermore, few examples of structural modulation of such  $\pi$ -oligomeric chains by incorporation of an aromatic moiety are reported.<sup>[34-36]</sup> Such an approach provides a new and versatile way to explore and optimize the optoelectronic properties of conjugated oligomers. Moreover, the use of a bifunctional aromatic moiety as a central unit provides a new and rapid divergent synthetic approach to prepare long conjugated oligomers.

As a result, we have set out to both develop new synthetic routes towards thiophene-containing enyne-based oligomers, and to study their photophysical behavior in detail. In this paper, we describe the synthesis of a novel series of highly soluble thiophene-containing oligodiacetylenes (ThODAs) and homocoupled ThODAs (HThODAs), which are presented in Scheme 1. In our approach the thiophene moiety is positioned either as a conjugation-extending endcap, as a central anchor unit, or both. The linear ThODA series **1-*n*** is endcapped with a trimethylsilyl moiety (TMS) and a thiophene group, while the **2-*n*** series has two thiophene endcaps, in contrast to **3-*n***, which has been synthesized by us previously<sup>[6]</sup> and is equipped with TMS and *t*-OMe endgroups. The banana-shaped ThODAs are constructed in a new, divergent way. A central thiophene molecule is used to couple two oligodiacetylene building blocks, resulting in a rapid extension of the oligomeric chain conjugation. The series **4-*n*** is equipped with two thiophene endcaps, whereas the **5-*n*** series has a  $C(CH_3)_2OMe$  and a thiophene endgroup. The homocoupled ThODAs **6-*n*** consist of two symmetric ThODA

subunits. All these novel oligomers with oligodiacyetylene subunits up to trimer are synthesized in high purity ( $\geq 99\%$ ), with moderate to high yields (30 – 90%). This allows the isolation of significant amounts of all members of these series (including the longest 4-3 ThODA with 20 conjugated  $\pi$ - $\pi$  bonds) and the systematic study of their optical properties. Therefore, we also report in detail on their optical properties using both steady-state and picosecond time-resolved optical spectroscopy.



Scheme 1. Series of novel ThODAs and HThODAs under present study with  $n = 1$ -3.

## 4.2 Results and Discussion

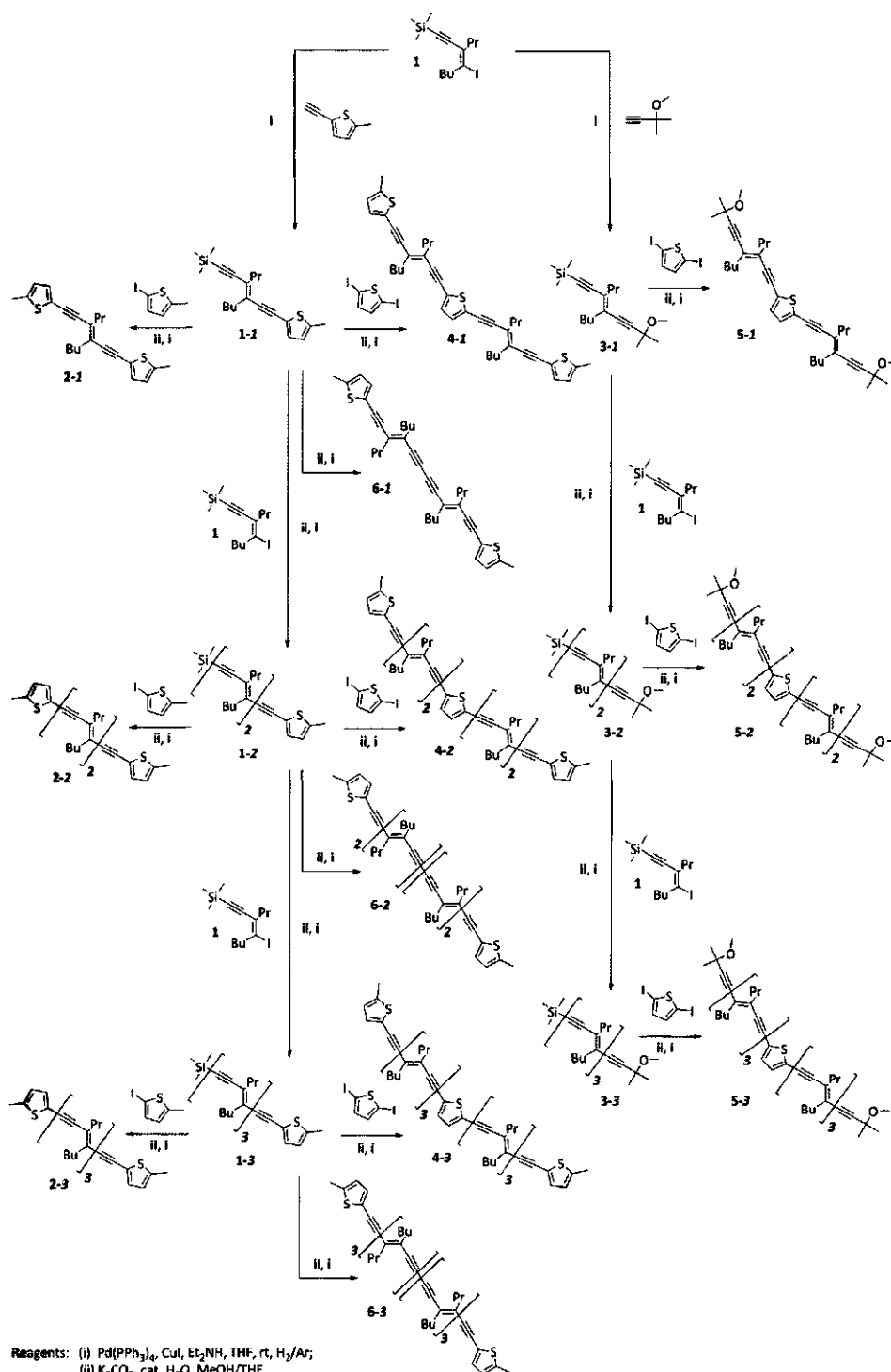
### 4.2.1 Synthesis of ThODAs and HThODAs

The ThODA and HThODA series were prepared according to the synthetic route illustrated in Scheme 2. The synthesis of oligodiacetylene building block **1** has been reported by us previously.<sup>[6]</sup> The 2-ethynyl-5-methylthiophene used to introduce a second thiophene endcap was synthesized from 2-carboxyl-5-methylthiophene *via* a short sequence including bromination of the carboxyl group and reduction of 2-(2,2-dibromovinyl)-5-methylthiophene. This thiophene endcap is introduced *via* a Sonogashira coupling of the iodoenyn **1** with the 2-ethynyl-5-methylthiophene, and results in the formation of **1-1**. Compound **1-1** was protodesilylated under alkaline conditions, and subjected to a catalytic coupling with 2-iodo-5-methylthiophene under reductive atmosphere to afford **2-1** bearing two thiophene endcaps. The use of a 1:1 mixture of H<sub>2</sub>/Ar and a large excess of iodothiophene provided a suppression of the homocoupling of terminal acetylenes down to 15 %. However, a negative side effect of this is a slow poisoning of the catalyst by the thiophene moiety. This resulted in somewhat lower yields compared to the analogous reaction with oligodiacetylenes.<sup>[6]</sup> Similar reaction conditions (10 equiv. of **1** and a reductive atmosphere) were chosen for the catalytic elongation of ThODA backbone. Iodoenyn **1** was recovered quantitatively after each step, which justified the use of this large excess. This chain extension is performed up to trimer *via* a sequence of protodesilylation of **1-*n*** followed by a Sonogashira coupling with **1**. After each step, a second thiophene endcap is introduced to yield **2-*n***.

The synthesis of the banana-shaped **4-*n*** and **5-*n*** series was performed *via* a Sonogashira coupling of two **1-*n*** or **3-*n*** building blocks, respectively, and a central 2,5-di-iodothiophene moiety. In order to achieve completion of this transformation, an excess of the oligodiacetylene moiety is used. Unfortunately, this results in slightly lower yields compared to the catalytic reaction of similar oligodiacetylenes due to an increased degree of homocoupling.

The synthesis of HThODAs **6-*n*** is performed quantitatively *via* a mild catalytic reaction under ambient air conditions: two protodesilylated building blocks **1-*n*** are coupled symmetrically to yield the corresponding HThODAs **6-*n*** up to a homocoupled trimer with two thiophene endcaps. The use of tetrakis (triphenylphosphine)palladium(0) under an oxygen atmosphere generates a Pd<sup>II</sup> catalyst *in situ*, which is the active catalyst for the homocoupling of terminal acetylenes.<sup>[8]</sup>





Scheme 2. Synthesis of ThODA and HThODA series based on a sequence of Sonogashira couplings.

### 4.2.2 Steady-state optical absorption in solution

The high solubility of the synthesized ThODAs and HThODAs, resulting from the asymmetric laterally attached alkyl side chains and the polar endcaps, allowed us to study their optical properties in solution. The ground-state optical absorption of all series was measured both in solution and as a drop-casted thin film (see Figure 1 for the absorption of these series in *n*-hexane). Additionally, Table 1 shows an overview of optical absorption characteristics of these oligomers measured in *n*-hexane, toluene and methanol solutions.

Table 1. Absorption data of oligomers under study in *n*-hexane, toluene and methanol.

oligomer (CL) <sup>[a]</sup>	$\lambda_{\max}^A$ [nm] ([eV])			$\epsilon_{\max}$
	<i>n</i> -hexane	toluene	methanol	<i>n</i> -hexane
1-1 (5)	327 (3.79)	332 (3.73)	327 (3.79)	20.0
1-2 (7)	360 (3.44)	365 (3.40)	360 (3.44)	23.1
1-3 (9)	386 (3.21)	393 (3.16)	386 (3.21)	49.4
2-1 (7)	355 (3.49)	360 (3.44)	355 (3.49)	25.4
2-2 (9)	380 (3.26)	386 (3.21)	380 (3.26)	32.4
2-3 (11)	396 (3.13)	403 (3.08)	395 (3.14)	57.8
4-1 (12)	403 (3.08)	410 (3.02)	402 (3.08)	61.4
4-2 (16)	419 (2.96)	426 (2.91)	417 (2.97)	71.4
4-3 (20)	429 (2.89)	433 (2.86)	<sup>[b]</sup>	100.4
5-1 (8)	373 (3.32)	378 (3.28)	372 (3.33)	34.9
5-2 (12)	407 (3.05)	412 (3.01)	404 (3.07)	54.4
5-3 (16)	421 (2.95)	427 (2.90)	418 (2.97)	94.2
6-1 (10)	377 (3.29)	385 (3.22)	382 (3.25)	50.4
6-2 (14)	412 (3.01)	419 (2.96)	410 (3.02)	81.9
6-3 (18)	426 (2.91)	434 (2.86)	<sup>[b]</sup>	153.1

[a] Conjugation length as total number of conjugated double and triple bonds. [b] Not obtained due to low solubility in methanol.

The steady-state absorption spectra recorded in all solvents show the expected red-shift of the maximum absorption peak ( $\lambda_{\max}^A$ ) with an increase of the conjugation length (CL = number of double and triple bonds). A similar dependence is observed for the extinction coefficient ( $\epsilon_{\max}$ ) determined in *n*-hexane. The evolution of  $\lambda_{\max}^A$  shows that the bathochromic shift ( $\Delta\lambda_{\max}^A$ ) decreases slightly with an increasing CL for all solvents, in line with observed trends

for oligodiacetylenes,<sup>[6]</sup> homocoupled oligodiacetylenes,<sup>[8]</sup> and oligothiophenes,<sup>[2]</sup> and as expected from simple 'particle-in-a-box' considerations.

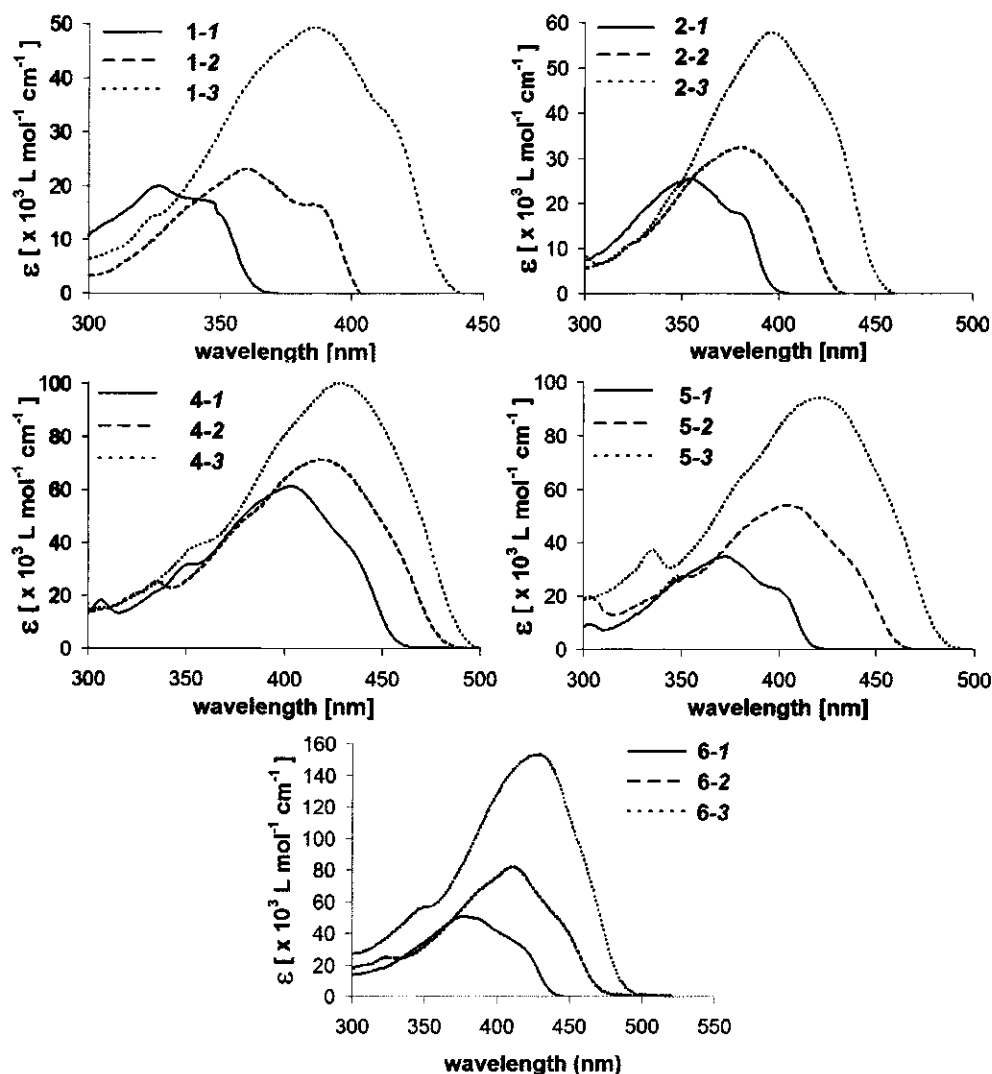


Figure 1. Electronic absorption spectra of the oligomers under study measured in *n*-hexane (*3-n* series published elsewhere)<sup>[6]</sup>.

Changing the solvent induces a small shift of  $\lambda_{\text{max}}^A$  as well. The bathochromic shift ranges from 0.03 eV for 4-3 up to 0.10 eV for 1-2 upon changing the solvent from *n*-hexane (*refr. index* = 1.375;  $E_T(30)$  = 31.0)<sup>[37]</sup> to toluene (*refr. index* = 1.50;  $E_T(30)$  = 33.9)<sup>[37]</sup>. This observation shows the stabilizing effect of an aromatic solvent on the excited state of these molecules.

This red-shift of  $\lambda_{\max}^A$  resembles values determined previously for oligodiacetylenes,<sup>[6]</sup> homocoupled oligodiacetylenes<sup>[8]</sup> and analogous to data reported for shorter diacetylene-based oligomers.<sup>[7, 10, 38-40]</sup> The shortest ThODA series 1-*n* displays similar  $\lambda_{\max}^A$  values in both hexane and methanol. The shift of  $\lambda_{\max}^A$  going from *n*-hexane to methanol (*refr. index* = 1.33;  $E_T(30)$  = 55.4 kcal/mol)<sup>[37]</sup> for other oligomers under study is marginal. We observed a small blue-shift of  $\lambda_{\max}$  (~ 0.2 eV) that is caused by destabilization of the excited state of these oligomers by a smaller solvent refractive index.<sup>[37, 41, 42]</sup> Plots of the maximum absorption, expressed in energy units, vs 1/CL for the oligomers under study are depicted in Figure 2 together with – for comparison – reported linear fits for oligodiacetylenes,<sup>[6]</sup> homocoupled oligodiacetylenes<sup>[8]</sup> and oligothiophenes from the literature.<sup>[2]</sup> For each of the five current series a linear correlation was observed, with  $r^2 \geq 0.99$ .

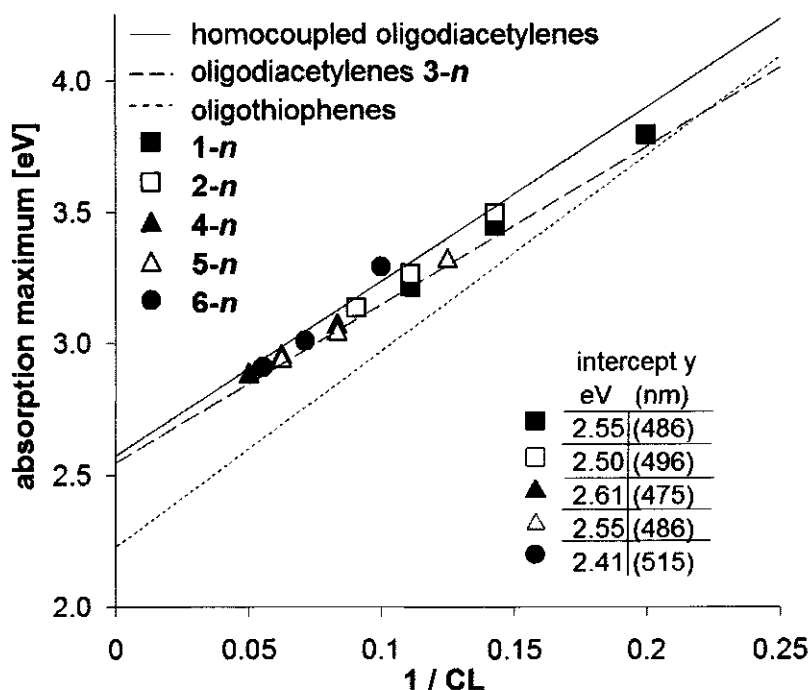


Figure 2. Energy of maximum absorption versus 1/CL of the ThODAs and HThODAs in *n*-hexane at micromolar concentrations ( $2 \cdot 10^{-6}$  M) and room temperature, together with linear fits of corresponding data reported for oligodiacetylenes,<sup>[6]</sup> homocoupled oligodiacetylenes,<sup>[8]</sup> and oligothiophenes.<sup>[2]</sup>

The optical absorption maxima for ThODAs and HThODAs are almost parallel to those of the diacetylene-based series. The extrapolated value of the absorption for the polymers ( $1/CL \rightarrow 0$ ) is nearly identical for all the thiophene-containing series (in between 2.61 and 2.41 eV)

and is basically identical to values derived from oligodiacetylenes (2.55 eV) and homocoupled oligodiacetylenes (2.56 eV). However, the values reported for the oligothiophenes are slightly lower (2.23 eV).<sup>[2]</sup> This is revealing in terms of the nature of the excited singlet states to which the oligomers are excited upon photon absorption. Both oligothiophenes (non-planar)<sup>[43]</sup> and oligodiacetylenes ( $C_{2h}$  symmetry)<sup>[40, 44]</sup> have two low-lying, planar excited singlet states ( $S_1$  and  $S_2$ ; Figure 3), but these are accessed with different ease.

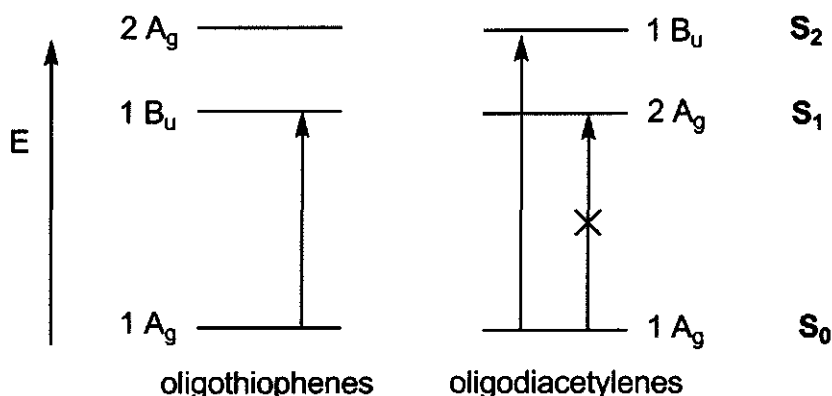


Figure 3. Schematic depiction of the electronic transitions in oligothiophenes<sup>[45, 46]</sup> and oligodiacetylenes<sup>[44]</sup> upon one-photon excitation.

From the  $A_g$  ground state in planar conjugated oligomers like ODAs, only the transition to the excited singlet state  $B_u$  is allowed; excitation to the second  $2A_g$  singlet state is symmetry forbidden.<sup>[40, 47]</sup> Because of these symmetry reasons, for the diacetylene-based oligomers only the transition to the  $S_2$  state is allowed.<sup>[6-8, 40, 47]</sup> For the oligothiophenes electronic excitation is to the  $S_1$  state.<sup>[2, 45]</sup> As a result, mixing in of thiophene moieties into an oligodiacetylene-based framework can qualitatively be expected to lead to higher excitation energies when compared to pure oligothiophenes, as is indeed observed. The absorption maxima of the thiophene-containing compounds generally resemble those of diacetylene-based oligomers with similar CL (see Figure 4 and Figure 6, *vide infra*). Whereas for all ThODA series the presence of thiophene moieties effects a marginal blue shift,  $\lambda_{\max}^A$  of the HThODA series, matches almost exactly the values reported for rod-like homocoupled oligodiacetylenes with identical CL.<sup>[8]</sup> Obviously, in these materials the thiophene moiety, which is positioned at the end of the homocoupled oligodiacetylene structure, results in an extension of the conjugation that is similar to chain prolongation with one oligodiacetylene unit. Comparison with e.g. series 4-n, which also features terminal thiophene moieties, thus shows that the excited state character is significantly affected by the central unit (thiophene or diacetylene) within the molecule.

The linear relation of the energy of maximum absorption with  $1/CL$  up to  $CL = 20$  indicates that for the thiophene-containing oligodiacetylenes the elongation of the conjugation length is preserved for all compounds under present study. The conjugation of ThODA and HThODA oligomeric chains is therefore not significantly reduced by kinks or torsions in the backbone.<sup>[6-8]</sup>

<sup>[8]</sup> The effective conjugation length (ECL) for these oligomers is therefore at least 20, and most likely  $> 20$  conjugated double and triple bonds.

### 4.2.3 Steady-state optical absorption in thin films

The optical absorption in the solid state of the members of ThODA and HThODA series that are solids at room temperature was investigated in drop-casted thin films. The absorption spectrum is recorded 12 hours after the start of the solvent evaporation from the quartz plate containing solid material prepared *via* drop-casting. [Unfortunately, the shorter oligomers such as **1-n** and **2-n** series and **5-1** and **5-2** are liquids, hampering such studies.] The absorption plots of the drop-casted thin films of **4-n** and **6-n** compared to solution plots are shown in Figure 4. The plot of **5-3** is similar, and is given in the Supporting Information (Subchapter 4.6, Figure 9). The solid-state absorption data of the solid oligomers under study are summarized in Table 2.

The solid-state absorption of ThODAs and HThODAs is characterized by three features:

- 1) a red-shifted  $\lambda_{\max}^A$  relatively to the absorption maxima in solution;
- 2) a clearly visible red-shifted shoulder and
- 3) an additional higher-wavelength absorption from 550 nm upwards

Table 2. Solid-state absorption data of **4-n**, **5c-3** and **6-n** series.

oligomer (CL) <sup>[a]</sup>	$\lambda_{\max}^{[b]}$	$\lambda_{\max}$ right shoulder <sup>[b]</sup>
<b>4-1</b> (12)	421 (2.95)	466 (2.66)
<b>4-2</b> (16)	441 (2.81)	484 (2.56)
<b>4-3</b> (20)	455 (2.73)	498 (2.49)
<b>5-3</b> (16)	444 (2.79)	492 (2.52)
<b>6-1</b> (12)	408 (3.04)	446 (2.78)
<b>6-2</b> (14)	437 (2.84)	479 (2.59)
<b>6-3</b> (18)	455 (2.73)	496 (2.50)

[a] Conjugation length (CL) as number of double and triple bonds. [b] Extinction is given in units of [nm] ([eV]).

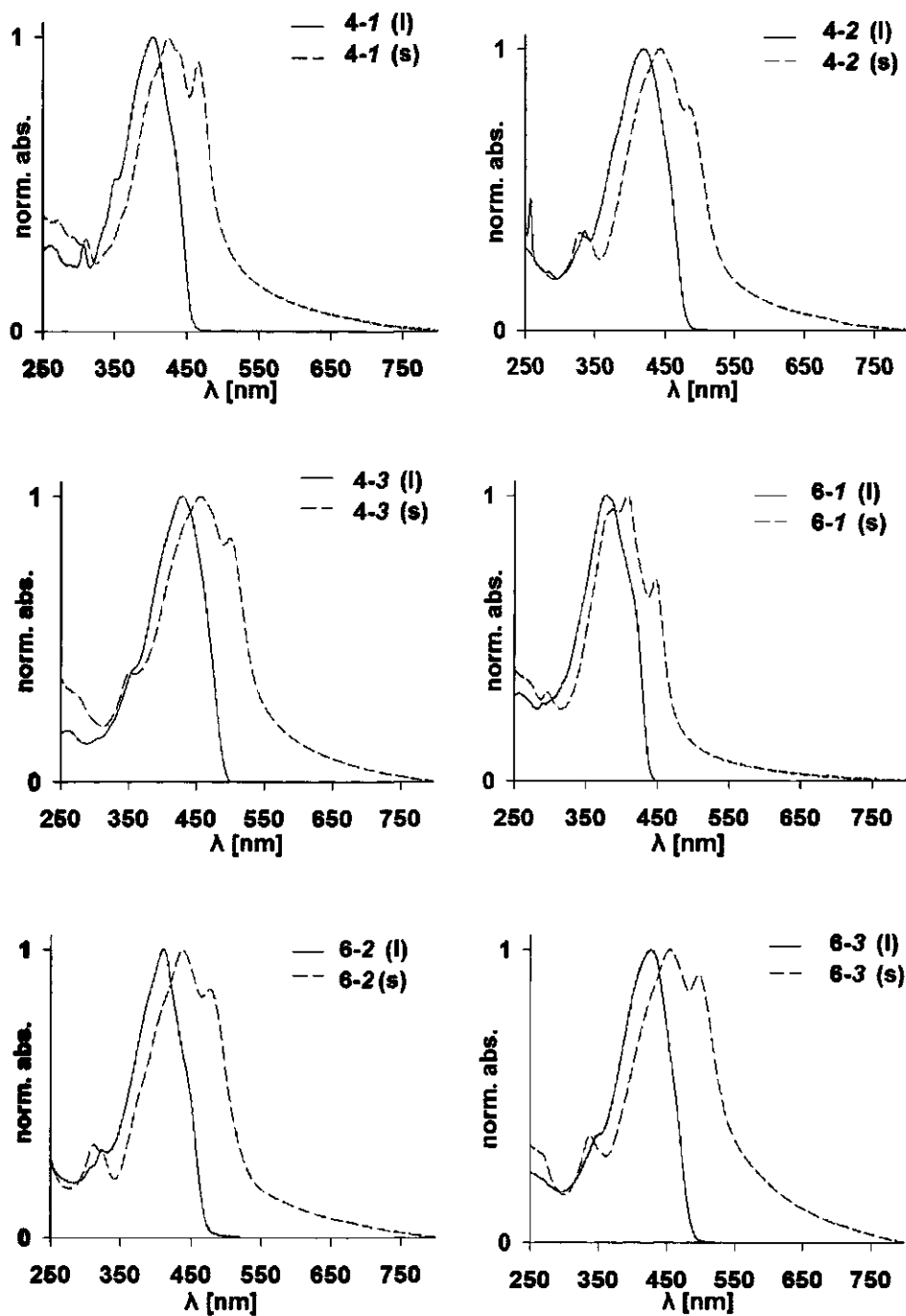


Figure 4. Normalized absorption spectra of 4-*n* and 6-*n* in solution (l) versus thin solid film (s).

The liquid-to-solid red-shift of  $\lambda_{\text{max}}^{\text{A}}$  for the 4-*n* series and for 5-3 is approximately 0.15 eV, and is slightly larger compared to the reported shift ( $\sim 0.10$  eV) for the ODAs 3-*n* series.<sup>[6]</sup> The HThODAs show an even larger liquid-to-solid red-shift ranging from 0.17 eV for 6-3 up to 0.25 eV for 6-1, compared to 0.07 eV as observed for homocoupled oligodiacetylenes.<sup>[9]</sup> The available data are used for a correlation between the reciprocal value of CL and the  $\lambda_{\text{max}}^{\text{A}}$  for both liquids and solids and compared to reported values of oligodiacetylenes<sup>[6]</sup> and homocoupled oligodiacetylenes<sup>[9]</sup> as drop-casted films (Figure 5).

Trend lines for the 4-*n* series and 5-3 are similar to that observed for (homocoupled) ODAs, pointing to a dominant effect of the ODA moieties in determining this liquid-to-solid effect. For the 6-*n* series it may tentatively be concluded that extension to an infinite polymer would yield a further reduction of the excitation energy in comparison to the analogous homocoupled ODAs, from 2.5 to  $\sim 2.3$  eV. Furthermore, we observe an additional electronic transition appearing at lower energy,  $\sim 0.26$  eV below the main absorption maxima, followed by a significant absorption increase in the range of 550 - 800 nm. This red-shifted shoulder positioned at higher wavelength region is already present for shorter oligomers in solution such as ThODAs 1-*n*, 2-1, 2-2 and 5-1 (Figure 1), but is absent in solutions of these longer hybrid oligomers. We interpret this to mean that for short ThODAs without central thiophene unit, the flat oligomeric geometry ( $\text{C}_{2h}$ -like) is dominant, as reported for rod-like oligodiacetylene chains.<sup>[40, 44]</sup> For longer oligomers, entropic reasons might also allow other geometries to play a role (e.g. with slight rotations around the C-C bonds), and the resulting peak broadening may make the lowest energy transition invisible as separate shoulder. In the solid state, interchain interactions may force planarity, and thus bring back the shoulder. Moreover, the significantly increased long-wavelength absorption (above 550 nm for longest oligomers under study) is caused by the intermolecular stacking of  $\pi$ -orbitals in the solid state, which is absent in diluted solution. Due to steric repulsion from the alkyl side chains, these oligomers do not show aggregation even in concentrated solution up to 5 mM.



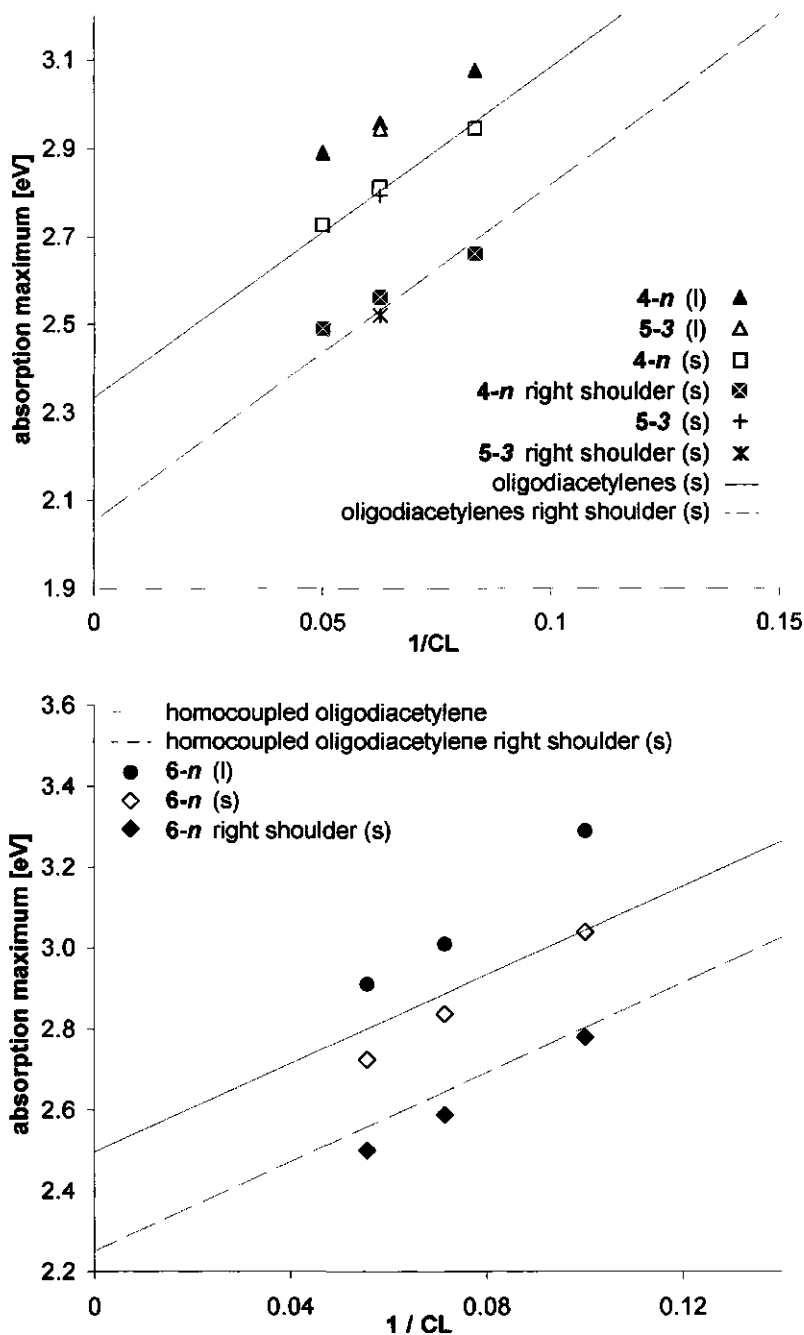


Figure 5.  $\lambda_{\max}^A$  of 4-*n*, 5-3 (top) and 6-*n* (bottom) in *n*-hexane solution ( $2 \cdot 10^{-6}$  M) (l) and drop-casted films (s) with  $\lambda_{\max}^A$  additional electronic transition compared to literature data of drop-casted films of oligodiacetylenes and homocoupled oligodiacetylenes as function of  $1/CL$ .

### 4.2.5 Steady-state fluorescence in solution

Emission spectra measured for homogeneous millimolar solutions of the ThODA and HThODA series were recorded in *n*-hexane, methanol and toluene. Table 3 summarizes the characteristic features of the steady-state fluorescence for these oligomers measured in *n*-hexane. Similar features were observed in methanol and toluene, and are given in the Supporting Information. These marked features are 1) a clear red-shift of the emission maxima ( $\lambda_{\text{max}}^{\text{E}}$ ) with increasing CL, 2) a sharp maximum of the fluorescence quantum yield ( $\Phi_{\text{f max}}$ ) for the oligomers with CL  $\leq 12$ , and 3) a resolved 0-0 transition (Figure 6). This last feature differs from the emission of diacetylene-based oligomers,<sup>[6, 8]</sup> where no distinguishable shoulder at the high-energy side of the fluorescence band was visible for these oligomers with CL  $\geq 6$ . For the linear ThODAs series 1-*n* and 2-*n* the maximum quantum yield of fluorescence is observed for the dimers 1-2 and 2-2, while in the linear HThODAs 6-*n* and the banana-shaped 4-*n* and 5-*n* ThODAs series the monomers display this maximum. Upon further chain elongation, the  $\Phi_{\text{f}}$  becomes marginal, likely as a result of highly efficient internal conversion.<sup>[45]</sup>

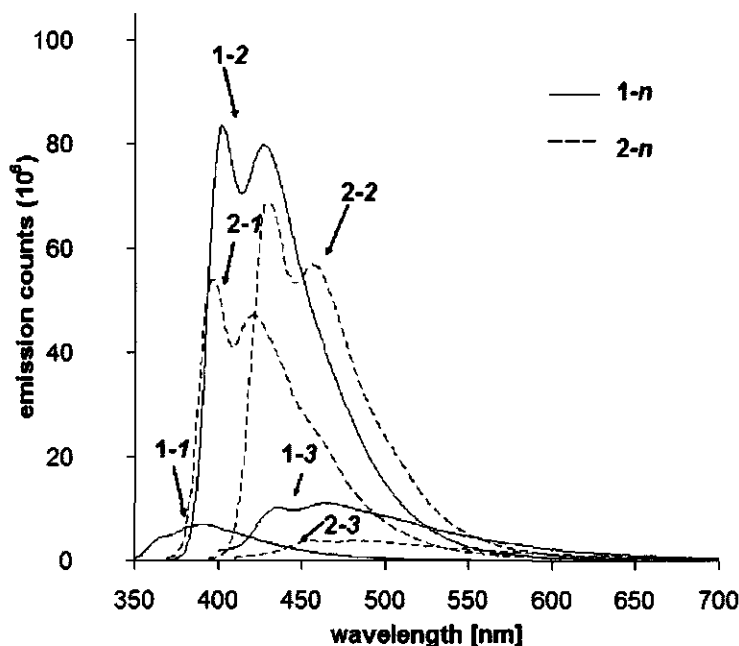


Figure 6a. Fluorescence spectra of ThODA series 1-*n* and 2-*n* measured in *n*-hexane. (Because of the marginal emission all spectra except 1-2, 2-1, 2-2, are multiplied by a factor of 5.)

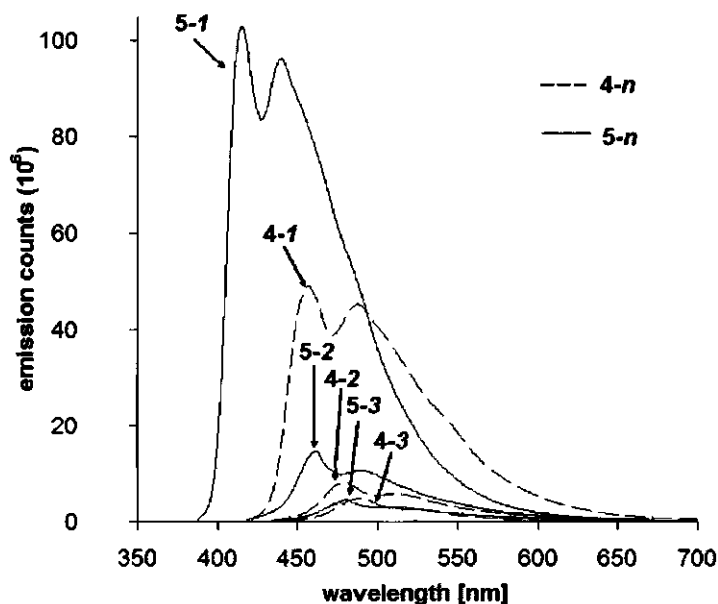


Figure 6b. Fluorescence spectra of ThODAs 4-*n* and 5-*n* measured in *n*-hexane. (Because of the marginal emission all spectra except 4-1 and 5-1 are multiplied by a factor of 5.)

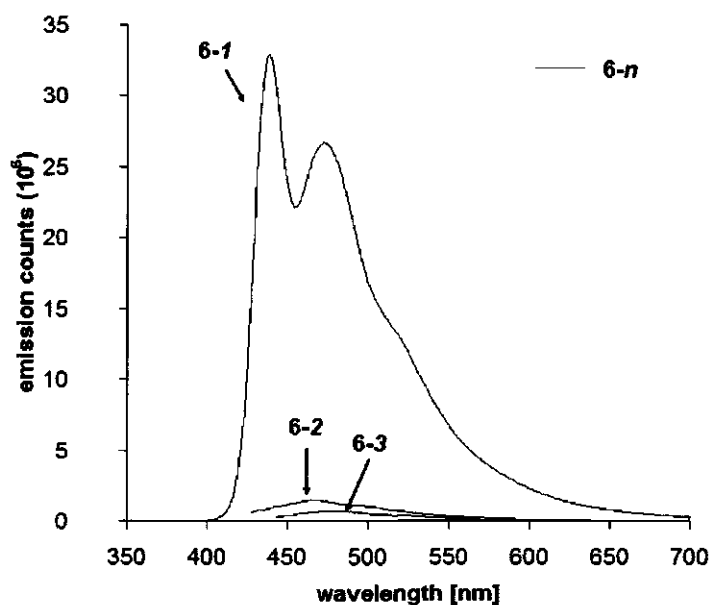


Figure 6c. Fluorescence spectra HThODA 6-*n* measured in *n*-hexane. (Because of the marginal emission all spectra except 6-1 are multiplied by a factor of 5.)

Table 3. Emission data of oligomers under study in *n*-hexane.

oligomer (CL) <sup>[a]</sup>	$\lambda_{\text{max}}^{\text{E}}$ [nm] ([eV])	Quantum Yield $\Phi_{\text{f}}$ <sup>[b,c]</sup>	Stokes shift [eV]
1-1 (5)	370 (3.35)	0.003	0.422
1-2 (7)	407 (3.05)	0.170	0.446
1-3 (9)	441 (2.81)	0.005	0.426
2-1 (7)	397 (3.12)	0.110	0.370
2-2 (9)	431 (2.88)	0.140	0.386
2-3 (11)	452 (2.74)	0.002	0.388
4-1 (12)	457 (2.71)	0.100	0.364
4-2 (16)	478 (2.59)	0.003	0.365
4-3 (20)	490 (2.53)	0.002	0.360
5-1 (8)	415 (2.99)	0.210	0.336
5-2 (12)	461 (2.69)	0.006	0.357
5-3 (16)	480 (2.58)	0.002	0.362
6-1 (10)	438 (2.83)	0.067	0.458
6-2 (14)	468 (2.65)	0.001	[d]
6-3 (18)	482 (2.57)	0.001	[d]

[a] Conjugation length (CL) as number of double and triple bonds; [b] Quantum yield determined by comparison with tryptophan:  $\Phi_{\text{f}} = 0.13$ ; <sup>[48]</sup> [c] Experimental error  $\pm 0.002$ ; [d] Not determined due to an absence of a visible 0-0 transition.

Changing the solvent from *n*-hexane to toluene induces a red-shift of  $\lambda_{\text{max}}^{\text{E}}$ . This red-shift is rather small (in between 0.04 and 0.06 eV) for ThODAs in toluene, but becomes slightly larger (0.10 eV) for the HThODA series. Increasing the polarity even more by changing the solvent to methanol results, only for the 1-*n* series, in a relatively large red-shift of the emission maximum of  $\sim 0.10$  eV. For all other oligomers under study this shift is smaller (0.02 eV for 2-*n*, 4-*n* and 5-*n*) or similar (0.09 eV for 3-*n*) compared to the red-shift in  $\pi$ -electron rich toluene. In line with this, the  $\lambda_{\text{max}}^{\text{E}}$  for ThODAs and HThODAs is highest in toluene except for the 1-*n*. For polar oligomers like 1-*n* with a -CMe<sub>2</sub>OMe endgroup, the solvent polarity plays an important role. For oligomers without (significant) dipole, the possibilities for increased  $\pi$ - $\pi$  interactions with the solvent (as in toluene) are obviously more important.

The emission quantum yield  $\Phi_{\text{f}}$  is highly dependent on the conjugation length. We observe a sharp maximum for  $\Phi_{\text{f}}$  in all solvents for relatively short ThODAs, viz.  $\Phi_{\text{f}}$  in *n*-hexane is highest for 1-2 ( $\Phi_{\text{f}} = 0.17$ ; CL = 7) and 2-2 ( $\Phi_{\text{f}} = 0.14$ ; CL = 9) and similar to  $\Phi_{\text{f}} = 0.16$  for an oligodiacetylene trimer with CL = 7.<sup>[6]</sup> For the longer series 4-*n*, 5-*n* and 6-*n*, the maximum  $\Phi_{\text{f}}$  is

recorded for their monomers **4-1** ( $\Phi_f = 0.10$ , CL = 12), **5-1** ( $\Phi_f = 0.21$ , CL = 8) and **6-1** ( $\Phi_f = 0.07$ , CL = 10). These values are – for **5-1** – five times larger than the marginal emission reported for ODAs with such CL values<sup>[6]</sup> or for HODAs (maximum  $\Phi_f = 0.041$ , reported for the homocoupled oligodiacetylene monomer with CL = 6).<sup>[8]</sup> This phenomenon shows that incorporation of thiophene moiety into oligodiacetylene framework increases  $\Phi_f$ .  $\Phi_f$  is further increased in toluene, which clearly indicates that an aromatic solvent stabilizes the intramolecular charge transfer in the excited state of the hybrid oligomers, which results not only in a fluorescence emission at longer wavelengths but effects also an increased efficiency thereof.

From the absorption and emission data the Stokes shifts in *n*-hexane were obtained (Table 3; for similar data in toluene and methanol see Table 4 in Supporting Information). These values are rather large (0.30 – 0.45 eV), and similar to those of ODAs<sup>[40]</sup> but slightly smaller than reported for oligothiophenes (~ 0.6 eV).<sup>[49, 50]</sup> For oligothiophenes the large Stokes shift is attributed to significant differences in geometry of the non-planar ground state and the planar excited state.<sup>[43, 50, 51]</sup> In contrast, for ODAs the  $S_2$  excitation (Figure 3) causes this large shift, which is followed by rapid internal conversion to the  $S_1$  state and fluorescence from there.<sup>[44]</sup> For the hybrid systems under study the planarity was investigated by DFT calculations (B3LYP/6-311G(d,p)) on **2-1** as depicted in Figure 7. The resulting geometry displays the planarity of this species, which implies that – in contrast to oligothiophenes – the observed large Stokes shift of the hybrid materials under present study is likely not due to large geometrical changes (such as rotations) upon excitation, but to excitation to a higher excited state, in line with Figure 3 (right). In other words, the order of the  $B_u$  and  $2A_g$  states seems fixed by the presence of the enyne moieties, even in molecules like **2-1** with two thiophene moieties and only one enyne unit.

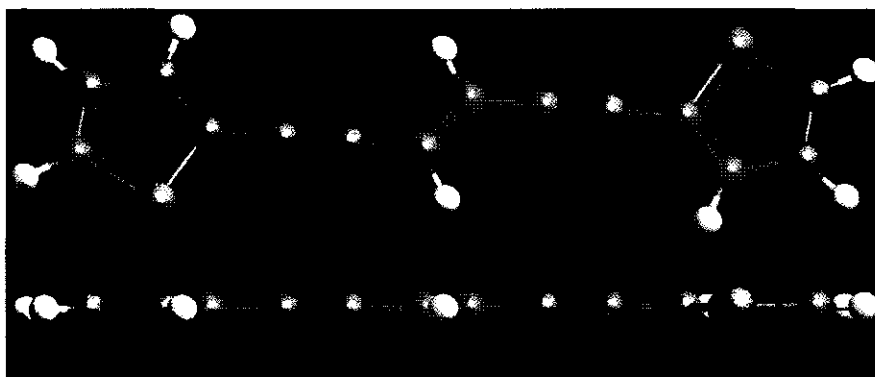


Figure 7. Planar geometry of ThODA oligomer **2-1** (front and side view; optimized at the B3LYP/6-311G(d,p) level of theory).

## 4.2.5 Fluorescence lifetimes and anisotropy

Picosecond time-resolved single photon counting at five different excitation wavelengths (295, 360, 380, 400, and 410 nm) was used to determine the fluorescence lifetimes ( $\tau_f$ ) of the oligomer series under study. The observed lifetimes for the ThODA and HThODA series measured in *n*-hexane are shown in Table 4, and fall typically in the 100 – 900 ps range.

Table 4. Fluorescence lifetimes  $\tau_f$ , their relative amplitudes *A*, the average lifetimes  $\tau_{\text{AVG}}$  and the rotation correlation time  $\tau_R$  of the ThODA and HThODA series in *n*-hexane.

oligomer (CL) <sup>[a]</sup>	$\tau_1 (A_1)$ <sup>[b]</sup>	$\tau_2 (A_2)$ <sup>[b]</sup>	$\tau_3 (A_3)$ <sup>[b]</sup>	$\tau_{\text{AVG}}$ <sup>[b, c]</sup>	$\tau_R$ <sup>[b, e]</sup>
1-1 (5)	10 (66) <sup>[d]</sup>	41 (29)	150 (5)	26	50
1-2 (7)	781 (100)				119
1-3 (9)	13 (9) <sup>[d]</sup>	204 (91)		187	200
2-1 (7)	200 (100)				205
2-2 (9)	839 (100)				250
2-3 (11)	7 (49) <sup>[d]</sup>	94 (51)		51	321
4-1 (12)	551 (100)				218
4-2 (16)	6 (49) <sup>[d]</sup>	300 (21)	793 (30)	304	643
4-3 (20)	3 (91) <sup>[d]</sup>	514 (9)		49	910
5-1 (8)	304 (100)				380
5-2 (12)	20 (92)	678 (8)		73	500
5-3 (16)	13 (100)				731
6-1 (10)	280 (100)				151
6-2 (14)	6 (72) <sup>[d]</sup>	84 (16)	742 (12)	107	441
6-3 (18)	[f]			[f]	[f]

[a] Conjugation length (CL) as number of double and triple bonds; [b]  $\tau_f$  [ps] (relative amplitudes); [c] Calculated using Eq. 1; [d] Values not accurate, as instrument response time is ~400 ps.; [e] Experimental error  $\leq 50$ ; [f] Not available due to marginal emission.

The decay curves of the compounds with lifetimes > 200 ps could all be fitted with one exponent. The compounds with marginal fluorescence displayed more complex decay kinetics, requiring a sum of two or three exponentials. In that case, the average lifetime  $\tau_{f, \text{AVG}}$  was calculated according to Equation 1:

$$\tau_{F,AVG} = \frac{A_1}{A_1 + A_2 + A_3} \tau_1 + \frac{A_2}{A_1 + A_2 + A_3} \tau_2 + \frac{A_3}{A_1 + A_2 + A_3} \tau_3 \quad (1)$$

where  $A_1$ ,  $A_2$  and  $A_3$  are the contributions of the decays obtained from the curve fitting. The evolution of  $\tau_F$  with increasing oligomeric chain length closely follows the trend shown for the fluorescence quantum yield (Table 3). We have determined the rotation correlation times ( $\tau_R$ ) for ThODAs and HThODAs in *n*-hexane, and the results are listed in Table 4.<sup>[48]</sup> Because the longer oligomers display marginal emission, the experimental error for these measurements was relatively high. The anisotropy lifetimes show an increase with the CL indicating an increased rotation time around perpendicular axis for longer oligomers. This is illustrated in Figure 8 where a linear dependence for  $\tau_R$  and the CL of the oligomers is depicted. This is as expected for conjugated oligomers with a linear increase in the distance between the terminal atoms going from one member of the series to the next, showing the rigidity of even the longest oligomers under present study.

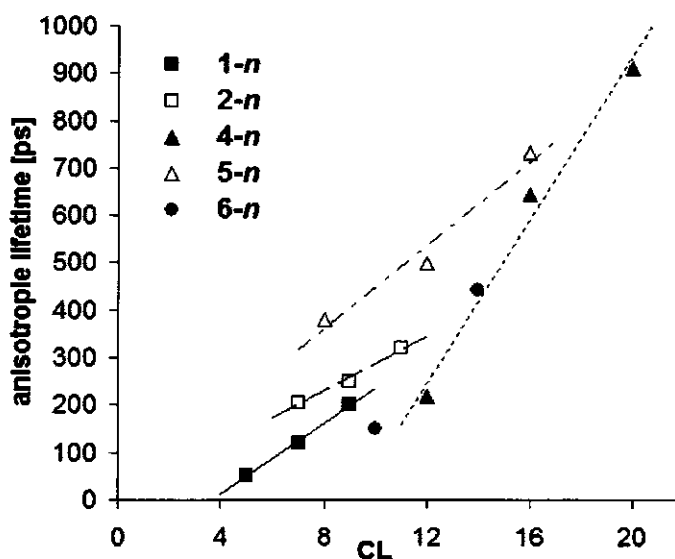


Figure 8. Anisotropy lifetimes vs. CL of ThODA and HThODA series.

## 4.3 Conclusion

Novel series of highly soluble oligodiacetylenes with thiophene moieties as endcap and/or as central unit were synthesized in high purity. These oligomers display photophysical properties in between those of oligodiacetylenes and homocoupled oligodiacetylenes on the one hand, and oligothiophenes on the other. Whereas the presence of thiophene units effects in the energy of excited states and the relaxation thereof, the nature of the lowest excited state of these hybrid materials ( $A_g$  or  $B_u$ ) is determined by the presence of enyne moieties, and for all compounds under present study a  $2A_g$  state. These oligomers show a clear linear increase in  $\lambda_{\max}$  for the  $\pi$ - $\pi^*$  transition with the conjugation length both in solution and in the drop-casted solid-state film. Optical absorption studies of the drop-casted films display a second red-shifted  $\lambda_{\max}^A$  and higher wavelength absorption, which are attributed to molecular planarization and aggregation, respectively. A more efficient  $\pi$ -electron delocalization along the oligodiacetylene backbone is obtained upon introduction of electron-rich thiophene moieties, which result in a red-shifted  $\lambda_{\max}$  of emission compared to oligodiacetylenes. This modulation also results in a significant increase of the quantum yield of emission up to a factor 5, in comparison to oligodiacetylenes and homocoupled oligodiacetylenes of the same conjugation length.

## 4.4 Experimental Section

### 4.4.1 Solvents and reagents

For all dry reactions performed under a steady stream of argon (or reductive atmosphere of argon/hydrogen mixture 1:1) the equipment was dried in an oven at 150 °C for several hours and allowed to cool down in an atmosphere of dry nitrogen or argon. Pure, dry, and degassed ether and tetrahydrofuran were obtained by distillation of the commercial material over sodium particles.  $\text{CH}_2\text{Cl}_2$  was distilled and dried over calcium hydride or sodium hydride. Dry DMF was purchased from Sigma-Aldrich and stored under argon. All other specified chemicals were commercially purchased (Aldrich, Fluka or Riedel-de Haën) and used without further purification.

### 4.4.2 General work up & purification procedure

Reaction monitoring and reagents visualization was performed on silica gel or reversed phase silica gel plates with UV-light (254 and 366 nm) combined with GC/MS. Usually the reaction mixture was diluted with water and extracted 3x with an organic solvent (petroleum ether 40-60, hexane, or ethyl acetate). The combined organic extracts were washed with brine and dried over anhydrous sodium sulfate prior to filtration and evaporation of the solvent under reduced pressure. Flash chromatography was performed on commercially available silica gel (0.035-0.070 nm pore diameter) and mixtures of freshly distilled petroleum ether 40/60 and ethyl acetate or reversed phase silica gel (0.04-0.06 nm pore diameter Screening Devices) with freshly distilled mixtures of acetonitrile and ethyl acetate. Final purification was



performed on Shimadzu preparative HPLC using a C18 column (Alltech Alltima 250 mm × 22mm; 5μ) with HPLC-grade water, acetonitrile and ethyl acetate mixture.

#### 4.4.3 Nuclear Magnetic Resonance spectroscopy and Mass Spectroscopy

$^1\text{H}$  NMR and  $^{13}\text{C}$  NMR spectra were determined on a Bruker CXP 300 NMR-spectrometer in  $\text{CDCl}_3$  solutions unless indicated otherwise. Chemical shifts are reported in ppm downfield relative to tetramethyl silane ( $\delta$  0 ppm for  $^1\text{H}$ ) or based on the solvent peak ( $\text{CDCl}_3$ ) ( $\delta$  77.00 ppm for  $^{13}\text{C}$  NMR) as an internal standard. HRMS was performed on Finnigan Mat95 mass spectrometer.

#### 4.4.4 Steady-state absorption and fluorescence

Absorption spectra of the oligodiacetylenes in *n*-hexane (spectrophotometric grade, Riedel-de Haën) and DCE (spectrophotometric grade, Sigma-Aldrich) were recorded using a Cary 100 UV-Vis spectrophotometer (scan range: 200 - 800 nm, scan rate: 300 nm min $^{-1}$ , data interval 0.5 nm) and steady-state fluorescence using a FLS920P Spectrometer (slit exc.: 2 nm, slit em.: 2 nm, step: 1.0, dwell: 0.2 s). Absorption spectra of oligodiacetylenes in film via drop casting were recorded on a Cary 50 UV-Vis spectrophotometer (scan range 200 - 850 nm, scan rate 300 nm/min, data interval 0.5 nm).

#### 4.4.5 Determination of fluorescence quantum yield in solution

In order to evaluate the fluorescence quantum yield ( $\Phi_F$ ) of the ODA's solution in *n*-hexane, toluene and methanol, the areas of the corrected emission spectra were compared to a spectrum of a reference molecule. A diluted solution of tryptophan in water was used, and a value of  $\Phi_R = 0.13$  was obtained at 25° C measured at 280 nm. The relevant fluorescence quantum yields of the ODAs were determined from the relationship:

$$\Phi_F = \Phi_R \frac{I}{I_R} \frac{OD_R}{OD} \frac{n^2}{n_R^2} \frac{RC_{\lambda_{exc,R}}}{RC_{\lambda_{exc}}} \quad (2)$$

where  $I$  and  $I_R$  are the integrated emission intensities of the ODA and tryptophan solutions, respectively, OD refers to the optical densities of the respective solutions and  $n$  is the refractive index. The ratio of  $RC_{\lambda_{exc}}$  is a correction factor for the lamp spectrum, due to the different excitation wavelength used for the determination of OD and  $I$  of the compound under study and tryptophan solution.

#### 4.4.5 Lifetime of fluorescence and fluorescence anisotropy in solution

The fluorescence lifetime and anisotropy were recorded using a FLS920P Spectrometer (Edinburgh Instruments) for time correlated photon counting (TCSP) (time set up: 5 or 10 ns, 4096 channels, 10000 counts). Pulsed diode lasers (372 nm, FWHM: 54 ps; 444 nm, FWHM: 63 ps) and pulsed LED's (283 nm, FWHM <500 ps; 304 nm, FWHM: < 350 ps) from PicoQuant were used as light sources. The anisotropy measurements were performed using vertical and horizontal polarizations. All other conditions and set-up were reported earlier by Van Hoek et al.<sup>[52-54]</sup>

#### 4.4.6 General method for protodesilylation of (Th)ODA series prior to catalytic chain elongation process as depicted in Figure 1

A solution of oligodiacetylene (1 eq) in THF/MeOH (1:1, 5ml/mmol) was stirred in round-bottomed flask.  $\text{H}_2\text{O}$  (3 drops/mmol) and  $\text{K}_2\text{CO}_3$  (2 eq) was added to the solution and stirred for 3 h. After working up following the general procedure, the terminal (Th)ODA was submitted to the catalytic chain elongation step as described below

#### 4.4.7 General method for catalytic Sonogashira coupling of terminal (Th)ODAs (1-*n*) or (3-*n*)<sup>[6]</sup> with iodo-diacetylene (1) as depicted in Figure 1

A mixture of ((E)-4-iodo-3-propyloct-3-en-1-ynyl)trimethylsilane (1; 10 eq.), Pd(PPh<sub>3</sub>)<sub>4</sub> (5 mol%), CuI (2 mol %), and dry, degassed diethyl amine (2 ml/mmol) and THF (5 ml/mmol) was placed anaerobically in a dried, brown two-necked round-bottomed flask, equipped with a magnetic stirrer, an argon/hydrogen in- and outlet, and a pressure-equalized dropping funnel containing terminal acetylene (1 eq.). The terminal (Th)ODA (1-*n*) or (3-*n*) was added slowly (over 6 h) to the stirred mixture under a constant flow of argon/hydrogen (1:1). The mixture was further stirred overnight at 25 °C, concentrated and filtrated over a short silica gel column (5% Et<sub>3</sub>N solution in petroleum ether 40/60). The residue was pre-purified on reversed phase silica (ACN/EtOAc) and finally purified on preparative HPLC to give pure (99%) elongated (Th)ODA (1-*n*) or (3-*n*)<sup>[6]</sup> respectively, while iodo-diacetylene (1) was recovered quantitatively.

#### 4.4.8 General method for catalytic Sonogashira coupling of protodesilylated members of ThODA series (1-*n*) with 2-iodo-5-methylthiophene as depicted in Figure 1

A mixture of 2-iodo-5-methylthiophene (3 eq.), Pd(PPh<sub>3</sub>)<sub>4</sub> (5 mol%), CuI (2 mol %), and dry, degassed diethyl amine (2 ml/mmol) and THF (5 ml/mmol) was placed anaerobically in a dried, brown two-necked round-bottomed flask, equipped with a magnetic stirrer, an argon/hydrogen in- and outlet, and a pressure-equalized dropping funnel containing terminal acetylene (1 eq.). The terminal ThODA (1-*n*) was added slowly (over 6 h) to the stirred mixture under a constant flow of argon/hydrogen (1:1). The mixture was further stirred overnight at 25 °C, concentrated and filtrated over a short silica gel column (petroleum ether 40/60). The residue was pre-purified on reversed phase silica (ACN/EtOAc) and finally purified on preparative HPLC to give pure (99 %) elongated ThODA (2-*n*).

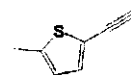
#### 4.4.9 General method catalytic Sonogashira coupling of protodesilylated members of ThODA series (1-*n*) or (3-*n*) with 2,5-diiodothiophene as depicted in Figure 1

A mixture of 2,5-diiodothiophene (3 eq.), Pd(PPh<sub>3</sub>)<sub>4</sub> (5 mol%), CuI (2 mol %), and dry, degassed diethyl amine (2 ml/mmol) and THF (5 ml/mmol) was placed anaerobically in a dried, brown two-necked round-bottomed flask, equipped with a magnetic stirrer, an argon/hydrogen in- and outlet, and a pressure-equalized dropping funnel containing terminal acetylene (1 eq.). The terminal ThODA (1-*n*) or (3-*n*)<sup>[6]</sup> was added slowly (over 6 h) to the stirred mixture under a constant flow of argon/hydrogen (1:1). The mixture was further stirred overnight at 25 °C, concentrated and filtrated over a short silica gel column (5% ethyl acetate in petroleum ether 40/60). The residue was pre-purified on reversed phase silica (ACN/EtOAc) and finally purified on preparative HPLC to give pure (99 %) elongated ThODA (4-*n*) or (5-*n*) respectively.

#### 4.4.10 General method for catalytic homocoupling of protodesilylated members of ThODA series (3-*n*) under Sonogashira conditions as illustrated in Figure 2

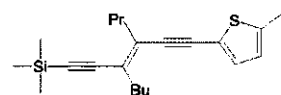
A mixture of terminal acetylene (3-*n*)<sup>[6]</sup>, Pd(PPh<sub>3</sub>)<sub>4</sub> (7 mol%), CuI (8 mol %), distilled diethyl amine (2 ml/mmol) and THF (5 ml/mmol) was placed in a round-bottomed flask, equipped with a magnetic stirrer. The mixture was stirred for 3 h at 25 °C under ambient atmosphere, concentrated and filtrated over a short silica gel column (5% ethyl acetate in petroleum ether 40/60). The residue was pre-purified on reversed phase silica (ACN/EtOAc) and finally purified on preparative HPLC to give pure (99.5%) HThODA (6-*n*).

## 4.4.11 2-ethynyl-5-methylthiophene



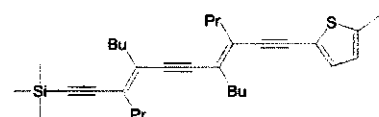
To a stirred and cooled (0 °C) solution of  $\text{PPh}_3$  (100 mmol, 26.2 gram) and  $\text{CBr}_4$  (50 mmol, 16.6 gram) in anhydrous dichloromethane (200 ml) under argon atmosphere was added in portions 2-thiophenecarbaldehyde (40 mmol, 4.48 gram). After completion (monitored on GC/MS and TLC), the crude reaction mixture was extracted as usual (see the general procedure) and purified on silica-gel column (petroleum ether 40/60). 2-(2,2-dibromovinyl)-5-methylthiophene was obtained as light, brown solid (38.3 mmol, 10.8 gram, 94% yield). To a stirred and cooled (-78 °C) solution of 2-(2,2-dibromovinyl)-5-methylthiophene (2.13 mmol, 0.6 gram) in anhydrous diethylether (30 ml) under argon atmosphere was added dropwise 1.7M solution of *n*-BuLi (4.27 mmol, 2.51 ml). After stirring for 30 min. the reaction mixture was allowed to warm up to room temperature. After completion (monitored on GC/MS and TLC), the reaction mixture was extracted as usual (see the general procedure) yielding 2-ethynyl-5-methylthiophene as pale brown liquid (1.87 mmol, 0.22 gram, 88%).  $^1\text{H}$  NMR:  $\delta$  = 2.48 (s, 3H), 3.30 (s, 1H), 6.64 (dq, 1H,  $J$  = 3Hz and 6Hz), 7.10 (d, 1H,  $J$  = 6Hz)  $^{13}\text{C}$  NMR:  $\delta$  = 15.32, 22.62, 80.37, 119.52, 125.15, 133.33, 142.36 HRMS: observed (122.0195) ; calculated (122.0191).

## 4.4.12 (E)-(3-butyl-4-(2-(5-methylthiophen-2-yl)ethynyl)hept-3-en-1-ynyl)trimethylsilane (1-1)



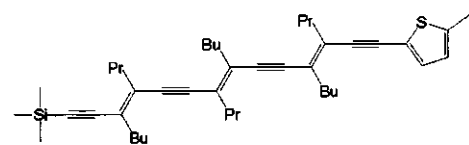
colorless oil (0.57 mmol, 0.197 g, 95%) from (1);  $^1\text{H}$  NMR:  $\delta$  = 0.22 (s, 9H), 0.97 (t, 3H,  $J$  = 7.2Hz), 0.98 (t, 3H,  $J$  = 7.4Hz), 1.38 (sextet, 2H  $J$  = 7.3Hz), 1.53-1.69 (m, 4H), 2.42 (t, 2H,  $J$  = 7.4Hz), 2.45-2.55 (m, 5H), 6.66 (m, 1H), 7.00 (d, 1H,  $J$  = 3.5Hz);  $^{13}\text{C}$  NMR:  $\delta$  = 0.0, 13.6, 13.9, 15.4, 21.7, 22.1, 30.5, 34.5, 36.8, 92.2, 92.3, 103.6, 104.7, 121.2, 125.4, 128.9, 130.8, 131.6, 142.2; HRMS: observed (342.1840); calculated (342.1838).

## 4.4.13 ((3E,7E)-4,7-dibutyl-8-(2-(5-methylthiophen-2-yl)ethynyl)-3-propylundeca-3,7-dien-1,5-diynyl)trimethylsilane (1-2)

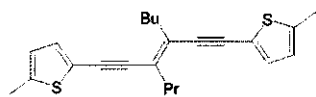


pale yellow oil (0.22 mmol, 0.106 g, 88%) from (1-1);  $^1\text{H}$  NMR:  $\delta$  = 0.23 (s, 9H), 0.96 (t, 6H,  $J$  = 7.4Hz), 0.99 (t, 6H,  $J$  = 7.9Hz), 1.31-1.48 (m, 4H), 1.52-1.74 (m, 8H), 2.42 (t, 2H,  $J$  = 7.4Hz), 2.45-2.58 (m, 9H), 6.67 (m, 1H), 7.01 (d, 1H,  $J$  = 3.6Hz);  $^{13}\text{C}$  NMR:  $\delta$  = 0.0, 13.6, 13.9, 14.0, 15.4, 21.7, 21.8, 22.1, 22.3, 22.4, 30.5, 30.8, 32.0, 34.8, 34.8, 37.0, 37.2, 92.2, 92.7, 98.5, 99.0, 103.8, 104.9, 121.3, 125.2, 125.5, 128.8, 129.2, 131.3, 131.6, 131.9, 142.2; HRMS: observed (490.3089); calculated (490.3090).

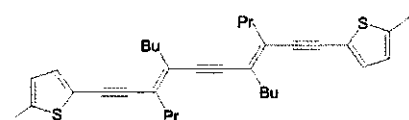
## 4.4.14 Trimethyl(((3E,7E,11E)-3,8,11-tributyl-12-(2-(5-methylthiophen-2-yl)ethynyl)-4,7-dipropylpentadeca-3,7,11-trien-1,5,9-triynyl)silane (1-3)



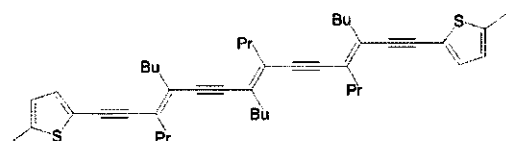
pale yellow oil (0.06 mmol, 0.036 g, 85%) from (1-2);  $^1\text{H}$  NMR:  $\delta$  = 0.23 (s, 9H), 0.91-1.02 (m, 18H), 1.32-1.48 (m, 6H), 1.52-1.71 (m, 12H), 2.37-2.58 (m, 15H), 6.67 (m, 1H,  $J$  = 3.6Hz), 7.01 (d, 1H,  $J$  = 3.6Hz);  $^{13}\text{C}$  NMR:  $\delta$  = 0.4, 13.6, 13.9, 14.0, 14.0, 15.4, 21.7, 21.8, 21.9, 22.1, 22.3, 22.3, 30.5, 30.8, 34.7, 34.8, 35.1, 37.0, 37.2, 37.3, 92.3, 92.8, 98.7, 99.1, 99.1, 103.8, 104.9, 121.3, 125.5, 128.8, 129.2, 129.3, 129.7, 131.3, 131.6, 142.2; HRMS: observed (638.4337); calculated (638.4342).

**4.4.15 (E)-2-methyl-5-(4-(2-(5-methylthiophen-2-yl)ethynyl)-3-propyloct-3-en-1-ynyl)thiophene (2-1)**


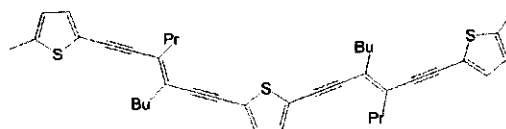
yellow oil (0.74 mmol, 0.217 g, 68%) from (1-1);  $^1\text{H}$  NMR:  $\delta$  = 0.96 (t, 3H,  $J$ =6.9Hz), 0.98 (t, 3H,  $J$ =6.9Hz), 1.45 (sextet, 2H,  $J$ =7.3Hz), 1.56-1.77 (m, 4H), 2.50 (s, 6H), 1.47-2.60 (m, 4H), 6.67 (m, 2H), 6.98 (d, 1H,  $J$ =3.5Hz), 6.99 (d, 1H,  $J$ =3.5Hz);  $^{13}\text{C}$  NMR:  $\delta$  = 13.7, 14.0, 15.4, 21.9, 22.2, 30.7, 34.6, 36.9, 92.1, 92.6, 92.7, 121.3, 125.5, 128.8, 129.3, 131.6, 142.2; HRMS: observed (366.1474); calculated (366.1476).

**4.4.15 2-((3E,7E)-4,7-dibutyl-8-(2-(5-methylthiophen-2-yl)ethynyl)-3-propylundeca-3,7-dien-1,5-diylnyl)-5-methylthiophene (2-2)**


yellow oil (0.07 mmol, 0.034 g, 53%) from (1-2);  $^1\text{H}$  NMR:  $\delta$  = 0.92-1.04 (m, 12H), 1.43 (sextet, 4H,  $J$ =7.2Hz), 1.54-1.74 (m, 8H), 2.46-2.58 (m, 14H), 6.67 (m, 2H), 7.00 (d, 1H,  $J$ =3.5Hz), 7.01 (d, 1H,  $J$ =3.5Hz);  $^{13}\text{C}$  NMR:  $\delta$  = 13.7, 14.0, 14.0, 15.4, 21.9, 21.9, 22.2, 22.3, 22.6, 30.8, 30.9, 34.8, 34.9, 37.0, 37.2, 92.3, 92.3, 92.8, 92.8, 98.9, 99.0, 121.3, 125.5, 128.8, 129.2, 129.3, 129.7, 131.6, 142.2; HRMS: observed (514.2727); calculated (514.2727).

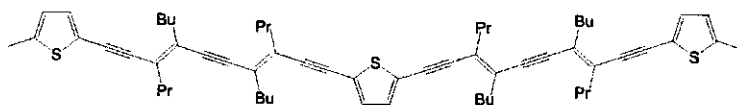
**4.4.16 2-((3E,7E,11E)-4,7-dibutyl-12-(2-(5-methylthiophen-2-yl)ethynyl)-3,8,11-tripropylhexadeca-3,7,11-trien-1,5,9-triynyl)-5-methylthiophene (2-3)**


yellow oil (0.03 mmol, 0.019 g, 40%) from (1-3);  $^1\text{H}$  NMR:  $\delta$  = 0.87-1.04 (m, 18H), 1.32-1.48 (m, 6H), 1.51-1.73 (m, 12H), 2.44-2.58 (m, 18H), 6.67 (d, 2H,  $J$ =3.6Hz), 7.00 (d, 1H,  $J$ =3.5Hz), 7.01 (d, 1H,  $J$ =3.5Hz);  $^{13}\text{C}$  NMR:  $\delta$  = 13.6, 14.0, 14.0, 14.0, 15.4, 21.9, 21.9, 22.1, 22.3, 22.3, 30.7, 30.9, 34.8, 34.9, 35.1, 37.0, 37.2, 37.3, 92.3, 92.3, 92.8, 92.9, 99.1, 99.2, 121.3, 125.5, 128.8, 129.2, 129.2, 129.3, 129.7, 129.8, 131.6, 142.2; HRMS: observed (662.3977); calculated (662.3979).

**4.4.17 2,5-bis((E)-3-butyl-4-(2-(5-methylthiophen-2-yl)ethynyl)hept-3-en-1-ynyl)thiophene (4-1)**


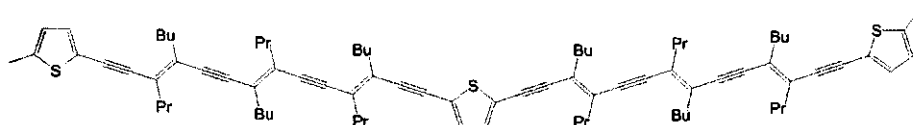
yellow solid (0.26 mmol, 0.164 g, 40%) from (1-1);  $^1\text{H}$  NMR:  $\delta$  = 1.01 (t, 6H,  $J$ =7.2Hz), 1.04 (t, 6H,  $J$ =7.2Hz), 1.45 (sextet, 4H,  $J$ =7.3Hz), 1.59-1.77 (m, 8H), 2.51 (s, 6H), 2.52-2.62 (m, 8H), 6.69 (m, 2H), 7.04 (d, 1H,  $J$ =3.5Hz), 7.05 (d, 1H,  $J$ =3.5Hz), 7.08 (s, 2H);  $^{13}\text{C}$  NMR:  $\delta$  = 13.7, 14.0, 15.5, 21.9, 22.1, 22.2, 22.5, 29.7, 30.8, 30.9, 31.7, 34.8, 36.8, 91.6, 92.8, 92.9, 94.8, 121.1, 125.0, 125.6, 128.3, 130.6, 131.4, 132.0, 142.5; HRMS: observed (620.2599); calculated (620.2605).

**4.4.18 2,5-bis((3E,7E)-4,7-dibutyl-8-(2-(5-methylthiophen-2-yl)ethynyl)-3-propylundeca-3,7-dien-1,5-diynyl)thiophene (4-2)**



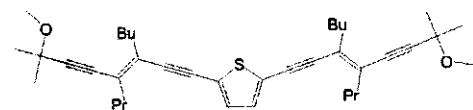
yellow/brown solid (0.02 mmol, 0.019 g, 30%) from (1-2);  $^1\text{H}$  NMR:  $\delta$  = 0.98 (t, 6H,  $J$ =7.3Hz), 0.99 (t, 6H,  $J$ =6.9Hz), 1.00 (t, 6H,  $J$ =7.3Hz), 1.02 (t, 6H,  $J$ =6.9Hz), 1.34-1.48 (m, 8H), 1.54-1.74 (m, 16H), 2.46-2.59 (m, 22H), 6.67 (m, 2H), 7.02 (d, 2H,  $J$ =3.5Hz), 7.06 (s, 2H);  $^{13}\text{C}$  NMR:  $\delta$  = 13.7, 14.0, 14.0, 15.4, 21.9, 22.0, 22.2, 22.3, 29.7, 30.8, 30.9, 34.9, 35.0, 36.9, 37.2, 91.5, 92.5, 92.8, 94.9, 98.8, 99.6, 121.2, 125.0, 125.5, 128.2, 129.1, 129.6, 131.0, 131.4, 131.7, 142.3; HRMS: observed (916.5116); calculated (916.5109).

**4.4.19 2,5-bis((3E,7E,11E)-3,8,11-tributyl-12-(2-(5-methylthiophen-2-yl)ethynyl)-4,7-dipropylpentadeca-3,7,11-trien-1,5,9-triynyl)thiophene (4-3)**



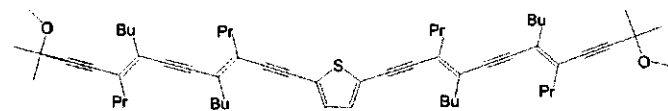
orange/brown solid (0.02 mmol, 0.028 g, 30%) from (1-3);  $^1\text{H}$  NMR:  $\delta$  = 0.92-1.04 (m, 36H), 1.33-1.49 (m, 12H), 1.54-1.74 (m, 24H), 2.45-2.59 (m, 30H), 6.67 (d, 2H,  $J$ = 3.7Hz), 7.02 (d, 2H,  $J$ =3.6Hz), 7.06 (s, 2H);  $^{13}\text{C}$  NMR:  $\delta$  = 13.7, 14.0, 14.0, 14.0, 15.4, 21.9, 22.0, 22.1, 22.3, 22.4, 30.8, 30.9, 30.9, 34.9, 35.0, 35.1, 36.9, 37.2, 37.3, 91.5, 92.4, 92.8, 95.0, 99.0, 99.1, 99.3, 99.8, 121.3, 125.0, 125.5, 128.2, 129.1, 129.3, 130.1, 131.0, 131.4, 131.7, 142.3; MALDI-TOF-MS: observed (1212.71); calculated (1212.76).

**4.4.20 2,5-bis((E)-3-butyl-7-methoxy-7-methyl-4-propylocta-3-en-1,5-diynyl)thiophene (5-1)**



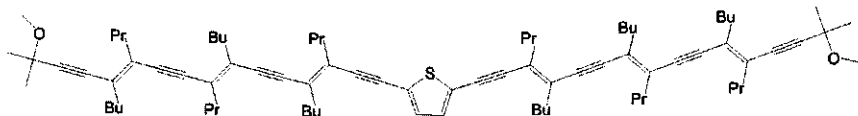
pale yellow oil (0.27 mmol, 0.157 g, 49%) from (3-1)<sup>[6]</sup>;  $^1\text{H}$  NMR:  $\delta$  = 0.94 (t, 6H,  $J$ =7.3Hz), 0.95 (t, 6H,  $J$ =7.4Hz), 1.37 (sextet, 4H,  $J$ =7.3Hz), 1.52 (s, 12H), 1.52-1.63 (m, 8H), 2.44 (t, 4H,  $J$ =7.2Hz), 2.45 (t, 4H,  $J$ =7.2Hz), 3.40 (s, 6H), 7.04 (s, 2H);  $^{13}\text{C}$  NMR:  $\delta$  = 13.6, 14.0, 21.8, 22.1, 28.4, 30.6, 34.8, 36.7, 51.8, 71.2, 83.7, 90.7, 94.2, 100.8, 124.9, 128.5, 130.3, 131.4; HRMS: observed (572.3691); calculated (572.3688).

**4.4.21 2,5-bis((3E,7E)-4,7-dibutyl-11-methoxy-11-methyl-3,8-dipropyldodeca-3,7-dien-1,5,9-triynyl)thiophene (5-2)**



yellow/orange oil (0.03 mmol, 0.262g, 46%) from (3-2)<sup>[6]</sup>;  $^1\text{H}$  NMR:  $\delta$  = 0.89-1.02 (m, 24H), 1.29-1.49 (m, 8H), 1.52 (s, 6H), 1.53-1.72 (m, 22H), 2.39-2.57 (m, 16H), 3.40 (s, 6H), 7.05 (s, 2H);  $^{13}\text{C}$  NMR:  $\delta$  = 13.6, 13.6, 14.0, 14.0, 21.8, 21.9, 22.1, 22.2, 22.7, 28.4, 30.7, 30.7, 34.9, 35.0, 36.9, 37.1, 51.7, 71.2, 84.0, 91.4, 94.8, 98.1, 99.1, 100.5, 125.0, 128.2, 129.3, 129.3, 131.0, 131.4; HRMS: observed (868.6197); calculated (868.6192).

**4.4.22 2,5-bis((3E,7E,11E)-3,8,11-tributyl-15-methoxy-15-methyl-4,7,12-tripropylhexadeca-3,7,11-trien-1,5,9,13-tetraynyl)thiophene (5-3)**



yellow/brown solid (0.02 mmol, 0.190 g, 66%) from **(3-3)**<sup>[6]</sup>; <sup>1</sup>H NMR:  $\delta$  = 0.90-1.00 (m, 36H), 1.30-1.49 (m, 12H), 1.52 (s, 12H), 1.53-1.70 (m, 24H), 2.41-2.56 (m, 24H), 3.40 (s, 6H), 7.06 (s, 2H); <sup>13</sup>C NMR:  $\delta$  = 13.6, 13.6, 14.0, 14.0, 21.8, 21.9, 21.9, 22.1, 22.2, 22.3, 28.4, 30.7, 30.7, 30.8, 34.9, 35.0, 35.1, 36.9, 37.1, 37.3, 51.7, 71.2, 84.0, 91.5, 94.9, 98.4, 98.8, 99.7, 100.4, 125.0, 128.2, 129.0, 129.1, 129.4, 130.0, 131.0, 131.4; HRMS: observed (1164.8670); calculated (1164.8696).

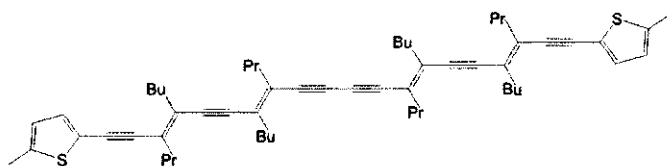
**4.4.23 2-((3E,9E)-4,9-dibutyl-10-(2-(5-methylthiophen-2-yl)ethynyl)-3-propyltrideca-3,9-dien-1,5,7-triynyl)-5-methylthiophene (6-1)**



yellow/brown solid (0.59 mmol, 0.320 g, 95%) from **(1-1)**; <sup>1</sup>H NMR:  $\delta$  = 0.97 (t, 6H,  $J$  = 7.3Hz), 0.99 (t, 6H,  $J$  = 7.3Hz), 1.41 (sextet, 4H,  $J$  = 7.4Hz), 1.55-1.72 (m, 8H), 2.43-2.65 (m, 14H), 6.61 (d, 1H,  $J$  = 3.5Hz), 6.68 (d, 1H,  $J$  = 3.5Hz), 7.03 (d, 2H,  $J$  = 3.7Hz); <sup>13</sup>C NMR:  $\delta$  = 13.6,

13.9, 15.4, 21.8, 22.1, 30.7, 34.8, 36.8, 82.9, 84.4, 92.4, 94.2, 120.9, 125.6, 127.8, 132.0, 133.6, 142.7; HRMS: observed (538.2729); calculated (538.2728).

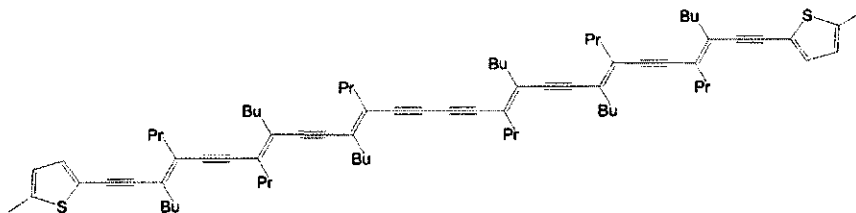
**4.4.24 2-methyl-5-((3E,7E,13E,17E)-4,7,14,17-tetrabutyl-18-(2-(5-methylthiophen-2-yl)ethynyl)-3,8,13-tripropylhenicosa-3,7,13,17-tetraen-1,5,9,11,15-pentaynyl)thiophene (6-2)**



dark orange solid (0.28 mmol, 0.230 g, 90%) from **(1-2)**; <sup>1</sup>H NMR:  $\delta$  = 0.80-1.03 (m, 24H), 1.40 (sextet, 8H,  $J$  = 7.3Hz), 1.55-1.72 (m, 16H), 2.43-2.65 (m, 22H), 6.67 (m, 2H), 7.02 (d, 2H,

$J$  = 3.7Hz); <sup>13</sup>C NMR:  $\delta$  = 13.6, 13.6, 13.9, 14.0, 15.4, 21.8, 21.9, 22.1, 22.3, 30.8, 30.8, 34.9, 35.2, 37.0, 37.2, 83.1, 84.7, 92.7, 92.7, 98.5, 100.9, 121.2, 125.5, 127.8, 129.0, 129.9, 131.7, 134.0, 142.4; HRMS: observed (834.5227); calculated (834.5232).

**4.4.25 2-((3E,7E,11E,17E,21E,25E)-4,7,12,17,22,25-hexabutyl-26-(2-(5-methylthiophen-2-yl)ethynyl)-3,8,11,18,21-pentapropylnonacosa-3,7,11,17,21,25-hexaen-1,5,9,13,15,19,23-heptaenyl)-5-methylthiophene (6-3)**



orange/brown solid (0.10 mmol, 0.110 g, 89%) from (1-3);  $^1\text{H}$  NMR:  $\delta$  = 0.88-1.03 (m, 36H), 1.33-1.44 (m, 12H), 1.50-1.70 (m, 24H), 2.43-2.65 (m, 30H), 6.67 (m, 2H), 7.01 (d, 2H,  $J$ =3.7Hz);  $^{13}\text{C}$  NMR:  $\delta$  = 13.6, 13.9, 14.0, 14.0, 15.4, 21.8, 21.9, 22.1, 22.3, 22.3, 30.8, 30.8, 34.8, 35.1, 37.0, 37.2, 37.3, 83.1, 84.8, 92.4, 92.8, 98.8, 99.0, 99.5, 101.1, 121.2, 125.5, 127.8, 129.0, 129.2, 129.4, 130.4, 131.6, 134.0, 142.3; HRMS: observed (1130.7749); calculated (1130.7736).

## 4.5 Acknowledgements

The authors thank the Dutch Technology Foundation STW for generous funding of this research (Project No. WPC 5740), Dr. Jan Kroon (ECN) and Dr. Joost Smits (Shell) for helpful discussions, Dr. M. A. Posthumus for performing HRMS experiments, Dr. Jacob Baggerman for the quantum chemical calculation of 2-1, and Ing. E. J. Bakx for performing MALDI-TOF MS experiments.

## 4.6 Supporting Information

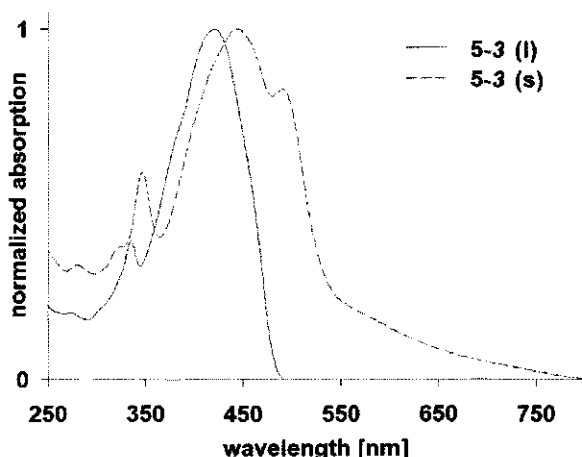


Figure 9. Normalized absorption spectra of 5-3 in solution (l) versus thin solid film (s).

Table 1. Emission data of oligomers under study in toluene and methanol.

oligomer (CL) <sup>[a]</sup>	$\lambda_{\text{max}}^{\text{E}}$ [nm] ([eV])		Quantum Yield $\Phi_{\text{f}}$ <sup>[b,c]</sup>		Stokes shift [eV]	
	toluene	methanol	toluene	methanol	toluene	methanol
1-1 (5)	377 (3.29)	386 (3.21)	0.003	0.002	0.446	[e]
1-2 (7)	415 (2.99)	417 (2.97)	0.229	0.045	0.409	0.471
1-3 (9)	452 (2.74)	470 (2.64)	0.017	0.010	0.412	[e]
2-1 (7)	405 (3.06)	398 (3.11)	0.160	0.023	0.383	0.377
2-2 (9)	440 (2.82)	434 (2.86)	0.250	0.130	0.394	0.406
2-3 (11)	463 (2.68)	460 (2.70)	0.005	0.006	0.399	0.444
4-1 (12)	467 (2.66)	460 (2.70)	0.190	0.110	0.369	0.372
4-2 (16)	489 (2.54)	483 (2.57)	0.011	0.006	0.375	0.406
4-3 (20)	500 (2.48)	[d]	0.006	[d]	0.384	[d]
5-1 (8)	421 (2.94)	416 (2.98)	0.240	0.220	0.335	0.353
5-2 (12)	470 (2.64)	461 (2.70)	0.015	0.011	0.371	0.380
5-3 (16)	490 (2.53)	478 (2.59)	0.005	0.005	0.373	0.372
6-1 (10)	449 (2.76)	447 (2.77)	0.160	0.089	0.459	0.472
6-2 (14)	492 (2.52)	490 (2.53)	0.002	0.001	[e]	[e]
6-3 (18)	502 (2.47)	[d]	0.001	[d]	[e]	[e]

[a] Conjugation length (CL) as number of double and triple bonds; [b] Quantum yield determined by comparison yield determined by comparison with tryptophan:  $\Phi_{\text{f}} = 0.13^{[48]}$ ; [c] Experimental error  $\pm 0.002$ ; [d] Not obtained due to low solubility in methanol; [e] Not determined due to an absence of a visible 0-0 transition.

## 4.7 References

- [1] J. M. Tour, *Chem. Rev.* **1996**, *96*, 537-553.
- [2] D. Fichou in *Handbook of oligo- and polythiophenes*, (WILEY-VCH Verlag GmbH, Weinheim, **1999**, p. 366.
- [3] H. Zuilhof, H. M. Barentsen, M. Dijk van, E. J. R. Sudhölter, R. J. O. M. Hoofman, L. D. A. Siebbeles, M. P. Haas de and J. M. Warman in *Polydiacetylenes*, (Ed. H. S. Nalwa), Academic Press, San Diego, San Francisco, New York, Boston, London, Sydney, Tokyo, **2001**, pp. 339-437.
- [4] J. Roncali, *Chem. Rev.* **1992**, *92*, 711-738.
- [5] J. Gierschner, J. Cornil and H.-J. Egelhaaf, *Adv. Mater.* **2007**, *19*, 173-191.
- [6] G. S. Pilzak, B. van Lagen, C. C. J. Hendrikx, E. J. R. Sudhölter and H. Zuilhof, *Chem. Eur. J.* **2008**, *14*, 7939-7950.



- [7] G. S. Pilzak, B. van Lagen, E. J. R. Sudhölter and H. Zuilhof, *Tetrahedron Lett.* **2008**, *49*, 4949-4952.
- [8] G. S. Pilzak, J. Baggerman, B. van Lagen, M. A. Posthumus, E. J. R. Sudhölter and H. Zuilhof, *Chem. Eur. J.* **2009**, *15*, 2296-2304.
- [9] M. Polhuis, C. C. J. Hendrikx, H. Zuilhof and E. J. R. Sudhölter, *Tetrahedron Lett.* **2003**, *44*, 899-901.
- [10] R. Giesa and R. C. Schulz, *Polym. Int.* **1994**, *33*, 43-60.
- [11] M. R. Bryce, M. A. Coffin, P. J. Skabara, A. J. Moore, A. S. Batsanov and J. A. K. Howard, *Chem. Eur. J.* **2000**, *6*, 1955-1962.
- [12] C. Czekelius, J. Hafer, Z. J. Tonzetich, R. R. Schrock, R. L. Christensen and P. Mueller, *J. Am. Chem. Soc.* **2006**, *128*, 16664-16675.
- [13] R. Sander, V. Stuempflen, J. H. Wendorff and A. Greiner, *Macromolecules* **1996**, *29*, 7705-7708.
- [14] R. E. Martin and F. Diederich, *Angew. Chem. Int. Ed.* **1999**, *38*, 1351-1377.
- [15] R. E. Martin, U. Gubler, J. Cornil, M. Balakina, C. Boudon, C. Bosshard, J.-P. Gisselbrecht, F. Diederich, P. Gunter, M. Gross and J.-L. Bredas, *Chem. Eur. J.* **2000**, *6*, 3622-3635.
- [16] J. F. Nierengarten, D. Guillon, B. Heinrich and J. F. Nicoud, *Chem. Commun.* **1997**, 1233-1234.
- [17] Y. Zhao and R. R. Tykwinski, *J. Am. Chem. Soc.* **1999**, *121*, 458-459.
- [18] Y. Zhao, R. McDonald and R. R. Tykwinski, *J. Org. Chem.* **2002**, *67*, 2805-2812.
- [19] S. C. Ciulei and R. R. Tykwinski, *Org. Lett.* **2000**, *2*, 3607-3610.
- [20] Y. Zhao, S. C. Ciulei and R. R. Tykwinski, *Tetrahedron Lett.* **2001**, *42*, 7721-7723.
- [21] G. Zotti, G. Schiavon, A. Berlin and G. Pagani, *Chem. Mater.* **1993**, *5*, 430-436.
- [22] G. Zotti, G. Schiavon, A. Berlin and G. Pagani, *Chem. Mater.* **1993**, *5*, 620-624.
- [23] G. Zotti, G. Schiavon, A. Berlin and G. Pagani, *Adv. Mater.* **1993**, *5*, 551-554.
- [24] W. Ten Hoeve, H. Wynberg, E. E. Havinga and E. W. Meijer, *J. Am. Chem. Soc.* **1991**, *113*, 5887-5889.
- [25] S. S. Zade and M. Bendikov, *J. Org. Chem.* **2006**, *71*, 2972-2981.
- [26] D. Fichou, G. Horowitz, B. Xu and F. Garnier, *Synth. Met.* **1990**, *39*, 243-259.
- [27] U. Segelbacher, N. S. Sariciftci, A. Grupp, P. Baeuerle and M. Mehring, *Synth. Met.* **1993**, *57*, 4728-4733.
- [28] C. Sauteret, J. P. Hermann, R. Frey, F. Pradère, J. Ducuing, R. H. Baughman and R. R. Chance, *Phys. Rev. Lett.* **1976**, *36*, 956-959.
- [29] A. F. Garito, C. C. Teng, K. Y. Wong and O. Zammani-Khamiri, *Mol. Cryst. Liq. Cryst.* **1984**, *106*, 219-258.
- [30] K. J. Donovan and E. G. Wilson, *Synth. Met.* **1989**, *28*, 569-574.
- [31] S. Spagnoli, K. J. Donovan, K. Scott, M. Somerton and E. G. Wilson, *Chem. Phys.* **1999**, *250*, 71-79.
- [32] S. Jo, H. Yoshikawa, A. Fujii and M. Takenaga, *Synth. Met.* **2005**, *150*, 223-226.
- [33] M. Schott, *Synth. Met.* **2003**, *139*, 739-742.
- [34] R. E. Martin, J. A. Wytke, F. Diederich, C. Boudon and J.-P. Gisselbrecht, *Helv. Chim. Acta* **1999**, *82*, 1470-1485.
- [35] U. Gubler, S. Concilio, C. Bosshard, I. Biaggio, P. Gunter, R. E. Martin, M. J. Edelmann, J. A. Wytke and F. Diederich, *Appl. Phys. Lett.* **2002**, *81*, 2322-2324.
- [36] Y. Nakano, K. Ishizuka, K. Muraoka, H. Ohtani, Y. Takayama and F. Sato, *Org. Lett.* **2004**, *6*, 2373-2376.
- [37] D. V. Matyushov, R. Schmid and B. M. Ladanyi, *J. Phys. Chem. B* **1997**, *101*, 1035-1050.
- [38] F. Wudl and S. P. Bitler, *J. Am. Chem. Soc.* **1986**, *108*, 4685-4687.
- [39] Y. Takayama, C. Delas, K. Muraoka and F. Sato, *Org. Lett.* **2003**, *5*, 365-368.
- [40] C. C. J. Hendrikx, M. Polhuis, A. Pul-Hootsen, R. B. M. Koehorst, A. Hoek van, H. Zuilhof and E. J. R. Sudhölter, *Phys. Chem. Chem. Phys.* **2005**, *7*, 548-553.
- [41] N. S. Bayliss and E. G. McRae, *J. Phys. Chem.* **1954**, *58*, 1002-1006.
- [42] C. Reichardt, *Solvents and Solvent Effects in Organic Chemistry*, Wiley-VCH, **2003**, p. 630.

- [43] H. Chosrovian, S. Rentsch, D. Grebner, D. U. Dahm, E. Birkner and H. Naarmann, *Synth. Met.* **1993**, *60*, 23-26.
- [44] G. M. Balkowski, M. Groeneveld, H. Zhang, C. C. J. Hendriks, M. Polhuis, H. Zuilhof and W. J. Buma, *J. Phys. Chem. A* **2006**, *110*, 11435-11439.
- [45] G. Lanzani, G. Cerullo, S. Stagira and S. De Silvestri, *J. Photochem. Photobiol. A Chem.* **2001**, *144*, 13-19.
- [46] S. Meng, J. Ma and Y. Jiang, *J. Phys. Chem. B* **2007**, *111*, 4128-4136.
- [47] B. E. Kohler and D. E. Schilke, *J. Chem. Phys.* **1987**, *86*, 5214-5215.
- [48] J. R. Lakowicz, *Principles of Fluorescence Spectroscopy*, Kluwer Academic / Plenum Publishers, **2006**, p. 420-421.
- [49] P. Garcia, J. M. Pernaut, P. Hapiot, V. Wintgens, P. Valat, F. Garnier and D. Delabouglise, *J. Phys. Chem.* **1993**, *97*, 513-516.
- [50] P. F. van Hutten, R. E. Gill, J. K. Herrema and G. Hadziioannou, *J. Phys. Chem.* **1995**, *99*, 3218-3224.
- [51] J. Gierschner, H. G. Mack, H. J. Egelhaaf, S. Schweizer, B. Doser and D. Oelkrug, *Synt. Met.* **2003**, *138*, 311-315.
- [52] A. Van Hoek and A. J. W. G. Visser, *Instrumentation Sci. Technol.* **1985**, *14*, 143 - 154.
- [53] E. G. Novikov, A. van Hoek, A. J. W. G. Visser and J. W. Hofstraat, *Optics Commun.* **1999**, *166*, 189-198.
- [54] A. V. Digris, V. V. Skakoun, E. G. Novikov, A. van Hoek, A. Claiborne and A. J. W. G. Visser, *Euro. Biophys. J.* **1999**, *28*, 526-531.

# Chapter 5

## Divergent Synthesis and Optoelectronic Properties of Oligodiacetylene Building Blocks

### Abstract

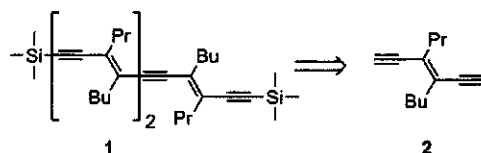
A new and divergent synthesis route to oligodiacetylene (ODA) building blocks has been developed via Sonogashira reaction under a reductive atmosphere. These central building blocks provide a new way for rapid preparation of long ODAs. In addition we report on their optoelectronic properties which are dependent on their endcap. Finally, the formation of their radical cations, and their optical properties and reactivity towards nucleophiles are investigated.

*This chapter was published: Gregor S. Pilzak, Barend van Lagen, Ernst J. R. Sudhölter, Han Zuilhof, Tetrahedron Letters, 2008, 49, 4949-4952.*

## 5.1 Introduction

The development of precisely defined  $\pi$ -conjugated oligomers has developed significantly in the last decade, since such monodisperse oligomers function as model systems to determine the evolution of the optical and electronic properties of the corresponding polymers.<sup>[1-3]</sup> Recently, our systematic studies of the optical properties of highly soluble all-*trans* oligodiacetylenes (ODA)<sup>[4]</sup> and homo-oligodiacetylenes (HODA)<sup>[5]</sup> has provided new information about the relationship between oligomer length (up to 8.2 nm) and the optoelectronic properties of polydiacetylene-related materials. This made it possible to distinguish intra- and intermolecular effects on the light absorption of these extended conjugated systems. However, the iterative synthesis of these materials is a rather time-consuming process, in which the oligomer backbone is extended with only one monomeric unit per elongation cycle. This chain extension could be substantially speeded up by using a central building block to couple two oligomers in just one elongation step. Moreover, such a building block should be designed in such a way that it does not alter the structure of the ODA backbone and can be implemented easily in existing ODA syntheses, to provide a new and fast way of preparing nanometer-sized ODAs.

In this study, a synthesis is presented of trimeric and monomeric central building blocks **1** and **2** for oligodiacetylene syntheses (Scheme 1). In addition, we have studied the influence of the endcaps on the optical properties of the oligomer backbone, and, for the first time the optoelectronic properties of the corresponding radical cations.



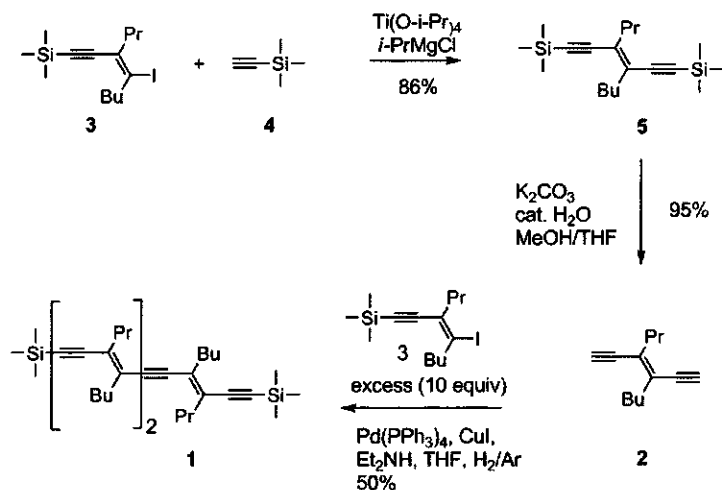
Scheme 1. Retrosynthesis of the oligodiacetylenes under present study.

## 5.2 Results and Discussion

### 5.2.1 Divergent synthesis of oligodiacetylene building blocks

The ODA building blocks **1** were prepared *via* a divergent approach as illustrated in Scheme 2. The ODA backbone bears two asymmetrical alkyl chains. These provide, firstly, steric hindrance, and therefore hamper interchain  $\pi$ - $\pi$  stacking. Secondly, their structural asymmetry is highly beneficial, as this improves substantially the solubility. Finally, the

trimethylsilyl (TMS) endcaps can be removed rapidly and quantitatively under mild, alkaline conditions yielding a terminal *bis*-acetylene that can be used as the central unit in a divergent synthesis of enediyne-containing materials. The synthesis of the *trans*-iodoenyne **3** is described elsewhere.<sup>4</sup> The mild coupling of the terminal acetylene **4** with **3** was performed via a Sonogashira reaction yielding ene-diyne **5** in 95% isolated yield. The alkaline protodesilylation of **5** proceeds quantitatively, and results in ene-diyne **2** bearing two terminal acetylene groups. The following divergent elongation step consists of catalytic coupling of **2** with two ODA blocks **3** under a diluted hydrogen atmosphere. This was done to prevent oxidation of the palladium catalyst, which would otherwise initiate polymerization of the terminal acetylenes.<sup>[6]</sup> Unreacted **3** was recovered quantitatively after the elongation step, which allowed the use of a large excess of this material. This elongation process adds eight conjugated C atoms to the ODA chain in a single reaction step. The catalytic coupling of *trans*-iodoenyne **3** to building block **1** can be repeated in this fashion to yield long-chain ODAs, or related materials.



Scheme 2. Divergent synthesis of oligodiacetylenes building blocks.

### 5.2.2 Steady-state optical absorption and fluorescence in solution

The ground state absorption and fluorescence emission of the newly synthesized building blocks **5** and **1** were recorded in *n*-hexane. In order to study the influence of the endcaps on the optoelectronic properties of the ODAs, a novel oligomer **6** was synthesized having methyl and  $-\text{C}(\text{CH}_3)_2\text{CH}_2\text{OCH}_3$  endcaps (Figure 1). The absorption and emission spectra of these ODAs

are shown in Figure 1 together with the literature data of previously synthesized ene-diyne **7** and ODA **8** with TMS and  $-\text{C}(\text{CH}_3)_2\text{CH}_2\text{OCH}_3$  endcaps.<sup>[4]</sup>

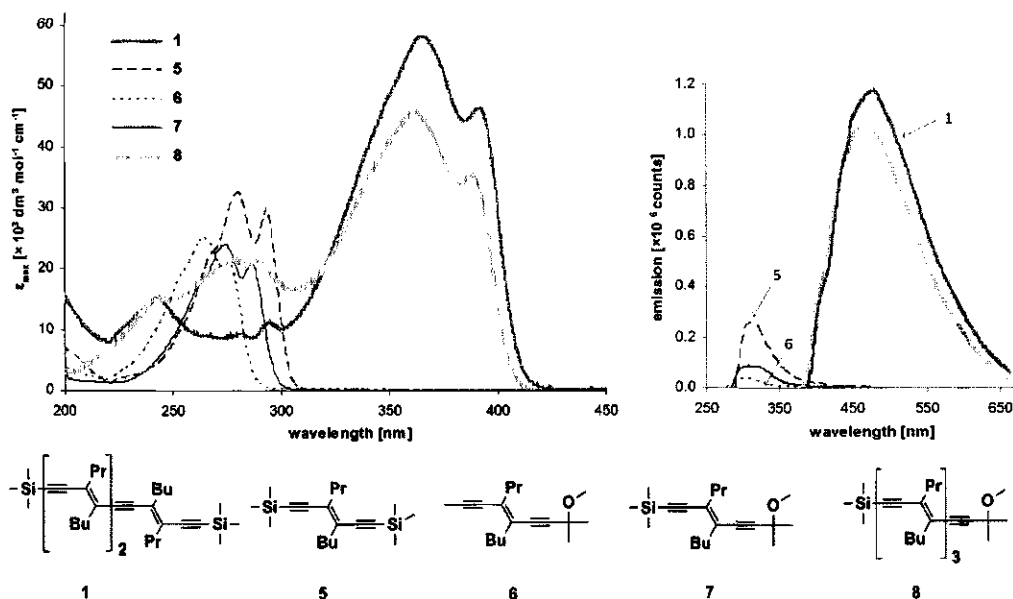


Figure 1. Electronic absorption (top) and emission (bottom) spectra of the ODA building blocks in *n*-hexane at micromolar concentrations ( $\sim 2 \cdot 10^{-6} \text{ M}$ ).

The steady-state optical absorption and fluorescence data of the oligoacetylenes under study are summarized in Table 1. The absorption spectra clearly show a bathochromic shift and an increase of the absorption with chain elongation. The  $\epsilon_{\text{max}}$  increases by 78% going from **5** with the conjugation length (CL) of 3 conjugated double and triple bonds, to **1** (CL = 7).

The optical properties of ODA building blocks are dominated by the  $\text{C}_{2h}$  symmetry that is present in fully stretched, planar oligomers, and their absorption spectrum is associated with the  $\text{S}_2 (1^1\text{B}_u) \leftarrow \text{S}_0 (1^1\text{A}_g)$  transition.<sup>[4, 7, 8]</sup> The influence of the endcap on the absorption is small but clear: a red-shift of 10 nm (0.17 eV) is induced when the less electron-donating Me-group in **6** is exchanged for a TMS-group in **7**.<sup>[9]</sup> Analogous but smaller effects were observed when the  $t\text{-CMe}_2\text{OMe}$  group was exchanged for a TMS group, that is, 5 nm (0.09 eV) and 4 nm (0.03 eV) for ODAs with CL of 3 and 7, respectively. Similar red-shifting of the absorption is reported for ODAs<sup>[8]</sup> and oligotriacetylenes<sup>[10]</sup> upon introduction of electron-donating end groups, whilst blue-shifts are observed when an electron-withdrawing endcap is added to carotenoid derivatives<sup>[11]</sup> and distyryl-benzenes.<sup>[12]</sup>

Table 1. Absorption and emission data of ODA building blocks as a millimolar solution ( $2 \cdot 10^{-6}$  M) in *n*-hexane.

ODA (CL) <sup>[a]</sup>	Absorption		Emission	
	$\lambda_{\text{max}}$ [nm] ([eV])	$\epsilon_{\text{max}}$ [ $\times 10^3 \text{ dm}^3 \text{ mol}^{-1} \text{ cm}^{-1}$ ]	$\lambda_{\text{max}}$ [nm] ([eV])	Fluor. Quant. Yield $\Phi_f$ <sup>[b,c]</sup>
1 (7)	365 (3.40)	58.2	480 (2.58)	0.177
5 (3)	279 (4.44)	32.7	310 (4.00)	0.010
6 (3)	264 (4.70)	25.2	305 (4.07)	0.002
7 (3)	274 (4.53)	24.0	307 (4.04)	0.004
8 (7)	361 (3.43)	45.7	471 (2.63)	0.159

[a] Conjugation length (CL) = number of double/triple bonds; [b] Quantum yield determined by comparison with quinine bisulfate in 0.1M H<sub>2</sub>SO<sub>4</sub>;  $\Phi_f = 0.535$ .<sup>[13]</sup>; [c] Exp. error  $\pm 0.002$ .

The extinction coefficient is also affected by the choice of the endcaps. The TMS-endcapped ODAs show higher absorptions in *n*-hexane compared to ODAs with poor electron-donating end groups. There is a substantial difference in  $\epsilon_{\text{max}}$  of  $\sim 30\%$  between the oligomers with two symmetrical end groups **1** and **5** compared to **7** and **8**, which have a dipole induced by a  $-\text{C}(\text{CH}_3)_2\text{CH}_2\text{OCH}_3$  endcap. This shows that the  $S_2 \leftarrow S_0$  transition for non-polar and dipole-less ODA building blocks is actually more probable in an apolar solvent. These observations are in line with the absorption increase for symmetrical HODAs in *n*-hexane compared to 1,2-dichloroethane (DCE).<sup>[5]</sup> Specifically, building block **1** is rather fluorescent ( $\Phi_f = 0.177$ ), keeping in mind the near-absence of fluorescence of PDAs, and the much lower quantum yield of fluorescence of **5** ( $\Phi_f = 0.010$ ). Apparently, the extension of the conjugated system increases the density of states near the excited state level, so as to increase the rate of radiationless decay at the cost of a decreased fluorescence efficiency.

As with the absorption, in comparison with a  $-\text{C}(\text{CH}_3)_2\text{CH}_2\text{OCH}_3$  endcap, a TMS group induces a red-shift of  $\sim 0.04$  eV of the emission maxima. This is a direct result of the increased electron density of the backbone induced by an electron-donating endcap, and is in line with the red-shift of the  $\lambda_{\text{max}}$  observed for the absorption. Electron-donating end groups also result in higher quantum yields for TMS-endcapped ODAs compared to oligomers with Me and  $-\text{C}(\text{CH}_3)_2\text{CH}_2\text{OCH}_3$  substituents, specifically for **5** versus **6** and **7** (5-fold and 2.5-fold increases, respectively). The building blocks with poor electron-donating endcaps show a marginal fluorescence, comparable to polydiacetylenes with typical values of  $\Phi_f \ll 0.001$ .<sup>[14]</sup>

### 5.2.3 Fluorescence lifetimes and anisotropy

Picosecond time-resolved single photon counting was used to determine the fluorescence lifetimes ( $\tau_F$ ) of the ODA building blocks (Table 2).

Table 2. Fluorescence lifetime  $\tau_F$  (in ps) and the rotation correlation times  $\tau_R$

ODA (CL) <sup>[a]</sup>	$\tau_F$ [ps]	$\tau_R$ [ps; $\pm 25$ ps]
1 (7)	560	130
5 (3)	$\sim 30^{[b]}$	55 <sup>[b]</sup>
6 (3)	$\sim 24^{[b]}$	55 <sup>[b]</sup>
7 (3)	$\sim 30^{[b]}$	65 <sup>[b]</sup>
8 (7)	596	155

[a] Conjugation length (CL) = number of double/triple bonds; [b] Values not accurate, as the instrument response time is 560 ps.

The recorded  $\tau_F$  matches rather closely the literature data of ODAs with the same CL,<sup>[4, 8]</sup> suggesting only marginal substituent effects on the quantum yield. Fluorescence depolarization ( $r$ ) of the ODA building blocks was determined by picosecond time-resolved fluorescence anisotropy measurements.<sup>[4, 5, 15]</sup> Since these rod-shaped oligomers possess a relatively large axial ratio, the rotation of the molecules around the longitudinal axis progresses – especially for **1** and **8** – evidently much faster compared to the rotation around the two short, perpendicular axes, which are not expected to differ significantly from each other. All the compounds under present study indeed display mono-exponential decay kinetics  $r(t)$  with an initial anisotropy value  $r_0$  determined by the angle  $\gamma$  between the absorption and emission transition moment and one rotation correlation time ( $\tau_R$ ).<sup>[13]</sup> For all the building blocks  $r_0$  was  $\sim 0.3$ , similar to that of trimeric ODAs investigated previously.<sup>[8, 14, 16]</sup> This indicates a small angle ( $\sim 15^\circ$ ) between absorption and emission transition moments.

### 5.2.4 ODA radical cations: Optical spectra and reactivity *via* nanosecond laser transient absorption spectroscopy

The use of conjugated materials in optoelectronic devices is limited frequently by the reactivity of the corresponding radical cations. We therefore employed nanosecond laser transient absorption spectroscopy to determine the optical absorption spectra of the ODA radical cations, and their reactivity towards a reactive nucleophile, nitrate.<sup>[17]</sup> Photo-induced



electron transfer was effected with positively charged sensitizers [*N*-methyl acridinium hexafluoro-phosphate ( $\text{NMA}^+$ )] to obtain the ODA radical cations very efficiently, *via* a reduction of the back electron transfer.<sup>[5, 18]</sup> An ODA solution in DCE was prepared with  $\text{NMA}^+$  and mesitylene as a co-sensitizer. Figure 2 shows the normalized UV-vis spectra of  $1^{+\bullet}$ ,  $5^{+\bullet}$  and  $6^{+\bullet}$  compared to the literature data of  $7^{+\bullet}$  and  $8^{+\bullet}$ .<sup>[18]</sup> The calculated extinction coefficients of ODA radical cations are  $\epsilon(1^{+\bullet}) = 10^3$ ,  $\epsilon(5^{+\bullet}) = 3.2 \times 10^2$  and  $\epsilon(6^{+\bullet}) = 2.0 \times 10^2 \text{ [M}^{-1}\text{cm}^{-1}]$  as determined by comparison with the extinction coefficient of quinuclidine ( $\epsilon = 2.5 \times 10^4$ ).<sup>[19]</sup>

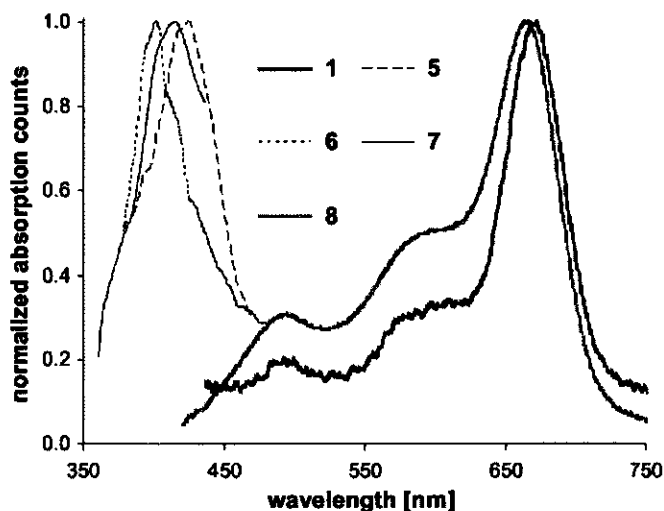


Figure 2. Transient absorption spectra of the radical cations of the ODA building blocks.

We observe a red-shift of the absorption of the radical cation of **1** versus **5** that is nearly identical to that of the neutral compounds: 1.06 eV for the radical cations compared to a red-shift of 1.04 eV for the absorption in their neutral form. This is somewhat surprising, as the lower-lying excited states of radical cations usually undergo a correspondingly smaller effect of differences in conjugation. Apparently, this is nearly completely compensated for by the larger effects of electron-donating substituents on these electron-poor systems. Theoretical studies that clarify this are clearly desired. The bathochromic shift of the absorption as a result of increasing the electron density of the backbone is again visible for the radical cations, that is, introducing a TMS endcap for ODAs with CL = 3, shifts the  $\lambda_{\text{max}}$  of the radical cation absorption with  $\sim 0.09$  eV relative to a *t*-CMe<sub>2</sub>OMe endcap. Again, this effect is near-identical as observed for the neutral compounds. However, this effect is smaller for longer ODAs with CL = 7, that is, 0.01 eV vs. 0.03 eV for the  $\lambda_{\text{max}}$  red-shift of the absorption of the neutral species.

Finally, the stability of the building blocks was studied as a function of the reactivity of the corresponding radical cations with a nucleophile. We used tetrabutylammonium nitrate (TBAN), which has a high solubility in DCE that minimizes aggregate formation. The results are given in Table 2. The data summarized in Table 2 reveal that the rate constants of nucleophilic attack on the radical cation decrease by roughly one order of magnitude in going from CL = 3 to CL = 7. These data suggest that significantly smaller reaction rates maybe observed with extended oligomers (up to CL = 30), which would be of interest for practical applications thereof. Such studies are currently in progress in our laboratories.

Table 2.  $\lambda_{\max}$  and lifetimes  $\tau$  of radical cations and rate constants  $k$  for nucleophilic attack of TBAN.

ODA (CL) <sup>[a]</sup>	$\lambda_{\max}$ [nm] ([eV])	$\tau$ [ $\mu$ s]	$k_{\text{TBAN}}$ [ $\text{M}^{-1} \text{s}^{-1}$ ]
1 (7)	671 (1.85)	50	$1.81 \times 10^9$
5 (3)	426 (2.91)	4	$8.02 \times 10^9$
6 (3)	403 (3.08)	5	$7.88 \times 10^9$
7 (3)	413 (3.00)	2	$\geq 1.0 \times 10^{10}$
8 (7)	666 (1.86)	52	$9.91 \times 10^8$

[a] CL = conjugation length as the number of double and triple bonds

## 5.3 Conclusion

We have developed a new and rapid divergent Sonogashira coupling for the synthesis of ODA building blocks. Absorption and emission spectra and reactivity of the corresponding radical cations confirm that the ODA with two terminal TMS groups is the most electron-rich ODA of a given conjugation length.

## 5.4 Experimental Section

### 5.4.1 Solvents and reagents

For all dry reactions performed under a steady stream of argon (or reductive atmosphere of argon/hydrogen mixture 1:1 v/v) the equipment was dried in an oven at 150 °C for several hours and allowed to cool down in an atmosphere of dry nitrogen or argon. Pure, dry, and degassed ether and tetrahydrofuran were obtained by distillation of the commercial material over sodium particles. CH<sub>2</sub>Cl<sub>2</sub> was distilled and dried over calcium hydride or sodium hydride. Dry DMF was purchased from Sigma-Aldrich and stored under argon. All other specified chemicals were commercially purchased (Aldrich, Fluka or Riedel-de Haën) and used without further purification.

### 5.4.2 General work up & purification procedure

Reaction monitoring and reagents visualization was performed on silica gel or reversed phase silica gel plates with UV-light (254 and 366 nm) combined with GC/MS. Usually the reaction mixture was diluted with water and extracted 3x with an organic solvent (petroleum ether 40-60, hexane, or ethyl acetate). The combined organic extracts were washed with brine and dried over anhydrous sodium sulfate prior to filtration and evaporation of the solvent under reduced pressure. Flash chromatography was performed on commercially available silica gel (0.035 - 0.070 nm pore diameter) and mixtures of freshly distilled petroleum ether 40/60 and ethyl acetate or reversed phase silica gel (0.04 - 0.06 nm pore diameter, Screening Devices) with freshly distilled mixtures of acetonitrile and ethyl acetate. Final purification was performed on Shimadzu preparative HPLC using a C18 column (Alltech Alltima 250 mm × 22mm; 5μ) with HPLC-grade water, acetonitrile and ethyl acetate mixture.

### 5.4.3 Nuclear Magnetic Resonance spectroscopy and Mass Spectroscopy

<sup>1</sup>H NMR and <sup>13</sup>C NMR spectra were determined on a Bruker CXP 300 NMR-spectrometer in CDCl<sub>3</sub> solutions unless indicated otherwise. Chemical shifts are reported in ppm downfield relative to tetramethylsilane ( $\delta$  = 0 ppm for <sup>1</sup>H) or based on the solvent peak (CDCl<sub>3</sub>) ( $\delta$  = 77.00 ppm for <sup>13</sup>C NMR) as an internal standard. HRMS was performed on Finnigan Mat95 mass spectrometer. MALDI-TOF MS analysis was performed on UltraFlex TOF (Bruker Daltonics Bremen).

### 5.4.4 Steady-state absorption and fluorescence

Absorption spectra of the oligodiacetylenes in *n*-hexane (spectrophotometric grade, Riedel-de Haën) and DCE (spectrophotometric grade, Sigma-Aldrich) were recorded using a Cary 100 UV-Vis spectrophotometer (scan range: 200 - 800 nm, scan rate: 300 nm min<sup>-1</sup>, data interval 0.5 nm) and steady-state fluorescence using a FLS920P Spectrometer (slit exc.: 2 nm, slit em.: 2 nm, step: 1.0, dwell: 0.2 s). Absorption spectra of oligodiacetylenes in film *via* drop casting were recorded on a Cary 50 UV-Vis spectrophotometer (scan range 200 - 850 nm, scan rate 300 nm/min, data interval 0.5 nm). Absorption spectra at low temperatures in methylcyclohexane (spectrophotometric grade, Sigma-Aldrich) were obtained with an LP920 spectrophotometer (Edinburgh Instruments Limited) fitted with a 450 W Xe arc lamp as probe-light source, a red-sensitive photomultiplier (R928, Hamamatsu) as detector and a cryostat (Optistat DN; Oxford Instruments, UK) with temperature controller (ITC 503S; Oxford Instruments, UK) as sample holder.

### 5.4.5 Determination of fluorescence quantum yield in solution

In order to evaluate the fluorescence quantum yield ( $\Phi_f$ ) of the ODA's solution in *n*-hexane and DCE, the areas of the corrected emission spectra were compared to a spectrum of a reference solution of quinine bisulfate in 0.1 M H<sub>2</sub>SO<sub>4</sub> measured at 366 nm having  $\Phi_f = 0.535$ .<sup>[13]</sup> The fluorescence quantum yields of the ODA's were determined using the relationship:

$$\Phi_f = \Phi_f \frac{I}{I_R} \frac{OD_R}{OD} \frac{n^2}{n_R^2} \quad (1)$$

where  $I$  and  $I_R$  are the integrated emission intensities of the ODA and quinine bisulfate solutions, respectively,  $OD$  refers to the optical densities of the respective solutions and  $n$  is the refractive index.

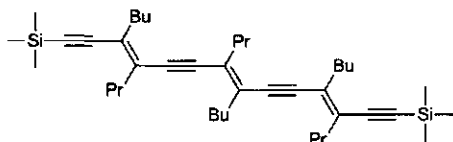
### 5.4.5 Lifetime of fluorescence and fluorescence anisotropy in solution

All spectroscopic measurements were carried out under magic angle condition unless stated otherwise to avoid the possible influence of rotational motions of the probe molecules. The fluorescence lifetime and anisotropy were recorded using a FLS920P Spectrometer (Edinburgh Instruments) for time correlated photon counting (TCSP) (time set up: 5 or 10 ns, 4096 channels, 10000 counts for 1-1 to 1-4, 1000 counts for 1-5 to 1-7). Pulsed diode lasers (372 nm, FWHM: 54 ps; 444 nm, FWHM: 63 ps) and pulsed LED's (283 nm, FWHM <500 ps; 304 nm, FWHM: < 350 ps) from PicoQuant were used as light sources. The anisotropy measurements were performed using vertical and horizontal polarizations.

### 5.4.5 Nanosecond laser flash photolysis

Nanosecond laser flash photolysis studies were carried out under magic angle condition using the third harmonic (355 nm, FWHM = 4 ns) of a Nd:YAG laser (Brilliant, Quantel Inc.). The transient spectra were obtained using an LP920 spectrophotometer (Edinburgh Instruments Limited) fitted with a 450 W Xe arc lamp as probe-light source and a red-sensitive photomultiplier (R928, Hamamatsu) and ICCD camera (DH720, Andor Technology) as detectors.

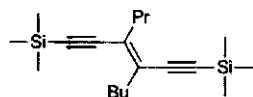
### 5.4.7 (4E,8E,12E)-5,9-dibutyl-4,13-bis(2(trimethylsilyl)ethynyl)-8,12-dipropylheptadeca-4,8,12-trien-6,10-diyne (1)



A solution of **5** (1 equiv.) in THF/MeOH (1:1, 5ml/mmol), H<sub>2</sub>O (3 drops/mmol) and K<sub>2</sub>CO<sub>3</sub> (2 equiv.) was stirred for 3 h. After working up (Et<sub>2</sub>O/H<sub>2</sub>O), drying (Na<sub>2</sub>SO<sub>4</sub>), and concentrating of the combined organic layers under *vacuo*, acetylene **2** was submitted as such to the chain elongation step. A mixture of **3** (10 equiv.),

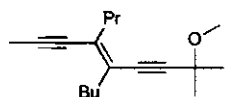
Pd(PPh<sub>3</sub>)<sub>4</sub> (5 mol%), CuI (2 mol%), dry, degassed Et<sub>2</sub>NH (2 ml/mmol) and THF (5 ml/mmol) was placed anaerobically in a dried, brown 2-necked round-bottom flask, equipped with an Ar/H<sub>2</sub> in- and outlet, and a pressure-equalizing dropping funnel containing **2** (1 equiv.). Compound **2** was added slowly (over 6 h) to the stirred mixture under a constant flow of Ar/H<sub>2</sub> (1:1), and stirring was continued overnight at 25 °C. Concentration, filtration over a short silica gel column (5% Et<sub>3</sub>N in pet-ether 40/60), prepurification on reversed phase silica (ACN/EtOAc, 7/3) and purification by prep. HPLC gave pure (99.5%) **1** (50% yield), whilst iodo-diacetylene **3** was recovered quantitatively. <sup>1</sup>H NMR (400 MHz, CDCl<sub>3</sub>): δ 0.21 (s, 18H), 0.90-0.95 (m, 18H), 1.29-1.41 (m, 6H), 1.54-1.62 (m, 12H), 2.32-2.49 (m, 12H); <sup>13</sup>C NMR (100 MHz, CDCl<sub>3</sub>): δ 0.0, 13.6, 13.6, 13.9, 14.0, 21.7, 21.9, 22.1, 22.3, 30.5, 30.8, 34.7, 35.0, 37.0, 37.3, 98.7, 99.1, 99.1, 103.8, 104.8, 128.8, 129.2, 129.7, 131.3; HRMS: observed 614.4699; calculated 614.4703.

### 5.4.8 (E)-4,5-bis(2-(trimethylsilyl)ethynyl)non-4-ene (5)



A mixture of (E)-4-iodo-3-propyloct-3-en-1-ynyl)trimethylsilane **3** (2.87 mmol, 1.00 g), ethynyltrimethylsilane **4** (5.77 mmol, 0.565 g), Pd(PPh<sub>3</sub>)<sub>4</sub> (0.14 mmol, 0.162 g), CuI (0.07 mmol, 0.013 g), and dry, degassed diethylamine (7.0 ml) and THF (18.0 ml) was placed anaerobically in a dried 50 ml two-necked round-bottom flask, equipped with an Ar in- and outlet, and a pressure-equalized dropping funnel. The mixture was stirred (4 h, 30 °C), concentrated and filtered over a short silica gel column (5% Et<sub>3</sub>N in pet-ether 40/60). Purification on reversed phase silica (ACN/EtOAc, 8.5:1.5) gave pure **5** (2.30 mmol, 0.731 g, 80 %) as a pale yellow oil. <sup>1</sup>H NMR (400 MHz, CDCl<sub>3</sub>): δ 0.27 (s, 18H), 0.929 (t, 3H, *J*=7.2Hz), 0.933 (t, 3H, *J*=7.2Hz), 1.27-1.41 (m, 2H), 1.48-1.63 (m, 4H), 2.35-2.43 (m, 4H); <sup>13</sup>C NMR (100 MHz, CDCl<sub>3</sub>): δ 0.0, 13.6, 13.9, 21.6, 22.1, 30.4, 34.4, 36.8, 103.8, 103.9, 104.4, 104.5, 130.5, 130.9; HRMS: observed 318.2196; calculated 318.2199.

### 5.4.9 (E)-5-butyl-8-methoxy-8-methyl-4-propylnona-4-en-2,6-diyne (6)



<sup>1</sup>H NMR (400 MHz, CDCl<sub>3</sub>): δ 0.91 (t, 3H, *J*=7.2 Hz), 0.92 (t, 3H, *J*=7.4 Hz), 1.26-1.42 (m, 2H), 1.47-1.62 (m, 4H), 1.49 (s, 6H), 2.04 (3H), 2.35-2.43 (m, 4H), 3.38 (s, 3H); <sup>13</sup>C NMR (100 MHz, CDCl<sub>3</sub>): δ 4.7, 13.6, 14.0, 21.7, 22.0, 28.5, 30.5, 34.3, 37.3, 51.7, 71.2, 79.0, 83.9, 94.3, 99.0, 127.8, 129.8; HRMS: observed 260.2143; calculated 260.2140.

## 5.5 Acknowledgements

The authors thank the Dutch Technology Foundation STW for generous funding of this research (Project No. WPC 5740), and Dr. Jan Kroon (ECN) for helpful discussions.

## 5.6 References

- [1] K. Müllen, *Pure & Appl. Chem.* **1993**, *65*, 89-96.
- [2] R. E. Martin and F. Diederich, *Angew. Chem. Int. Ed.* **1999**, *38*, 1350-1377.
- [3] J. Gierschner, J. Cornil and H.-J. Egelhaaf, *Adv. Mater.* **2007**, *19*, 173-191.
- [4] G. S. Pilzak, B. van Lagen, C. C. J. Hendrikx, E. J. R. Sudhölter and H. Zuilhof, *Chem. Eur. J.* **2008**, *14*, 7939-7950.
- [5] G. S. Pilzak, J. Baggerman, B. van Lagen, M. A. Posthumus, E. J. R. Sudhölter and H. Zuilhof, *Chem. Eur. J.* **2009**, *15*, 2296-2304.
- [6] A. Elangovan, Y.-H. Wang and T.-I. Ho, *Org. Lett.* **2003**, *5*, 1841-1844.
- [7] B. E. Kohler and D. E. Schilke, *J. Chem. Phys.* **1987**, *86*, 5214-5215.
- [8] C. C. J. Hendrikx, M. Polhuis, A. Pul-Hootsen, R. B. M. Koehorst, A. Hoek van, H. Zuilhof and E. J. R. Sudhölter, *Phys. Chem. Chem. Phys.* **2005**, *7*, 548-553.
- [9] K. van Alem, G. Lodder and H. Zuilhof, *J. Phys. Chem. A* **2002**, *106*, 10681-10690.
- [10] R. E. Martin, U. Gubler, J. Cornil, M. Balakina, C. Boudon, C. Bosshard, J.-P. Gisselbrecht, F. Diederich, P. Günter, M. Gross and J.-L. Brédas, *Chem. Eur. J.* **2000**, *6*, 3622-3635.
- [11] Y. Deng, G. Gao, Z. He and L. D. Kispert, *J. Phys. Chem. B* **2000**, *104*, 5651-5656.
- [12] M. S. Liu, X. Jiang, S. Liu, P. Herguth and A. K.-Y. Jen, *Macromolecules* **2002**, 3532-3538.

- [13] J. R. Lakowicz, *Principles of Fluorescence Spectroscopy*, Kluwer Academic / Plenum Publishers, **2006**, p. 420-421.
- [14] H. Zuilhof, H. M. Barentsen, M. Dijk van, E. J. R. Sudhölter, R. J. O. M. Hoofman, L. D. A. Siebbeles, M. P. Haas de and J. M. Warman in *Polydiacetylenes*, (Ed. H. S. Nalwa), Academic Press, San Diego, San Francisco, New York, Boston, London, Sydney, Tokyo, **2001**, pp. 339-437.
- [15] P. Kapusta, R. Erdmann, U. Ortmann and M. Wahl, *J. Fluoresc.* **2003**, *13*, 179-183.
- [16] G. M. Balkowski, M. Groeneveld, H. Zhang, C. C. J. Hendrikx, M. Polhuis, H. Zuilhof and W. J. Buma, *J. Phys. Chem. A* **2006**, *110*, 11435-11439.
- [17] I. R. Gould, D. Ege, J. E. Moser and S. Farid, *J. Am. Chem. Soc.* **1990**, *112*, 4290-4301.
- [18] G. S. Pilzak, S. Fratiloiu, F. Grozema, J. Baggerman, E. J. R. Sudhölter, L. D. A. Siebbeles and H. Zuilhof, *J. Chem. Phys. B submitted* **2009**.
- [19] J. P. Dinnocenzo and T. E. Banach, *J. Am. Chem. Soc.* **1989**, *111*, 8646-8653.

# Chapter 6

## Radical Cations of all-*trans* Oligodiacetylenes: Optical Absorption and Reactivity towards Nucleophiles

### Abstract

High yields of the radical cations of oligodiacetylenes have been prepared by photo-induced electron transfer using a positively charged co-sensitizer and by pulse radiolysis. The absorption maxima of the ODA radical cations show a bathochromic shift to the infrared region and a large increase of their lifetimes with chain elongation. Their reactivity towards nucleophiles decreases for longer ODAs, illustrating clearly the stabilizing effect of charge delocalization along the oligomeric chain. This also implies a very low reactivity of ODA radical cations towards trace amounts of water in optoelectronic devices.

*This chapter was accepted for publishing: Gregor S. Pilzak, Silvia Fratiloiu, Jacob Baggerman, Ferdinand C. Grozema, Ernst J. R. Sudhölter, Laurens. D. A. Siebbeles, and Han Zuilhof, The Journal of Physical Chemistry B, 2009.*

## 6.1 Introduction

Polydiacetylenes (PDAs) are interesting materials for a variety of optoelectronic devices, including photovoltaics.<sup>[1]</sup> PDA one-dimensional organic quantum wires<sup>[1-3]</sup> are unique due to their formation by topochemical polymerization from crystalline diacetylenes.<sup>[4]</sup> These PDA molecular wires can transfer charges between sites in a molecular electronic device.<sup>[5, 6]</sup> Moreover, in their pure, neutral state these materials behave as one-dimensional, wide-band gap semiconductors,<sup>[7]</sup> but they can be made conductive by injection of charges from electrodes, photoexcitation, or chemical doping.<sup>[8]</sup> The performance of PDA derivatives as a candidate in optoelectronic devices depends on the properties of the excess charges. This aspect of PDA chains is not well understood because of the rather large heterogeneity in conjugation length in polymeric materials. Therefore, in this study, the corresponding charged monodisperse oligodiacylenes (ODAs) are used as model compounds to determine the evolution of the optoelectronic properties as function of the conjugation length. The synthesis of the ODA series under study and their optoelectronic characterization is described by us elsewhere.<sup>[9-11]</sup> The ODA series **1-n** is depicted in Figure 1.

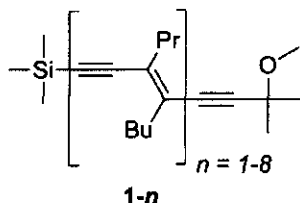


Figure 1. ODAs series **1-n** of which the radical cations are prepared and studied in the present study.

An important requirement for optoelectronic materials in many devices is the stability of their radical cations against nucleophilic attack from water. Therefore, nanosecond laser transient absorption spectroscopy is used to obtain and investigate the optical absorption of these ODA radical cations in the 350 - 850 nm range. To verify the nature of these transients, these radical cations were independently prepared by pulse radiolysis, and studied by visible/near-infrared (VIS/NIR) spectroscopy in the range of 500 - 2100 nm (0.6 - 2.5 eV). In addition, their lifetimes and reactivity towards nucleophiles are discussed on the basis of time-resolved nanosecond laser flash spectroscopy,<sup>[12]</sup> with an eye to the potential of this type of materials for optoelectronic devices.



## 6.2 Results and Discussion

### 6.2.1 ODA radical cations: Optical spectra and reactivity *via* nanosecond laser transient absorption spectroscopy

To study the optical spectra and reactivity of ODA radical cations in solution, time-resolved photoinduced electron transfer is well-tested approach.<sup>[13]</sup> To this aim, the quantum yield of formation using photoinduced electron transfer needs to be as high as possible. Therefore, use was made of a scheme involving positively charged sensitizers that maximizes  $k_{\text{separation}}$  and thus minimizes back electron transfer, and a large excess of co-sensitizer. This scheme is depicted in Figure 2.<sup>[14]</sup> The ODAs under study were dissolved in 1,2-dichloroethane along with *N*-methyl acridinium hexafluorophosphate ( $\text{NMA}^+$ ; sensitizer) and mesitylene ( $\text{MES}$ ; co-sensitizer).<sup>[15]</sup>

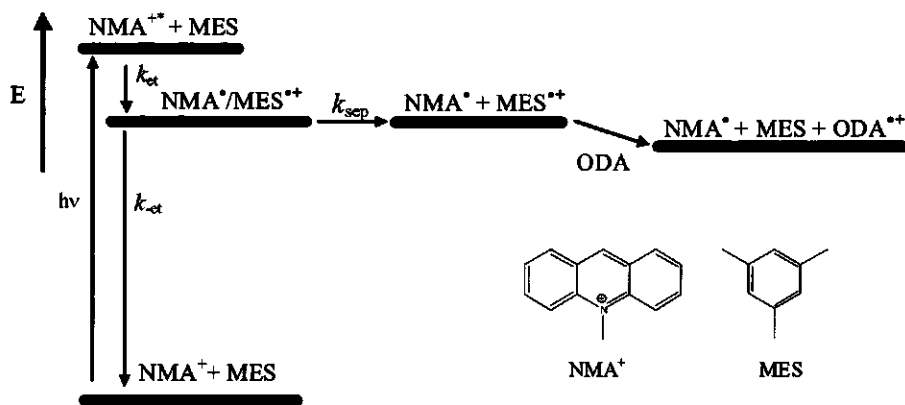


Figure 2. Energy scheme of the formation of ODA radical cations using  $\text{NMA}^+$  as sensitizer and mesitylene ( $\text{MES}$ ) as co-sensitizer.

The major advantage of using a co-sensitizer is that it can be added in high concentrations, which ensures that  $\text{NMA}^{**}$  reacts preferably with  $\text{MES}$ , rather than with  $\text{ODA}$ . In this way the excitation energy of the short-lived  $\text{NMA}^{**}$  is efficiently captured.<sup>[16]</sup> High concentrations of the  $\text{ODA}$  itself gives undesirable side effects,<sup>[17]</sup> partially because it may display direct photochemistry upon intense irradiation and because  $\text{ODA}$  might be reactive towards  $\text{ODA}^{**}$ . The high concentrations of co-sensitizer also certify that equal amounts of radical cation  $\text{ODA}^{**}$  are formed in different experiments, regardless of the precise concentration of the  $\text{ODA}$ . [The

absorption spectra of  $\text{NMA}^+$ ,  $\text{NMA}^\bullet$ ,  $\text{MES}$  and  $\text{MES}^{2+}$  are given in the Supporting Information; Figure 8, Chapter 6.7.]

Argon was flushed through the medium to remove oxygen, and this provides  $\text{NMA}^\bullet$  with sufficient kinetic stabilization that it does not decay significantly within the time scales relevant for this study. As a result of this non-reactivity and because of the constant amount of  $\text{NMA}^\bullet$  that is formed irrespective of the ODA that is studied, the spectrum of  $\text{NMA}^\bullet$  can be subtracted from the measured transient spectrum. Since the oxidation potential of the co-sensitizer  $\text{MES}$  (2.11 V)<sup>[18]</sup> is significantly higher than that of all the ODAs under study diffusion-controlled electron transfer will occur in all cases.

Figure 3 presents the thus obtained optical spectra of the ODA radical cations, and illustrates the dependence of  $\lambda_{\text{max}}$  for the ODA radical cations on the number of enynic units  $n$ . For the determined spectra of  $1\text{-}1^{2+}$  to  $1\text{-}6^{2+}$  the maximum absorption peak ( $\lambda_{\text{max}}$ ) shifts evidently into the near infra-red region with an increase of the oligomer length. The detection range of the detector used in this experimental setup prevented recording of signals above 850 nm, where  $1\text{-}7^{2+}$  and  $1\text{-}8^{2+}$  should be expected (see for those spectra the pulse radiolysis experiments below). The plot of  $\lambda_{\text{max}}$  of  $\text{ODA}^{2+}$  versus  $1/\text{CL}$  (Figure 4; conjugation length  $\text{CL}$  = total number of conjugated double and triple bonds) displays a linearity similar to the trend that was shown for  $\lambda_{\text{max}}$  of the ground-state absorption in our previous studies of the neutral *all-trans* ODAs,<sup>[9, 19]</sup> homocoupled ODAs,<sup>[20]</sup> and thiophene-containing ODAs<sup>[21]</sup> with an extrapolated  $\lambda_{\text{max}}$  for the radical cation of an idealized isolated PDA polymer chain of 1228 nm.

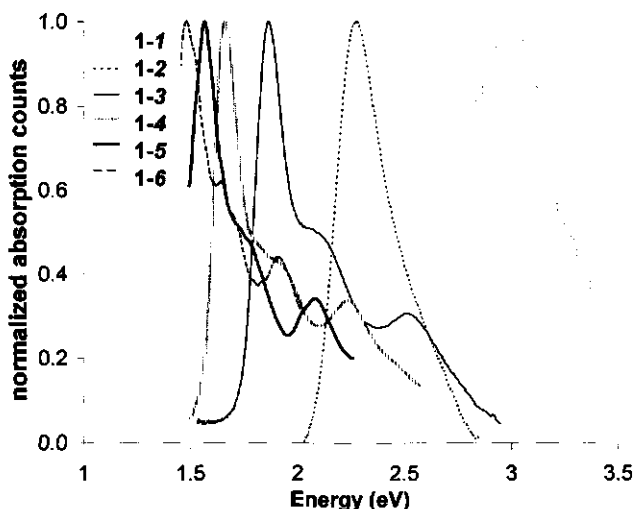


Figure 3. Normalized transient absorption spectra of the radical cations of methoxy-endcapped ODAs  $1\text{-}n$  ( $n = 1 - 6$ ).

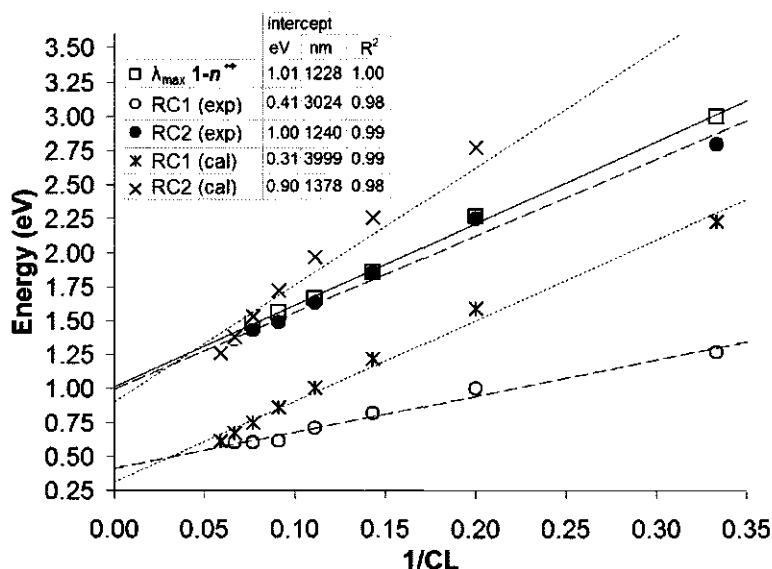


Figure 4.  $\lambda_{\max}$  for the ODA<sup>••</sup> series 1- $n$  ( $n = 1 - 6$ ) and experimental and calculated transition energies (RC1 and RC2) of the ODA<sup>••</sup> series 1- $n$  ( $n = 1 - 8$ ) versus  $1/CL$  in DCE solution.

With time-resolved absorption measurements, the lifetimes  $\tau$  of the ODA<sup>••</sup> series 1- $n^{**}$  ( $n = 1 - 6$ ) were determined. The decay curves of the ODA<sup>••</sup> series 1- $n$  ( $n = 1 - 6$ ) could all be fitted with one exponential function, yielding one value for the lifetime  $\tau$  resulting from slow reaction with the solvent (Table 1).  $\tau$  shows a regular increase with chain elongation going from 2  $\mu$ s for 1-1<sup>••</sup> to 450  $\mu$ s for 1-6<sup>••</sup>, due to increased stabilization of the ODA<sup>••</sup> via delocalization of charge along the oligomer chain.

Table 1. Maxima of the optical absorption  $\lambda_{\max}$  and lifetimes  $\tau$  of ODA radical cations 1- $n^{**}$ , and rate constants  $k$  for nucleophilic attack of methanol and tetrabutylammonium nitrate (TBAN).

1- $n^{**}$ (CL) <sup>[a]</sup>	$\lambda_{\max}$ [nm] ([eV])	$\tau$ [ $\mu$ s]	$k_{\text{MeOH}}$ [ $\text{M}^{-1} \text{s}^{-1}$ ]	$k_{\text{TBAN}}$ [ $\text{M}^{-1} \text{s}^{-1}$ ]
1-1 <sup>••</sup> (3)	413 (3.00)	2 <sup>[b]</sup>		$\geq 1.0 \cdot 10^{10}$
1-2 <sup>••</sup> (5)	547 (2.27)	32	$4.15 \cdot 10^4$	$2.38 \cdot 10^9$
1-3 <sup>••</sup> (7)	666 (1.86)	52	$2.94 \cdot 10^4$	$9.91 \cdot 10^8$
1-4 <sup>••</sup> (9)	748 (1.66)	372	$6.62 \cdot 10^3$	$4.24 \cdot 10^8$
1-5 <sup>••</sup> (11)	794 (1.56)	431		$2.32 \cdot 10^8$
1-6 <sup>••</sup> (13)	840 (1.48)	450		$1.29 \cdot 10^8$

[a] Conjugation length (CL) = number of double/triple bonds; [b] Low signal-to-noise ratio prevents accurate results.

One of the requirements for optoelectronic materials in many devices is the stability of their radical cations against nucleophilic attack from water. Since the low solubility of water in DCE (2 g/l)<sup>[22]</sup> yields water clusters,<sup>[23]</sup> the effective concentration of water does not increase linearly with the amount of water added, and the reactivity of this nucleophile changes with its concentration. Therefore, methanol was chosen as a model nucleophile, since its significantly higher solubility diminishes aggregate formation, which makes it a reasonable model compound for water. It turned out (see Table 1) that  $1-n^{+\bullet}$  did not react fast with methanol, i.e. extended ODA radical cations are not very reactive towards MeOH, and thus likely even less reactive towards less nucleophilic water. In fact, already for  $1-4^{+\bullet}$  the reaction rate  $k$  turned out to be  $< 10^4 \text{ M}^{-1}\text{s}^{-1}$ , and longer, less reactive ODA radical cations could even not be studied in this manner anymore. To extend the range over which the nucleophilic reactivities of  $\text{ODA}^{+\bullet}$  could be studied, the reactivity towards the stronger nucleophile nitrate was investigated. The lifetime decays of the radical cations  $\text{ODA}^{+\bullet}$  were recorded in the presence of methanol for  $1-2^{+\bullet}$  up to  $1-4^{+\bullet}$ , and towards tetrabutylammonium nitrate (TBAN) for  $1-1^{+\bullet}$  up to  $1-6^{+\bullet}$ . The results are summarized in Table 1. The data in Table 1 also reveal that the rate constants are roughly logarithmically decreasing with an increasing number of monomeric units. This finding confirms that the ODA radical cations are stabilized by the extensive charge delocalization, and thus less prone to nucleophilic attack, e.g.  $1-6^{+\bullet}$  reacts  $\sim 4$  times slower than  $1-4^{+\bullet}$  with TBAN. This decrease in reaction rate constant suggests  $k_{\text{MeOH}}$  for  $1-6^{+\bullet} < 2000 \text{ M}^{-1}\text{s}^{-1}$ , and presumably  $k_{\text{MeOH}}$  for  $1-8^{+\bullet}$  is  $<< 1000 \text{ M}^{-1}\text{s}^{-1}$ . This implies that the radical cation of longer ODAs, and thus of PDA chains, will remain stable in the presence of traces of water that may be present in a device, which of course makes these longer oligomers and polymers more useful for a broad application range of optoelectronic devices.

## 6.2.2 ODA radical cations: Optical spectra and reactivity *via* pulse radiolysis absorption spectroscopy

Measurements of the optical absorption spectra of the radical cations of ODA were also performed using pulse radiolysis transient absorption spectroscopy (detailed information is given in the Experimental Section). Figure 5 shows transient changes in optical absorption observed upon irradiation of an oxygen-saturated solution ( $[\text{O}_2] = 11.9 \text{ mM}$  at 1 atm and  $25^\circ\text{C}$ ) of  $1-4$  in benzene at different wavelengths.

Irradiation of benzene solutions leads to the formation of benzene radical cations ( $\text{C}_6\text{H}_6^{+\bullet}$ ), excited states ( $\text{C}_6\text{H}_6^*$ ) and excess electrons ( $\text{e}^-$ ).<sup>[24-26]</sup> The excited states that are produced on radiolysis either decay rapidly (singlets) or are deactivated by the presence of oxygen (triplets). The latter process leads to the formation of singlet oxygen, which could react with the ODAs,

resulting in oxidation products. Although the formation of these oxidation products is likely and it is not possible to prevent this, we have not observed any notable decay of the ODAs at the radiation doses used to obtain the spectra reported here. Radiation doses of at least an order of magnitude larger were necessary to observe decay of the ODAs in the ground state and cation spectra. The excess electrons generated during irradiation are highly mobile ( $0.13 \text{ cm}^2 \text{ V}^{-1} \text{ s}^{-1}$ )<sup>[27]</sup> and can react rapidly ( $< 1 \text{ ns}$ ) with oxygen ( $\text{O}_2$ ) with a rate constant of  $1.5 \times 10^{11} \text{ M}^{-1} \text{ s}^{-1}$ ,<sup>[28]</sup> yielding oxygen anions ( $\text{O}_2^-$ ). This reaction competes with addition of the excess electrons to the ODA studied, yielding the corresponding radical anion (here:  $1\text{-}4^{\bullet-}$ ).

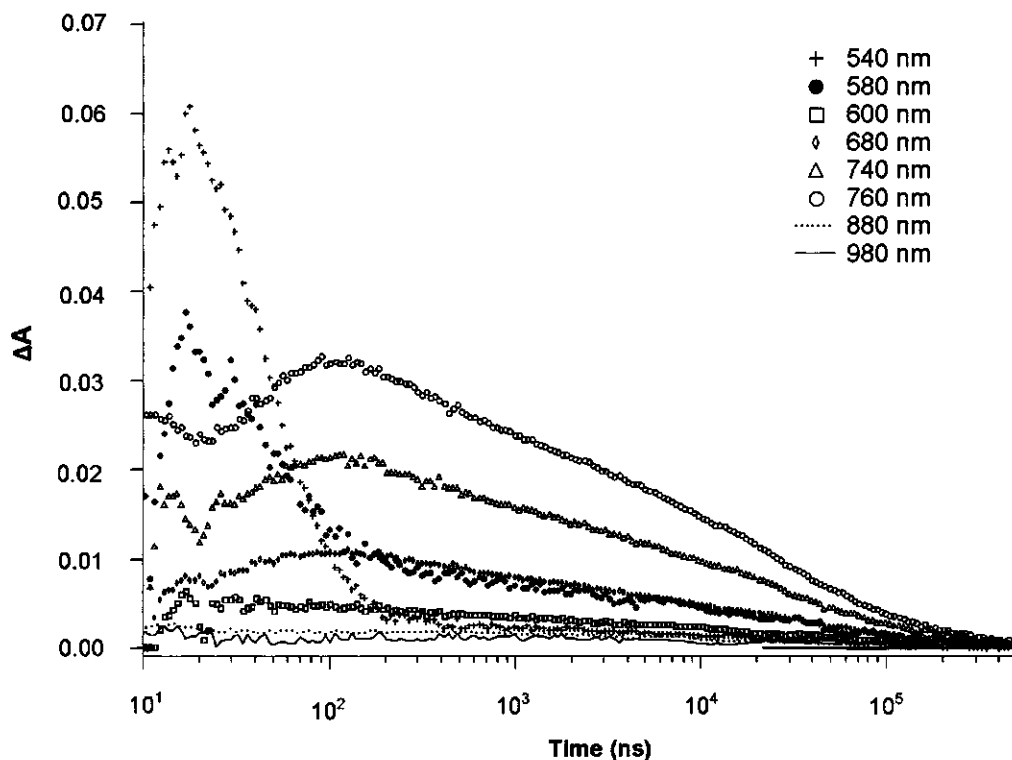


Figure 5. Optical absorption transients due to the positive and negative charges on  $1\text{-}4$  (1 mM) observed upon irradiation of  $\text{O}_2$ -saturated benzene solutions at different wavelengths. Note: The wavelength-dependent Cerenkov radiation prevents measurements during and directly after the electron pulse.

The time scale on which diffusion-controlled electron attachments occur can be calculated if the rate constant and the concentration are known. The rate constant ( $k$ ) for a charge transfer controlled by diffusion of the charge can be calculating using Equation 1:

$$k = 4\pi RD \quad (1)$$

in which  $R$  is the reaction radius and  $D$  is the diffusion coefficient of the charge. The diffusion coefficient of the charge can be obtained from the charge carrier mobility using the Einstein relation (2):

$$D = \frac{\mu k_B T}{e} \quad (2)$$

Taking a value for electron mobility in benzene equal to  $0.13 \text{ cm}^2 \text{V}^{-1} \text{s}^{-1}$  at room temperature<sup>[27]</sup> and assuming a typical reaction radius of  $1 \text{ nm}$ ,<sup>[29]</sup> the rate constant of the reaction of excess electrons with **1-4** is estimated to be  $2.46 \times 10^{12} \text{ M}^{-1} \text{s}^{-1}$ . Knowing the concentration of **1-4** in benzene ( $1 \text{ mM}$ ), the reaction of the excess electrons with the oligomer takes place in about  $4.5 \text{ ns}$ . Indeed, in the optical absorption transients at  $540$  and  $580 \text{ nm}$  (Figure 4), it can be seen that during the pulse ( $5 \text{ ns}$ ) **1-4**<sup>•−</sup> radical anions have already been formed. Note that only a small fraction of electrons react with **1-4**; the majority attaches onto  $\text{O}_2$ : the time scale for this reaction is  $\sim 0.6 \text{ ns}$  for a rate constant of  $1.5 \times 10^{11} \text{ M}^{-1} \text{s}^{-1}$  and  $[\text{O}_2] = 11.9 \text{ mM}$ . However, the transient optical absorption at short times in Figure 4 is due to the fraction of electrons that does react with **1-4**, while the rapid decay of **1-4**<sup>•−</sup> is due to the electron transfer from **1-4**<sup>•−</sup> to  $\text{O}_2$  ( $\text{O}_2$  has a high electron affinity).

Due to the fact that the ionization potential of **1-4** is lower than that of benzene, the benzene radical cations formed upon irradiation will undergo charge transfer to **1-4** according to Equation 3:



The time scale at which the **1-4**<sup>•+</sup> is formed can be estimated from the rate constant and the concentration of the solution. The hole mobility in benzene is  $4 \times 10^{-4} \text{ cm}^2 \text{V}^{-1} \text{s}^{-1}$  at room temperature.<sup>[30]</sup> Assuming a reaction radius of  $1 \text{ nm}$ ,<sup>[29]</sup> the rate constant for the reaction of  $\text{C}_6\text{H}_6^{•+}$  with **1-4** is calculated to be  $7.56 \times 10^9 \text{ M}^{-1} \text{s}^{-1}$ . For  $[\text{1-4}] = 1 \text{ mM}$ , this yields a radical cation formation time of  $130 \text{ ns}$ . This is in reasonable agreement with the rise of the optical absorption transients on a time scale of  $100 - 110 \text{ ns}$  in Figure 4. The decay of the optical absorption in Figure 4 is due to the reaction of the **1-4**<sup>•+</sup> with  $\text{O}_2$  anions, yielding neutral **1-4** and oxygen.

Due to the fact that at short wavelengths the decay of the radical anions of **1-4** takes place at similar times as the formation of the radical cations of **1-4**, in the optical absorption spectra of the charged ODAs an absorption feature is obtained at short wavelengths, which is attributed to the radical anion. Indeed, this can be seen in Figure 5, which shows the optical absorption spectra of the radical cations of **1-*n*** oligomers ( $n = 2 - 8$ ). The first absorption peak

(noted RC1 in Figure 1) corresponds to the low-energy band of the radical cations. This peak appears at 1.27 eV for  $1-2^{+\bullet}$  and shifts towards lower energies with increasing the length of the oligomer: 1.0 eV for  $1-3^{+\bullet}$ , 0.82 eV for  $1-5^{+\bullet}$ , etc. These values are also shown in Table 2. Note that for the longer chains ( $1-7$  and  $1-8$ ) the low-energy band RC1 shifts below 0.6 eV, which is the instrumental lower limit.

The high-energy band (denoted RC2) shifts as well with increasing chain length, as seen and discussed from the laser transient absorption data in Figure 3 (*vide supra*). The absorption maxima of the RC2 band are presented in Table 1, and display a near-identical fit with  $1/CL$  that confirms that the same species is observed. In addition, the observed values agree very well with the flash photolysis data, indicating that these spectra belong to the same species, for which the small differences between these two data sets are likely predominantly caused by solvent effects. The RC2 band of the absorption spectra  $1-3^{+\bullet}$  has a shoulder towards higher energy. This shoulder is near-absent in  $1-2^{+\bullet}$ , seems most pronounced in  $1-4^{+\bullet}$  (also obvious in the photolysis spectra, as can e.g. be clearly seen in the overlay with the photolysis spectrum of  $1-4^{+\bullet}$ , see Figure 6) and subsequently becomes less pronounced with increasing chain length. In order to establish whether this shoulder corresponds to a different absorption feature or to a vibrational progression belonging to the same electron excitation, quantum chemical calculations of the optical absorption spectra of  $1-n^{+\bullet}$  have been performed and they will be discussed in the next section (*vide infra*).

In the optical spectra of  $1-3^{+\bullet}$  can be observed as well another absorption feature at high energy (at about 2.5 eV). The energy of this peak decreases with increasing the chain length and is attributed to the absorption due the ODA<sup>n</sup> radical anions. In Figure 6 this absorption is indicated as RA2, as preliminary calculations suggest that it belongs to the second excited state. The presence of such radical anions in these pulse radiolysis experiments was confirmed by additional pulse radiolysis experiments in tetrahydrofuran (THF)<sup>[31]</sup> on compound  $1-4$ . It is interesting to note that the RA2 band is significantly shifted with respect to the RC2 band, which is uncommon in conjugated oligomers. This suggests that the electronic structure of the radical anion differs significantly from that of the cation. The nature of the radical anion states in these ODAs is under current investigation and a detailed discussion is outside the scope of this paper.

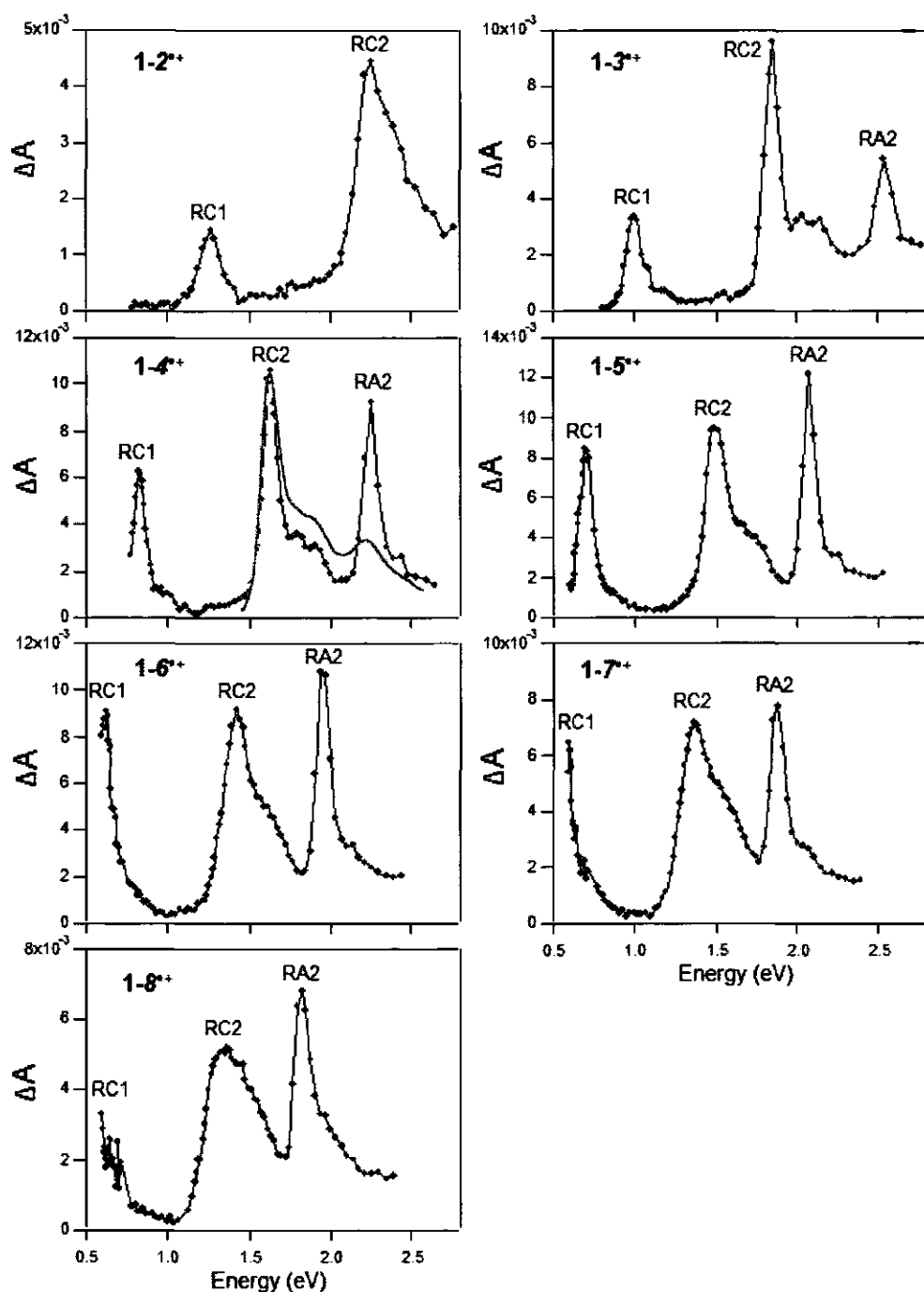


Figure 6. Optical absorption spectra of the radical cations  $1-n^{+}$  in benzene, RC1 and RC2 and an overlay with the transient absorption spectra of  $1-4^{+}$  (continuous gray line). (Note that these spectra show as well the absorption RA2 due to the formation of the radical anions  $1-n^{-}$ ). Calculated optical absorption spectra of ODA radical cations



The optical absorption spectra of charged oligodiacetylenes were calculated as described in the Computational Methodology section. The energy transitions of ODA radical cations are presented in Table 2 together with their oscillator strength and the relative contribution of  $\alpha$ - and  $\beta$ -spin electrons of excited state configurations, and compared with experiment. The experimental optical absorption spectrum of  $1\text{-I}^{+\bullet}$  suggests an absorption band with the maximum of absorption above 2.8 eV. In the radiolysis measurements the maximum of absorption could not be measured (it exceeds the instrumental limit), but photolysis studies show that  $1\text{-I}^{+\bullet}$  absorbs at 410 nm (3.02 eV; see also ref. 9c). The DFT calculations predict two electronic transitions for this radical cation. According to the DFT calculations, the first transition (denoted RC1) appears at 2.23 eV and it has a very small oscillator strength (0.09). Therefore it is likely that this transition could not be observed in the experimental spectra. The second energy transition of  $1\text{-I}^{+\bullet}$  is denoted RC2 and appears at 3.64 eV. This calculated value is higher than the experimental one (3.02 eV), which clearly indicates that DFT overestimates the absorption energy. The agreement of the experimental values with the calculations becomes much better with increasing chain length, as it can be seen from the values in Table 2.

For the longer ODA radical cations the DFT calculations predict two transitions energies. These transition energies can be explained in terms of a molecular orbital model, shown schematically in Figure 7a. This model has been used previously to describe the transition energies for the charged phenylenevinylene<sup>[9, 32-34]</sup> and fluorene oligomers.<sup>[35]</sup> The model considers that removal of an electron introduces additional transitions with lower energy than the one of the neutral compound. Since the molecular orbital model is derived from the polaron model<sup>[36]</sup> the energy levels between additional transitions will be named after the polaronic levels, P1 and P2. According to this model, in ODA radical cations the P1 level is singly occupied, while P2 represents the lowest unoccupied molecular orbital. The highest doubly occupied molecular orbital is indicated as H, while the second empty level for cations is denoted L (see Figure 7a). In the last column of Table 2 the relative contributions of excited state configurations are presented in terms of this model. The lowest transition (RC1) of ODA radical cations is dominated by the configuration in which an electron from the highest doubly occupied molecular orbital is excited to the singly occupied molecular orbital (H $\rightarrow$ P1). The second RC2 transition corresponds mainly to excitation of an electron from the singly occupied molecular orbital to the lowest unoccupied molecular orbital (P1 $\rightarrow$ P2).

Figure 4 shows the calculated transition energies of the ODA radical cations as a function of chain length in comparison with  $\lambda_{\text{max}}$  determined for the  $1\text{-n}^{+\bullet}$ . The maximum of absorption rapidly decreases with increasing of chain length, indicating delocalization of the positive

charge along the oligomer chain. A similar monotonous decrease of the transition energies with increasing chain length was previously found from TDDFT calculations on phenylenevinylene radical cations,<sup>[33, 34]</sup> and fluorene-based cations.<sup>[35, 37]</sup> This indicates that the complete  $\pi$ -system is involved in the excitation, which is indeed confirmed by investigation of the orbitals that are active in these transitions according to the TD-DFT calculations.

Table 2. Experimental and calculated transition energies, calculated oscillator strengths and relative contribution of  $\alpha$ - and  $\beta$ -spin electrons of excited state configuration for ODA radical cations  $1-n^{+*}$  ( $n = 1 - 8$ ).

$1-n^{+*}$ (CL) <sup>[a]</sup>	Experimental Energy (eV)	Calculated Energy (eV)	Oscillator strength	Composition of excited state configuration
$1-1^{+*}$ (3)		2.23	0.09	$0.79\beta(H \rightarrow P1) + 0.19\alpha(P1 \rightarrow P2)$
	> 2.8	3.64	0.75	$0.56\alpha(P1 \rightarrow P2) + 0.16\beta(H \rightarrow P1) + 0.11(H-1 \rightarrow P1)$
$1-2^{+*}$ (5)	1.27	1.59	0.06	$0.68\beta(H \rightarrow P1) + 0.32\alpha(P1 \rightarrow P2)$
	2.25	2.78	1.19	$0.41\alpha(P1 \rightarrow P2) + 0.21\beta(H \rightarrow P1) + 0.14\alpha(H \rightarrow P2) + 0.13\beta(H-1 \rightarrow P1)$
$1-3^{+*}$ (7)	1.00	1.22	0.08	$0.65\beta(H \rightarrow P1) + 0.34\alpha(P1 \rightarrow P2)$
	1.85	2.26	1.53	$0.38\alpha(P1 \rightarrow P2) + 0.21\beta(H \rightarrow P1) + 0.19\alpha(H \rightarrow P2)$
	2.03 <sup>[b]</sup>			
$1-4^{+*}$ (9)	0.82	1.01	0.10	$0.66\beta(H \rightarrow P1) + 0.34\alpha(P1 \rightarrow P2)$
	1.63	1.97	2.81	$0.53\alpha(P1 \rightarrow P2) + 0.27\beta(H \rightarrow P1) + 0.12\beta(H \rightarrow P2)$
	1.80 <sup>[b]</sup>			
$1-5^{+*}$ (11)	0.71	0.86	0.15	$0.67\beta(H \rightarrow P1) + 0.33\alpha(P1 \rightarrow P2)$
	1.49	1.72	3.70	$0.59\alpha(P1 \rightarrow P2) + 0.29\beta(H \rightarrow P1)$
	1.65 <sup>[b]</sup>			
$1-6^{+*}$ (13)	0.61	0.75	0.20	$0.69\beta(H \rightarrow P1) + 0.31\alpha(P1 \rightarrow P2)$
	1.43	1.53	4.26	$0.61\alpha(P1 \rightarrow P2) + 0.28\beta(H \rightarrow P1)$
$1-7^{+*}$ (15)	< 0.6 <sup>[c]</sup>	0.67	0.28	$0.70\beta(H \rightarrow P1) + 0.29\alpha(P1 \rightarrow P2)$
	1.36	1.38	4.63	$0.61\alpha(P1 \rightarrow P2) + 0.26\beta(H \rightarrow P1)$
$1-8^{+*}$ (17)	< 0.6 <sup>[c]</sup>	0.61	0.37	$0.72\beta(H \rightarrow P1) + 0.28\alpha(P1 \rightarrow P2)$
	1.36	1.26	4.88	$0.61\alpha(P1 \rightarrow P2) + 0.24\beta(H \rightarrow P1)$

[a] Conjugation length (CL) = number of double/triple bonds; [b] Energies corresponding to the shoulder of the RC2 band from the spectra in Figure 5; [c] Energy of the shoulder towards higher energy of the RC2 for  $1-6^{+*}$  and  $1-7^{+*}$  could not be precisely determined.

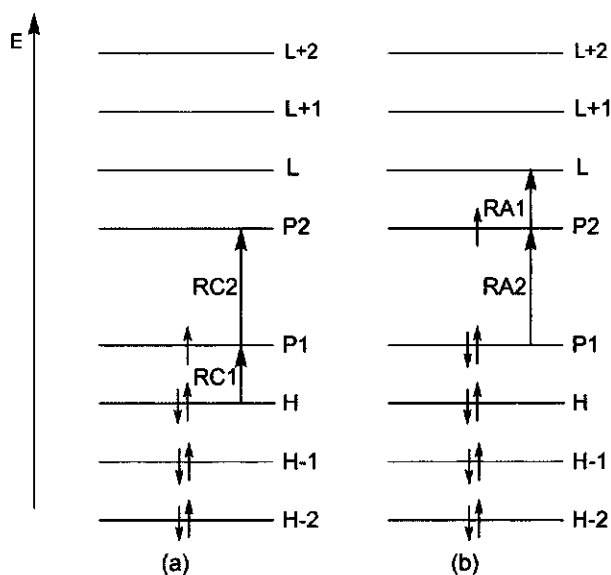


Figure 7. Molecular orbital model for (a) cations and (b) anions for oligodiacetylene oligomers. The electronic transitions are also represented.

## 6.3 Conclusion

The radical cations of a series of monodisperse oligodiacetylenes ( $\text{ODA}^{+\bullet}$ ) were prepared independently in two ways, namely by photoinduced electron transfer in argon-saturated 1,2-dichloroethane and pulse radiolysis in  $\text{O}_2$ -saturated benzene. For these radical cations the optical spectra (in the range of 0.6 - 2.8 eV) and reactivity towards nucleophiles were determined. The optical spectra obtained in these experiments were compared with simulated spectral data obtained from time-dependent DFT calculations. The optical absorption spectra of this  $\text{ODA}^{+\bullet}$  series show upon extension of the conjugated chain a monotonous red-shift of  $\lambda_{\text{max}}$ . The quantum chemical calculations confirm this, showing that the excitation involves the complete  $\pi$ -system. In additions, they suggest that the lowest electronic transition is mainly due to the promotion of an electron from the highest doubly occupied orbital to the singly occupied orbital. The reactivity towards nucleophiles decreases significantly with a more extended conjugation, to values  $\ll 1000 \text{ M}^{-1}\text{s}^{-1}$  for the reactivity of water. This implies that this aspect of ODAs is compatible with their use in a range of optoelectronic devices.

## 6.4 Experimental Section

### 6.4.1 Nanosecond laser flash photolysis

Nanosecond laser flash photolysis studies were carried out using the third harmonic (355 nm, FWHM = 4 ns) of a Nd:YAG laser (Brilliant, Quantel Inc.). The transient spectra were obtained using an LP920 spectrophotometer (Edinburgh Instruments Limited) fitted with a 450 W Xe arc lamp as probe-light source and a red-sensitive photomultiplier (R928, Hamamatsu) and ICCD camera (DH720, Andor Technology) as detectors.

### 6.4.2. Pulse radiolysis experiments

Dilute solutions of ODA oligomers **1-n** were prepared using UV-spectroscopic grade benzene. The solutions were bubbled with benzene-saturated oxygen for 20 min. The pulse radiolysis technique was used to generate charge carriers on isolated ODA oligomers in benzene solutions. Solutions of **1-n** were irradiated with 5 ns pulses of 3 MeV electrons from a Van de Graaff accelerator. The charges were detected by time-resolved visible/near-infrared (VIS/NIR) spectroscopy in the range of 500 - 2100 nm (0.6 - 2.5 eV), as reported previously for phenylenevinylene<sup>[32, 33, 38]</sup> and fluorene oligomers.<sup>[35]</sup> Because both positive and negative charges can be generated using oxygen-saturated benzene solutions, the experiments have been performed also using tetrahydrofuran as solvent, since it is known from literature that this leads only to the generation of negative species. The absorption spectra of the ODA radical cations and anions were measured by following the transient changes in absorbance of the solution at different wavelengths. The spectra are normalized to the radiation dose in the electron pulse, which is proportional to the charge,  $Q$ .

### 6.4.3 Quantum chemical calculations

The geometries of the radical cations under study were optimized using the Amsterdam Density Functional (ADF) Theory program,<sup>[39]</sup> using the Local Density Approximation (LDA) with exchange and correlation functionals based on Vosko-Wilk-Nusair (VWN) parameterization of electron gas data.<sup>[40]</sup> The Generalized Gradient Approximation (GGA)<sup>[41]</sup> corrections by Becke<sup>[42]</sup> (exchange) and Perdew<sup>[43]</sup> (correlation) were included. All DFT calculations were performed with an atomic basis set of Slater-type orbitals (STOs) of double- $\zeta$  quality including one set of polarization functions on each atom (DZP basis set in ADF). For open-shell systems unrestricted DFT calculations have been used. In all calculations the propyl and *n*-butyl chains were replaced by hydrogen atoms. This simplification is not expected to significantly affect the optical absorption spectra of ODA radical cations, because the presence of alkyl substituents does not create any significant steric effects.

The optical absorption spectra of ODA radical cations were calculated by Time-Dependent Density Functional Theory (TDDFT)<sup>[44]</sup> in ADF. The absorption energies were computed using the TZP (Slater-type orbitals of triple- $\zeta$  quality including one set of polarization functions on each atom) basis set and the Becke-Perdew functional.

## 6.5 Acknowledgements

The authors thank the Dutch Technology Foundation STW for generous funding of this research (Project No. WPC 5740).

## 6.6 Supporting Information

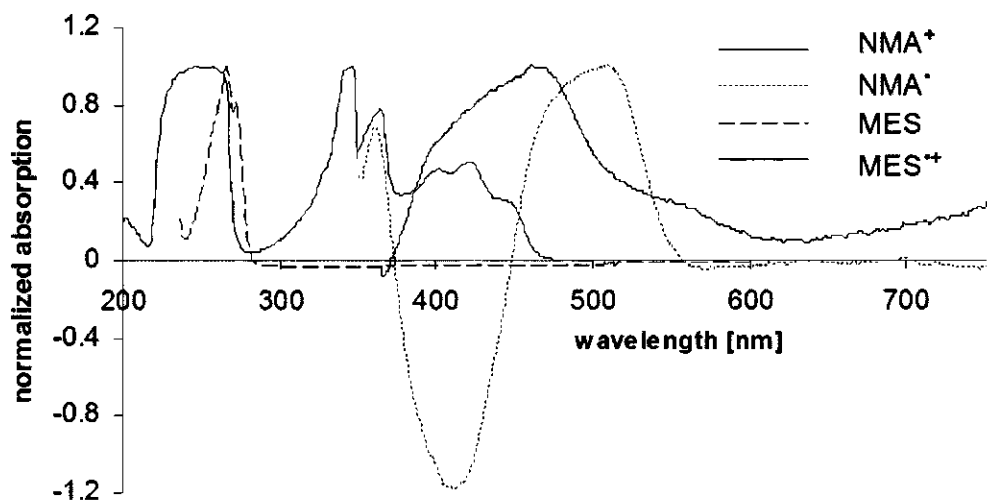


Figure 8. Normalized absorption spectra of  $\text{NMA}^+$ ,  $\text{NMA}^\bullet$ , MES and  $\text{MES}^{\bullet+}$  in 1,2-dichloroethane (at room temperature).

## 6.7 References

- [1] H. Zuilhof, H. M. Barentsen, M. Dijk van, E. J. R. Sudhölter, R. J. O. M. Hoofman, L. D. A. Siebbeles, M. P. Haas de and J. M. Warman in *Polydiacetylenes*, (Ed. H. S. Nalwa), Academic Press, San Diego, San Francisco, New York, Boston, London, Sydney, Tokyo, **2001**, pp. 339-437.
- [2] S. Jo, H. Yoshikawa, A. Fujii and M. Takenaga, *Synth. Met.* **2005**, *150*, 223-226.
- [3] M. Schott, *Synth. Met.* **2003**, *139*, 739-742.
- [4] V. Enkelmann, *Adv. Polym. Sci.* **1984**, *63*, 91-136.
- [5] K. J. Donovan and E. G. Wilson, *Synth. Met.* **1989**, *28*, 569-574.
- [6] S. Spagnoli, K. J. Donovan, K. Scott, M. Somerton and E. G. Wilson, *Chem. Phys.* **1999**, *250*, 71-79.
- [7] D. S. Boudreaux, *Chem. Phys. Lett.* **1976**, *38*, 341-345.
- [8] T. A. Skotheim, R. L. Elsenbaumer and J. R. Reynolds, *Handbook of Conducting Polymers*, Marcel Dekker: New York, **1998**, p.
- [9] G. S. Pilzak, B. van Lagen, C. C. J. Hendrikx, E. J. R. Sudhölter and H. Zuilhof, *Chem. Eur. J.* **2008**, *14*, 7939-7950.
- [10] G. M. Balkowski, M. Groeneveld, H. Zhang, C. C. J. Hendrikx, M. Polhuis, H. Zuilhof and W. J. Burma, *J. Phys. Chem. A* **2006**, *110*, 11435-11439.
- [11] G. S. Pilzak, B. van Lagen, E. J. R. Sudhölter and H. Zuilhof, *Tetrahedron Lett.* **2008**, *49*, 4949-4952.
- [12] I. R. Gould, D. Ege, J. E. Moser and S. Farid, *J. Am. Chem. Soc.* **1990**, *112*, 4290-4301.
- [13] G. J. Kavarnos, *Fundamentals of photo-induced electron transfer* VCH, Weinheim, Germany, **1993**, p. 359.

- [14] J. P. Dinnocenzo, H. Zuilhof, D. R. Lieberman, T. R. Simpson and M. W. McKechney, *J. Am. Chem.* **1997**, *119*, 994-1004.
- [15] K. P. Dockery, J. P. Dinnocenzo, S. Farid, J. L. Goodman, I. R. Gould and W. P. Todd, *J. Am. Chem. Soc.* **1997**, *119*, 1876-1883.
- [16] W. P. Todd, J. P. Dinnocenzo, S. Farid, J. L. Goodman and I. R. Gould, *J. Am. Chem. Soc.* **1991**, *113*, 3601-3602.
- [17] N. P. Schepp and L. J. Johnston, *J. Am. Chem. Soc.* **1994**, *116*, 10330-10331.
- [18] D. Chiapperino, S. McIlroy and D. E. Falvey, *J. Am. Chem. Soc.* **2002**, *124*, 3567-3577.
- [19] C. C. J. Hendriks, M. Polhuis, A. Pul-Hootsen, R. B. M. Koehorst, A. Hoek van, H. Zuilhof and E. J. R. Sudhölter, *Phys. Chem. Chem. Phys.* **2005**, *7*, 548-553.
- [20] G. S. Pilzak, J. Baggerman, B. van Lagen, M. A. Posthumus, E. J. R. Sudhölter and H. Zuilhof, *Chem. Eur. J.* **2009**, *15*, 2296-2304.
- [21] G. S. Pilzak, K. van Gruijthuijsen, R. H. van Doorn, B. van Lagen, E. J. R. Sudhölter and H. Zuilhof, *Chem. Eur. J.* *accepted* **2009**.
- [22] D. J. Henderson and W. Schmickler, *J. Chem. Soc., Faraday Trans.* **1996**, *92*, 3839-3842.
- [23] C. Jolicoeur and A. Cabana, *Can. J. Chem.* **1968**, *46*, 567-570.
- [24] R. Cooper and J. K. Thomas, *J. Chem. Phys.* **1968**, *48*, 5097-5102.
- [25] W. F. Schmidt and A. O. Allen, *J. Phys. Chem.* **1968**, *72*, 3730-3736.
- [26] N. Gee and G. R. Freeman, *Can. J. Chem.* **1992**, *70*, 1618-1622.
- [27] K. Shinsaka and G. R. Freeman, *Can. J. Chem.* **1974**, *52*, 3495-3506.
- [28] F. C. Grozema, R. J. O. M. Hoofman, L. P. Candeias, M. P. de Haas, J. M. Warman and L. D. A. Siebbeles, *J. Phys. Chem. A* **2003**, *107*, 5976-5986.
- [29] J. M. Warman, P. P. Infelta, M. P. de Haas and A. Hummel, *Chem. Phys. Lett.* **1976**, *43*, 321-325.
- [30] S. S.-S. Huang and G. R. Freeman, *J. Chem. Phys.* **1980**, *72*, 1989-1993.
- [31] H. D. Burrows, M. da G. Miguel, A. P. Monkman, L. E. Horsburgh, I. Hamblett and S. Navaratnam, *J. Chem. Phys.* **2000**, *112*, 3082-3090.
- [32] F. C. Grozema, L. P. Candeias, M. Swart, P. T. van Duijnen, J. Wildeman, G. Hadziannou, L. D. A. Siebbeles and J. L. Warman, *J. Chem. Phys.* **2002**, *117*, 11366-11378.
- [33] S. Fratiloïu, L. P. Candeias, F. C. Grozema, J. Wildeman and L. D. A. Siebbeles, *J. Phys. Chem. B* **2004**, *108*, 19967-19975.
- [34] S. Fratiloïu, F. C. Grozema and L. D. A. Siebbeles, *J. Phys. Chem. B* **2005**, *109*, 5644-5652.
- [35] S. Fratiloïu, F. C. Grozema, Y. Koizumi, S. Seki, A. Saeki, S. Tagawa, S. P. Dudek and L. D. A. Siebbeles, *J. Phys. Chem. B* **2006**, *110*, 5984-5993.
- [36] K. Fesser, A. R. Bishop and D. K. Campbell, *Phys. Rev. B* **1983**, *27*, 4804-4825.
- [37] S. Fratiloïu, S. M. Fonseca, F. C. Grozema, H. D. Burrows, M. L. Costa, A. Charas, J. Morgado and L. D. A. Siebbeles, *J. Phys. Chem. C* **2007**.
- [38] S. Fratiloïu, K. Senthilkumar, F. C. Grozema, H. Christian-Pandya, Z. I. Niazimbetova, Y. J. Bhandari, M. E. Galvin and L. D. A. Siebbeles, *Chem. Mater.* **2006**, *18*, 2118-2129.
- [39] G. te Velde, F. M. Bickelhaupt, E. J. Baerends, C. F. Guerra, S. J. A. van Gisbergen, J. G. Snijders and T. Ziegler, *J. Comp. Chem.* **2001**, *22*, 931-967.
- [40] S. H. Vosko, L. Wilk and M. Nusair, *Can. J. Phys.* **1980**, *58*, 1200.
- [41] F. Jensen, *Introduction to computational chemistry*, John Wiley & Sons Ltd., Chichester, **1999**, p. 130.
- [42] A. D. Becke, *Phys. Rev. A* **1988**, *38*, 3098-3100.
- [43] J. P. Perdew and W. Yang, *Phys. Rev. B* **1986**, *33*, 8800-8802.
- [44] R. Leeuwen, *Int. J. Mod. Phys. B* **2001**, *15*, 1969-2023.

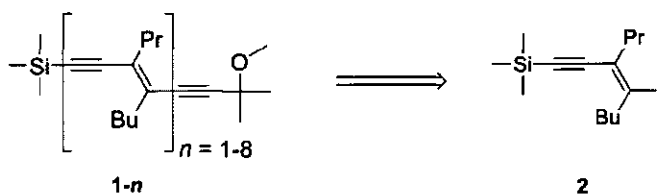
# ***Chapter 7***

## **Summary and General Discussion**

## Synthesis

Electronic properties of  $\pi$ -conjugated polymers resemble those of metals and semiconductors, but show in addition potential advantages with respect to processing and mechanical properties.<sup>[1]</sup> Among  $\pi$ -conjugated polymers, polydiacetylenes (PDAs) hold special interest because of their different morphologies, i.e. single crystal, drop-casted films, Langmuir films and bilayer vesicles in aqueous dispersions, and are also of interest for their nonlinear optical properties.<sup>[2, 3]</sup> As for almost all polymers, the detailed study of the optoelectronics of extended PDAs with high molecular weight is hampered by a broad molecular weight distribution and, often, a low solubility. The studies on monodisperse series of oligodiacylenes (ODAs), that are presented in this thesis, are performed to provide models for the less precise defined higher molecular weight PDAs. These studies deal with the development of multimiligram-scale syntheses of different series of monodisperse and highly soluble oligomers based on a repetitive diacetylene unit (Scheme 1). Their optoelectronic properties were studied as a function of the conjugation length, in both solution and in the solid state, to provide detailed information about the influence of the aggregation state. Therefore, this study accurately addresses the long-standing issue in the literature regarding high wavelength absorption of PDAs,<sup>[3]</sup> i.e. the origin of the visible light absorption of these polymers.

A high solubility of ODAs is required to study their optoelectronic properties in solution. This is clearly demonstrated in Chapter 2 by means of the synthesis of a series of highly soluble oligodiacylenes (ODAs) up to the octamer. The backbone of these ODAs consists of the enyne unit bearing propyl and butyl side chains (Scheme 1).



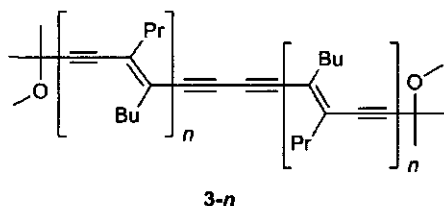
Scheme 1. ODA series **1-n** bearing solubility-enhancing side chains synthesized from enyne building block **2**.

These solubility-enhancing alkyl chains of different lengths prevent intermolecular interactions, i.e. stacking, between the adjacent ODA chains in micromolar solutions. Additionally, the polar *tert*-OMe endcap increases the polarity of the ODAs, which improves the solubility and purification procedure of the oligomers. The synthesis of the ODA series was performed using a sequence of catalytic couplings of the enyne building block **2** with



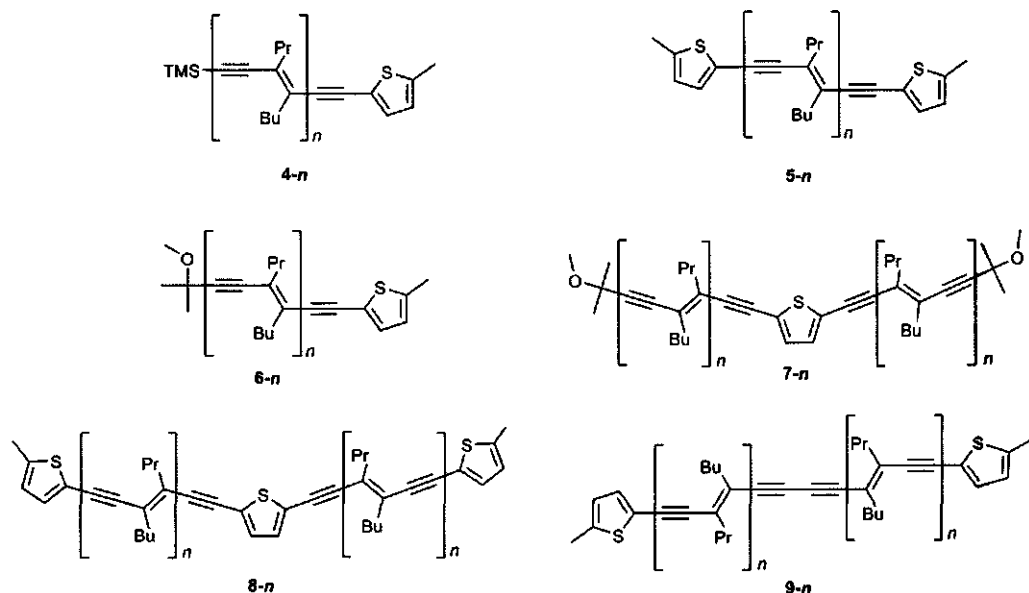
protodesilylated **1-*n*** (Scheme 1). An important requirement for the iterative oligomer synthesis is the high yield of the elongation step. This was achieved by a Sonogashira reaction under reductive atmosphere. This significantly decreased the amount of homocoupling of terminal acetylenes.<sup>[4]</sup> Prior to the chain elongation process the building block **2** was synthesized on a multigram scale with an overall yield of 60%, using titanium-mediated, regioselective coupling of a terminal and an internal acetylene<sup>[5, 6]</sup> followed by a sequence of alkylation and iodination reactions (Chapter 2, Scheme 2).<sup>[7, 8]</sup>

The synthesis of novel homocoupled ODA (HODA) series ranging up to 30 conjugated double and triple bonds and having an estimated length of 8.2 nm is described in Chapter 3. HODAs are constructed by coupling two symmetrical oligodiacetylene units efficiently in one catalytic step. This reaction doubles the overall conjugation length of the oligomer (Scheme 2). ODA chains deployed in the key-step condensation reaction were synthesized up to heptamer using the approach as depicted in Scheme 2. In contrast to the ODA chain elongation process (Chapter 2, Scheme 4), the homocoupling reaction was induced by the use of palladium(II) catalyst under ambient air and proceeded in very high yields (>90 %).



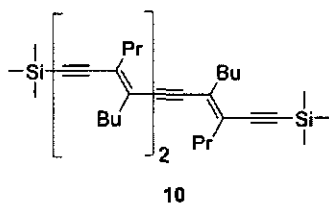
Scheme 2. HODA series ranging from monomer **3-1** ( $C_{34}H_{50}O_2$  and  $M_r = 490.38$ ) to heptamer **3-7** ( $C_{166}H_{242}O_2$  and  $M_r = 2267.67$ ).

In Chapter 4 the synthesis of an ODA-like series containing a thiophene moiety as a central unit and/or endcap (ThODAs series **4-*n*** up to **8-*n***) and HODAs series with thiophene moieties as endcaps (HThODAs series **9-*n***) is presented (Scheme 3). Five novel series of these diacetylene-based materials were synthesized and characterized from monomer up to the trimer and including the longest **9-3** ThODA with 20 conjugated  $\pi$ - $\pi$  bonds. Series **4-*n*** up to **6-*n*** were synthesized following the iterative sequence of Sonogashira couplings between the building block and the protodesilylated ODA chain. The members of **5-*n*** and **6-*n*** series were endcapped with a thiophene moiety after each elongation step. The series **7-*n*** and **8-*n*** were synthesized using a divergent approach. As a result, two ODA chains of equal length were coupled using 2,5-diiodothiophene as a central linker in a catalytic chain elongation step. Finally, the HThODA series **9-*n*** was prepared by homocoupling of two **4-*n*** oligomer chains.



Scheme 3. The synthesized and investigated series of novel ThODAs and HThODAs with  $n = 1-3$ .

Chapter 5 describes a new divergent route to synthesize longer ODAs such as **10** (Scheme 5), i.e. by adding two building blocks to a terminal *bis*-acetylene (Chapter 5, Scheme 2). The effect of an apolar endcap, the trimethylsilyl (TMS)-group, is studied in comparison with the previous synthesized monomer **1-1** and trimer **1-3** (Scheme 2).



Scheme 5. Divergent approach to synthesize monodisperse ODA **10**.

In Chapter 6 radical cations derived from the ODA series **1- $n$**  (Scheme 1) are prepared in two independent ways, and their optical absorption spectra are determined in the visible/near-infrared (VIS/NIR) region (500 - 2100 nm = 0.6 - 2.5 eV). The use of time-resolved spectroscopy shows that these radical cations react only slowly with water, which shows that these materials are kinetically stable with respect to trace amounts of water as may be present in optoelectric devices.

## Optoelectronics

The steady-state optical absorption spectra determined for all series in solution show a red-shift of the absorption maximum ( $\lambda_{\text{max}}^{\text{A}}$ ) and an increase of the molar extinction coefficient ( $\epsilon_{\text{max}}$ ) with an increasing number of repeating units. The correlation of the  $\lambda_{\text{max}}^{\text{A}}$  with the reciprocal conjugation length (CL) is linear for all these enyne-based materials both in solution and in drop-casted films, which indicated that the conjugation in these materials is not significantly reduced by possible kinks or torsions in the backbone. Extrapolation of  $\lambda_{\text{max}}^{\text{A}}$  values to infinite CL values yields maximum absorption wavelengths of  $\sim 500$  nm. This is significantly lower than those reported in literature for PDAs ( $>600$  nm).<sup>[3]</sup> Furthermore, these oligomers do not show any aggregation in concentrated solution (up to 5 mM) due to steric repulsions between the alkyl side chains.

Some new features were observed in the solid-state absorption spectra of all solid oligomers:

- a red-shifted  $\lambda_{\text{max}}^{\text{A}}$  relatively to the absorption maxima in solution;
- a clearly visible red-shifted shoulder; and
- an additional higher-wavelength absorption at  $\geq 550$  nm.

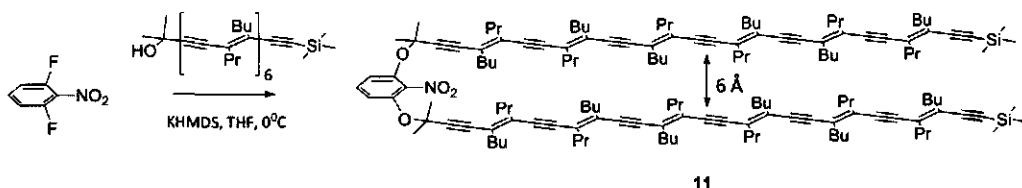
This is explained by increased interchain interactions in the solid state, which force the molecules to planarity. The highly shifted long-wavelength absorption (above 550 nm for longest oligomers under study) is obviously caused by intermolecular stacking of  $\pi$ -orbitals in the solid state, which is absent in diluted solution.

The emission maxima  $\lambda_{\text{max}}^{\text{E}}$  show an increase with chain elongation for all oligomers under study. Measurement of the Stokes shifts shows that these are relatively large (0.30 – 0.45 eV), although somewhat smaller than for pure oligothiophenes.<sup>[9, 10]</sup> Since the hybrid materials under present study are planar in the electronic ground state, this observation is explained by excitation of ThODAs and HThODAs to the  $S_2$  state (similar as observed in ODAs).<sup>[11]</sup> This implies that even in the presence of a small number of enyne moieties in the chain, the photophysics of hybrid thiophene-enyne materials is dominated by these enyne moieties.

The fluorescence quantum yield  $\Phi_f$  displays a clear maximum at CL = 7 – 12, and quickly reduces to marginal values for longer oligomers. This trend is in line with the observation that PDA polymers show marginal fluorescence quantum yields.<sup>[3, 12]</sup> The fluorescence lifetimes are relatively short ( $\tau_f < 900$  ps) and decrease upon chain elongation for all enyne-based materials. The observed correlation time  $\tau_R$  of the molecule in its fully extended conformation provides additional evidence that the conjugation in enyne-based materials is not significantly hampered by kinks or torsions, because otherwise  $\tau_R$  would have increased less than linearly with CL or the length of the fully extended system.

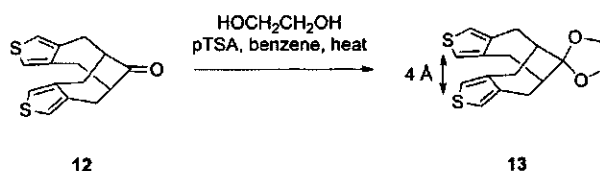
## General Discussion: Future Prospects

Since interchain  $\pi$ - $\pi$  interactions are now shown to have a dominant effect on the photophysics, new model compounds can be proposed for detailed investigations of  $\pi$ - $\pi$  interactions. For example, a covalent linkage of two oligomeric chains with  $C_{2h}$  symmetry would ideally result in two (near-) parallel ODA chains that are locked on top of one another, corresponding to a case in which the interchain interactions are maximized. An example is depicted in Scheme 6 were two hexamers **1-6** endcapped with  $-C(CH_3)_2CH_2OH$  and trimethylsilyl group are coupled *via* an ether bond to 1,3-difluoro-2-nitrobenzene.<sup>[13]</sup> The resulting stacked ODA **11** has an estimated distance between two adjacent chains of approximately 6 Å.



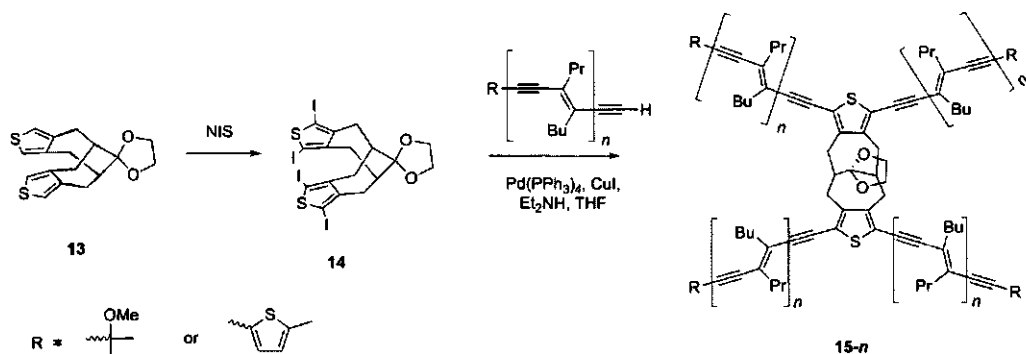
Scheme 6. Stacked  $\pi$ -conjugated ODA hexamers as molecular models to examine interchain interactions in  $\pi$ -conjugated materials.

Moreover, a similar model to study the influence of interchain  $\pi$ - $\pi$  interactions on the optoelectronic properties of an oligomer chain is proposed for hybrid enyne-based oligomers such as ThODAs series with a central thiophene unit (Scheme 7).



Scheme 7. Ketalization of *bis*-thieno-fused bicyclo[4.4.1]undecanone **12**.

This approach is based on the ketalization of *bis*-thieno-fused bicyclo[4.4.1]undecanone **12** with ethylene glycol. This locks the bicycloalkane into a chair-chair conformation in which the thiophene rings are stacked having a mutual distance of  $\sim 4$  Å.<sup>[14]</sup> Chain elongation of enyne-based material is initiated by tetra-halogenation of ketal **13**, followed by Sonogashira coupling with protodesilylated ODA chain **1-*n*** or **3-*n*** (Scheme 8). The oligomer series **15-*n*** are stacked analogues of **6-*n*** and **7-*n***, respectively.

Scheme 8. Model for stacked ThODAs 15-*n*.

Given the rapid growth of possibilities to accurately compute the optical spectra of  $\pi$ -conjugated materials (such as has been performed in Chapter 6 for the radical cations of ODAs), it would be of significant interest to further investigate theoretically the excited states properties of the enyne-based materials. Two topics had attracted our special interest: 1) the effect of small torsions within the polymer backbone on both  $\lambda_{\text{max}}^{\text{A}}$  and oscillator strength; 2) the effect of stacking of two parallel (or nearly parallel) oligomers on these properties. The success of such an approach hinges to a great deal on the increased capacity of DFT and DFT-like methods to describe non-covalent interactions in a quantitatively correct manner. Here the developments by e.g. Truhlar *et al.*,<sup>[15]</sup> and Grimme *et al.*<sup>[16]</sup> show great potential, and point to the possibility that such accurate computations come within reach soon.

There is a lot of scientific interest in polymers such as poly(*p*-phenylenevinylene) (PPV) for use as active layers in Polymer Light-Emitting Diodes (PLED), since it is possible to tune their emission.<sup>[17]</sup> Synthesized enyne-based oligomers offer an advantage over their polymeric counterparts due to their high purity, which may contribute to increased device efficiencies and stabilities. Furthermore, these oligomers can be used to fabricate multilayer structures to boost device efficiencies even further.<sup>[18]</sup> In addition, follow-up investigations of the electroluminescence of the synthesized materials as emitting/conductive layers in systems such as Organic Light-Emitting Diodes (OLED) are highly recommended. Such a study should focus on the performance of OLED devices incorporating an active region of the enyne-based materials presented here. This will provide a new scientific playground to explore the potential of these materials as candidates in optoelectronic devices.

## References

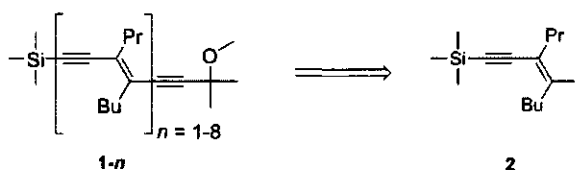
- [1] M. Schott in *Photophysics of Molecular Materials*, (Ed. G. Lanzani), Wiley-VCH, Weinheim, **2006**, pp. 49-151.
- [2] A. F. Garito, C. C. Teng, K. Y. Wong and O. Zammani-Khamiri, *Mol. Cryst. Liq. Cryst.* **1984**, *106*, 219-258.
- [3] H. Zuilhof, H. M. Barentsen, M. Dijk van, E. J. R. Sudhölter, R. J. O. M. Hoofman, L. D. A. Siebbeles, M. P. Haas de and J. M. Warman in *Polydiacetylenes*, (Ed. H. S. Nalwa), Academic Press, San Diego, San Francisco, New York, Boston, London, Sydney, Tokyo, **2001**, pp. 339-437.
- [4] A. Elangovan, Y.-H. Wang and T.-I. Ho, *Org. Lett.* **2003**, *5*, 1841-1844.
- [5] F. Sato and S. Okamoto, *Adv. Synth. Catal.* **2001**, *343*, 759-784.
- [6] K. Fukuhara, Y. Takayama and F. Sato, *J. Am. Chem. Soc.* **2003**, *125*, 6884-6885.
- [7] Y. Takayama, C. Delas, K. Muraoka, M. Uemura and F. Sato, *J. Am. Chem. Soc.* **2003**, *125*, 14163-14167.
- [8] Y. Takayama, C. Delas, K. Muraoka and F. Sato, *Org. Lett.* **2003**, *5*, 365-368.
- [9] P. F. van Hutten, R. E. Gill, J. K. Herrema and G. Hadziioannou, *J. Phys. Chem.* **1995**, *99*, 3218-3224.
- [10] P. Garcia, J. M. Pernaut, P. Hapiot, V. Wintgens, P. Valat, F. Garnier and D. Delabouglise, *J. Phys. Chem.* **1993**, *97*, 513-516.
- [11] G. M. Balkowski, M. Groeneveld, H. Zhang, C. C. J. Hendrikx, M. Polhuis, H. Zuilhof and W. J. Buma, *J. Phys. Chem. A* **2006**, *110*, 11435-11439.
- [12] R. Lécuyer, J. Berrehar, C. Lapersonne-Meyer and M. Schott, *Phys. Rev. Lett.* **1998**, *80*, 4068-4071.
- [13] T. F. Woiwode, C. Rose and T. J. Wandless, *J. Org. Chem.* **1998**, *63*, 9594-9596.
- [14] K. M. Knoblock, C. J. Silvestri and D. M. Collard, *J. Am. Chem. Soc.* **2006**, *128*, 13680-13681.
- [15] Y. Zhao and D. G. Truhlar, *Acc. Chem. Res.* **2008**, *41*, 157-167.
- [16] T. Schwabe and S. Grimme, *Acc. Chem. Res.* **2008**, *41*, 569-579.
- [17] H. C. Christian-Pandya, S. Vaidyanathan and M. E. Galvin in *Applications and Devices Based on Conjugated Polymers* (Eds.: T. A. Skotheim and J. R. Reynolds), CRC Press, Boca Raton, **2007**, pp. 1245-1279.
- [18] F. Zhang, A. Petr, U. Kirbach and L. Dunsch, *J. Mater. Chem.* **2003**, *13*, 265-267.

# Samenvatting

## Synthese

De elektronische eigenschappen van  $\pi$ -geconjugeerde polymeren lijken in vele opzichten op die van metalen en halfgeleiders, maar tonen daarnaast ook potentiële voordelen met betrekking tot hun mechanische eigenschappen voor mogelijke toepassing in opto-elektronische apparaten.<sup>[1]</sup> De klasse van polydiacetylenen zijn uniek binnen deze groep van polymeren door een combinatie van niet-lineaire optische eigenschappen en een uiteenlopende vaste stofmorfologie zoals ondermeer de eenkristallen, de dunne films, Langmuir films aan wateroppervlakken en de bilaag vesikels.<sup>[2, 3]</sup> Zoals geldt voor de meeste polymeren met een hoog molecuulgewicht, wordt een gedetailleerde studie van de opto-elektronische eigenschappen belemmerd door een brede molecuulgewichtsdistributie en, daarmee vaak samenhangend, een lage oplosbaarheid. Het onderzoek aan monodisperse reeksen van oligodiacetylenen (ODAs), zoals die beschreven zijn in dit proefschrift, dienen dan ook als een modelsysteem voor de hoogmoleculaire en minder goed gedefinieerde polydiaceylenen (PDAs). Dit onderzoek omvat de ontwikkeling van de synthese van verschillende reeksen monodisperse en zeer goed oplosbare oligomeren op multigramschaal (Schema 1). De opto-elektronische eigenschappen van deze ODAs is bestudeerd als een functie van de conjugatielengte in zowel oplossing als in de vaste toestand. Dit onderzoek richt zich in meer detail op de oorsprong van de lichtabsorptie van PDAs bij lange golflengtes.<sup>[3]</sup>

Een goede oplosbaarheid van de ODAs is noodzakelijk om hun optoelektronische eigenschappen in oplossing te kunnen bestuderen. In hoofdstuk 2 wordt de succesvolle synthese van uitstekend oplosbare ODAs, tot aan het octameer, beschreven. De hoofdketen van deze ODAs bestaat uit de repeterende enyn-eenheid met *n*-propyl en *n*-butyl zijketens. (Schema 1).



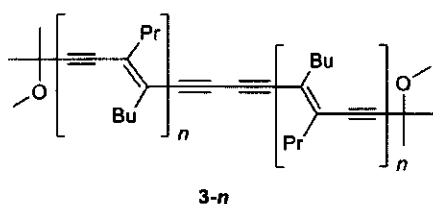
Schema 1. ODA reeks 1-*n* met oplosbaarheidverhogende zijketens gesynthetiseerd uit de enyn bouwsteen 2.

Deze alkylketens, hinderen intermoleculaire interacties tussen de geconjugeerde hoofdketens ("stacking"), waardoor de kristalpakking wordt gefrustreerd. Hierdoor neemt de

oplosbaarheid toe. Bovendien zorgen deze alkylketens ervoor dat in oplossing mogelijke intermoleculaire interacties tussen de  $\pi$ -geconjugeerde ketens wordt gehinderd. De gebruikte *tert*-OMe eindgroep draagt vanwege zijn polariteit mogelijk ook bij aan de oplosbaarheidsverhoging. De synthese van deze ODAs is uitgevoerd door een aantal opeenvolgende, katalytische verlengingsstappen tussen de enyn-bouwsteen **2** en de ontschermde trimethylsilyl eenheid **1-n** (Schema 1).

Een belangrijke eis die gesteld is aan deze iteratieve oligomeer synthese is de gewenste hoge opbrengst ieder van deze verlengingsstappen. Dit is bereikt door een Sonogashira koppeling onder reducerende atmosfeer uit te voeren. Hierdoor wordt de gevormde hoeveelheid homogekoppeld product tussen eindstandige acetylenen significant verminderd.<sup>[4]</sup> Voorafgaand aan de ketenverlenging wordt de bouwsteen **2** gesynthetiseerd op multigramschaal met een opbrengst van 60%, door middel van een regioselective titanium koppeling tussen een eindstandige en een intern acetyleen<sup>[5, 6]</sup> gevolgd door alkylering en jodering (Hoofdstuk 2, Schema 2).<sup>[7, 8]</sup>

In hoofdstuk 3 wordt de synthese van een nieuwe serie homo-gekoppelde ODAs (HODAs) beschreven. De langste gesynthetiseerde HODA bevat 30 geconjugeerde dubbele en drievoudige bindingen en heeft een geschatte lengte van maar liefst 8.2 nm! Deze HODAs worden bereid door twee symmetrische oligodiacetyleen-eenheden te koppelen in één katalytische stap. (Schema 2). De hiervoor gebruikte ODA ketens variëren van een monomeer tot een heptamer (Schema 2). In tegenstelling tot de ketenverlenging van het ODA reeks **1-n** (Hoofdstuk 2, Schema 4), kan deze palladium gekatalyseerde reactie onder lucht atmosfeer worden uitgevoerd en wordt een zeer hoge opbrengst van meer dan 90% verkregen.

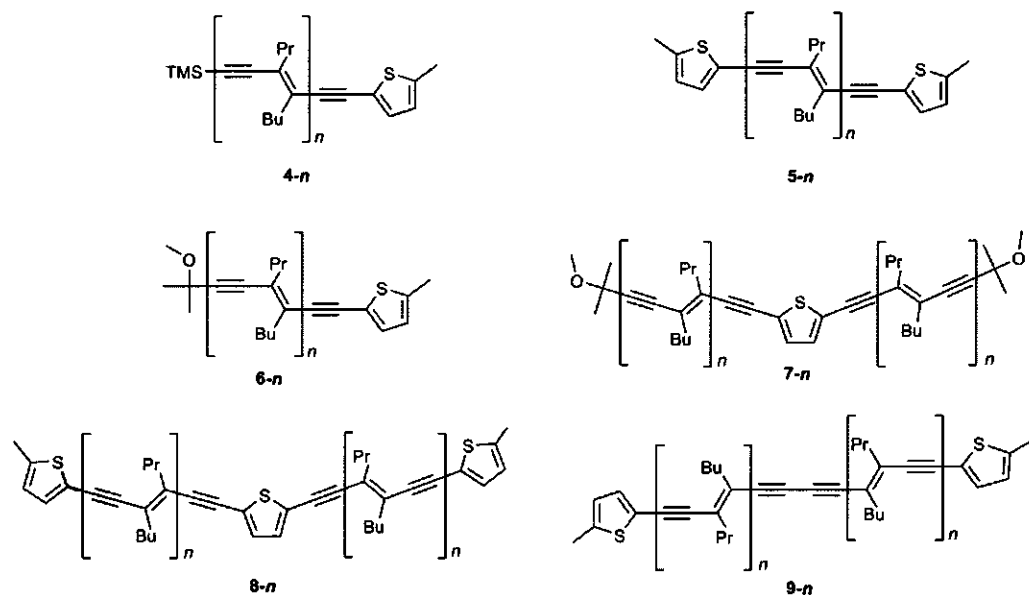


Schema 2. HODA reeks variërende van een monomeer **3-1** ( $C_{34}H_{50}O_2$  and  $M_r = 490.38$ ) tot een heptameer **3-7** ( $C_{166}H_{242}O_2$  and  $M_r = 2267.67$ ).

In hoofdstuk 4 wordt de synthese van een aantal enyn-thiofeen hybride materialen beschreven. De thiofeengroep fungeert hierin als een centrale brug (ThODAs reeks **4-n** tot **8-n**) en/of als eindgroep (HThODAs reeks **9-n**) (Schema 3). In totaal zijn vijf nieuwe reeksen gesynthetiseerd. De langste geconjugeerde verbinding **9-3** ThODA bevat 20 geconjugeerde  $\pi$  bindingen. De reeksen van **4-n** tot **6-n** zijn alle gesynthetiseerd via een iteratieve procedure

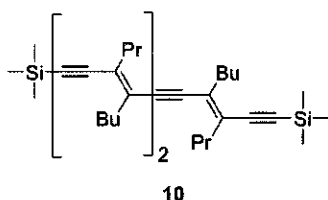


van Sonogashira koppelingen tussen de bouwstenen en de ontschermd trimethylsilyl eenheid. De reeksen **5-n** en **6-n** zijn na elke verlengingsstap voorzien van een thiofeen eindgroep. De reeksen **7-n** en **8-n** zijn gesynthetiseerd door twee ODA ketens van gelijke lengte te koppelen via 2,5-dijoodthiofeen. De HThODA reeks **9-n** is gesynthetiseerd door twee **4-n** oligomeren van een gelijke lengte aan elkaar te koppelen.



Schema 3. De gesynthetiseerde en onderzochte reeksen van ThODAs and HThODAs met  $n = 1-3$ .

In Hoofdstuk 5 wordt een nieuwe, divergente route beschreven om lange ODAs zoals bijvoorbeeld **10** (Schema 5) te synthetiseren door twee bouwstenen te verbinden aan een terminaal *bis*-acetyleen (Hoofdstuk 5, Schema 2). Het effect van een apolair eindgroep, zoals de trimethylsilyl (TMS)-groep, is bestudeerd in vergelijking met monomeer **1-1** en trimeer **1-3** (Schema 2).



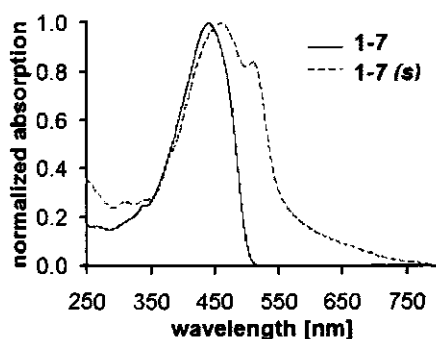
Schema 5. Divergente synthese van monodisperse ODA **10**.

In hoofdstuk 6 wordt de synthese van ODA reeks 1-*n* en de respectievelijke radicaal kationen (Schema 1) beschreven. De optische absorptiespectra van deze verbindingen zijn bepaald in het zichtbare en nabij-infrarood (VIS/NIR) gebied (500-2100 nm = 0.6-2.5 eV). Het gebruik van tijdsopgeloste spectroscopische metingen toont aan dat deze radicaal kationen slechts zeer langzaam met water reageren. Ze zijn dus kinetisch stabiel. Dat is belangrijk om te weten, omdat spoortjes water altijd aanwezig kunnen zijn in opto-electronische experimenten.

## Opto-elektronika

De 'steady-state' optische absorptie eigenschappen van de ODA reeksen zijn bepaald in oplossing en in dunne films. De resultaten laten eenduidig een roodverschuiving van het absorptiemaximum ( $\lambda_{\text{max}}^A$ ) zien, evenals een verhoging van de molaire extinctie coëfficiënt ( $\epsilon_{\text{max}}$ ) indien het aantal repeterende monomerische eenheden toeneemt. De correlatie tussen  $\lambda_{\text{max}}^A$  en de reciproke conjugatielengte (CL) is lineair voor alle bestudeerde reeksen, zowel in een oplossing als in dunne film. Deze waarneming laat eenduidig zien dat de conjugatie in deze moleculen niet gehinderd wordt door knikken of torsies in de hoofdketen. Extrapolatie van  $\lambda_{\text{max}}^A$  naar oneindige CL resulteert in een maximum absorptie golflengte van 500 nm. Dit is veel lager dan de gerapporteerde literatuurwaarden voor PDAs (> 600 nm).<sup>[3]</sup> Aggregatie in geconcentreerde oplossingen van deze oligomeren (tot 5 mM) kan worden uitgesloten. De vermoede sterische hindering door de aanwezige alkylketens blijkt dus te werken.

Een aantal nieuwe eigenschappen zijn waargenomen in de absorptiespectra van dunne films van de onderzochte oligomeren (Figuur 1): a) een verdere roodverschuiving van  $\lambda_{\text{max}}^A$  in vergelijking met de waargenomen maxima in oplossing; b) een duidelijk zichtbare roodverschoven schouder; en c) een extra lange golflente absorptie bij  $\geq 550$  nm.



Figuur 1. Genormaliseerde absorptie spectrum van HODA 1-7 in oplossing en in dunne film (s).

Dit wordt geïnterpreteerd door de aanwezigheid van een nagenoeg vlakke geometrie van de oligomeren. De additionele roodverschuiving van de lange golflengte absorptie ( $> 550$  nm voor de langste oligomeren) wordt veroorzaakt door een intermoleculaire interactie ("stacking") van de  $\pi$ -systemen, welke niet voorkomt in oplossing.

De emissie maxima  $\lambda_{\text{max}}^{\text{E}}$  verschuiven ook naar langere golflengte met een toegenomen ketenlengte voor alle bestudeerde oligomeren. De gemeten Stokes-verschuiving is relatief groot (0.30 – 0.45 eV), maar is enigszins kleiner dan gemeten voor de oligothiofenen.<sup>[9, 10]</sup> Deze hybride materialen hebben een planaire geometrie in de elektronische grondtoestand en exciteren naar een  $S_2$  toestand (zoals gevonden voor ODAs).<sup>[11]</sup> Deze bevinding laat zien dat de fotofysica van een hybride thiofeen-enyn materiaal bepaald wordt door de enyn eenheid.

De fluorescentie quantumopbrengst  $\Phi_f$  vertoont een duidelijk maximum bij CL = 7 - 12, en neemt snel af tot een marginale waarde voor de langere oligomeren. Deze tendens komt overeen met de gevonden marginale fluorescentie quantumopbrengst voor PDA polymeren.<sup>[3]</sup>

<sup>[12]</sup> De gevonden fluorescentie levensduur is relatief kort ( $\tau_f < 900$  ps) en neemt verder af met toenemende ketenlengte voor alle enyn-gebaseerde materialen. De waargenomen correlatietijd  $\tau_R$  van het molecuul in een volledig gestrekte conformatie levert een extra aanwijzing op dat de conjugatie van enyn-gebaseerde materialen niet belemmerd wordt door knikken of torsies in het systeem.

## References

- [1] M. Schott in *Photophysics of Molecular Materials*, (Ed. G. Lanzani), Wiley-VCH, Weinheim, **2006**, pp. 49-151.
- [2] A. F. Garito, C. C. Teng, K. Y. Wong and O. Zammani-Khamiri, *Mol. Cryst. Liq. Cryst.* **1984**, *106*, 219-258.
- [3] H. Zuilhof, H. M. Barentsen, M. Dijk van, E. J. R. Sudhölter, R. J. O. M. Hoofman, L. D. A. Siebbeles, M. P. Haas de and J. M. Warman in *Polydiacetylenes*, (Ed. H. S. Nalwa), Academic Press, San Diego, San Francisco, New York, Boston, London, Sydney, Tokyo, **2001**, pp. 339-437.
- [4] A. Elangovan, Y.-H. Wang and T.-I. Ho, *Org. Lett.* **2003**, *5*, 1841-1844.
- [5] F. Sato and S. Okamoto, *Adv. Synth. Catal.* **2001**, *343*, 759-784.
- [6] K. Fukuhara, Y. Takayama and F. Sato, *J. Am. Chem. Soc.* **2003**, *125*, 6884-6885.
- [7] Y. Takayama, C. Delas, K. Muraoka, M. Uemura and F. Sato, *J. Am. Chem. Soc.* **2003**, *125*, 14163-14167.
- [8] Y. Takayama, C. Delas, K. Muraoka and F. Sato, *Org. Lett.* **2003**, *5*, 365-368.
- [9] P. F. van Hutten, R. E. Gill, J. K. Herrema and G. Hadzioannou, *J. Phys. Chem.* **1995**, *99*, 3218-3224.
- [10] P. Garcia, J. M. Pernaut, P. Hapiot, V. Wintgens, P. Valat, F. Garnier and D. Delabouglise, *J. Phys. Chem.* **1993**, *97*, 513-516.
- [11] G. M. Balkowski, M. Groeneveld, H. Zhang, C. C. J. Hendrikx, M. Polhuis, H. Zuilhof and W. J. Buma, *J. Phys. Chem. A* **2006**, *110*, 11435-11439.
- [12] R. Lecuillier, J. Berrehar, C. Lapersonne-Meyer and M. Schott, *Phys. Rev. Lett.* **1998**, *80*, 4068-4071.

## Dankwoord

Op deze plaats wil ik iedereen bedanken die heeft bijgedragen aan het totstandkomen van dit proefschrift. Velen hebben mij tijdens dit onderzoek met raad en daad terzijde gestaan. Enkele personen wil ik echter in het bijzonder noemen.

Allereerst wil ik mijn promotoren, Prof. H. Zuilhof en Prof. E.J.R. Sudhölter, bedanken voor het feit dat ik dit onderzoek onder hun supervisie mocht uitvoeren op het Laboratorium voor Organische Chemie. Beste Han, je hebt vanaf het begin een grote invloed gehad op dit onderzoek. Enerzijds door mij de ruimte en tijd te geven voor de oligomeer synthese, anderzijds door vele goede adviezen en nodige toelichtingen over de fotofysica. Ik heb er veel van geleerd! Beste Ernst, bedankt voor je altijd aanwezige enthousiasme en optimisme, vele goede ideeën en interesse voor dit onderzoek. De regelmatige contacten, ook na je vertrek uit Wageningen, heb ik bijzonder gewaardeerd.

Naast mijn begeleiders wil ik graag mijn collega's bedanken voor de uiterst prettige samenwerking. Als eerste wil ik Barend van Lagen noemen. Barend, je hebt het meeste bijgedragen aan de spectroscopische en in de laatste fase van dit onderzoek ook de fotofysische metingen. Jouw pragmatische aanpak en persoonlijke betrokkenheid, ook buiten het onderzoek, heb ik zeer gewaardeerd! Jacob Baggerman wil ik langs deze weg eveneens bedanken voor zijn belangrijke bijdrage aan de opto-elektronica. Maarten Posthumus ben ik zeer erkentelijk voor de uiterst nauwkeurige HRMS metingen en zijn boeiende en uitgebreide toelichtingen. Elbert van der Klift en Frank Claassen ben ik dankbaar voor hun hulp bij de analyse en de zuivering van de verbindingen.

De leden van de gebruikerscommissie, dr. Jan Kroon, dr. Herman Schoo en dr. Joost Smits, ben ik eveneens dank verschuldigd voor hun bijdrage tijdens de jaarlijkse vergaderingen.

Tijdens mijn onderzoek heb ik het genoegen gehad om een aantal studenten te mogen begeleiden. Ik wil in het bijzonder Kitty van Gruijthuisen en Reindert van Doorn bedanken: mede dankzij jullie inspanningen is de synthese en de karakterisering van de hybride oligomeren gelukt!

Tevens is dit een goed moment om alle collega promovendi, postdocs en medewerkers van het Laboratorium voor Organische Chemie te bedanken voor de gezellige jaren die ik hier gehad heb: ORC was voor mij een fijne werkplek. My sincere thanks are extended to my paranims, Ganesan and Ioan, for their support and benevolent help.

Mijn Moeder, mijn familie en vrienden wil ik bedanken voor de belangstelling die ze getoond hebben in de voortgang van het onderzoek en de noodzakelijke ondersteuning om dat te voltooien.

Finally, I would like to express special thanks to Agnieszka for her love and support. Without your help and encouragement, this study would not have been completed.

*Gregor*

## **CURRICULUM VITAE**

Gregor Pilzak werd geboren op 19 augustus 1976 te Kraków. Na het behalen van HAVO (1996) en VWO (1997) diploma aan het Graafschap College te Doetinchem werd in september 1997 begonnen met de studie Moleculaire Wetenschappen aan de Wageningen Universiteit. Tijdens deze studie werd onder leiding van dr. B. Jansen en Prof. dr. Æ. de Groot een afstudeer onderzoek verricht bij de vakgroep Organische Chemie op het gebied van de natuurstofsynthese getiteld: "Intermediaren voor de stereoselectieve synthese van het fungitoxische isozonanol". Daarnaast werd onder leiding van dr. R.H. Blaauw (Chiralix) en Prof. dr. F.P.J.T. Rutjes (Radboud Universiteit Nijmegen) een stage onderzoek verricht, getiteld: "Stereoselective synthesis of functionalized heterocycles and amino acid derivatives". Begin 2003 werd het doctoraal examen behaald en vanaf februari 2003 tot mei 2007 werd hij aangesteld als Onderzoeker in Opleiding bij het Laboratorium voor Organische Chemie van Wageningen Universiteit. Hier werd het in dit proefschrift beschreven onderzoek verricht onder leiding van Prof. dr. H. Zuilhof en Prof. dr. E.J.R. Sudhölter. Sinds oktober 2007 is hij werkzaam als Senior Scientist bij Mercachem B.V. te Nijmegen.

## List of publications

### Divergent Synthesis and Optoelectronic Properties of Oligodiacetylene Building Blocks

*Tetrahedron Letters*

Volume 49, Issue 33, Date: June 3, 2008, Pages: 4949–4952

**Gregor S. Pilzak**, Barend van Lagen, Ernst J. R. Sudhölter, Han Zuilhof

### Synthesis and Optical Properties of All-trans-Oligodiacetylenes

*Chemistry - A European Journal*

Volume 14, Issue 26, Date: September 8, 2008, Pages: 7939–7950

**Gregor S. Pilzak**, Barend van Lagen, Cindy C. J. Hendrikx, Ernst J. R. Sudhölter, Han Zuilhof

### Synthesis and Optoelectronic Properties of Nanometer-Sized and Highly Soluble Homocoupled Oligodiacetylenes

*Chemistry - A European Journal*

Volume 15, Issue 10, Date: February 23, 2009, Pages: 2296–2304

**Gregor S. Pilzak**, Jacob Baggerman, Barend van Lagen, Maarten A. Posthumus, Ernst J. R. Sudhölter, Han Zuilhof

### Hybrid Conjugated Organic Oligomers Consisting of Oligodiacetylene and Thiophene Units: Synthesis and Optical Properties

*Chemistry - A European Journal*

accepted, 2009

**Gregor S. Pilzak**, Kitty van Gruijthuisen, Reindert H. van Doorn, Barend van Lagen, Ernst J. R. Sudhölter, Han Zuilhof

### Radical Cations of All-trans Oligodiacetylenes: Optical Absorption and Reactivity towards Nucleophiles

*The Journal of Physical Chemistry B*

accepted, 2009

**Gregor S. Pilzak**, Silvia Fratiloiu, Jacob Baggerman, Ferdinand C. Grozema, Ernst J. R. Sudhölter, Laurens. D. A. Siebbeles, and Han Zuilhof

## Overview of completed training activities

### *Discipline specific activities*

#### *Meetings*

Design and Synthesis, Structure and Reactivity, Biomolecular Chemistry, NWO, Lunteren, the Netherlands	2004-2007
Wageningen Symposium of Organic Chemistry, KNCV, Wageningen, the Netherlands	2004, 2006
Dutch Polymer Institute meeting, Eindhoven, the Netherlands	2005
Sollar Cell Day, ECN, Utrecht, the Netherlands	2006

#### *General courses*

Advanced Organic Chemistry Course, Laboratory for Organic Chemistry, WUR, Wageningen, the Netherlands	2003-2007
---	-----------

#### *Optionals*

Preparation of research proposal	
Literature study, Laboratory for Organic Chemistry, WUR, Wageningen, the Netherlands	2003-2007
Laboratory for Organic Chemistry Colloquia, WUR, Wageningen, the Netherlands	2003-2007

Het onderzoek in dit proefschrift werd financieel ondersteund door de Nederlandse Technologiestichting STW.